Effect of Displacement Feedback Control on the Frequencies of Cantilevered Beams with Tip Mass and Axial Load using Piezo Actuators

Malesela K. Moutlana

In fulfillment of a Master of Science in Mechanical Engineering

College of Agriculture, Engineering and Science, University of KwaZulu-Natal

School of Engineering

January 2014

Supervisor:

Prof. Sarp Adali

Declaration 1

Supervisor:

As the candidate's Supervisor I agree/do not agree to the submission of this dissertation.

Signed:……(Prof. Sarp Adali) Date:……

Candidate:

I, Malesela Kenneth Moutlana (207528577) declare that:

(i) The research reported in this dissertation, except where otherwise indicated, is my original work.

(ii) This dissertation has not been submitted for any degree or examination at any university.

(iii) This dissertation does not contain other person's data, pictures, graphs or other information, unless specifically acknowledged as being sourced from other persons.

(iv) This dissertation does not contain other person's writing, unless specifically acknowledged as being sourced from other researchers. Where written sources have been quoted, then:

   a) their words have been re-written but the general information attributed to them has been referenced;

   b) where their exact words have been used, their writing has been placed inside quotation marks, and referenced.

(v) Where I have reproduced a publication of which I am an author, co-author or editor, I have indicated in detail which part of the publication was actually written by myself alone and have fully referenced such publication.

(vi) This dissertation does not contain text, graphics or tables copied and pasted from the Internet, unless specifically acknowledged, and the source being detailed in the dissertation and in the References sections.

Signed:……..….(MK Moutlana) Date:……

Declaration 2

Conferences

1. Moutlana MK (2009) Analytical model for a study of a composite cantilevered beam with piezo actuators attached to the top and bottom surface. *15th International Conference on Composite Structures* (ICCS-15), 15-17 June 2009, Porto, Portugal. Presentation
2. Moutlana MK (2013) Effect of piezoelectric control on a cantilever beam with extended tip mass and axial load. Proceedings of *1st International Conference on Composite and Biocomposites and Nanocomposites* (ICCBN-1), 2 – 4 December 2013, Durban. pp.555-575
3. Moutlana MK (2014) Use of piezo actuators to maximize the fundamental frequency and the gaps. Proceedings of *9th South African Conference on Computational and Applied Mechanics* (SACAM2014), 14-16 January 2014, Somerset West.
   To appear

Journal publications

1. Moutlana MK and Adali S (2014) Vibration of a Cantilever Beam with extended tip mass subject to piezoelectric control *R&D Journal SAIMechE* Stellenbosch.
   (Corresponding author: MK Moutlana)
   Submitted
2. Moutlana MK and Adali S (2014) Effect of piezo voltage polarity on the frequencies and frequency gaps of piezoelectric beams.
   In preparation

In these publications, I, MK Moutlana was the main author and Prof. S Adali was the supervisor of MSc research.

Signed:……..….(MK Moutlana) Date:……

Acknowledgments

I would like to thank Prof. Sarp Adali for supervising my research in this project and for his support. His knowledge, guidance and experience has encouraged and motivated me throughout my research. I would like to thank my family: Rose my wife, the kids Keletso, Tswelopele and Thato for their support and inspiration. I would also like thank my parents who remain a shining beacon in my life. I love you very much.

Abstract

Summary: *This work provides a study of the natural frequencies of a cantilevered beam with tip mass and axial load. Displacement feedback control is applied using piezo actuators attached to the top and bottom of the beam. The center of gravity of the mass and its rotary inertia are accounted for in the solution.*

Abstract: The analysis of flexible components is essential to provide for the successful design of various engineering structures. This study provides an analytical solution to the dynamic behavior of a cantilevered beam carrying a mass at the free end, while being subjected to constant axial load. The structure is modeled using the Euler-Bernoulli theory and the contributions of the mass, thickness and stiffness of the piezoelectric actuators to the structure are taken into account. The effects of the piezo input voltage polarity is also taken into account.

The natural frequencies of the beam can be altered by applying a voltage in the desired polarity and thereby causing an extension or contraction in the piezo actuator. This mechanical response alters the frequencies of the piezoelectric beam. The piezoelectric effect causes a compression or extension strain when a voltage is applied along the direction of polarization. The strain in the piezoelectric beam causes a moment at the free end, which directly affects the natural frequencies. By applying a voltage in the same or opposite direction of the poling of the piezo, the result is a compression or extension perpendicular to the poling. An applied voltage in the same direction can be considered positive and reduces the frequencies, whilst in the opposite direction negative and increases the natural frequencies. In this investigation the piezo layer thickness is varied, which in turn allows for a variable voltage input. For a thicker layer, the voltage can be increased and the actuation strain increased.

The frequency content of the dynamically varying forces applied to a structure has the potential to excite the structure at one or more of its natural frequencies. Using piezo actuators, the natural frequencies and the natural frequency gaps can be maximized. Maximizing the natural frequencies is useful to avoid resonance when the external excitation frequency is less than the natural frequency.

Keywords: Piezo, vibrations, natural frequencies, Euler-Bernoulli, tip mass, axial load.

Table of Contents

Declaration 1 ii

Supervisor: ii

Candidate ii

Declaration 2 iii

Conferences iii

Journal publications iii

Acknowledgments iv

Abstract v

List of figures ix

List of figures in appendix xii

List of tables xiii

List of tables in appendix xvi

Nomenclature xvii

Chapter 1 – Introduction 20

1.1 Background and motivation 20

1.2 Literature review **23**

1.3 Research objectives 30

Chapter 2 – Piezoelectric composite beam 33

2.1 Derivation of the governing equations for the beam and the piezo layers 33

2.1.1 Moment-curvature relation for beam 33

2.1.2 Governing equations for composite beam 36

2.1.3 Constitutive equations for piezo layers 37

2.2 Solution of the governing equations by separation of variables 48

2.3 Boundary conditions 51

2.4 Determination of the natural frequencies of the beam 54

2.5 Orthogonality of the modes 60

Chapter 3 - Computation of the natural frequencies 66

3.1 Natural frequencies for a cantilevered beam.....66

3.2 Natural frequencies for a beam with tip mass and axial load.....67

3.2.1 First natural frequencies (ω_1).....67

3.2.2 Second natural frequencies (ω_2) 71

3.2.3 Third natural frequencies (ω_3) 74

3.2.4 Fourth natural frequencies (ω_4).....78

3.3 Change in natural frequencies for varying axial load, tip mass and voltage.....81

3.3.1 First natural frequencies (fundamental mode) 81

3.3.2 2^{nd}, 3^{rd} and 4^{th} Natural frequency (higher modes).....85

3.4 Natural frequencies versus change in tip mass.....85

3.5 Percentage change in natural frequencies with change in axial load 95

Chapter 4 – Computation of frequencies with an extended tip mass 99

4.1 Determination of the natural frequencies for a beam with an extended tip mass and tip inertia.....99

4.2 Natural frequencies for a beam with extended tip mass.....103

4.3 Fundamental frequencies for a beam with an extended tip mass and rotary inertia 106

4.3.1 Natural frequencies of a beam with a tip mass, $b_1 = 0$ 106

4.3.2 Natural frequencies of a beam with extended tip mass and rotary inertia for $b_1 = L/2$ 111

4.3.3 Natural frequencies of a beam with extended tip mass and rotary inertia for $b_1 = L/1$.....114

Chapter 5 – Effect of actuator thickness and voltage polarity on the frequencies 119

5.1 Fundamental frequencies for a beam with different actuator thicknesses 119

5.2 Effect of voltage polarity on frequencies 123

5.2.1 Increase in the fundamental frequency 123

5.2.2 Increase in frequency gap between the fundamental and second natural frequency 125

Chapter 6 – Mode shapes of vibrating piezoelectric beam 130

6.1 First mode shapes for a beam with a concentrated tip mass 130

6.2 Mode shapes for a beam with an extended tip mass and rotary inertia ($b_1 > 0$) 135

Chapter 7 – Dynamic behaviour of a piezoelectric beam subject to initial conditions .137

7.1 Initial value problem and the eigenfunction expansion series 137

7.2 Convergence of the eigenfunction series expansion 140

7.3 Complete dynamic solution..... 144

7.4 Oscillation of the beam for $b_1 = 0$ 150

7.5 Oscillation of the beam for $b_1 = L/2$ 153

7.6 Oscillation of the beam for $b_1 = L/1$ 155

7.7 Amplitude spectrum for the cantilevered beam 157

Chapter 8 – Conclusions..... 163

8.1 Conclusion..... 163

8.2 Future research 165

Bibliography 166

Appendix..... 172

A1. Second natural frequencies. 172

A2. Third natural frequencies. 175

B1. Natural frequencies with $b_1 = L/10$. 181

B2. Natural frequencies with $b_1 = L/5$. 183

C1. Mode shapes 0V and 1000V for $\eta = 0$ 185

C2. Mode shapes for different tip masses $k = 0$..... 187

List of figures

Figure 2.1: Uniform beam under free vibration....33
Figure 2.2: Single deformed fiber(s) along the length of the beam....34
Figure 2.3: Internal shear forces, moments and external forces on the beam....36
Figure 2.4: Cross-sectional area of beam....37
Figure 2.5: Cross-sectional area of beam indicating the dimensions of the composite....39
Figure 2.6: Beam with concentrated mass at the free end....53
Figure 2.7: Cantilever sandwiched between two piezo electric actuators....54
Figure 2.8: Compression and Extension due to piezo material poling and input voltage polarity for piezo....58
Figure 3.1a: Change in fundamental frequency vs axial Load ratio: Voltage = 0V....67
Figure 3.1b: Change in fundamental frequency vs axial load ratio: Voltage = 100V....68
Figure 3.1c: Change in fundamental frequency vs axial load ratio: Voltage = 500V....69
Figure 3.1d: Change in fundamental frequency vs axial load ratio: Voltage = 1000V....70
Figure 3.2a: Change in 2nd frequency vs axial load ratio: Voltage = 0V....71
Figure 3.2b: Change in 2nd frequency vs axial load ratio: Voltage = 100V....72
Figure 3.2c: Change in 2nd frequency vs axial load ratio: Voltage = 500V....73
Figure 3.2d: Change in 2nd frequency vs axial load ratio: Voltage = 1000V....74
Figure 3.3a: Change in 3rd frequency vs axial load ratio: Voltage = 0V....75
Figure 3.3b: Change in 3rd frequency vs axial load ratio: Voltage = 100V....76
Figure 3.3c: Change in 3rd frequency vs axial load ratio: Voltage = 500V....77
Figure 3.3d: Change in 3rd frequency vs axial load ratio: Voltage = 1000V....77
Figure 3.4a: Change in 4th frequency vs axial load ratio: Voltage = 0V....78
Figure 3.4b: Change in 4th frequency vs axial load ratio: Voltage = 100V....79
Figure 3.4c: Change in 4th frequency vs axial load ratio: Voltage = 500V....80
Figure 3.4d: Change in 4th frequency vs axial load ratio: Voltage = 1000V....81
Figure 3.5a: Percentage change in natural frequency ($\eta = 0$)....83
Figure 3.5b: Percentage change in natural frequency ($\eta = 0.1$)....83
Figure 3.5c: Percentage change in natural frequency ($\eta = 1$)....84
Figure 3.5d: Percentage change in natural frequency ($\eta = 5$)....84
Figure 3.6a: 1st Frequency vs tip mass ratio: Voltage = 0V....86
Figure 3.6b: 1st Frequency vs tip mass ratio: Voltage = 100V....87

Figure 3.6c: 1st Frequency vs tip mass ratio: Voltage = 500V.....87
Figure 3.6d: 1st Frequency vs tip mass ratio: Voltage = 1000V 88
Figure 3.7a: 2nd Frequency vs tip mass ratio: Voltage = 0V.....88
Figure 3.7b: 2nd Frequency vs tip mass ratio: Voltage = 100V 89
Figure 3.7c: 2nd Frequency vs tip mass ratio: Voltage = 500V.....90
Figure 3.7d: 2nd Frequency vs tip mass ratio: Voltage = 1000V 90
Figure 3.8a: 3rd Frequency vs tip mass ratio: Voltage = 0V 91
Figure 3.8b: 3rd Frequency vs tip mass ratio: Voltage = 100V.....91
Figure 3.8c: 3rd Frequency vs tip mass ratio: Voltage = 500V 92
Figure 3.8d: 3rd Frequency vs tip mass ratio: Voltage = 1000V.....92
Figure 3.9a: 4th Frequency vs tip mass ratio: Voltage = 0V 93
Figure 3.9b: 4th Frequency vs tip mass ratio: Voltage = 100V 93
Figure 3.9c: 4th Frequency vs tip mass ratio: Voltage = 500V 94
Figure 3.9d: 4th Frequency vs tip mass ratio: Voltage = 1000V 94
Figure 3.10a: Changes in the natural frequency (ω_1) vs axial load for V = 0V 97
Figure 3.10b: Changes in the natural frequency (ω_1) vs axial load for V = 100V.....97
Figure 3.10c: Changes in the natural frequency (ω_1) vs axial load for V = 500V 97
Figure 3.10d: Changes in the natural frequency (ω_1) vs axial load for V = 1000V.....97
Figure 3.11a: Changes in the natural frequency (ω_2) vs axial load for V = 0V 98
Figure 3.11b: Changes in the natural frequency (ω_2) vs axial load for V = 1000V.....98
Figure 3.12a: Changes in the natural frequency (ω_3) vs axial load for V = 0V 98
Figure 3.13a: Changes in the natural frequency (ω_4) vs axial load for V = 0V 98
Figure 3.12b: Changes in the natural frequency (ω_3) vs axial load for V = 1000V.....98
Figure 3.13b: Changes in the natural frequency (ω_4) vs axial load for V = 1000V.....98
Figure 4.1: Cantilever beam with an extended tip mass 99
Figure 4.2: Lowest Natural frequencies of system at k = +0.8 and η = 10 105
Figure 4.3a: Natural frequency vs axial load and tip mass for b_1 = 0 and V = 0V 107
Figure 4.3b: Natural frequency vs axial load and tip mass for b_1 = 0 and V = 100V 108
Figure 4.3c: Natural frequency vs axial load and tip mass for b_1 = 0 and V = 500V 109
Figure 4.3d: Natural frequency vs axial load and tip mass for b_1 = 0 and V =1000V 110
Figure 4.4a: Natural frequency vs axial load and tip mass for b_1 = L/2 and V = 0V.....111
Figure 4.4b: Natural frequency vs axial load and tip mass for b_1 = L/2 and V =100V 112
Figure 4.4c: Natural frequency vs axial load and tip mass for b_1 = L/2 and V =500V 113
Figure 4.4d: Natural frequency vs axial load and tip mass for b_1 = L/2 and V =1000V.....114

Figure 4.5a: Natural frequency vs axial load and tip mass for $b_1 = L/1$ and $V = 0$V 115
Figure 4.5b: Natural frequency vs axial load and tip mass for $b_1 = L/1$ and $V = 100$V 116
Figure 4.5c: Natural frequency vs axial load and tip mass for $b_1 = L/1$ and $V = 500$V 117
Figure 4.5d: Natural frequency vs axial load and tip mass for $b_1 = L/1$ and $V = 1000$V 118
Figure 5.1: 1st Natural frequency vs axial load for different voltages ($b_1 = 0$).....120
Figure 6.1: 1st Mode shape of vibration with inactive piezo actuators for Voltage = 0V.....131
Figure 6.2: 1st Mode shape of vibration with active piezo actuators for Voltage = 1000V..132
Figure 6.3: 1st Mode shape of vibration with inactive piezo actuators for Voltage = 0V.....133
Figure 6.4: 1st Mode shape of vibration with active piezo actuators for Voltage =1000V...134
Figure 7.1: Convergence of eigenfunction expansion for Voltage = 0V 141
Figure 7.2: Convergence of eigenfunction expansion for Voltage = 0V 142
Figure 7.3: Convergence of eigenfunction expansion for Voltage =1000V 143
Figure 7.4: Convergence of eigenfunction expansion for Voltage =1000V 144
Figure 7.5: Right angled triangle that shows the relation between (ϕ) and (G).....149
Figure 7.6: Phase angle (ϕ) and period ($\mathcal{T}$) of oscillation.....149
Figure 7.7: Frequencies for controlled and uncontrolled beams for $b_1 = 0$. (a) $\eta = 0$, (b) $\eta = 0.1$, (c) $\eta = 1$ and (d) $\eta = 5$ 152
Figure 7.8: Frequencies for controlled and uncontrolled beams for $b_1 = L/2$. (a) $\eta = 0$, (b) $\eta = 0.1$, (c) $\eta = 1$ and (d) $\eta = 5$ 154
Figure 7.9: Frequencies for controlled and uncontrolled beams for $b_1 = L/1$. (a) $\eta = 0$, (b) $\eta = 0.1$, (c) $\eta = 1$ and (d) $\eta = 5$ 156
Figure 7.10: (a) to (d): Oscillation of uncontrolled beam and controlled beams. (e) to (h): Amplitude spectrum of uncontrolled beams. (i) to (l): Amplitude spectrum of controlled beams; $\eta = 0$ 0V 1000V.....159
Figure 7.11: (a) to (d): Oscillation of uncontrolled beam and controlled beams. (e) to (h): Amplitude spectrum of uncontrolled beams. (i) to (l): Amplitude spectrum of controlled beams; $\eta = 0.1$ 0V 1000V.....160
Figure 7.12: (a) to (d): Oscillation of uncontrolled beam and controlled beams. (e) to (h): Amplitude spectrum of uncontrolled beams. (i) to (l): Amplitude spectrum of controlled beams; $\eta = 1$ 0V 1000V.....161
Figure 7.13: (a) to (d): Oscillation of uncontrolled beam and controlled beams. (e) to (h): Amplitude spectrum of uncontrolled beams. (i) to (l): Amplitude spectrum of controlled beams; $\eta = 5$ 0V 1000V.....162

List of figures in appendix

Figure A1 1: Natural frequency vs axial load: Tip mass ratio (η = 0) 172
Figure A1 2: Natural frequency vs axial load: Tip mass ratio (η = 0.1) 172
Figure A1 3: Natural frequency vs axial load: Tip mass ratio (η = 1.0) 173
Figure A1 4: Natural frequency vs axial load: Tip mass ratio (η = 5.0) 173
Figure A1 5: Natural frequency vs axial load: Tip mass ratio (η = 10) 174
Figure A2 1: Natural frequency vs axial load: Tip mass ratio (η = 0) 175
Figure A2 2: Natural frequency vs axial load: Tip mass ratio (η = 0.1) 175
Figure A2 3: Natural frequency vs axial load: Tip mass ratio (η = 1.0) 176
Figure A2 4: Natural frequency vs axial load: Tip mass ratio (η = 5.0) 176
Figure A2 5: Natural frequency vs axial load: Tip mass ratio (η = 10) 177
Figure A3 1: Natural frequency vs axial load: Tip mass ratio (η = 0) 178
Figure A3 2: Natural frequency vs axial load: Tip mass ratio (η = 0.1) 178
Figure A3 3: Natural frequency vs axial load: Tip mass ratio (η = 1.0) 179
Figure A3 4: Natural frequency vs axial load: Tip mass ratio (η = 5.0) 179
Figure A3 5: Natural frequency vs axial load: Tip mass ratio (η = 10) 180
Figure B1 1: Changes in the natural frequency vs axial load and tip mass ($b_1 = L/10$) 181
Figure B1 2: Changes in the natural frequency vs axial load and tip mass ($b_1 = L/10$) 181
Figure B1 3: Changes in the natural frequency vs axial load and tip mass ($b_1 = L/10$) 182
Figure B1 4: Changes in the natural frequency vs axial load and tip mass ($b_1 = L/10$) 182
Figure B2 1: Changes in the natural frequency vs axial load and tip mass ($b_1 = L/5$) 183
Figure B2 2: Changes in the natural frequency vs axial load and tip mass ($b_1 = L/5$) 183
Figure B2 3: Changes in the natural frequency vs axial load and tip mass ($b_1 = L/5$) 184
Figure B2 4: Changes in the natural frequency vs axial load and tip mass ($b_1 = L/5$) 184
Figure C1 1: First four mode shapes for k = +0.8 185
Figure C1 2: .First four mode shapes for k = 0 185
Figure C1 3: First four mode shapes for k = -1 186
Figure C1 4: First four mode shapes k = -2 186
Figure C2 1: Fundamental mode shapes 187
Figure C2 2: Second mode shapes 187
Figure C2 3: Third mode shapes 187
Figure C2 4: Fourth mode shapes 187

List of tables

Table 1.1: Four beam theories that are taken into consideration. 24
Table 2.1: Material and geometric properties of the composite beam.....58
Table 2.2: Polarity of voltage input for piezo actuators.....58
Table 3.1a: 1st frequencies of the beam with a tip mass and axial load: Voltage = 0V. 67
Table 3.1b: 1st frequencies of the beam with a tip mass and axial load: Voltage = 100V. 68
Table 3.1c: 1st frequencies of the beam with a tip mass and axial load: Voltage = 500V. 69
Table 3.1d: 1st frequencies of the beam with a tip mass and axial load: Voltage = 1000V. 70
Table 3.2a: 2nd frequencies of the beam with a tip mass and axial load: Voltage = 0V. 71
Table 3.2b: 2nd frequencies of the beam with a tip mass and axial load: Voltage = 100V. 72
Table 3.2c: 2nd frequencies of the beam with a tip mass and axial load: Voltage = 500V. 73
Table 3.2d: 2nd frequencies of the beam with a tip mass and axial load: Voltage = 1000V…74
Table 3.3a: 3rd frequencies of the beam with a tip mass and axial load: Voltage = 0V.....75
Table 3.3b: 3rd frequencies of the beam with a tip mass and axial load: Voltage = 100V. 76
Table 3.3c: 3rd frequencies of the beam with a tip mass and axial load: Voltage = 500V.....76
Table 3.3d: 3rd frequencies of the beam with a tip mass and axial load: Voltage = 1000V. ...77
Table 3.4a: 4th frequencies of the beam with a tip mass and axial load: Voltage = 0V.....78
Table 3.4b: 4th frequencies of the beam with a tip mass and axial load: Voltage = 100V. 79
Table 3.4c: 4th frequencies of the beam with a tip mass and axial load: Voltage = 500V.....80
Table 3.4d: 4th frequencies of the beam with a tip mass and axial load: Voltage = 1000V. ...81
Table 3.5a: 1st Mode frequencies (ω_1) with tip mass ratio, η = 0 83
Table 3.5b: 1st Mode frequencies (ω_1) with tip mass ratio, η = 0.1 83
Table 3.5c: 1st Mode frequencies (ω_1) with tip mass ratio, η = 1 84
Table 3.5d: 1st Mode frequencies (ω_1) with tip mass ratio, η = 5 84
Table 4.1: Lowest natural frequencies for k = +0.8 and η = 10. 105
Table 4.2a: 1st Frequency of a beam with a tip mass (b_1 = 0) and rotary inertia at 0V. 107
Table 4.2b: 1st Frequency of a beam with a tip mass (b_1 = 0) and rotary inertia at 100V. 108
Table 4.2c: 1st Frequency of a beam with a tip mass (b_1 = 0) and rotary inertia at 500V. 109
Table 4.2d: 1st Frequency of a beam with a tip mass (b_1 = 0) and rotary inertia at 1000V…110
Table 4.3a: 1st Frequency of a beam with a tip mass (b_1 = L/2) and rotary inertia at 0V.....111
Table 4.3b: 1st Frequency of a beam with a tip mass (b_1 = L/2) and rotary inertia at 100V. 112
Table 4.3c: 1st Frequency of a beam with a tip mass (b_1 = L/2) and rotary inertia at 500V..113

Table 4.3d: 1st Frequency of a beam with a tip mass ($b_1 = L/2$) and rotary inertia at 1000V. 114
Table 4.4a: 1st Frequency of a beam with a tip mass ($b_1 = L/1$) and rotary inertia at 0V. 115
Table 4.4b: 1st Frequency of a beam with a tip mass ($b_1 = L/1$) and rotary inertia at 100V. 116
Table 4.4c: 1st Frequency of a beam with a tip mass ($b_1 = L/1$) and rotary inertia at 500V..117
Table 4.4d: 1st Frequency of a beam with a tip mass ($b_1 = L/1$) and rotary inertia at 1000V. 118
Table 5.1: Fundamental frequency of a beam with a tip mass ($b_1 = 0$), axial load ratio ($k = 0$), beam thickness ($h_b = 8$mm) and top and bottom piezo ($h_1 = h_2 = 2$mm). 121
Table 5.2: Fundamental frequency of a beam with a tip mass ($b_1 > 0$), axial load ratio ($k = 0$), beam thickness ($h_b = 8$mm) and top and bottom piezo ($h_1 = h_2 = 2$mm). 122
Table 5.3: Fundamental frequencies for uncontrolled beam $^{-}_{+}V = 0$V 124
Table 5.4: Fundamental frequencies for controlled beam $^{+}_{-}V = 1000$V 124
Table 5.5: Fundamental frequencies for controlled beam $^{+}_{-}V = 2000$V 124
Table 5.6: Percentage change in fundamental frequency between uncontrolled $^{-}_{+}V = 0$V and controlled beam $^{+}_{-}V = 1000$V 125
Table 5.7: Percentage change in fundamental frequency between uncontrolled $^{-}_{+}V = 0$V and controlled beam $^{+}_{-}V = 2000$V 125
Table 5.8a: 1st frequencies for uncontrolled beam $^{-}_{+}V = 0$V 126
Table 5.8b: Reduced 1st frequencies for controlled beam $^{+}_{-}V = 1000$V 126
Table 5.8c: Reduced 1st frequencies for controlled beam $^{+}_{-}V = 2000$V 126
Table 5.9a: 2nd frequencies for uncontrolled beam $^{-}_{+}V = 0$V 126
Table 5.9b: Reduced 2nd frequencies for controlled beam $^{+}_{-}V = 1000$V 126
Table 5.9c: Reduced 2nd frequencies for controlled beam $^{+}_{-}V = 2000$V 126
Table 5.10: Difference between 1st and 2nd frequencies for uncontrolled beam $^{-}_{+}V = 0$V ...127
Table 5.11: Difference between 1st and 2nd reduced frequencies for controlled beam $^{+}_{-}V = 1000$V 127
Table 5.12: Difference between 1st and 2nd reduced frequencies for controlled beam $^{+}_{-}V = 2000$V 127

Table 5.13: Percentage change in frequency gap between uncontrolled $\bar{}_{+}V = 0\text{V}$ and controlled beam $\overset{+}{-}V = 1000\text{V}$ ……..…….128

Table 5.14: Percentage difference in frequency gap between uncontrolled $\bar{}_{+}V = 0\text{V}$ and controlled beam $\overset{+}{-}V = 2000\text{V}$ 128

Table 7.1: Tip deflection contribution of individual eigenfunctions with $\bar{}_{+}V = 0\text{V}$ for varying axial load ratios(*k*)…….……...…..……145

Table 7.2: Tip deflection contribution of individual eigenfunctions with $\bar{}_{+}V = 0\text{V}$ for varying mass ratios (η)…. 146

Table 7.3: Tip deflection contribution of individual eigenfunctions with $\overset{+}{-}V = 1000\text{V}$ for varying axial load ratios (*k)*. 146

Table 7.4: Tip deflection contribution of individual eigenfunctions with $\overset{+}{-}V = 1000\text{V}$ for varying mass ratios (η). 147

List of tables in appendix

Table A1 1: 2nd Mode frequencies (ω_2) with tip ass ratio, η = 0.....172
Table A1 2: 2nd Mode frequencies (ω_2) with tip ass ratio, η = 0.1.....172
Table A1 3: 2nd Mode frequencies (ω_2) with tip ass ratio, η = 1.....173
Table A1 4: 2nd Mode frequencies (ω_2) with tip ass ratio, η = 5.....173
Table A1 5: 2nd Mode frequencies (ω_2) with tip ass ratio, η = 10.....174
Table A2 1: 3rd Mode frequencies (ω_3) with tip ass ratio, η = 0 175
Table A2 2: 3rd Mode frequencies (ω_3) with tip ass ratio, η = 0.1 175
Table A2 3: 3rd Mode frequencies (ω_3) with tip ass ratio, η = 1 176
Table A2 4: 3rd Mode frequencies (ω_3) with tip ass ratio, η = 5 176
Table A2 5: 3rd Mode frequencies (ω_3) with tip ass ratio, η = 10 177
Table A3 1: 4th Mode frequencies (ω_4) with tip ass ratio, η = 0 178
Table A3 2: 4th Mode frequencies (ω_4) with tip ass ratio, η = 0.1 178
Table A3 3: 4th Mode frequencies (ω_4) with tip ass ratio, η = 1 179
Table A3 4: 4th Mode frequencies (ω_4) with tip ass ratio, η = 5 179
Table A3 5: 4th Mode frequencies (ω_4) with tip ass ratio, η = 10 180
Table B1 1: Natural frequencies of a beam with a concentrated tip mass (b_1 = *L/10*) including the effects rotary inertia at 0V.....181
Table B1 2: Natural frequencies of a beam with a concentrated tip mass (b_1 = *L/10*) including the effects rotary inertia at 100V.....181
Table B1 3: Natural frequencies of a beam with a concentrated tip mass (b_1 = *L/10*) including the effects rotary inertia at 500V.....182
Table B1 4: Natural frequencies of a beam with a concentrated tip mass (b_1 = *L/10*) including the effects rotary inertia at 1000V.....182
Table B2 1: Natural frequencies of a beam with a concentrated tip mass (b_1 = *L/5*) including the effects rotary inertia at 0V.....183
Table B2 2: Natural frequencies of a beam with a concentrated tip mass (b_1 = *L/5*) including the effects rotary inertia at 100V.....183
Table B2 3: Natural frequencies of a beam with a concentrated tip mass (b_1 = *L/5*) including the effects rotary inertia at 500V.....184
Table B2 4: Natural frequencies of a beam with a concentrated tip mass (b_1 = *L/5*) including the effects rotary inertia at 1000V.....184

Nomenclature

β – Axial load parameter, (1/m^2)

ε_{xx} – Strain in the longitudinal direction

ε_1 – Strain in the lower piezo due to applied voltage

ε_2 – Strain in the top piezo due to applied voltage

η – Dimension-less mass ratio = $m_T/(m_c L)$

ρ_b – Density, (kg/m^3)

ρ_1 – Density of bottom piezo, (kg/m^3)

ρ_2 – Density of top piezo, (kg/m^3)

σ_{xx} – Stress in the longitudinal direction, (N/m^2)

ω – Natural frequency, (1/s)

ω_n – nth Mode natural frequency, (1/s)

a – Frequency parameter, (1/m)

a_n – Frequency parameter for nth mode, (1/m)

A_b – Cross-sectional area of beam, (m^2)

A_1 – Cross-sectional area of bottom piezo, (m^2)

A_2 – Cross-sectional area of top piezo, (m^2)

$b(x)$ – Width of beam, (m)

C_A – Combined top and bottom piezo effects, (N)

C_{a1} – Piezo constant for bottom piezo, (N)

C_{a2} – Piezo constant for top piezo, (N)

E_c – Young's Modulus for composite/lamina, (N/m^2)

E_b – Young's Modulus for beam, (N/m^2)

E_1 – Young's Modulus for piezo at bottom surface, (N/m^2)

E_2 – Young's Modulus for piezo at top surface, (N/m^2)

$f(x,t)$ – Transverse loading of beam

h_b – Height of beam, (m)

h_1 – Height of piezo of bottom piezo, (m)

h_2 – Height of piezo of top piezo, (m)

I_b – Moment of inertia for the beam, (m^4)

I_c – Moment of inertia for the composite/lamina, (m^4)

I_1 – Moment of inertia for the piezo at bottom surface, (m^4)

I_2 – Moment of inertia for the piezo at top surface, (m^4)

k – Dimensionless axial load ratio

L – Length of beam, (m)

$\mathcal{L}$ – Distance along the beam were inertia is considered, (m)

m_c – Mass per unit length of composite, (kg/m)

m_T – Mass at tip of beam, (kg)

$M_c(x,t)$ – Moment distribution along the composite, (Nm)

M_b – Moment contribution from the beam, (Nm)

M_1 – Moment contribution from the bottom piezo, (Nm)

M_2 – Moment contribution from the top piezo , (Nm)

M_p – Piezo moment contribution due to applied voltage, (Nm)

M_{P1} – Moment contribution from the bottom piezo due to applied voltage, (Nm)

M_{P2} – Moment contribution from the top piezo due to applied voltage, (Nm)

$N(x)$ – Axial load, (N)

P_{cr} –Euler's critical buckling load, (N)

p_1, p_2 – Characteristic values, (m^{-1})

p_{1n}, p_{2n} – Characteristic values for n^{th} mode, (m^{-1})

$Q(x,t)$ – Shear force distribution along the beam, (N)

t – Time, (s)

$\mathcal{T}$ – Period of oscillation

$T(t)$ – Time function

$X(x)$ – Transverse displacement along the length of beam

x – Length-wise coordinate in the x-direction

y – Length-wise coordinate in the y-dir.

$w(x,t)$ – Transverse displacement of beam as a function of time.

V^{p1} – Applied voltage for bottom piezo, (V/mm)

V^{p2} – Applied voltage for top piezo, (V/mm)

Chapter 1 – Introduction

1.1 Background and motivation

Structural mechanics, in a broad sense, is the science concerned with the design of various structures (e.g. beams, plates, shells, strings, etc.) bearing in mind the strength, stiffness and stability. In this study we analyze the dynamic behavior of a cantilevered beam subjected to various loading conditions. Research into the analysis of flexible components is essential to successful design of robots, machines, space structures and other engineering structures. Due to the dynamically varying loads experienced by these engineering structures, there is a potential to excite the structure to a point of resonance. Design engineers should always be mindful of the natural frequencies of a structure in order to minimize large displacements and fatigue due vibrations.

In this study we study a cantilevered beam subjected to an axial load. Following that, we will add a concentrated mass at the free end, and the natural frequencies and mode shapes will be generated for different loading conditions. A concentrated mass is infinitesimal and therefore has no volume and this serves as an ideal case to establish a benchmark for investigating a more realistic case were the mass has some volume. In the latter case the center of gravity of the mass will not coincide with the free end of the beam and therefore rotary inertia will be taken into account.

This research demonstrates how we can alter the vibration characteristics of a cantilevered beam with a mass at the free end and an axial load using piezo actuators. Piezo materials can be described in the electro-mechanical context under the field of piezoelectricity. Piezoelectricity is a charge that accumulates in certain materials when they are subjected to some form of structural deformation. The other more attractive property of piezo material is that these materials will deform when subjected to an electric field. This phenomenon is called the piezoelectric effect. Piezoelectric materials can be manufactured such that the piezoelectric effect is totally reversible; meaning that, if a material is subject to an electric field it will deform and as soon as the electric field is removed it goes back to its original shape. The converse is also true, that if we subject a material to an external load, an electric field will build up and as soon as we remove the load the electric field vanishes. When an

electric field is applied to a material the strain generated can be used to change the shape of the structure. Also, when a piezo material is deformed, a voltage is generated which can be a measure for assessing the extent of the deformation. This property of piezo-electric materials can be utilized such that the materials can be employed as a sensor or an actuator.

Lead-Zirconate-Titanate(PZT) ceramics were discovered in 1954 and have been widely used depending on the desired physical effects in the system. The piezoelectric effect will manifest itself in four forms i.e. sensors, generators, actuators and transducers. Sensors and generators will produce an electric charge due to an applied external load. When used as sensors, the magnitude of the electric charge can be used to determine the extent of the deformation and when used as generators we can harvest parasitic mechanical energy due to vibration for storage to run small electric circuits. Piezo material can generate large amounts of force (in the order of 1000 Newtons) at extremely small strokes in piezo stacks, for instance; and can therefore be used as actuators. With a combination of sensing and actuating we can design transducers were both the direct piezoelectric effects and its inverse are used to our advantage.

In order to alter the dynamic characteristics of the cantilever with the end condition as mentioned above, a piezo material layer of uniform width is attached to the top and the bottom of the beam to form a composite structure. By applying and electric field to the piezo layers the strain induced at the top and bottom of the beam has an effect on the natural frequencies of vibration of the structure. In this study we will demonstrate that we can alter the natural frequency and quantify the extent of those changes.

This control strategy assists us in altering the natural frequencies of the structure using piezoelectric actuators. This is referred to as active control, whereas in passive control, the structure is built to absorb the external energy input thereby reducing the energy dissipation by the primary structure. Passive control tends to add more mass on the structure in the form of springs, shock absorbers and dampers. This is undesirable in space structures since one has to minimize the load/cargo one can carry to space. Piezoelectricity technology has also found various applications in modern technologies including the transport industry. The piezoelectric effect is being used in engineering structures to determine the health of structures and monitor performance.

Knock sensors, distance sensors and fuel injection systems employ piezo technology in current designs of land transportation. Piezo material can be used as an accelerometer to measure the seismic changes between a vibrating structure and a mass. The piezo material converts the vibrations into electric pulses which can be measured to determine the dynamics of the system. Distance sensors employ the same principle in terms of detecting back and forward movement. In fuel injection systems it has been found that piezo electric material provide much quicker response time than conventional magnetic technologies, where fuel consumption could be lowered and efficiency improved significantly. Noise reduction can also be achieved in the cabins of transportation vehicles by attenuating the external vibrations of wings, rotor blades, engine parts, etc.

In the aviation industry piezo materials are gaining prominence in various applications in structural defect monitoring, cabin noise reduction, energy harvesting, vibration control of the wings, rotors, etc. This research will demonstrate the effectiveness of piezo actuators in changing the natural frequencies of a cantilevered beam carrying a mass at the free end while being subjected to a uniform axial load. The findings of this research will be useful in application such as wings design for fixed wing planes and also provide some insights into the design of helicopter rotor blades. As the rotor blades turn on a helicopter, an axial load directed at the pivot is induced which is analogous to the model being investigated in this research. Micro Air Vehicles (MAV) and Unmanned Aerial Vehicles (UAV) which are used in military reconnaissance and surveillance have improved significantly in performance under extreme environments as a result of research conducted into the use of smart (piezo-electric) materials (Janker *et al.*, 2008). Piezo-electric technology has proven to be very effective in solving these vibration problems due its light weight, reliability, can be incorporated in the structure (as in composites) and provide structural intelligence (act as both sensors and actuator).

In this investigation we examine a cantilevered beam with a tip mass while being subjected to an axial load. To this end, we derive the equation of motion governing transverse displacements of the beam and solve the equations analytically to arrive at a closed-form solution. The method of separation of variables is used to solve the differential equations of motion to generate the eigenvalues and the eigenfunctions. By inducing a potential across the piezo actuators it is demonstrated that there is a significant change in the frequencies of the structure under certain loading conditions.

1.2 Literature review

The Euler-Bernoulli model dates back to the 18th century, when two researchers discovered that the curvature along an elastic beam subjected to bending is proportional to the bending moment at that point. Daniel Bernoulli (1700-1782) was a pioneer in developing the differential equations to describe the vibrations of a beam. Leonhard Euler (1707-1783) investigated the shape of elastic columns under various loading condition and together they proposed what is known as the Euler-Bernoulli beam theory which is sometimes called: Bernoulli-Euler beam theory, Euler beam theory, Bernoulli beam theory or the classic beam theory (Magrab, 2007).

This theory is one of the most commonly used due to its simplicity and provides reasonable engineering approximations to a multitude of problems encountered in vibration of slender beams. The Euler-Bernoulli theory tends to overestimate the frequencies compared to other theories that were later developed, i.e. the Rayleigh beam theory (1877) and Timoshenko beam theory (1922), according to Meirovitch (2001). The theories mentioned above can be summarized in Table 1.1 below where the following basic assumptions are taken into account (Hans *et al*., 1999):

1. The length of the beam is much larger than the width and thickness
2. The material conforms to Hooke's law
3. The effects underlined by Poisson are insignificant
4. The neutral and the centroidal axes coincide
5. The neutral axis remains perpendicular to the cross-sectional planes after deformation
6. The small angle assumption can be used due to small angular rotations.

The Rayleigh beam theory provides an improvement in the Euler-Bernoulli beam theory by taking into account the effects of the rotation of the cross-section and as a result, it corrects the error in overestimation encountered when using the classic beam theory (Meirovitch, 2001). The Rayleigh models have also been employed for static analysis and later extended for dynamic analysis (Kim and Jones, 1991).

Table 1.1: Four beam theories that are taken into consideration.

Beam theory	Bending moment	Lateral displacement	Shear deformation	Rotary inertia
Euler-Bernoulli	X	X	0	0
Rayleigh	X	X	0	X
Shear	X	X	X	0
Timoshenko	X	X	X	X

Piezoelectric materials were discovered in the early 1880 by Jacques Currie and Pierce Currie. These materials have found great use in the post-World War II era in applications ranging from audio speakers, gas stove igniters, electric motors, aerospace and satellite technologies, where they are utilized as actuators and sensors (Sadek *et al.*, 2009). The piezoelectric effect has been proven to be effective in shape control of engineering structures due to its ability to behave as an actuator. When used as an actuator, the applied voltage across the piezoelectric produces a strain. Kapuria and Alan (2006) studied a one dimensional hybrid piezoelectric beam to analyze the electric degrees freedom and the accuracy of the model is verified using ABAQUS as a benchmark. Further studies were performed by Weinberg (1999) to describe in detail one-dimensional analysis of piezoelectric bending actuators using energy methods.

Shudong and Siyuan (2012) extended the study of unimorphs with a rigid mass while observing the behaviour of the beam under free vibration. Piezoelectric beams can be classified into unimorphs, bimorphs and triple or multi-layer benders (Devoe and Pisano, 1997). Unimorphs are beams with a piezo layer attached to the bottom or the top of the elastic column, a bimorph has a piezo actuator on the bottom and top of the elastic column and a multi-layer can have different lay-ups. Multi-layer piezo or multi-morph beams were investigated by Lee *et al.*, (2005) to obtain the natural frequencies and maximum displacement; and the theoretical and experimental results were found to be in agreement. Emerging technologies such as micro air vehicles, micro robotics that require a large force to mass ratio and high displacements are constantly being advanced with the incorporation of piezo actuators (Wood *et al.*, 2005).

Recent applications of piezoelectricity have been focused on energy harvesters, where the piezo materials are used to scavenge energy from vibrating machines. The strain due the amplitudes of vibration are converted into an electric field and the energy from the induced

electric potential can be used to power equipment such as remote sensors, monitoring equipment, cabin equipment in vehicles and low power electric devices. The use of piezo ceramics in converting ambient vibrations into electricity is arguably one of the most studied topics in the field of vibrations (Cook-Chennault *et al.*, 2008). These materials convert an electric signal to physical motion by causing a strain in the direction of polarization of the piezoelectric material and visa-versa. The piezo is transversely isotropic and is poled in the thickness direction (*y-dir*). The poling direction determines whether the piezo actuator undergoes a contraction or expansion in the *x-z* plane perpendicular to the *y*-direction.

The strain in the piezoelectric actuators depends on the polarity of the input. The piezo actuator in a composite beam undergoes a longitudinal tensile or compressive load depending on the induced voltage. The electrical input connections can be arranged in a parallel or series configuration depending on the desired directions of the input voltage polarities, which causes longitudinal contraction or expansion strain effects on the piezo electric benders as observed by Lumentut and Howard (2011). For example, when the piezo element is not deformed and the poling direction is perpendicular to the piezo actuator length, the poling direction can be considered to be in the positive *y*-axis direction. Consequently, if a positive voltage is applied to the piezo, the polarization behaves in the same direction to the poling direction resulting in a compressive stress in the longitudinal direction of the beam and if a negative voltage is applied the polarization behaves in the opposite direction of the poling direction resulting in a tensile stress. The piezo actuator circuitry can be wired to accommodate and adjust the varying polarities.

The constitutive relations for parallel and series connections are explored in more detail by Park and Moon (2004). The application of the electric field to the actuators can be accomplished using several traditional methods, where the first method requires only a single voltage source. For a series configuration, the same voltage field is applied across the top and bottom actuator and the poling direction of the piezoelectric material is opposite. In a parallel configuration, the center electrode is grounded and a voltage is applied to the outer electrodes (Wang *et al.*, 1999). The difference in these two approaches is that for series configurations, twice the voltage is required for the same amount of strain as opposed to a parallel configuration. The voltage field can be applied independently to the top and bottom piezo actuator by using dual voltage sources, where the sources are 180^{o} out of phase with

each other. The application of the field for each actuator must take into account the poling direction of the piezoelectric layer.

The piezoelectric material inputs are interchangeable, i.e. for a voltage input the result is a strain and for a strain input, the result is a voltage. As a result of this property, if a piezoelectric material experiences a compressive strain in the longitudinal direction a voltage is produced in the poling direction of the material and a tensile strain produces a voltage in the opposite direction (Shu and Lien, 2006). The induced strain can be used to cause a desired motion on the surface of a structure and therefore manipulate the vibration characteristics of the structure (Bailey and Hubbard, 1985). This unique characteristic of these materials have been exploited in vibration control of space structures. This is attributed to the vacuum environment, where modern materials being used lack other means of damping vibrations such as air drag. PZT transducers are manufactured on a ceramic based on titanates of barium or lead zirconia.

Piezoelectric ceramics are composed of small perovskite crystals. These crystals are made up of a small tetravalent metal ion in a lattice of large divalent metal ions. The small tetravalent metal ion is normally titanium or zirconium and the large divalent metal ion is usually lead. Each of these perovskite crystals exhibits a dipole moment after processing (APC International LTD, 2013). The manufacturing of PZT ceramics involves the mixing of fine powders of the constituent metal oxides in appropriate quantities. The homogenous powder is then combined with an organic binder and the necessary shape or form of transducer is produced, for example, disks, plates and strips.

These shapes are heated for a specific time at a desired temperature causing the powder to sinter. At a temperature just below melting, the atoms in the powder diffuse and the powder material forms a dense crystalline structure (PI Ceramics GmbH, 2013). When a voltage potential is applied across the PZT ceramic material above Curie temperature the crystals remain in a simple cubic symmetry and do not exhibit a dipole moment. When the temperature drops below the Curie point, the crystals exhibit a dipole moment due to the tetragonal symmetry of the structure. The adjoining crystals form regions of local alignment called domains. The aligned domains stretch by a small amount within the micrometer range in the poling direction, resulting in a residual strain in the piezo material after the poling voltage potential is removed (APC International LTD, 2013).

The combined domains cause a net dipole moment and thus a net polarization. The application of this electric potential below the Curie point is called poling. When the electric field is removed the domains remain locked and the material is permanently polarized. The poling of the domains is what gives the material the piezoelectric effect. The rigidity of these ceramic materials makes them especially suited for converting electric energy into mechanical work and vice versa. A comprehensive review and discussion of these smart materials is available in various publications by Banks *et al*., (1996), Smith (2005) and Preumont (2011).

There are detailed models of actuation using piezoelectric transducers have that been presented by (Bailey and Hubbard, 1985; Crawley and de Luise, 1990; Drozdov and Kalamkarov, 1996). In earlier beam theory, according to the theories mentioned above, it was assumed that the cross-sectional area is symmetric so that the neutral and the centroidal axes coincide. For non-symmetric beams it is critical that the moment of inertia of the tip mass should be expressed at the end of the beam which would require a shift of the centroidal mass moment of inertia to this point (Meriam and Kraige, 2001). Since the beam is made up of different materials, the varying material stiffness's in the composite will require that the location of the modulus weight should be determined to indicate the neutral axis of the composite (Lin and Huang, 1999).

PZT piezo actuators are used widely in the vibration control and are preferred because of their mechanical power to produce a controlling force and mechanical simplicity (Sadek *et al.*, 2009). Improved actuation can be achieved more effectively with ceramic piezoelectric materials due to fast response time. Piezo material actuators are highly reliable and can withstand billions of cycles without experiencing significant deterioration in mechanical performance. Due to the high modulus of elasticity of ceramics, the stiffness of the actuators has to be taken into consideration and also the fact that the lamina may be non-symmetric. New models were explored by several engineers including Brissaud *et al.,* (2003), where one has to take into account the position of the neutral axis in the analytical model. These models were developed for non-symmetric actuation, were the piezoelectric actuator is bonded to the top or bottom surface of the beam. It is compulsory to account for the elastic and geometric parameters in the analysis of non-symmetric bimorph actuators. In addition, the analytical model for a clamped free bimorph shows that the

increase in electrode thickness causes a decrease in transverse free end displacement according to Brissaud *et al.,* (2003). The electrodes of the piezo material are bonded perfectly to the piezo actuator and column. The thickness of the electrodes is very small (in the range of 0-10μm) compared to the piezo layers and the column such that the deformations are small and the material behaviour is assumed linear. The material geometric and dissipative non-linearities are not pronounced according to Stanton *et al.,* (2010).

Many models have been developed in recent years, but most of these models placed more emphasis on the control of a single end condition. For example, Burke and Hubbard (1987) developed a simply supported model with an axial load, Pourki (1993) developed a models to investigate different piezo patch geometric shapes that could be utilized to achieve maximum vibration control, Yim and Singh (2002) developed a model for a cantilever with a linear spring at the free end and Mansou *et al*., (2010) developed models for energy harvesting from ambient structural vibrations. The following assumptions can be made with regards to the voltage induced piezo layers (Oliviera *et al.*, 2004):

1. Strain distribution is constant along the thickness
2. Strain distribution is linear through the thickness
3. Effects of the bonding layer are negligible (shear-lag is negligible)
4. The piezo actuator induces strain in the *x*-direction only

A detailed survey of sandwich structures with piezoelectric materials used for vibration control and vibration suppression is outlined in publications by Benjeddou (2000) and Trindale *et al*., (2002). The majority of these publications are devoted to the analysis of linear models used to describe the mechanical behavior of piezo composites or piezo laminated structures. Belouettar *et al*., (2008) have advanced these investigations to cover the areas of nonlinear vibrations of sandwiched beams. Dunsch and Breguet (2007) presented a unified approach using superposition of piezoelectric action on the moments and forces acting on the bender, enabling the determination of strains and stresses at different points along the piezoelectric bender. The analytical model developed in this unified approach can be utilized to systematically optimize the various parameters.

Previous work by Fridman and Abramovich (2007) focused on the behavior of a composite beam subject to external loading condition and its behavior as the applied load approaches the

critical buckling load. Their findings included the fact that with different lay-ups one could manipulate the critical buckling load for a beam. The maximum compressive load applied to the beam can be reduced to a fraction of the critical buckling load determined from the properties of the host material, e.g. aluminium. Piezoelectric composite beams undergo a compressive axial load when a voltage is applied in the poling direction. The induced axial load in the longitudinal directions will affect the critical buckling load. This buckling phenomenon is categorized into two different forms: divergence and flutter according to Naschie MSEL (1990). Divergence occurs when the natural frequency is zero and flutter occurs when two natural frequencies combine and this is referred to as Beck's problem (Rezazadeh *et al*., 2009).

There have been recent investigations performed on a cantilevered beam with tip mass. Mei (2011) used a wave-based approach to study the effects of a lumped mass on the vibration of a cantilevered beam. In this study, the effects of rotary inertia on the beam and the lumped mass were included and the vibrations of the structure were not controlled. This approach allowed for the determination of the modes of vibration and the effects of the lumped mass.

Gökdağ and Kopmaz (2005) investigated coupled bending and torsional vibration on beam with different end attachments. A concentrated tip mass was applied to beams of varying cross-sections and therefore various centroidal axes, to quantify the effects on the natural frequencies. Further studies have been conducted where the moment of inertia of the tip mass contains some of the geometric characterization of the tip mass volume in case the point mass assumption fails due to a relatively large mass (Erturk, 2012). In this study, the distance to the centroid of the extended mass is included in the analysis to determine the effects on the frequencies of vibration.

Boundary value problems governing the vibration of beams can be solved by using the method of separation of variables (Edwards Jr., 1989). This technique involves determining the eigenvalues and eigenfunctions that satisfy the differential equation of motion, the boundary condition and the initial values. These eigenfunctions provide an accurate approximation to a controlled vibration case (Kayacik *et al.*, 2008). The resultant eigenfunctions form a complete solution that resembles a set of harmonics, each with its own amplitude and unique frequency. The analysis of these harmonics can be accomplished by

means of the approach used by de Silva (2000), by defining the amplitude and frequency of each eigenfunction to determine its effect on the overall dynamics of the vibration.

Boundary control of the beam is achieved by means of distributed parameter system (DPS) where the piezo actuator functions appear as moments at the boundaries (Sadek *et al.*, 2009). Distributed parameter control with discreet actuators may lead to the truncation of the model whereas distributed parameter control with distributed parameter actuators avoids these pitfalls according to Bailey and Hubbard (1985). The direct and reverse effects of uniformly distributed piezoelectric layer modeling have been studied by Gaudenzi *et al.*, (2000) and Qiu *et al.*, (2007). The displacement feedback employed in this investigation can be used in the vibration to control the distributed parameter system and this is demonstrated in the studies by Inman (2001) and Gardonio *et al.*, (2005).

1.3 Research objectives

The aim of this investigation is to develop a model to simulate the vibration characteristics of a cantilevered piezoelectric beam with tip mass and axial load. The cantilevered beam is a composite beam with piezo actuator bonded to the top and bottom surface. The piezo actuators are utilized to modify the vibration characteristics of the system. In order to achieve the aim of controlling and analyzing the vibration characteristics of the model using piezoelectric actuators the following objectives must be met,

1. Development of the piezo-beam equations using the constitutive relations of piezoelectric materials
2. Development of the equations of motion governing the vibration of the piezo beam
3. Simulations to compare the frequencies of uncontrolled and controlled beam
4. Computation of the percentage changes in frequency for uncontrolled and controlled beam
5. Investigation of the effects of piezo layer thickness
6. Investigation of the effects of voltage input polarity for the different layers with a view to increase frequency gaps
7. Investigation of the vibration of the beam subject to initial conditions

In this dissertation we will not study the shear deformations in the beam but rotary inertia is included when a tip mass is added to the free end of the beam. The Euler- Bernoulli model is utilized initially and later augmented with the Rayleigh beam theory to include rotary inertia. To satisfy the stated objectives the research is divided into three major categories:
(1) Problem formulation, (2) Simulations and (3) Vibration under initial conditions.

Problem formulation: This stage involves the assessment of the mechanical structure subjected to vibration. An axially loaded beam with tip mass is investigated to analyze a typical engineering structure. This stage involves the modeling of the piezoelectric composite and formulating the equations of motion. It also involves formulating the stress strain relationships which are used for developing these equations. The constitutive relations for the piezo actuator and the equations of motion are combined to develop a transverse displacement function. The material properties (Young's modulus, density, etc.) of PZT and the column are of the same order of magnitude as the elastic column, and therefore the investigation accounts for the material properties of the host and the piezoelectric materials.

The presence or absence of the piezo layer at the top or bottom of the composite will be shown to have an effect on the symmetry and position of the neutral axis of the beam. The model should show that an electric field applied to the top or bottom piezo actuator will also have an effect on the frequencies of vibration. The piezoelectric beam model is developed such that the input voltage can be varied in an individual layer without affecting the input voltage in the other layer. The piezo actuators are powered by two voltage sources and allows for the ability to switch the polarity of the source. In this study, the model developed would be robust enough to analyze both symmetric and non-symmetric lamina.

Simulations: At this stage we develop a displacement feedback control system to compare the oscillations of a beam without an electric field to a beam with an induced electric field. In the investigation below, the study will show that by using piezo-electric actuators, it is possible to increase or decrease the natural frequencies of vibration. The solution is presented in the form of an eigenfunction series expansion.

Vibration under initial conditions: The infinite series of eigenfunctions is reduced to a finite set and the level of accuracy required to satisfy the initial conditions is established. The initial conditions involve an initial displacement and velocity for the tip of the piezoelectric

beam. The contribution of the various eigenfunctions to the total solution is also demonstrated. The frequencies of oscillation for uncontrolled and controlled beams will be compared to quantify the level of efficacy in the reduction of the vibrations.

Chapter 2 – Piezoelectric composite beam

2.1 Derivation of the governing equations for the beam and the piezo layers

2.1.1 Moment-curvature relation for beam

Piezo materials have a special property that allows the conversion of electric voltage into a mechanical strain, and vice-versa. These materials can be incorporated into mechanical structures to form composite structures. A voltage input induces a strain which can be used to change the dynamic characteristic behaviour of the structure. The effect of piezo-electricity on the natural frequencies of a cantilevered beam made from an elastic column and piezo actuators can be modeled as a lamina or composite beam. In Figure 2.1 below, a uniform beam is vibrating freely under constant axial load $N(x)$. The left-end of the beam is clamped to a support, while the right-hand side is allowed to move freely in the *y-dir*. Let $w(x,t)$ be the transverse displacement of the beam anywhere along the *x-dir*. at any time.

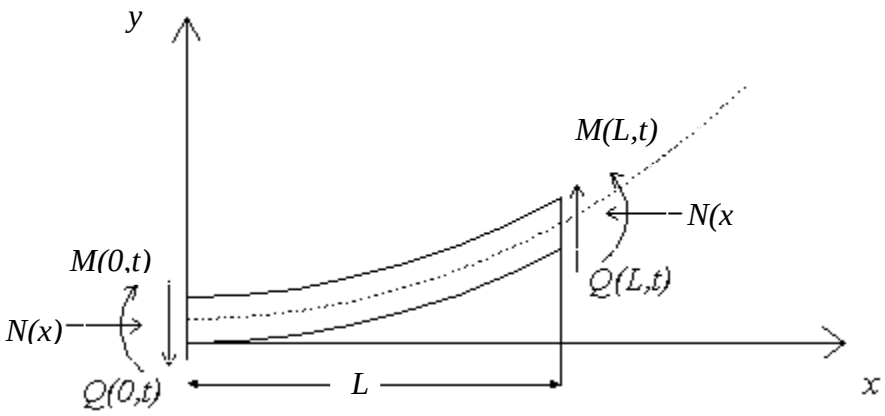

Figure 2.1: Uniform beam under free vibration

The Euler-Bernoulli theory can be applied to the deformation of the beam, where the fiber along the neutral axis of the beam experiences zero strain. The fibers above the neutral axis experience a contraction, whilst the fibers at the bottom of the neutral axis experience an extension. According to this theory: (1) the neutral axis remains un-deformed, (2) plane sections normal to the neutral axis remain normal and plane to the neutral axis when a load is

applied, and (3) the transverse normal's experience zero strain along the normal direction. When the beam is deflected, a fiber can be isolated to form a basis for the discussion as shown in the Figure 2.2 below.

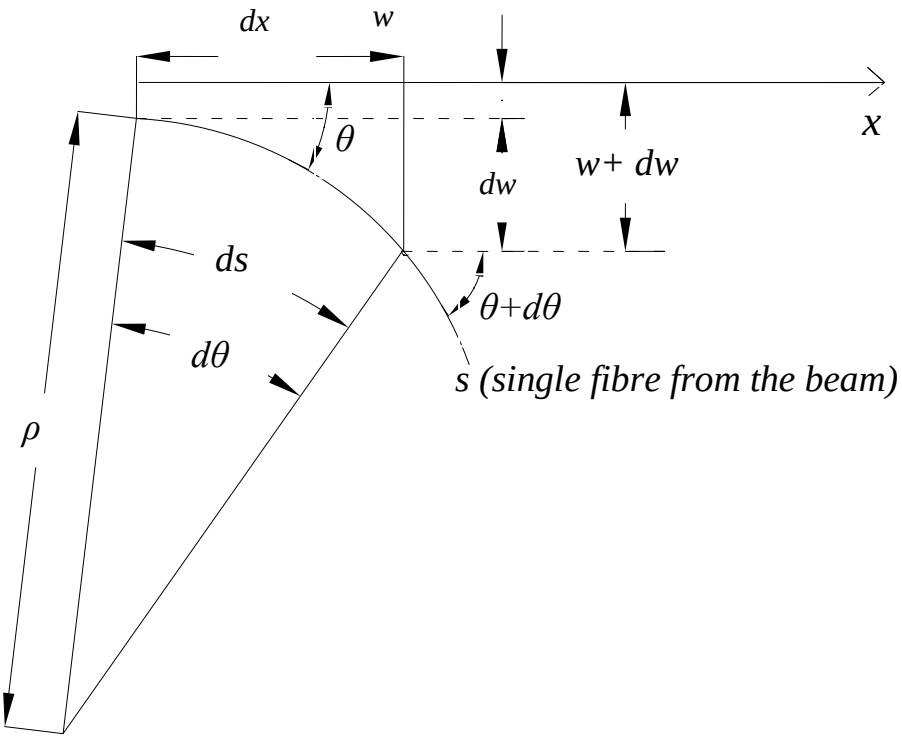

Figure 2.2: Single deformed fiber(s) along the length of the beam

We can deduce from Figure 2.2 that the following relation holds.

$$\frac{d\theta}{ds} = \frac{1}{\rho} \tag{2.1}$$

furthermore,

$$\varepsilon_x(y) = -y \cdot \frac{d\theta}{ds} = -(y/\rho) \tag{2.2}$$

and,

$$\sigma_x(y) = E_c \cdot \varepsilon_x = -y \cdot (E_c/\rho) \tag{2.3}$$

The resultant bending moment due to σ_x must equal the integral of the bending moment across the surface area and thus:

$$M_c = -\int_A y \cdot [\sigma_x dA] \tag{2.4a}$$

and,

$$M_c = -(E_c / \rho) \cdot \int_A y^2 dA \tag{2.4b}$$

also,

$$I_c = \int_A y^2 dA \tag{2.4c}$$

therefore,

$$M_c = -E_c I_c \cdot \frac{1}{\rho} \qquad \text{and,} \quad \frac{1}{\rho} = \frac{d\theta}{ds} \tag{2.4d}$$

It can be shown that the following relation holds:

$$\frac{d\theta}{ds} = \frac{\dfrac{d^2 w}{dx^2}}{\left[1 + \left(\dfrac{dw}{dx}\right)^2\right]^{\frac{3}{2}}} \tag{2.5}$$

when $\left(\dfrac{dw}{dx}\right)^2 << 1$ the slope and the deflection are small it leads to the following moment curvature relation:

$$\frac{d^2 w}{dx^2} = -\frac{M_c(x)}{E_c I_c} \tag{2.6}$$

$$M_c(x) = M_b + M_1 + M_2 + M_p \tag{2.7}$$

where, $M_c(x)$ is the combined moment contribution from the elastic beam, the piezo material and the applied electric potential on the piezo. When the beam moves from its natural position; internal forces, shear forces and moments acting on each infinitesimal element of the beam are induced, as shown in Figure 2.3. The element has a length *dx* along the beam in the *x*-direction.

2.1.2 Governing equations for composite beam

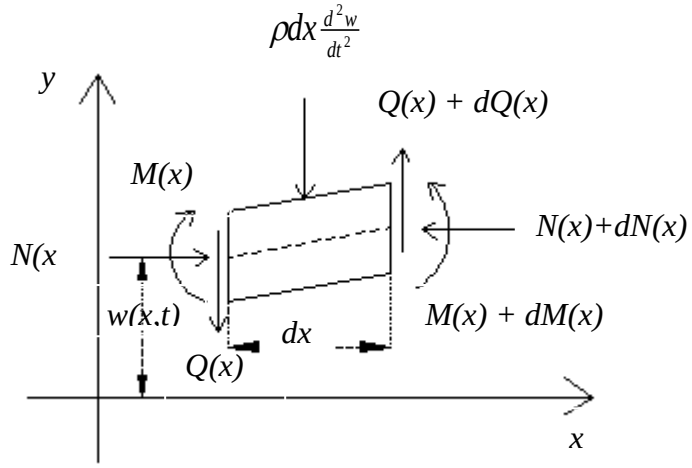

Figure 2.3: Internal shear forces, moments and external forces on the beam

Taking the sum of the forces and moments in both co-ordinates (x and y) we derive the equilibrium conditions for the element in a form of these equations:

$$\frac{\partial Q(x,t)}{\partial x} - \rho \frac{\partial^2 w(x,t)}{\partial t^2} = 0 \tag{2.8}$$

$$\frac{\partial M(x,t)}{\partial x} + N(x)\frac{\partial w(x,t)}{\partial x} + Q(x,t) = 0 \tag{2.9}$$

The piezo-actuator layer is bonded to the top and bottom of the beam. The strain induced on the piezo, through a voltage input signal, provides for active control of the vibrations. Looking at the cross-section of the beam, we derive the relationship between stress and strain. The stresses in the y and z direction can be regarded small, and therefore negligible. Figure 2.4 shows a cross-sectional area of the beam with the stress contribution from the different materials.

2.1.3 Constitutive equations for piezo layers

The beam can be treated as a lamina with the piezo-electric material inducing a strain on the top and bottom surface of the beam. The equation of state for the induced stress-strain for a piezo material (of the *D-form*) can be written as (Smith, 2005),

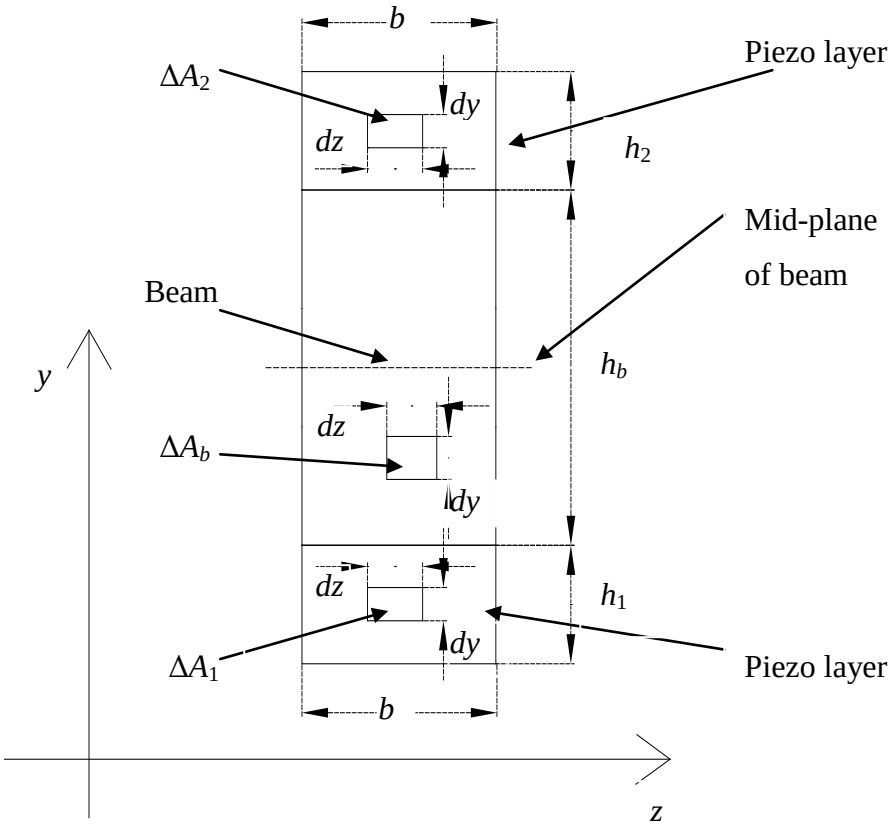

Figure 2.4: Cross-sectional area of beam

$$\varepsilon_p = S_{pq}^{E}\sigma_q + d_{ip}E_i \tag{2.10}$$

and,

$$D_i = d_{iq}\sigma_q + \varepsilon_{ik}^{\sigma}E_k \tag{2.11}$$

where, p,q = 1……6 and i,k = 1,2,3 and S_{pq}^{E}, d_{ip} and $\varepsilon_{ik}^{\sigma}$ represent the elastic compliance, piezoelectric strain/charge coefficient and the electric permittivity, respectively. D_i and E_k represent the electric displacement and the electric field, respectively. For an unconstrained piezo actuator the strain can be written as:

$$\varepsilon_{xx}^{p} = d_{31}E_3 = d_{31}\frac{V^{p}}{h_p} \tag{2.12}$$

where, d_{31} is the transformed piezoelectricity constant, h_p is the piezo thickness and V^p is the applied voltage. The stress strain relationship in each layer of the lamina can be expressed as follows:

$$\sigma_{xx} = E_b\varepsilon_{xx} \qquad \text{Beam layer} \tag{2.13a}$$

$$\sigma_{xx} = E_1(\varepsilon_{xx} - \varepsilon_p) \qquad \text{Bottom piezo layer} \tag{2.13b}$$

$$\sigma_{xx} = E_2(\varepsilon_{xx} - \varepsilon_p) \qquad \text{Top piezo layer} \tag{2.13c}$$

ε_{xx} is the strain in the x-direction only; E_b , E_1 and E_2 are the Young's Modulus for the beam and the piezo layers respectively and ε_p the strain due to the applied voltage. For a beam whose cross-section dimensions are small relative to the span, the stresses and the strains are very small in the y and z directions and therefore negligible, $\varepsilon_{yy} = \varepsilon_{zz} = 0$. However, this assumption would be unjustified if there was a uniformly distributed load acting at the top of the beam. The lateral and transverse displacements are used to define the strain in the beam.

$$u_x = u_0(x) + y\frac{dw(x)}{dx} \tag{2.14}$$

and,

$$u_y = w(x) \tag{2.15}$$

also,

$$\varepsilon_{xx} = \frac{du_0(x)}{dx} + y\frac{dw^2(x)}{dx^2} \tag{2.16}$$

therefore,

$$\sigma_{xx} = E_2[u'_0(x) + yw''(x) - \varepsilon_2] \qquad +\frac{h_b}{2} \le y \le \frac{h_b}{2} + h_2 \tag{2.17a}$$

$$\sigma_{xx} = E_b[u'_0(x) + yw''(x)] \qquad -\frac{h_b}{2} \le y \le +\frac{h_b}{2} \tag{2.17b}$$

$$\sigma_{xx} = E_1[u'_0(x) + yw''(x) - \varepsilon_1] \qquad -\frac{h_b}{2} \le y \le -\frac{h_b}{2} - h_1 \tag{2.17c}$$

where, $u'_0(x)$ is the initial value of the strain and (′) indicates the derivative with respect to x, $\partial/\partial x$ The initial strain in the column is caused by the axial force. The piezo is perfectly bonded to the beam such that the longitudinal strain in the lamina varies linearly from the center of the beam to the top and bottom surfaces. The stress at the interface between the different materials exhibit discontinuities and the stress vary linearly through the thickness of each particular layer based on the stiffness properties of each layer. By integrating the stress throughout the cross-sectional area, A_b, A_1 and A_2 in Figure 2.4, the resultant in-plane normal force (F_L) in the *x-dir* can be calculated using equation 2.18 and 2.20 below:

$$F_L = \int_A \sigma_{xx} dA \tag{2.18}$$

The beam can be modeled as a composite made out of three different materials; two piezo actuators and an elastic beam, see Figure 2.4. The stress resultant is sum of the stresses in each layer of the composite. The maximum stress occurs at the outer most surface in each layer and the stresses tend to zero as we approach the neutral axis of the composite. The fiber along the neutral axis experiences zero strain in the case of zero axial force. For a symmetric composite the neutral axis is half-way along the height of the beam.

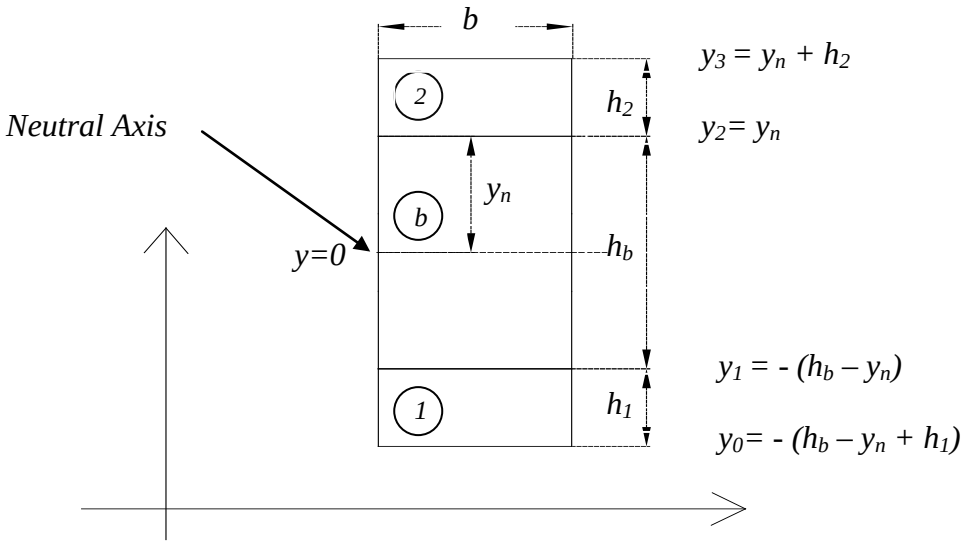

Figure 2.5: Cross-sectional area of beam indicating the dimensions of the composite

If the top layer and bottom layer of the piezo actuators are of different thickness, material and dissimilar induced voltage, the composite becomes anti-symmetric and it is necessary to locate position of the neutral axis (y_n) from the interface between the top piezo layer and the elastic column as indicated in Figure 2.5. To determine the neutral axis the longitudinal forces in the composite must be equal to zero therefore from equations 2.17 and 2.18 and Figure 2.5:

$$F_L = \int_{A_1} \sigma_{xx} dA + \int_{A_b} \sigma_{xx} dA + \int_{A_2} \sigma_{xx} dA \tag{2.19}$$

$$F_L = b(x)\int_{y_0}^{y_1} E_1[u'_0(x) + y\kappa - \varepsilon_1]dy + b(x)\int_{y_1}^{y_2} E_b[u'_0(x) + y\kappa]dy + b(x)\int_{y_2}^{y_3} E_2[u'_0(x) + y\kappa - \varepsilon_2]dy \tag{2.20a}$$

where,

$$\kappa = \frac{d^2w}{dx^2}, \qquad u'_0(x) = \frac{du_0}{dx} \text{ and } dA = b(x)dy \tag{2.20a}$$

This investigation focuses on a beam with an applied constant axial force along the beam were the lateral deflections are small and linear elastic behavior is assumed, the longitudinal forces are either zero or constant in the case of bending, axial compression and extension in free vibration (Gere *et al.*, 2009). It follows that the initial longitudinal deflection does not change along the beam and the second derivative of the longitudinal force along the beam can be ignored. Therefore equation 2.18 simplifies to the following:

$$\sum_{k=1}^{k=n} \iint (\sigma_{xx} dA)_k = 0 \tag{2.21}$$

where,

$$(\sigma_{xx})_k = E_k(y)_k \kappa \tag{2.22}$$

and,

$$dA_k = b(x)dy \tag{2.23}$$

therefore,

$$\sum_{k=1}^{k=n} E_k b(x)\kappa \int_{y_{k-1}}^{y_k} y dy = 0 \tag{2.24}$$

For a constant width ($b(x)$ = constant) and curvature for all three materials:

$$\sum_{k=1}^{k=n} E_k \left(y_k^2 - y_{k-1}^2\right) = 0 \tag{2.25}$$

Using Figure 2.5 the above summation can be used to solve and determine y_n, which is the distance from the interface of the top piezo and the elastic column to the neutral axis.

$$E_1(y_1^2 - y_0^2) + E_b(y_2^2 - y_1^2) + E_2(y_3^2 - y_2^2) = 0 \tag{2.26}$$

Substituting the values for $y_{0...3}$ into equation 2.26 the position of the *neutral axis* can be determined from the following relationship:

$$y_n = \frac{E_1 h_1^2 - E_2 h_2^2 + E_b h_b^2 + 2E_1 h_b h_1}{2\left(E_1 h_1 + E_b h_b + E_2 h_2\right)} \tag{2.27a}$$

For a symmetric beam, with $h_1 = h_2 = h$ and $E_1 = E_2$, equation 2.27a reduces to $y_n = -h_b/2$, which is the mid-plane of the composite beam. As $E_1 \rightarrow 0$, the bottom piezo layer can be neglected and the neutral axis is located at:

$$y_n = \frac{-E_2 h_2^2 + E_b h_b^2}{2\left(E_2 h_2 + E_b h_b\right)} \tag{2.27b}$$

Further, by letting $E_b \rightarrow 0$, the elastic column can be neglected and only the top piezo layer is taken into account making $y_n = -h_2/2$, which corresponds to the results obtained by Smith, (2005). In equation 2.27a, when $E_2 \rightarrow 0$ the top piezo layer is neglected and the neutral axis is expressed as:

$$y_n = \frac{+E_b h_b^2 + E_1 h_1^2 + 2E_1 h_1 h_b}{2\left(E_1 h_1 + E_b h_b\right)} \tag{2.27c}$$

Further setting $E_b \rightarrow 0$ in the above equation the result is $y_n = +(h_1/2 + h_{b)}$, which corresponds to the results obtained by (Gere *et al.*, 2008). It is therefore correct to deduce that when the Young's modulus for the beam tends to zero the neutral axis of the composite is at the midpoint of the distance between the two piezo layers, when the Young's modulus of the piezo actuators remain large and equal ($E_1 = E_2 >> 0$).

The bending moment (M_Z) in the *z*-direction includes contributions from the beam and the piezo layers combined and therefore the bending moment can be calculated by summing the contributions across the cross-sectional area, i.e.

$$M_Z = b(x)\int_A \sigma_{xx} y dy \tag{2.28}$$

The internal strain in the different layers in the composite and the position of the neutral plain will assist in the definition of the bending characteristics of the beam, when the beam is in a state of equilibrium. From the stress in the different layers, the moments and the longitudinal forces across the cross-section of the composite can be calculated by integrating the stresses over the areas covered by the beam and the piezo actuators. Equation 2.28 defines the moments experienced by the composite, where $b(x)$ is the width of the composite along the *x*-direction, σ_{xx} is the stress across the cross-section and y is the position from the neutral axis along the transverse direction. After inserting equation 2.26 into equation 2.28, the moment across the composite can be expanded and represented in equation 2.29 as the sum across the three different cross sections.

$$\int_{-(h_b+h_1)}^{+h_2} E_c (y-y_n)^2 dy = \int_{-(h_b+h_1)}^{-h_b} E_1 (y-y_n)^2 dy + \int_{-h_b}^{0} E_b (y-y_n)^2 dy + \int_{0}^{+h_2} E_2 (y-y_n)^2 dy \tag{2.29}$$

The left side of equation 2.29 is the combined moment of the composites beam, while the right hand side represents the contributions from the different layers, i.e. the beam and the top and bottom piezo actuator. The neutral axis (y_n) is defined in equation 2.27 and together with equation 2.30 the combined Young's modulus (E_c) for the composite beam can be resolved.

$$\left[\frac{1}{3}E_c\left(y-y_n\right)^3\right]_{-(h_b+h_1)}^{+h_2}=\left[\frac{1}{3}E_1\left(y-y_n\right)^3\right]_{-(h_b+h_1)}^{-h_b}+\left[\frac{1}{3}E_b\left(y-y_n\right)^3\right]_{-h_b}^{0}+\left[\frac{1}{3}E_2\left(y-y_n\right)^3\right]_{0}^{+h_2} \quad (2.30)$$

After inserting the integration limits and solving equation 2.30 for E_c the results are the following:

$$E_c=\frac{E_1\left[-\left(h_b+y_n\right)^3+\left(h_b+h_1+y_n\right)^3\right]+E_b\left[\left(h_b+y_n\right)^3-y_n^3\right]+E_2\left[\left(h_2-y_n\right)^3+y_n^3\right]}{\left(h_2-y_n\right)^3-\left(-h_b-h_1-y_n\right)^3} \quad (2.31)$$

E_c is the combined stiffness of the elastic column and the piezo layers. The longitudinal force in the composite relationship states that:

$$F_L=b(x)\int_{-(h_b+h_1)}^{+h_2}E_c\kappa\left(y-y_n\right)dy \quad (2.32)$$

Were F_L is the longitudinal force and κ is the curvature. Thus the moment-curvature relation for the composite beam can be expressed as:

$$M_c=-\int_{-(h_b+h_1)}^{+h_2}E_c b(x)\frac{\partial^2 w}{\partial x^2}\left(y-y_n\right)^2 dy \quad (2.33a)$$

$$=-E_c I_c(x)\frac{\partial^2 w}{\partial x^2} \quad (2.33b)$$

Therefore the combined moment of inertia for the composite beam can be expressed in equation 2.34 where dA is an infinitesimal area of the composite shown in Figure 2.4.

$$I_c=\int_A y^2 dA \quad (2.34)$$

Using equations 2.28, 2.33 and 2.34, we derive the combined moment of inertia of the composite beam, which includes all the material properties associated with each layer that

would have an effect on the bending of the composite, i.e. the dimensions and stiffness of the different layers in the structure.

$$I_c(x) = \frac{b(x)}{3}\left[(h_2 - y_n)^3 - (-h_b - h_1 - y_n)^3\right] \tag{2.35}$$

In the limit as $E_2 \rightarrow 0$ and $E_1 \rightarrow 0$, $h_2 \rightarrow 0$ and $h_1 \rightarrow 0$, the bottom and top piezo actuators have no effect because the stiffness and the geometric proportions become non-existent (zero).

$$I_c(x) = \frac{b(x)}{3}\left[(-y_n)^3 + (h_b + y_n)^3\right] \tag{2.36}$$

This leads to a reduction of equation 2.36 to equation 2.37 which is the moment of inertia for a symmetrical cross-section beam. This is the moment of inertia for rectangular cross-section beam.

$$I_c(x) = \frac{b(x)h_b^{\,3}}{12} \tag{2.37}$$

The moment contribution by the piezo layer can be expressed in equation 2.38 below, where M_p is the moment due to the applied electric potential. E_c is the effective Young's modulus due to the elastic beam and top and bottom piezo material.

$$M_z(x,t) = u'_0(x)\int_{A_B} E_c y dy + \kappa \int_{A_B} E_c y^2 dy - M_p(x,t) \tag{2.38a}$$

$$\kappa = 1/\rho_c \quad , \quad \text{and} \quad M_p(x,t) = M_{P1}(x,t) + M_{P2}(x,t) \tag{2.38a}$$

where ρ_c is the radius of curvature for the composite, M_{P1} and M_{P2} are voltage induced moments in the piezo layers.

From Figure 2.5, the neutral axis is calculated to be at a distance (y_n) from the interface between the top piezo actuator and the elastic beam. The moment induced by both actuators

is calculated using the interface between the top layer and the beam as the pivot. And thus the moment due to bottom piezo becomes:

$$M_{P1}(x,t) = -\int_{A_p} E_1 \varepsilon_1 y dy \tag{2.39a}$$

$$= -E_1 \int_{-(h_b+h_1)}^{-(h_b)} d_{31} \frac{V^p}{h_1} b(x)\left(y - \left(-y_n\right)\right) dy$$

$$= -E_1 d_{31} \frac{V^{P1}}{h_1} b(x)\left[\frac{1}{2}\left(y - \left(-y_n\right)\right)^2\right]_{-(h_b+h_1)}^{-(h_b)}$$

$$= -\frac{1}{2} E_1 d_{31} V^{P1} b(x)\left(h_1 + 2h_b - 2y_n\right)$$

$$= -\frac{1}{2} d_{31} V^{P1} b(x) E_1 \left(\frac{E_2 h_2\left(h_1 + h_2 + 2h_b\right) + E_b h_b\left(h_1 + h_b\right)}{\left(E_1 h_1 + E_b h_b + E_2 h_2\right)}\right) \tag{2.39b}$$

where, $V^{P1} = g_{d1} w(L,t)$ and g_{d1} is the control voltage gain used to control the strain in the piezo actuator. As $h_2 \to 0$, the top piezo layer will have no structural effect on the lamina and therefore it will not exert a moment on the beam and its control effectiveness is insignificant. When the reference point for the neutral axis is at the top surface of the beam and $h_2 = 0$, equation 2.39b reduces to the results obtained by Bailey *et al.*, (1985) and Kalamkarov *et al.*, (1996).

Let,
$$C_{a1} = \frac{1}{2} d_{31} b(x) E_1 \left(\frac{E_2 h_2\left(h_1 + h_2 + 2h_b\right) + E_b h_b\left(h_1 + h_b\right)}{\left(E_1 h_1 + E_b h_b + E_2 h_2\right)}\right) g_{d1} \tag{2.40}$$

where C_{a1} is the piezo constant on the bottom. From equations 2.39b and 2.40 it follows that:

$$M_{P1}(x,t) = C_{a1} w(L,t) \tag{2.41}$$

Moving the reference point or pivot from the interface between the top piezo and the elastic column and locating it at the center of the beam, C_{a1} then becomes,

$$C_{a1} = \frac{1}{2} d_{31} b(x) E_1 \left(\frac{-E_2 h_2 (h_1 + h_2 + 2h_b) - E_b h_b (h_1 + h_b)}{(E_1 h_1 + E_b h_b + E_2 h_2)} \right) g_{d1} \tag{2.42}$$

The moment due to the top piezo is:

$$M_{P2}(x,t) = -\int_{A_p} E_2 \varepsilon_2 y dy \tag{2.43a}$$

$$= -E_2 \int_0^{+h_2} d_{31} \frac{V^{P2}}{h_2} b(x)(y - y_n) dy$$

$$= -E_2 d_{31} \frac{V^{P2}}{h_2} b(x) \left[\frac{1}{2} (y - y_n)^2 \right]_0^{+h_2}$$

$$= -E_2 d_{31} \frac{V^{P2}}{h_2} b(x) \left(\frac{h_2}{2} (h_2 - 2y_n \right)$$

$$= \frac{1}{2} E_2 d_{31} V^{P2} b(x)(h_2 - 2y_n)$$

$$= \frac{1}{2} d_{31} V^{P2} b(x) E_2 \left(h_2 - \frac{E_1 h_1 (h_1 + 2h_b) - E_2 h_2^2 + E_b h_b^2}{(E_1 h_1 + E_b h_b + E_2 h_2)} \right) \tag{2.43b}$$

where, $V^{P2} = g_{d2} w(L,t)$ and g_{d2} is the control voltage gain.

Let,
$$C_{a2} = \frac{1}{2} d_{31} b(x) E_2 \left(h_2 - \frac{E_1 h_1 (h_1 + 2h_b) - E_2 h_2^2 + E_b h_b^2}{(E_1 h_1 + E_b h_b + E_2 h_2)} \right) g_{d2} \tag{2.44}$$

where C_{a2} is the piezo constant on the top. From equations 2.43b and 2.44 it follows that:

$$M_{P2}(x,t) = C_{a2} w(L,t) \tag{2.45}$$

As $h_1 \to 0$, the bottom piezo layer has no structural effect on the lamina and therefore it will not exert a moment on the beam and its control effectiveness is insignificant. If we take the

reference point for the neutral axis to be at the top surface of the beam, between the top piezo layer and the elastic column, equation 2.44 reduces to the results obtained by Smith (2005).

Again, if the reference point or pivot is shifted from the interface between the top piezo and the beam and located at the center of the beam, C_{a2} then becomes:

$$C_{a2} = \frac{1}{2} d_{31} b(x) E_2 \left(\frac{E_1 h_1 \left(h_1 + h_2 + 2h_b \right) + E_b h_b \left(h_2 + h_b \right)}{\left(E_1 h_1 + E_b h_b + E_2 h_2 \right)} \right) g_{d2} \tag{2.46}$$

From comparing equations 2.42 and 2.46 it is noted that when the material properties and geometric proportions are identical for the bottom and top piezo the moments are equal in magnitude for a similar voltage input. Then the combined piezo moment effect due to the input voltage on the top and bottom layers and the tip displacement can be written as:

$$M_p(x,t) = C_{A0} w(L,t) \tag{2.47}$$

where,

$$C_{A0}(x,t) = C_{a1}(L,t) + C_{a2}(L,t) \tag{2.48}$$

And the combined moment for the whole beam can be written as:

$$M_c(x,t) = E_c I_c(x) \frac{\partial^2 w(x,t)}{\partial x^2} - M_p(x,t) \tag{2.49}$$

Inserting equation 2.49 into equation 2.9, the shearing force *Q(x,t)* can be expressed in terms of the displacement variables, *w*(*x*,*t*).

$$Q(x,t) = -\left[\frac{\partial}{\partial x} \left(E_c I_c(x) \frac{\partial^2 w(x,t)}{\partial x^2} \right) + N(x) \frac{\partial w(x,t)}{\partial x} + \frac{\partial M_p(x,t)}{\partial x} \right] \tag{2.50}$$

From equations 2.8 and 2.50 the equation of motion can be expressed in terms of the displacement variables as,

$$\frac{\partial^2}{\partial x^2}\left(E_c I_c(x)\frac{\partial^2 w}{\partial^2 x}\right)+\frac{\partial}{\partial x}\left(N(x)\frac{\partial w}{\partial x}\right)+\frac{\partial^2 M_P(x,t)}{\partial x^2}+\rho A(x)\frac{\partial^2 w}{\partial t^2}=f(x,t) \quad (2.51)$$

Where $f(x,t)$ is the external transverse load per unit length. This load includes conservative and non-conservative loads, such as gravity and viscous damping. Equation 2.51 represents the partial differential equation describing the motion of the beam at any point along the beam at any time, and equations 2.49 and 2.50 represent the moment and shear distribution along the beam, respectively.

2.2 Solution of the governing equations by separation of variables

In this study the width of the piezo layers are kept constant along the length of the beam to facilitate a uniformly distributed parameter approach, where the applied voltage is kept constant along the length of beam. A piezo layer is attached to the bottom and top of an elastic beam and therefore the piezo term, $M_p(x,t)$, appears in the differential equation of motion (equation 2.51). This piezo term is a constant along the beam and therefore the second derivative for the piezo term is zero and does not appear in equation 2.52 below. In free vibration the external transverse load is set to zero, $f(x,t) = 0$, in equation 2.51 and the axial force, $N(x)$, is kept the constant along the length of the beam. The beam cross-section is kept constant and therefore the height of both piezo layers and elastic beam remain constant along the composite. This problem can be solved by obtaining the eigenvalues and taking the sum of the eigenfunctions. After the above modifications, the equation of motion 2.51 reduces to equation 2.52.

$$E_c I_c \frac{\partial^4 w}{\partial x^4} + N\frac{\partial^2 w}{\partial x^2} + \rho A\frac{\partial^2 w}{\partial t^2} = 0 \quad (2.52)$$

For this partial differential equation a separable solution of the form below is assumed.

$$w(x,t) = \sum_{n=1}^{\infty} X_n(x)T_n(t) \quad (2.53)$$

Where X is a function of x only, T is function of t only and n is the n^{th} mode of vibration.

Inserting equation 2.53 into equation 2.52; and taking the cross-section of the beam and the axial load to be constant along the length of the beam; we arrive at the following equation in the spatial domain and in the time domain.

$$E_c I_c X_n''''(x) T_n(t) + N X_n''(x) T_n(t) + \rho A X_n(x) \ddot{T}_n(t) = 0 \tag{2.54}$$

This equation becomes equation 2.55 after rearrangement, such the left hand side only contains the terms in the spatial variable, $X(x)$; and the right hand side contains the terms in the time domain, $T(t)$.

$$\frac{E_c I_c X_n''''(x) + N X_n''(x)}{X_n(x)} = -\frac{m_c \ddot{T}_n(t)}{T_n(t)} \tag{2.55}$$

where, $m_c = \rho A$ (mass/unit length for the composite column) and $\rho A = \rho_1 A_1 + \rho_b A_b + \rho_2 A_2$. For the above relation to be true, it follows that the right-hand-side and the left-hand-side of equation 2.55 must be equal to a constant. A constant λ_n, is chosen such that both the RHS and the LHS of equation 2.55 are equal to the constant (λ_n) and two differential equations can be derived and these are shown in equations 2.56 and 2.57. By definition, $\lambda_n = \rho A \omega_n^2$.

$$X_n''''(x) + \frac{N}{E_c I_c} X_n''(x) - \frac{\lambda_n}{E_c I_c} X_n(x) = 0 \tag{2.56}$$

$$m_c \ddot{T}_n(t) + \lambda_n T_n(t) = 0 \tag{2.57}$$

where (') and (.) are the derivatives with respect to space and time respectively, ω_n is the natural frequency for the n^{th} mode of vibration. Equations 2.58a and 2.58b below demonstrate the relation between the natural frequency and the other parameters of the system.

$$\beta^2 = \frac{N}{E_c I_c}; \qquad a_n^4 = \frac{m_c \omega_n^2}{E_c I_c} \tag{2.58a}$$

$$\frac{\lambda_n}{m_c} = \omega_n^2; \qquad N = k \cdot P_{cr} \tag{2.58b}$$

where, β^2 is the axial load parameter, a_n^4 is the frequency parameter, N is the axial load, P_{cr} is the critical buckling of a beam under compressive axial loading and k is a proportionality constant (k = -10.0……+0.8). A negative proportionality constant indicates a tensile load and a positive constant indicates a compressive load.

$$P_{cr} = \frac{\pi^2 E_c I_c}{4L^2} \tag{2.59}$$

After separation of variables, the solution can be expressed in the space and time domain, independently. The equations are:

$$X_n''''(x) + \beta^2 X_n''(x) - a_n{}^4 X_n(x) = 0 \tag{2.60}$$

and,

$$\ddot{T}_n(t) + \omega_n^2 T_n(t) = 0 \tag{2.61}$$

The general solution to equation 2.60 and 2.61 are:

$$X_n(x) = A_n \sin p_{2n}x + B_n \cos p_{2n}x + C_n \sinh p_{1n}x + D_n \cosh p_{1n}x \tag{2.62}$$

and,

$$T_n(t) = E_n \sin \omega_n t + F_n \cos \omega_n t \tag{2.63}$$

where,

$$p_{1n} = \sqrt{\frac{-\beta^2 + \sqrt{\left(\beta^2\right)^2 + 4a_n^4}}{2}} \quad \text{and} \quad p_{2n} = \sqrt{\frac{\beta^2 + \sqrt{\left(-\beta^2\right)^2 + 4a_n^4}}{2}}$$

where A_n, B_n, C_n, and D_n, are constants to be determined from the boundary conditions; and E_n and F_n from the initial conditions. The characteristic equation can be used to determine the natural frequencies from the stipulated boundary conditions, which are clamped-free in this case.

2.3 Boundary conditions

Discreet elements can be attached to the ends of the beam and they will have an effect on the vibration profile of the beam. For the clamped end of the beam the displacement and slope are zero, thus:

$$w(0,t) = 0 \quad \text{and} \quad \frac{w(0,t)}{\partial x} = 0 \tag{2.64}$$

At the free end, the moment and shear force are non-zero because of the piezo and concentrated mass and thus an additional moment and a force term are added, implying:

$$E_c I_c \frac{\partial^2 w(L,t)}{\partial x^2} - M_p(L,t) = 0 \tag{2.65}$$

and,

$$m_T \frac{\partial^2 w(L,t)}{\partial t^2} - E_c I_c \frac{\partial^3 w(L,t)}{\partial x^3} - N \frac{\partial w(L,t)}{\partial x} = 0 \tag{2.66}$$

where, the shear boundary condition is time dependent. In order to separate the time and space dependency from the boundary conditions we assume a separable solution of this form:

$$w(L,t) = \sum_{n=1}^{\infty} X_n(L) T_n(t) \tag{2.67}$$

where $w(L,t)$ is the tip displacement, ω_n is the natural frequency of vibration and $X_n(L)$ is the spatial solution of the vibration of the beam evaluated at $x = L$. Substituting equation 2.67 into equation 2.65 the following moment at the tip of the beam is derived:

$$E_c I_c \frac{\partial^2 X_n(L) T_n(t)}{\partial x^2} - C_{A0} X_n(L) T_n(t) = 0 \tag{2.68}$$

From equation 2.42, 2.44 and 2.47, it follows that:

$$E_c I_c \frac{\partial^2 X_n(L)}{\partial x^2} - (C_{a1} + C_{a2}) X_n(L) = 0 \tag{2.69}$$

and the combined moment experienced by the beam is:

$$\frac{\partial^2 X_n(L)}{\partial x^2} - C_A X_n(L) = 0 \tag{2.70}$$

where,

$$C_A = -\frac{d_{31} b(x)}{E_c I_c}\left(\frac{E_1 E_b h_b (h_1 + h_b)}{2(E_1 h_1 + E_b h_b)}\right) g_{d1} - \frac{d_{31} b(x)}{E_c I_c}\left(\frac{2E_2^2 h_2^2 + E_2 h_2 E_b h_b - E_2 E_b h_b^2}{2(E_b h_b + E_2 h_2)}\right) g_{d2} \tag{2.71}$$

Thus, equation 2.69 can be written in short form as follows:

$$X_n''(L) - C_A X_n(L) = 0 \tag{2.72}$$

Substituting equation 2.67 into equation 2.66, such that ω_n is the natural frequency of the tip of the beam, the natural frequency of motion of the tip mass should be the same as that of the beam. Figure 2.6 shows the concentrated mass at the tip of the beam (the mass is dimensionless). Therefore the shear boundary condition simplifies to the expression in the equation below.

$$m_T \frac{d^2\left(X_n(L) T_n(t)\right)}{dt^2} - E_c I_c \frac{d^3\left(X_n(L) T_n(t)\right)}{dx^3} - N \frac{d\left(X_n(L) T_n(t)\right)}{dx} = 0 \tag{2.73}$$

$$m_T X_n(L) \ddot{T}_n(t) - E_c I_c \frac{d^3 X_n(L)}{dx^3} T_n(t) - N \frac{dX_n(L)}{dx} T_n(t) = 0 \tag{2.74}$$

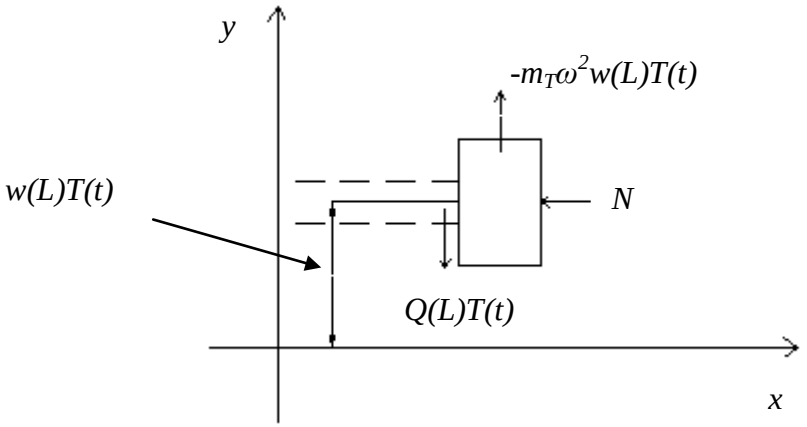

Figure 2.6: Beam with concentrated mass at the free end

using equation 2.61 above.

$$m_T X_n(L)\left(-\omega^2 T_n(t)\right) - E_c I_c \frac{d^3 X_n(L)}{dx^3} T_n(t) - N \frac{dX_n(L)}{dx} T_n(t) = 0 \qquad (2.75)$$

and dividing equation 2.75 by $T_n(t)$, it is reduced to equation 2.76 below, where the boundary condition appears in terms of the spatial variable alone.

$$-m_T X_n(L)\left(\omega_n^2\right) - E_c I_c \frac{d^3 X_n(L)}{dx^3} - N \frac{dX_n(L)}{dx} = 0 \qquad (2.76)$$

Rearranging equation 2.76, and writing it in reduced notation results in the boundary condition in equation 2.77, after dividing and multiplying the first term by m_c and dividing all the terms by $E_c I_c$.

$$X_n''' + \frac{N}{E_c I_c} X_n' + \frac{m_T}{m_c} \cdot \frac{m_c \omega^2}{E_c I_c} X_n = 0 \qquad \text{at } x = L \qquad (2.77)$$

And finally, in the space frame, the shear boundary condition at the free end due to the mass is expressed in equation 2.78.

$$X_n''' + \beta^2 X_n' + \eta a_n^4 \; X_n = 0 \qquad \text{at } x = L \qquad (2.78)$$

where, β^2 is the axial load parameter, a_n^4 is the frequency parameter and $\eta = m_T / m_c$ is the ratio of the concentrated tip mass to the mass of the composite beam. From equation 2.65, M_p is the uniformly distributed moment generated by the piezo layer on the beam due to the input voltage. The piezo layer is bonded to the top and bottom surface of the beam as indicated in Figure 2.7. Although the piezo is mounted along the length of the beam (at $0 < x < L$), the moment manifests itself only at the boundary.

2.4 Determination of the natural frequencies of the beam

To find the natural frequencies of the beam, it is necessary to satisfy the boundary conditions at the clamped end and at the free end of the beam. The natural frequencies are used to determine the mode shapes. These boundary conditions imply the following on the boundary after using equation 2.67 in the space frame.

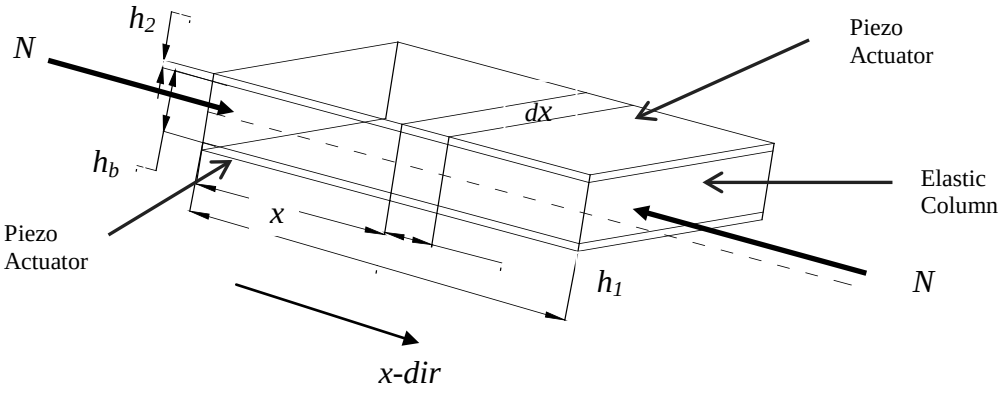

Figure 2.7: Cantilever sandwiched between two piezo electric actuators

At **x = 0**:

$$X_n(0) = 0 \quad \text{and} \quad \frac{dX_n(0)}{dx} = 0 \tag{2.79}$$

At **x = L**:

$$\frac{d^2 X_n(L)}{d^2 x} - C_A X_n(L) = 0 \tag{2.80}$$

$$\frac{d^3 X_n(L)}{dx^3} + \beta^2 \frac{dX_n(L)}{dx} + \eta a_n{}^4 X_n(L) = 0 \tag{2.81}$$

The general solution from the previous section, mentioned below in equation 2.82a will be used in the four boundary conditions above.

$$X_n(x) = A_n \sin p_{2n}x + B_n \cos p_{2n}x + C_n \sinh p_{1n}x + D_n \cosh p_{1n}x \tag{2.82a}$$

After inserting the general equation into the boundary conditions in equations 2.79 at $x = 0$, and dropping the subscript (n) two variables can be eliminated and represent the general solution in terms of two variables C and B. The constants A, B, C and D are unique for each and every mode of vibration because each and every mode corresponds to a unique natural frequency depending on the loading conditions.

$$D = -B; \text{ and } A = -\frac{p_1}{p_2}C \tag{2.83b}$$

Hence our general solution equation 2.82a becomes,

$$X(x) = C\left(\sinh p_1x - \frac{p_1}{p_2}\sin p_2x\right) + B(\cos p_2x - \cosh p_1x) \tag{2.84}$$

The general solution can be substituted into the two boundary conditions on the free-end of the beam at $x = L$, to arrive at two equations with the two unknown constants C and B. These two equations are used to determine the characteristic equation in order to find the natural frequencies. One of the variables is undetermined and can be set to unity. The boundary conditions, equations 2.80 and 2.81 are converted into equation 2.84 and 2.85 after inserting the general solution and some simplification.

$$\begin{aligned} &C\left[\frac{p_1}{p_2}\left(p_2^2 + C_A\right)\sin p_2L + \left(p_1^2 - C_A\right)\sinh p_1L\right] \\ &- B\left[\left(p_2^2 + C_A\right)\cos p_2L + \left(p_1^2 - C_A\right)\cosh p_1L\right] = 0 \end{aligned} \tag{2.85}$$

and,

$$
\begin{aligned}
&C\left[\begin{aligned}&\frac{p_1}{p_2}(p_2^3\cos p_2L-\beta^2 p_2\cos p_2L-\eta a^4\sin p_2L)\\&+(p_1^3\cosh p_1L+\beta^2 p_1\cosh p_1L+\eta a^4\sinh p_1L)\end{aligned}\right]\\
&+B\left[\begin{aligned}&(p_2^3\sinh p_1L-\beta^2 p_2\sin p_2L+\eta a^4\cos p_2L)\\&-(p_1^3\sinh p_1L+\beta^2 p_1\sinh p_1L+\eta a^4\cosh p_1L)\end{aligned}\right]=0
\end{aligned}
\tag{2.86}
$$

For the characteristic equation solve for *C* in equation 2.84 and substitute the results into equation 2.85, and *B* remains undetermined or an arbitrary constant. The constant *B* can be set to unity. After simplification the characteristic equation can be expressed in equation 2.86. Equation 2.86 is used to determine the infinite set of natural frequencies which are associated with the subscript (*n*) in equation 2.82a.

$$
\begin{aligned}
&2a^4+2a^4\cosh p_1L\cos p_2L+\frac{\beta^4C_A}{a^2}\sinh p_1L\sin p_2L-a^2\beta^2\sinh p_1L\sin p_2L\\
&+\eta a^2\left(p_1^2+p_2^2\right)\left(p_2\sinh p_1L\cos p_2L-p_1\cosh p_1L\sin p_2L\right)\\
&-\frac{C_A\left(2a^4+\beta^4\right)}{a^2}\sinh p_1L\sin p_2L+\beta^2C_A\cosh p_1L\cos p_1L\\
&-\beta^2C_A+\beta^4\cos p_2L=0
\end{aligned}
\tag{2.87}
$$

To verify the characteristic equation, set the piezo constant to zero and the result is equation 2.87, which corresponds to the characteristic equation obtained by (Shaker, 1975) in a study on vibration of a beam with axial load and a concentrated mass, which is given as:

$$
\begin{aligned}
&2a^4+\left(2a^4+\beta^4\right)\cosh p_1L\cos p_2L-a^2\beta^2\sinh p_1L\sin p_2L\\
&+\eta a^2\left(p_1^2+p_2^2\right)\left(p_2\sinh p_1L\cos p_2L-p_1\cosh p_1L\sin p_2L\right)=0
\end{aligned}
\tag{2.88}
$$

Furthermore, if the axial force is set to zero, the result is the frequency equation for cantilevered beam with a concentrated tip mass only, which is also obtained by Edwards, Jr *et al.*, (1989).

$$
\begin{aligned}
&\eta a^2\left(p_1^2+p_2^2\right)\left(p_2\sinh p_1L\cos p_2L-p_1\cosh p_1L\sin p_2L\right)+\\
&2a^4+2a^4\cosh p_1L\cos p_2L=0
\end{aligned}
\tag{2.89}
$$

When the mass at the tip is zero we have the characteristic equation for an ordinary clamped-free beam (Ertuk, 2012):

$$2a^4 + 2a^4 \cosh p_1 L \cos p_2 L = 0 \tag{2.90}$$

For known values of β^2, C_A, L and η the characteristic equation 2.86 can be solved numerically for the roots. There will be an infinite number of roots or natural frequencies (ω_n). The natural frequencies for the characteristic equation 2.86 will be determined from the roots (R_n), which are determined from the relationship between the characteristic value (a_n) and the length (L) of the beam.

To find the roots of the characteristic equation 2.86, let $R_n^4 = a_n^4 L^4$, such that R_n becomes a non-dimensional constant, then $a_n = R_n / L$. Inserting a_n into equation 2.60:

$$X_n''''(x) + \beta^2 X_n''(x) - \left(\frac{R_n}{L}\right)_n^4 X_n(x) \ = 0 \tag{2.91}$$

but, by using equation 2.58a; $a_n^4 = \left(m_c \omega_n{}^2\right) \!/ \left(E_c I_c\right)$ then:

$$\left(\frac{R_n}{L}\right)^4 = \frac{m_c \omega_n{}^2}{E_c I_c} \tag{2.92}$$

therefore,

$$\omega_n = \left(\frac{R_n}{L}\right)^2 \sqrt{\frac{E_c I_c}{m_c}} \tag{2.93}$$

using the following relationship R_n can be determined numerically and thus the characteristic value (a_n).

The material and geometric properties for the elastic beam and the piezo actuators are listed in Table 2.1. The length of the column is chosen to be L = 0.146m to facilitate a comparison with the table of findings by Young *et al.*, (1949). The natural frequencies for a clamped-free

beam in their study corresponds with those in this study for all the first four modes of vibration when the tip mass ratio, axial load ratio and piezo-electric voltage are set to zero.

Table 2.1: Material and geometric properties of the composite beam.

	Aluminum Beam	Bottom piezo material (Fiji C-82)	Top piezo material (Fiji C-82)
Young's Modulus	$E_b = 76 \times 10^9$ N/m^2	$E_1 = 59 \times 10^9$ N/m^2	$E_2 = 59 \times 10^9$ N/m^2
Density	$\rho_{b = 2840}$ kg/m^3	$\rho_{1 = 1800}$ kg/m^3	$\rho_{2 = 1800}$ kg/m^3
Thickness	$h_b = 10$mm	$h_1 = 1$mm	$h_2 = 1$mm
Width	$b(x) = 0.0127$m	$b(x) = 0.0127$m	$b(x) = 0.0127$m
Length	$L = 0.146$m	$L = 0.146$m	$L = 0.146$m
Piezo electric constant	--	$d_{31} = 260 \times 10^{-12}$ m/V	$d_{31} = 260 \times 10^{-12}$ m/V

The characteristic equation 2.86 is dependent on C_A, the combined top and bottom piezo effect. The piezo effects are caused by the voltage applied and manifests at the boundary in the form of moments. These effects are included in the moment boundary condition in equation 2.70 which is used to determine the natural frequencies. It can be concluded that the natural frequencies of the system depend on the voltage applied. When applying the voltage to the piezo actuators the polarity or direction if the voltage input has a significant effect on the natural frequencies. The polarity has the effect of increasing or decreasing the natural frequencies depending on the mechanical response of the piezo materials. The two critical parameters that determine the mechanical response of the actuator are poling direction of the piezo material and the direction of the input voltage, see Figure 2.8.

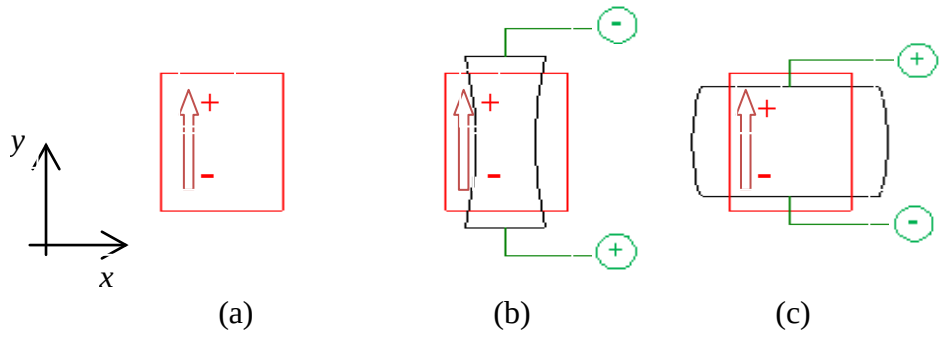

Figure 2.8: Compression and Extension due to piezo material poling and input voltage polarity for piezo

Figure 2.8(a) shows a piezo material poled in the *y*-direction and Figure 2.8(b) and 2.8(c) shows the piezoelectric beam with a positive and negative applied voltage potential, respectively. In Figure 2.8(b), the piezo material extends in length in the *y*-direction whilst contracting in the *x*-direction and in Figure 2.8(c) the piezo material contracts in the *y*-direction whilst it extends in the *x*-direction. A contraction in the *x*-direction represents a compressive load and an extension in the *x*-direction represents a tensile load in the longitudinal direction. The effects of compressive and tensile load on the natural frequency are shown in Table 2.2. These results also shows the effects of the input voltage polarity which has been observed by other researchers. According to literature, applying equal opposite voltages to the piezoelectric layers poled in the transverse direction results in a compressive or tensile mechanical stress on the beam (Abedinnasab *et al*., 2008). Table 2.2 indicates that, by controlling the polarity of the voltage input to the piezo layers, the natural frequencies can be increased or reduced.

Table 2.2: Polarity of voltage input for piezo actuators.

Voltage	Tension(T) Compression(C)	Frequency	Voltage	Tension(T) Compression(C)	Frequency
$V^{p1} = +1000\text{V}$ $V^{p2} = +1000\text{V}$ $(^{+}_{+}V = 1000\text{V})$	T C	1.8750 4.6941 7.8548 10.996	$V^{p1} = 0\text{V}$ $V^{p2} = +1000\text{V}$ $(^{0}_{+}V = 1000\text{V})$	-- C	1.8352 4.6857 7.8518 10.994
$V^{p1} = -1000\text{V}$ $V^{p2} = -1000\text{V}$ $(^{-}_{-}V = 1000\text{V})$	C T	1.875 4.6941 7.8548 10.996	$V^{p1} = -1000\text{V}$ $V^{p2} = 0\text{V}$ $(^{-}_{0}V = 1000\text{V})$	C --	1.8352 4.6857 7.8518 10.994
$V^{p1} = +1000\text{V}$ $V^{p2} = -1000\text{V}$ $(^{+}_{-}V = 1000\text{V})$	T T	1.9453 4.7107 7.8606 10.999	$V^{p1} = 0\text{V}$ $V^{p2} = -1000\text{V}$ $(^{0}_{-}V = 1000\text{V})$	-- T	1.9115 4.7025 7.8577 10.997
$V^{p1} = -1000\text{V}$ $V^{p2} = +1000\text{V}$ $(^{-}_{+}V = 1000\text{V})$	C C	1.7925 4.6772 7.8489 10.993	$V^{p1} = +1000\text{V}$ $V^{p2} = 0\text{V}$ $(^{+}_{0}V = 1000\text{V})$	T --	1.9115 4.7025 7.8577 10.997

A positive input voltage causes the bottom piezo (p_1) to exert a tensile load on the composite and a negative voltage exerts a compressive load on the column. A negative voltage exerts a tensile load on the top piezo actuator (p_2) and the opposite voltage exerts a compression. If the bottom and top piezo actuators exert loads in opposite direction and the natural frequencies remain unchanged because the net sum of the forces is zero.

However, if both piezo actuators exert a tensile load the whole column experiences a symmetric tensile load which results in the increase in the natural frequencies of the system. This is indicated in the tables for a positive voltage for bottom piezo (p_1) and negative voltage for top piezo (p_2) $^{+}_{-}V = 1000\text{V}$. The superscript and subscript indicates the polarity of the input voltage. An input voltage of $^{-}_{+}V = 1000\text{V}$ exerts a compressive load on the column resulting in a reduction in the natural frequencies.

2.5 Orthogonality of the modes

If a sequence of real functions $X_n(x)$ {for $n = 1\ldots\infty$} has a property that over an interval:

$$\int_a^b \left[P_1(x) X_n(x) \cdot X_m(x) + P_2(x) \frac{dX_n(x)}{dx} \cdot \frac{dX_m(x)}{dx} \right] dx = \delta_{nm} N_n \tag{2.94}$$

where δ_{nm} is the Kronecker delta function ($\delta_{nm} = 1$ for $n = m$ and $\delta_{nm} = 0$ for $n \neq m$), then the set of functions are said to form an orthogonal set (Balachandran, 2009). $P_1(x)$ and $P_2(x)$ are the weighting functions on the interval where $\sqrt{N}$ is the norm of the function. If we assume that a_n^4 is a set of eigenvalues or characteristic values and $X_n(x)$ is the set of eigenfunctions associated with the set, this set provides the solution to the equation of motion of the beam in equation 2.94a and 2.94b, such that m and n are arbitrary integers greater than zero.

$$X_n''''(x) + \beta^2 X_n''(x) - a_n^4 X_n(x) = 0 \tag{2.94a}$$

$$X_m''''(x) + \beta^2 X_m''(x) - a_m^4 X_m(x) = 0 \tag{2.94b}$$

Multiplying equation 2.94a by X_m and equation 2.94b by X_n, where X_n and X_m are distinct solutions to the equations of motion and integrating over the whole length of the column ($0 \le x \le L$) we arrive at the following relations,

$$\int_0^L X_m X_n'''' dx + \beta^2 \int_0^L X_m X_n'' dx - a_n^4 \int_0^L X_m X_n dx = 0 \tag{2.95a}$$

$$\int_0^L X_n X_m'''' dx + \beta^2 \int_0^L X_n X_m'' dx - a_m^4 \int_0^L X_n X_m dx = 0 \tag{2.95b}$$

Integrating the first two terms of equation 2.95a and 2.95b by parts we arrive at the following equations:

$$\left[X_m X_n'''\right]_0^L + \beta^2 \left[X_m X_n'\right]_0^L + \int_0^L X_m'' X_n'' dx - \beta^2 \int_0^L X_m' X_n' dx - a_n^4 \int_0^L X_m X_n dx = \left[X_m' X_n''\right]_0^L \tag{2.96a}$$

$$\left[X_n X_m'''\right]_0^L + \beta^2 \left[X_n X_m'\right]_0^L + \int_0^L X_n'' X_m'' dx - \beta^2 \int_0^L X_n' X_m' dx - a_m^4 \int_0^L X_n X_m dx = \left[X_n' X_m''\right]_0^L \tag{2.96b}$$

Subtract equation 2.96b from equation 2.96a, and since the subscripts of the functions in the third and fourth integration terms on the LHS can be interchanged, these terms cancel out and vanish. Inserting the integration limits into equation 2.96a and 2.96b, the results are:

$$\begin{aligned} &X_m(L)X_n'''(L) - X_m(0)X_n'''(0) + \beta^2 X_m(L)X_n'(L) - \beta^2 X_m(0)X_n'(0) \\ &- X_n(L)X_m'''(L) + X_n(0)X_m'''(0) - \beta^2 X_n(L)X_m'(L) - \beta^2 X_n(0)X_m'(0) \\ &= \left[X_m' X_n'' - X_m' X_n''\right]_0^L \end{aligned} \tag{2.97}$$

The term on the RHS of equation 2.97 will be treated by first considering the moment boundary condition at the free end ($x = L$).

$$X_n''(L) - C_A X_n(L) = 0 \tag{2.98a}$$

$$X_m''(L) - C_A X_m(L) = 0 \tag{2.98b}$$

Multiplying equation 2.98a by X_m and equation 2.98b by X_n, where X_n and X_m are distinct solutions to the equations of motion and integrating over the whole length of the column $(0 \le x \le L)$ we arrive at the following relations:

$$X_m X_n'' - C_A X_m X_n = 0 \tag{2.99a}$$

$$X_n X_m'' - C_A X_n X_m = 0 \tag{2.99b}$$

Subtracting equation 2.99b from equation 2.99a and integrating over the domain the results are:

$$\int_0^L X_m X_n'' dx - \int_0^L X_n X_m'' dx - \int_0^L C_A X_m X_n dx + \int_0^L C_A X_n X_m = 0 \tag{2.100}$$

Integrate the first two terms of equation 2.100 by parts and factor C_A from the last two terms:

$$\left[X_m X_n'\right]_0^L - \left[X_n X_m'\right]_0^L - \int_0^L X_m' X_n' dx + \int_0^L X_n' X_m' dx - C_A\left(\int_0^L X_m X_n dx - \int_0^L X_n X_m dx\right) = 0 \tag{2.101}$$

In equation 2.101 the subscripts for the last four terms on the LHS are interchangeable and therefore those terms vanish leaving us with the following:

$$\left[X_m X_n' - X_n X_m'\right]_0^L = 0 \tag{2.102}$$

From the LHS of equation 2.97 above, after inserting the integration limits, the terms associated with the displacement and gradient at the fixed end vanish and the result is the following:

$$X_m(L)X_n'''(L) - X_n(L)X_m'''(L) + \beta^2 X_m(L)X_n'(L) - \beta^2 X_n(L)X_m'(L) = \left[X_m' X_n'' - X_m' X_n''\right]_0^L \tag{2.103}$$

But $X_n''(L) = C_A X_n(L)$ therefore the RHS of equation 2.103 becomes:

$$\left[X_m^{'} C_A X_n - X_n^{'} C_A X_m\right]_0^L = 0 \tag{2.104}$$

All the displacements and the slopes at the fixed end of the beam are zero and cause the associated terms in equation 2.104 to vanish after inserting the appropriate integration limits such that:

$$C_A\left[X_m^{'}(L) X_n(L) - X_n^{'}(L) X_m(L)\right] = 0 \tag{2.105}$$

Using the boundary conditions at the fixed end ($X_n(0) = 0$ and $X_n^{'}(0) = 0$ where $x = 0$) and grouping the terms with X_m and X_n in equation 2.96a and 2.96b, respectively, we arrive at equations 2.106a and 2.106b.

$$X_m(L)\left[X_n^{'''}(L) + \beta^2 X_n^{'}(L)\right] + \int_0^L X_m^{''} X_n^{''} dx - \beta^2 \int_0^L X_m^{'} X_n^{'} dx - a_n^4 \int_0^L X_m X_n dx = X(L)_m^{'} X_n^{''}(L). \tag{2.106a}$$

$$X_n(L)\left[X_m^{'''}(L) + \beta^2 X_m^{'}(L)\right] + \int_0^L X_n^{''} X_m^{''} dx - \beta^2 \int_0^L X_n^{'} X_m^{'} dx - a_m^4 \int_0^L X_n X_m dx = X(L)_n^{'} X_m^{''}(L) \tag{2.106b}$$

After inserting the boundary conditions at the fixed end the associated terms vanish and we are left to satisfy the boundary conditions at the free end. Now using the boundary conditions at the free end, $x = L$, i.e.

$$X_n^{'''}(L) + \beta^2 X_n(L) + \eta a_n{}^4 X_n(L) = 0 \quad \text{and} \quad X_n^{''}(L) - C_A X_n(L) = 0$$

using equations 2.106a, 2.106b and the above boundary conditions, after simplifying we arrive at equations 2.107a and 2.107b.

$$X_m(L)\left[-\eta a_n^4 X_n(L)\right] + \int_0^L X_m^{''} X_n^{''} dx - \beta^2 \int_0^L X_m^{'} X_n^{'} dx - a_n^4 \int_0^L X_m X_n dx = X_m^{'}(L) X_n^{''}(L) \tag{2.107a}$$

$$X_n(L)\left[-\eta a_m^4 X_m(L)\right]+\int_0^L X_n'' X_m'' dx-\beta^2\int_0^L X_n' X_m' dx-a_m^4\int_0^L X_n X_m dx=X_n'(L)X_m''(L) \qquad (2.107b)$$

Subtracting equation 2.107b from equation 2.107b we arrive at equation 2.108 and factor the out the like terms on the LHS of this equation to arrive at equation 2.109.

$$\left(a_n^4-a_m^4\right)\eta X_n(L)X_m(L)+\left(a_n^4-a_m^4\right)\int_0^L X_n X_m dx=X_m'(L)X_n''(L)-X_n'(L)X_m''(L) \qquad (2.108)$$

$$\left(a_n^4-a_m^4\right)\left[\eta X_n(L)X_m(L)+\int_0^L X_n X_m dx\right]=X_m'(L)X_n''(L)-X_n'(L)X_m''(L) \qquad (2.109)$$

Inserting the moment boundary condition at the free end ($x = L$), the RHS of equation 2.109 leads to:

$$\left(a_n^4-a_m^4\right)\left[\eta X_n(L)X_m(L)+\int_0^L X_n X_m dx\right]=C_A[X_m'(L)X_n(L)-X_n'(L)X_m(L)] \qquad (2.110)$$

where, equation 2.105 shows that the RHS of equation 2.110 is zero.

$$\left(a_n^4-a_m^4\right)\left[\eta X_n(L)X_m(L)+\int_0^L X_n X_m dx\right]=0 \qquad (2.111)$$

Since the natural frequencies are distinct, the eigenvalues will be distinct and therefore $a_n^4 \neq a_m^4$, then the term inside the square brackets must be equal to zero for equation 2.111 to be true. The eigenvalues associated with these eigenfunctions will lead to an orthogonal relationship:

$$\int_0^L X_n X_m dx+\eta X_n(L)X_m(L)=\delta_{nm}N_n \qquad (2.112)$$

where δ_{nm} is the Kronecker delta and N_n is the norm

$$N_n = \int_0^L X_n^2(x)dx + \eta X_n^2(L) \tag{2.113}$$

and equation 2.114 can be written as:

$$\int_0^L \left[1 + \eta\delta(x-L)\right] X_n(L) X_m(L) dx = \delta_{nm} N_n \tag{2.114}$$

where, $\delta(x-L)$ is the delta function, $P_1(x) = 1 + \eta\delta(x-L)$ and $P_2(x) = 0$ are the weighting functions.

Chapter 3 - Computation of the natural frequencies

3.1 Natural frequencies for a cantilevered beam

The natural frequencies of a beam with a tip mass, axial load and a piezo actuator can be determined from the characteristic equation obtained in equation 2.86 of Section 2.4. After some simplification it can be written as equation 3.1 below:

$$\begin{aligned} &2a^4 - \beta^2 C_A(2 + \cosh p_1 L \cos p_2 L) + \left(2a^4 + \beta^4\right)\cosh p_1 L \cos p_2 L \\ &- a^2\beta^2 \sinh p_1 L \sin p_2 L + \frac{2C_A}{a^2}\left(\beta^4 + a^4\right)\sinh p_1 L \sin p_2 L \\ &+ \eta a^2\left(p_1^2 + p_2^2\right)\left(p_2 \sinh p_1 L \cos p_2 L - p_1 \cosh p_1 L \sin p_2 L\right) = 0 \end{aligned} \tag{3.1}$$

The roots of equation 3.1 are the eigenvalues of the solution and are used to determine the natural frequencies of the beam. The natural frequencies are calculated for varying tip mass and varying axial load for a piezo input voltages of 0V, 100V, 500V and 1000V. This study pays attention to the first four natural frequencies of the system, i.e. 1st (fundamental), 2nd, 3rd and 4th natural frequencies. More frequencies can be added to improve the accuracy of the solution. It is demonstrated later in Chapter 7 that four eigenfunctions are adequate to approximate the exact solution with a small residual. The results are plotted in the Figures 3.1a to 3.4d below. The voltage input into the piezo material produce a strain resulting in moments at the boundaries and changes the natural frequencies.

When the piezo layers are deactivated, the results of this study can be compared to the results obtained by other researchers. If the axial load is removed and there remains only the tip mass, the natural frequencies are listed in Table3.1a for zero axial load ratio (k = 0) are obtained. These are the same natural frequencies obtained by Balachandran *et al*., (2009). When the tip mass is removed and the axial load is retained, the natural frequencies generated are the same as those generated by Shaker, (1975).

In this investigation, an analysis is conducted into the influence of the axial load, tip mass and the piezo voltage input, with the main emphasis being on the piezo. The tip mass is considered infinitesimal. Later we consider an extended mass with a center of gravity that

does not necessarily coincide with the tip of the beam. In that case, the rotary inertia of the tip mass is taken into account. This case will be presented later in Chapter 4.

3.2 Natural frequencies for a beam with tip mass and axial load

3.2.1 First natural frequencies (ω_1)

Table3.1a to Table 3.1d below indicate the change in natural frequency with respect to axial load and tip mass ratio. Figures 3.1a to 3.4d are the graphs generated from Table3.1a to 3.1d. From the figures it is noted that as the axial force is increased, the natural frequency increases, and the reverse occurs as the tip mass is increased the natural frequency decreases.

Table 3.1a: 1st frequencies of the beam with a tip mass and axial load: Voltage = 0V.

	Voltage = 0V/mm (ω_1)				
Axial load Ratio (k)	$\eta = 0$	$\eta = 0.1$	$\eta = 1$	$\eta = 5$	$\eta = 10$
0.8	1.27	1.17	0.84	0.58	0.49
0.4	1.66	1.52	1.10	0.77	0.65
0	1.88	1.72	1.25	0.87	0.74
-1	2.19	2.03	1.48	1.03	0.87
-6	2.87	2.68	1.99	1.40	1.18
-10	3.15	2.96	2.22	1.56	1.32

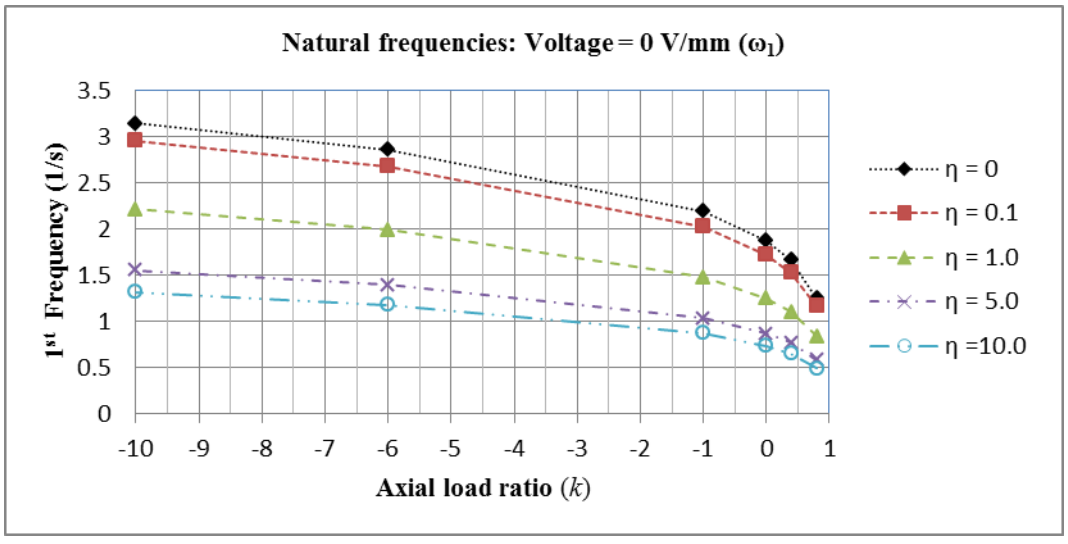

Figure 3.1a: Change in fundamental frequency vs axial Load ratio: Voltage = 0V

The natural frequency is highest for maximum axial tensile load and zero tip mass ratios for all modes of vibration. In the first mode, the natural frequencies vary non-linearly in a monotonic manner but in the higher modes the variation tends to be more linear as indicated in the graphs of the higher modes, Figure 3.2a to 3.4d.

Table 3.1b: 1st frequencies of the beam with a tip mass and axial load: Voltage = 100V.

	Voltage = 100 V/mm (ω_1)				
Axial load Ratio (k)	η = 0	η = 0.1	η = 1	η = 5	η =10
0.8	1.27	1.14	0.82	0.57	0.48
0.4	1.65	1.51	1.09	0.76	0.64
0	1.87	1.72	1.24	0.87	0.73
-1	2.19	2.02	1.47	1.03	0.87
-6	2.86	2.68	1.99	1.40	1.18
-10	3.15	2.96	2.21	1.56	1.32

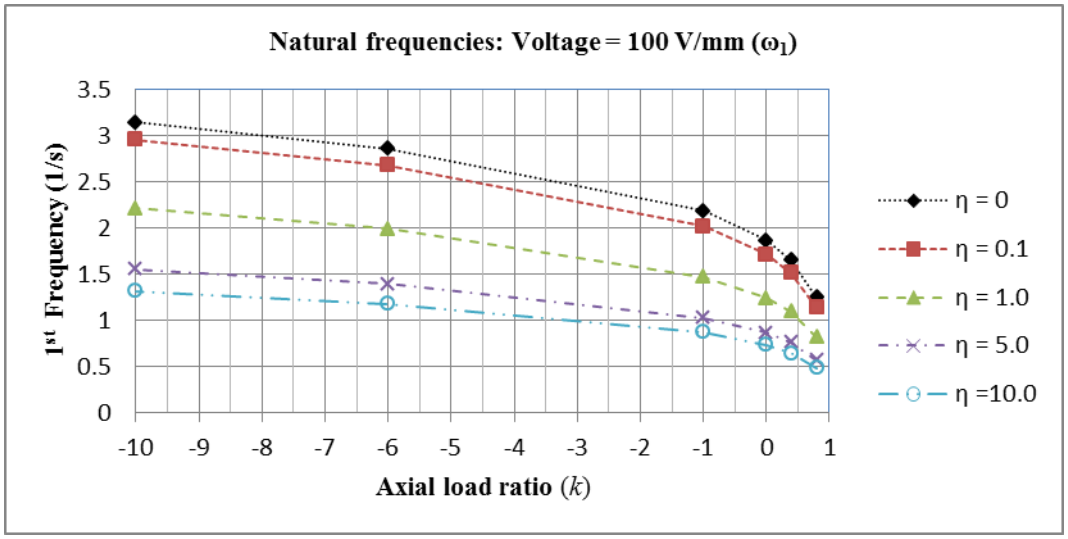

Figure 3.1b: Change in fundamental frequency vs axial load ratio: Voltage = 100V

When the axial mass ratio is zero (η = 0), the axial load ratio is compressive (k = +0.8) and the piezo layers are inactive $(\overset{-}{+}V = 0\text{V})$, the natural frequency of the beam is ω_1 = 1.2472s^{-1} in the first mode. When a maximum voltage $(\overset{-}{+}V = 1000\text{V})$ is applied, the natural frequency decreases to ω_1 = 0.7051s^{-1}, which is percentage difference of 44%; indicating that the natural frequency of vibration can be controlled using piezo actuators.

The change in natural frequency becomes less pronounced when the axial load ratio goes from compressive to tensile. At an axial load ratio (k = -1) the percentage difference is 1.83% and beyond that, at (k = -6) the difference is less than 1%. There is a point between (k = -1) and (k = -6) where the piezo loses its efficacy. This efficacy cut-off point is investigated later in the study.

Table 3.2c: 1st frequencies of the beam with a tip mass and axial load: Voltage = 500V.

	Voltage = 500 V/mm (ω_1)				
Axial load Ratio (k)	η = 0	η = 0.1	η = 1	η = 5	η =10
0.8	1.11	1.02	0.73	0.51	0.43
0.4	1.61	1.47	1.06	0.80	0.62
0	1.84	1.69	1.22	0.85	0.72
-1	2.18	2.01	1.46	1.02	0.86
-6	2.86	2.67	1.99	1.39	1.18
-10	3.15	2.95	2.21	1.55	1.31

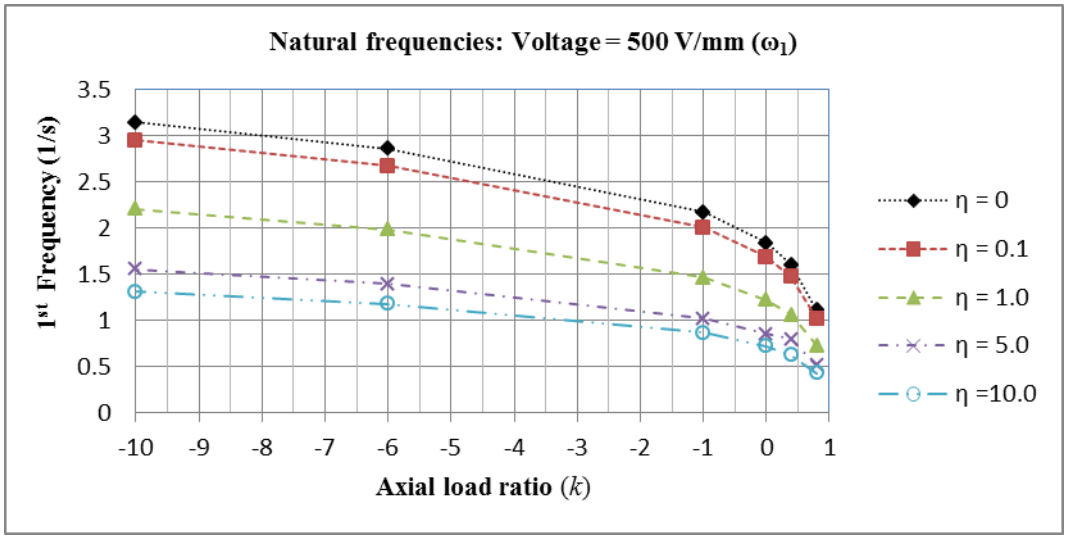

Figure 3.1c: Change in fundamental frequency vs axial load ratio: Voltage = 500V

From Table3.1a to Table 3.1d and the Figures 3.1a to 3.4d it is noted that as the axial force ratio increases and the tip mass ratio is kept constant the natural frequencies increase, similar to a guitar string. The lowest frequencies occur when the beam is in compression. When keeping the axial load constant and increasing the tip mass the natural frequencies are reduced significantly. The axial load and the tip mass have opposite effects on the natural

frequencies and both are dominant beyond a particular threshold, such that the piezo actuator loses control effectiveness.

In tensile load, the gradient of the curves for frequency versus axial load ratio are smaller than in compression. In compression at maximum input voltage the slope is steeper than the slopes of the curves at lower voltages (0V, 100V, 500V). This shows that the most effective control can be achieved at a voltage of 1000V. The maximum input voltage is limited to 1000V/mm to prevent piezo breakdown and to facilitate for a bench mark comparison with other reseachers.

Table 3.1d: 1st frequencies of the beam with a tip mass and axial load: Voltage = 1000V.

	Voltage = 1000 V/mm (ω_1)				
Axial load Ratio (k)	η = 0	η = 0.1	η = 1	η = 5	η =10
0.8	0.66	0.73	0.53	0.37	0.31
0.4	1.54	1.41	1.02	0.71	0.60
0	1.79	1.65	1.19	0.83	0.70
-1	2.15	1.99	1.45	1.01	0.85
-6	2.86	2.67	1.98	1.39	1.18
-10	3.14	2.95	2.21	1.55	1.31

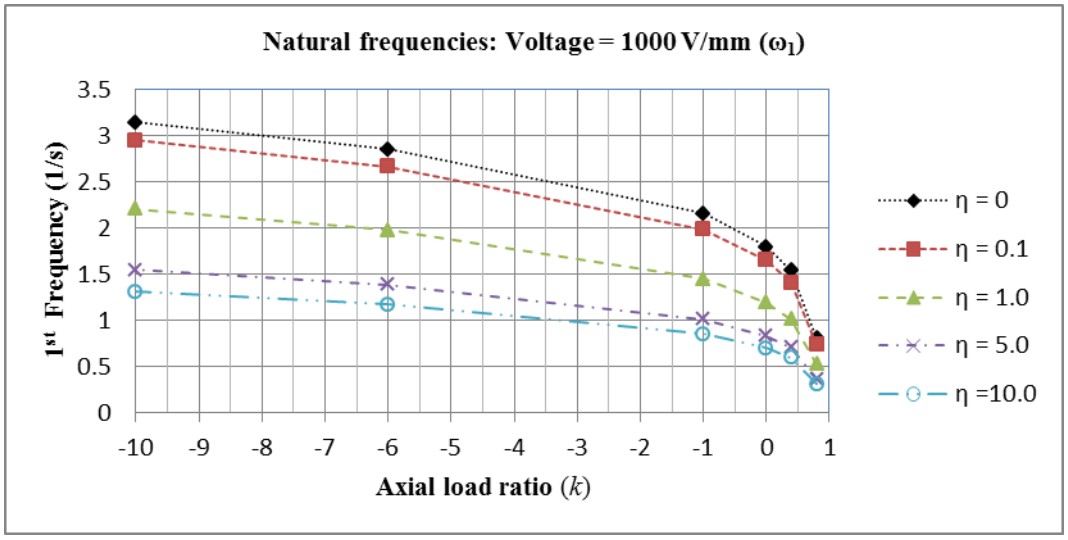

Figure 3.1d: Change in fundamental frequency vs axial load ratio: Voltage = 1000V

From Figures 3.1a and 3.1d it can observe that the frequencies at k = -10 are identical to two decimal places. Tables 3.1c and 3.1d show that there is an overall drop in natural frequency

when the voltage is increased from 0V to 1000V and the axial load ratio is $-1 \leq k \leq +0.8$. At k = -6 and k = -10 the difference is very small, see Figures 3.1a to 3.1d. That shows that there is a loss of control effectiveness of the piezo actuators beyond a certain axial load ratio.

3.2.2 Second natural frequencies (ω_2)

In the 2nd mode of vibration the maximum natural frequency (ω_2 = 5.9240s^{-1}) occurs at maximum tensile load ratio (k = -10) and the minimum natural frequency (ω_2 = 4.5310s^{-1}) occurs at the critical axial load ratio (k = +0.8.) We also note that as the tip mass ratio is increased the natural frequency drops.

Table 3.2a: 2nd frequencies of the beam with a tip mass and axial load: Voltage = 0V.

	Voltage = 0V/mm (ω_2)				
Axial load Ratio (k)	η = 0	η = 0.1	η = 1	η = 5	η =10
0.8	4.53	4.26	3.93	3.85	3.84
0.4	4.62	4.33	3.98	3.90	3.89
0	4.69	4.40	4.03	3.95	3.94
-1	4.88	4.56	4.15	4.06	4.05
-6	5.55	5.17	4.64	4.52	4.51
-10	5.92	5.52	4.94	4.81	4.79

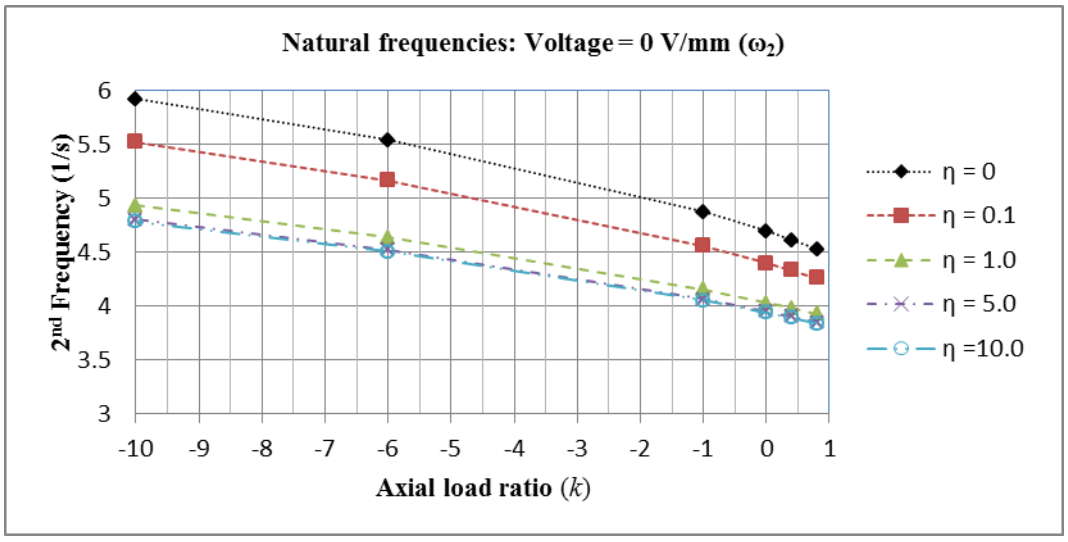

Figure 3.2a: Change in 2nd frequency vs axial load ratio: Voltage = 0V

The gradients of the curves in Figures 3.2a to 3.2d are uniform, indicating that the change is almost linear at the higher modes of vibration. The maximum percentage change is slightly less than 0.5% when the input voltage is $\bar{+}V = 1000\text{V}$. The observation from Table 3.2a and 3.2d is that beyond η = 0.1, as the tip mass ratio increases the percentage difference drops and becomes negligible.

Table 3.2b: 2nd frequencies of the beam with a tip mass and axial load: Voltage = 100V.

	Voltage = 100V/mm (ω_2)				
Axial load Ratio (k)	η = 0	η = 0.1	η = 1	η = 5	η =10
0.8	4.53	4.26	3.92	3.85	3.84
0.4	4.61	4.33	3.98	3.90	3.89
0	4.69	4.40	4.03	3.95	3.94
-1	4.87	4.56	4.15	4.06	4.05
-6	5.54	5.16	4.64	4.52	4.51
-10	5.92	5.52	4.94	4.81	4.79

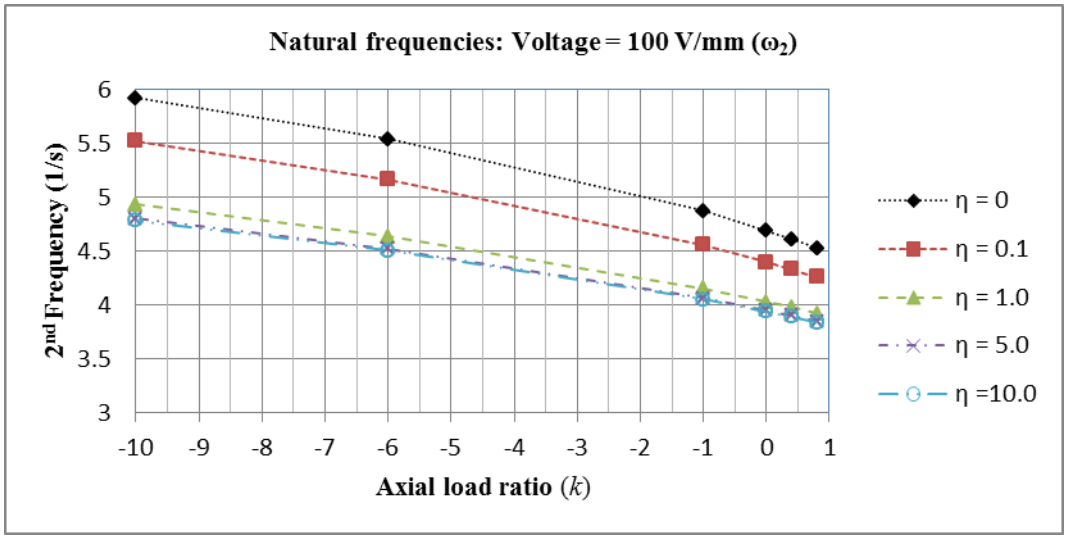

Figure 3.2b: Change in 2nd frequency vs axial load ratio: Voltage = 100V

The ineffenctiveness of the piezo can also be observed in the higher modes of vibration, see results in Appendix A1 to A3. The piezo actuator has insufficient or no control in the higher mode of vibration except for the fundamental mode (ω_1). At the higher modes, when the tip mass is kept constant and the input voltage is varied, the curves overlap. This implies that the voltage has no effect on the natural frequencies.

In the 2nd mode of vibration shown in Figure 3.2c and 3.2d, when the input voltage is $\overset{-}{+}V = 500\text{V}$ and 1000V the gradient of the curves is approximately linear and the natural frequencies are impossible to differentiate to two decimal places, see Tables 3.2c and 3.2d. That only confirms that the piezo actuators has an insignificant effect on the higher modes of vibration and that only the fundumental mode can be controlled effectively. Lastly, the curves of Figures 3.2a to 3.2d are identical in the second mode of vibration regardless of the electric field induced.

Table 3.2c: 2nd frequencies of the beam with a tip mass and axial load: Voltage = 500V.

	Voltage = 500V/mm (ω_2)				
Axial load Ratio (k)	η = 0	η = 0.1	η = 1	η = 5	η =10
0.8	4.52	4.25	3.92	3.85	3.84
0.4	4.61	4.33	3.98	3.90	3.89
0	4.69	4.39	4.03	3.95	3.94
-1	4.87	4.55	4.15	4.06	4.05
-6	5.54	5.16	4.64	4.52	4.51
-10	5.92	5.52	4.94	4.81	4.79

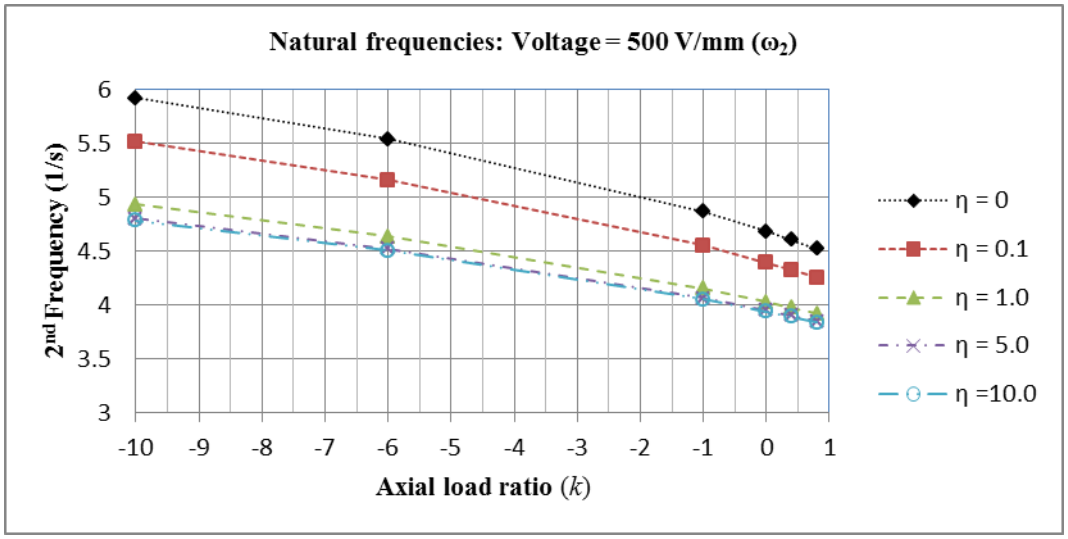

Figure 3.2c: Change in 2nd frequency vs axial load ratio: Voltage = 500V

Table 3.2d: 2nd frequencies of the beam with a tip mass and axial load: Voltage = 1000V.

	Voltage = 1000V/mm (ω_2)				
Axial load Ratio (k)	η = 0	η = 0.1	η = 1	η = 5	η =10
0.8	4.51	4.25	3.92	3.85	3.84
0.4	4.60	4.32	3.98	3.90	3.89
0	4.68	4.39	4.03	3.95	3.94
-1	4.86	4.55	4.15	4.06	4.05
-6	5.54	5.16	4.64	4.52	4.51
-10	5.92	5.52	4.94	4.81	4.79

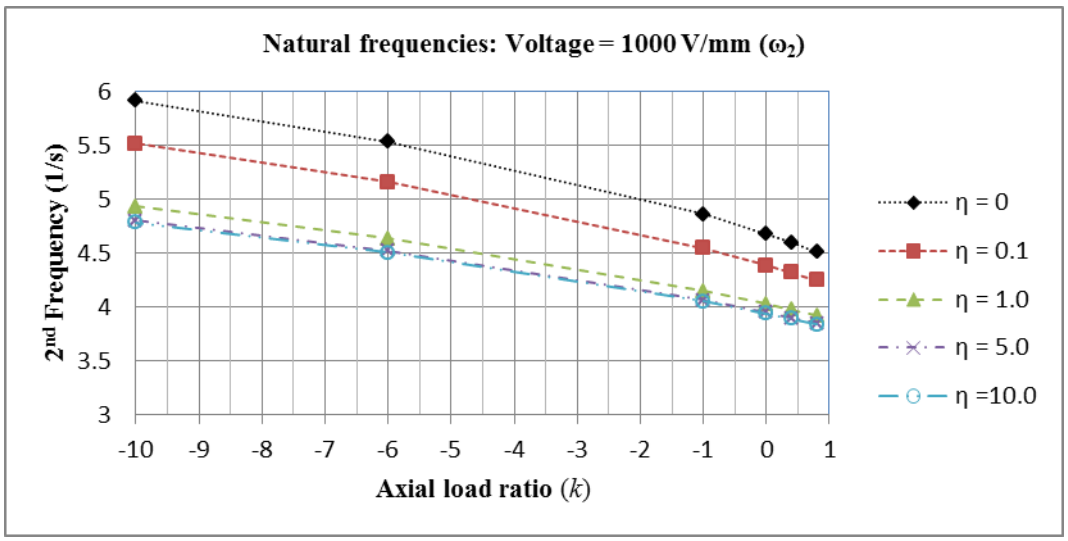

Figure 3.2d: Change in 2nd frequency vs axial load ratio: Voltage = 1000V

3.2.3 Third natural frequencies (ω_3)

In the 3rd mode of vibration when the tip mass is zero, the maximum natural frequency is ω_3 = 8.6870s^{-1} and the minimum natural frquency is ω_3 = 7.7750s^{-1} for axial load ratio k = -10 and k = +0.8 at zero voltage, respectively. The trends in the natural frequency are as previously observed in the first and second mode. The natual frequencies at maximum voltage ($\bar{+}V = 1000$V) are very similar as shown in Table 3.3a and 3.3d. It is also evident that for all k and η > 0.1, the natural frequencies are identical regardless of input voltage to the piezo actuators. The percentage change in the natural frequency is less than 0.1% for zero

tip mass ratio (η = 0) and decreases to less than 0.006% for tip mass ratio (η = 10), see Appendix A2.

Table 3.3a: 3rd frequencies of the beam with a tip mass and axial load: Voltage = 0V.

	Voltage = 0V/mm (ω_3)				
Axial load Ratio (k)	η = 0	η = 0.1	η = 1	η = 5	η =10
0.8	7.78	7.38	7.07	7.02	7.01
0.4	7.82	7.42	7.10	7.05	7.05
0	7.86	7.45	7.13	7.08	7.08
-1	7.95	7.54	7.21	7.16	7.15
-6	8.39	7.92	7.55	7.50	7.49
-10	8.69	8.19	7.80	7.74	7.73

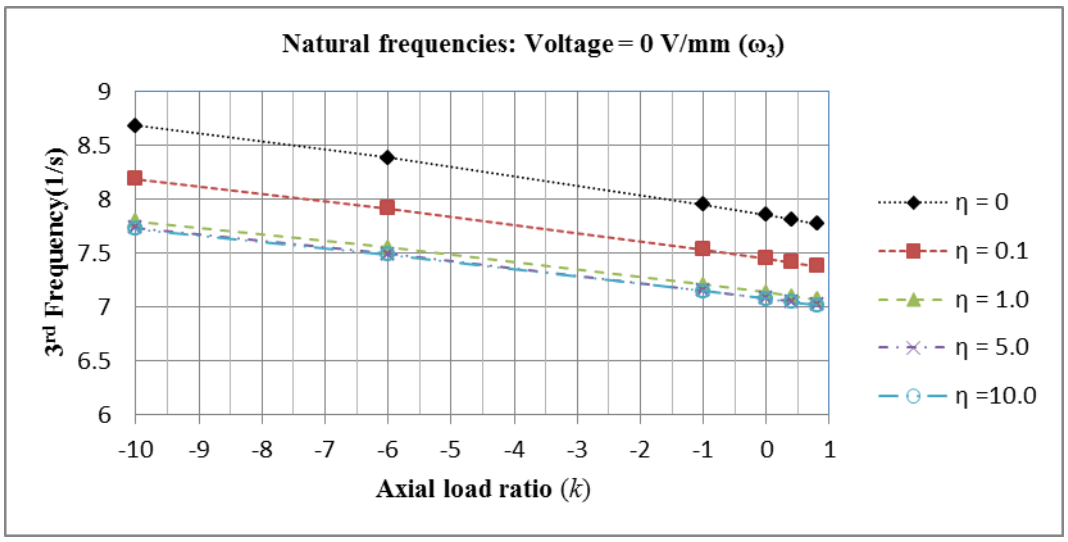

Figure 3.3a: Change in 3rd frequency vs axial load ratio: Voltage = 0V

From the data in Figures A1-1 to A3-4 in Appendix A1 to A3, it can be concluded that in the second, third and fourth modes of vibration , the piezo actuators have minimal control over the vibrations of the system. It is also observed from the Tables 3.3a to 3.4d, that the natural frequencies for the system are identical to two decimal places in the third mode. It is also noted that as the tip mass increseases the natural frqeuncies become identical for varying voltage inputs. That leads to the conclusion that as we increas the tip mass ratio, the piezo actuators have absolutly no effect vibrations of the beam and the tip mass is the dominant parameter. In Figures 3.2a to 3.2d it is noted that in the higher modes of vibratio the curves at tip mass ratio η = 5 and η = 10 overlap and the frequencies are identical.

Table 3.3b: 3rd frequencies of the beam with a tip mass and axial load: Voltage = 100V.

	Voltage = 100V/mm (ω_3)				
Axial load Ratio (k)	$\eta = 0$	$\eta = 0.1$	$\eta = 1$	$\eta = 5$	$\eta = 10$
0.8	7.77	7.38	7.07	7.02	7.01
0.4	7.81	7.42	7.10	7.05	7.05
0	7.85	7.45	7.13	7.08	7.08
-1	7.95	7.53	7.21	7.16	7.15
-6	8.39	7.92	7.55	7.50	7.49
-10	8.69	8.19	7.80	7.74	7.73

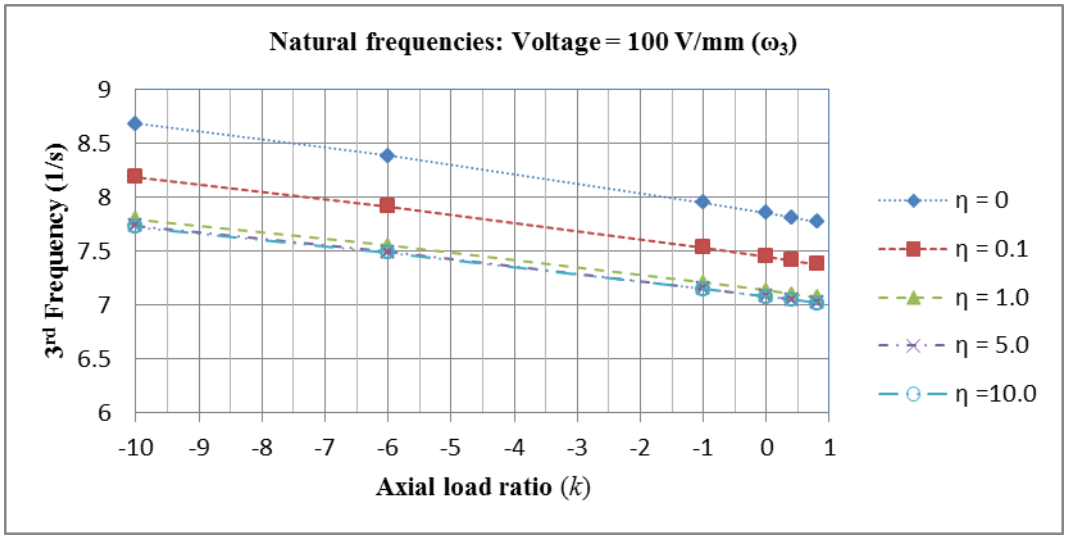

Figure 3.3b: Change in 3rd frequency vs axial load ratio: Voltage = 100V

This leads to the conclusion that beyond $\eta \geq 5$ the natural frequencies are constant or converge to a particular value. This further indicates that the cantilever starts to behave like a clamped-pinned beam because of the large mass at the tip.

Table 3.3c: 3rd frequencies of the beam with a tip mass and axial load: Voltage = 500V.

	Voltage = 500V/mm (ω_3)				
Axial load Ratio (k)	$\eta = 0$	$\eta = 0.1$	$\eta = 1$	$\eta = 5$	$\eta = 10$
0.8	7.77	7.38	7.07	7.02	7.01
0.4	7.81	7.42	7.10	7.05	7.05
0	7.85	7.45	7.13	7.08	7.08
-1	7.95	7.53	7.21	7.16	7.15
-6	8.38	7.92	7.55	7.50	7.49
-10	8.69	8.19	7.80	7.74	7.73

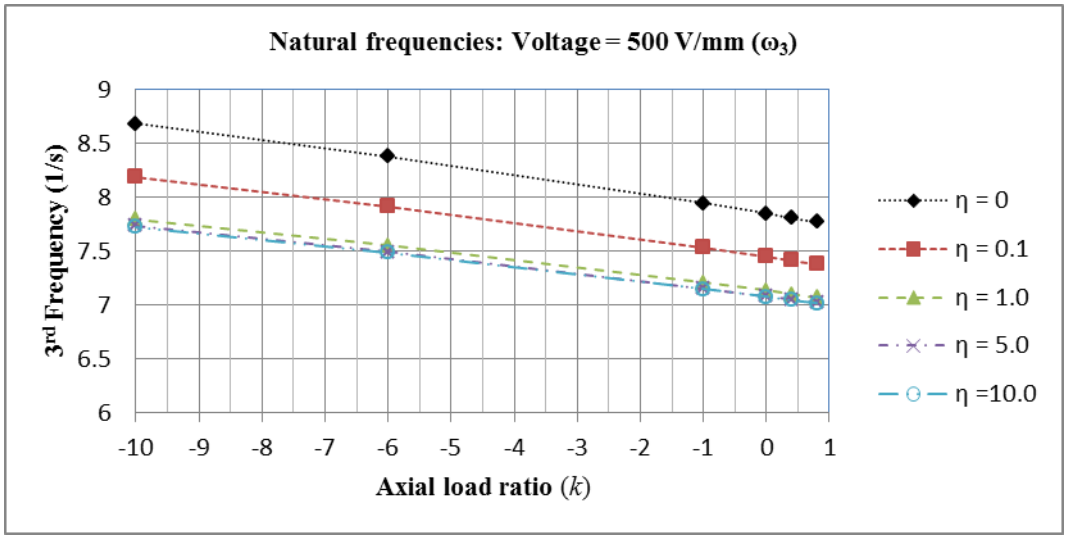

Figure 3.3c: Change in 3rd frequency vs axial load ratio: Voltage = 500V

Table 3.3d: 3rd frequencies of the beam with a tip mass and axial load: Voltage = 1000V.

	Voltage = 1000V/mm (ω_3)				
Axial load Ratio (k)	$\eta = 0$	$\eta = 0.1$	$\eta = 1$	$\eta = 5$	$\eta = 10$
0.8	7.77	7.38	7.07	7.02	7.01
0.4	7.81	7.41	7.10	7.05	7.05
0	7.85	7.45	7.13	7.08	7.08
-1	7.95	7.53	7.21	7.16	7.15
-6	8.38	7.92	7.55	7.50	7.49
-10	8.68	8.19	7.80	7.74	7.73

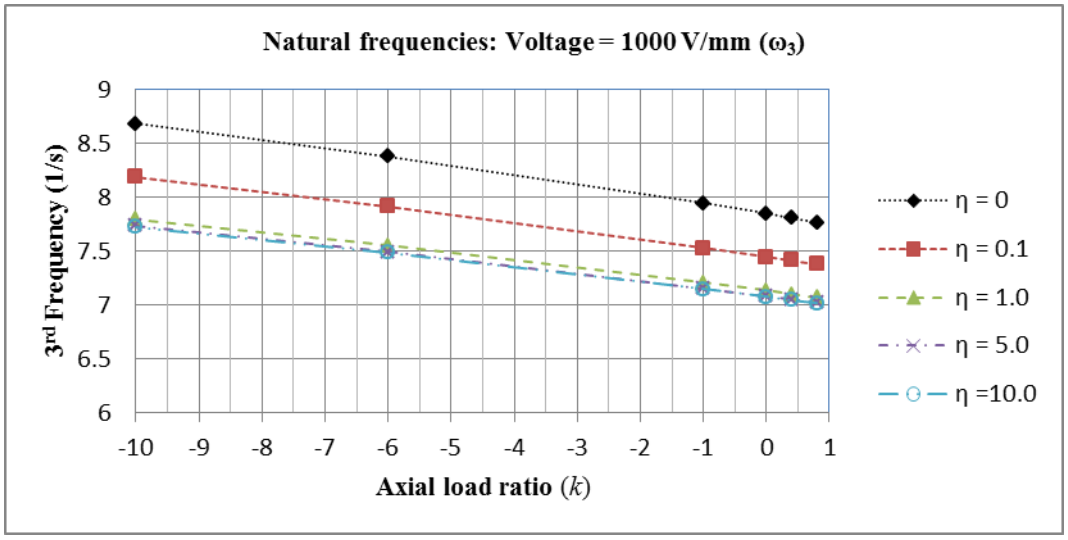

Figure 3.3d: Change in 3rd frequency vs axial load ratio: Voltage = 1000V

3.2.4 Fourth natural frequencies (ω_4)

In the 4th mode of vibration the natural frequency band is between $10s^{-1}$ and $11s^{-1}$, see Figures 3.4a to 3.4d. The percantage differences in the natural frequency for zero tip mass (η = 0) to maximum tip mass ratio (η = 10) for a maximum compressive load (k = +0.8) and maximum tension (k = -10) are approximately 7% in the fourth mode compared to about 60% in the first mode for an uncontrolled beam ($\bar{+}V = 0\text{V}$).

Table 3.4a: 4th frequencies of the beam with a tip mass and axial load: Voltage = 0V.

	Voltage = 0V/mm (ω_4)				
Axial load Ratio (k)	η = 0	η = 0.1	η = 1	η = 5	η =10
0.8	10.94	10.47	10.21	10.18	10.17
0.4	10.97	10.50	10.23	10.20	10.19
0	11.00	10.52	10.26	10.22	10.22
-1	11.06	10.58	10.31	10.27	10.27
-6	11.37	10.86	10.57	10.53	10.53
-10	11.60	11.06	10.77	10.73	10.72

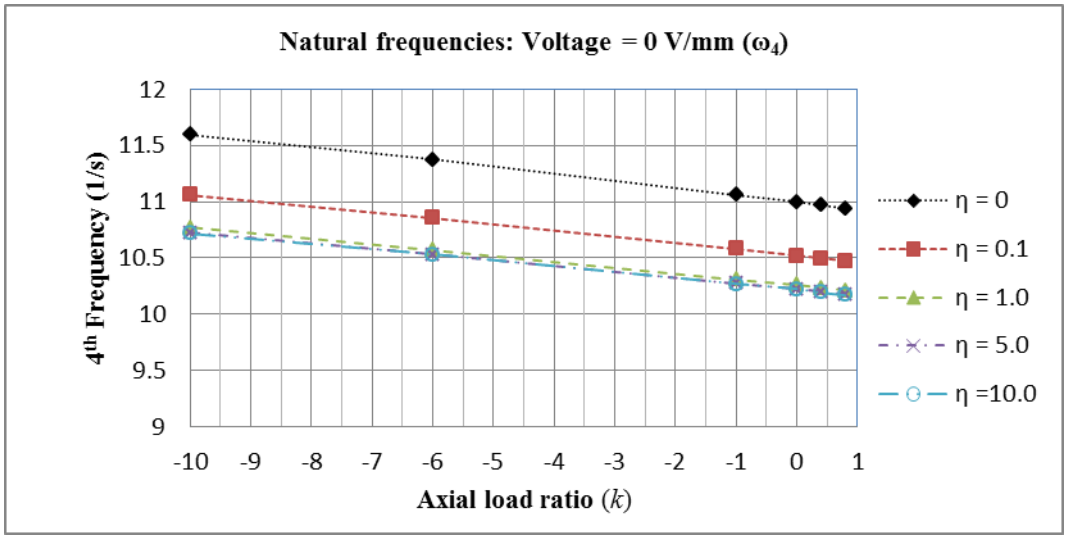

Figure 3.4a: Change in 4th frequency vs axial load ratio: Voltage = 0V

As the mode number increases the frequency band narrows from 60% to 23% to 10% and to 7% in the 1st , 2nd , 3rd and 4th modes of vibration, respectively. For a controlled beam ($\bar{+}V = 1000\text{V}$) the frequency is approximaely 78% in the 1st mode and 7% in the fourth

mode. In the fourth mode the difference is approximately 7% for both uncontrolled and controlled beam. This shows the eneffectiveness of the piezo actuators in the higher modes. These frequencies will converge as the mode number increases to infinity, $n \rightarrow \infty$. In the higher modes, when the axial load is kept constant and the tip mass is increased steadily, the difference in succesive frequencies becomes smaller, see Table A1a to A3e in Appendix A1 to A3.

Table 3.4b: 4th frequencies of the beam with a tip mass and axial load: Voltage = 100V.

	Voltage = 100V/mm (ω_4)				
Axial load Ratio (k)	η = 0	η = 0.1	η = 1	η = 5	η =10
0.8	10.94	10.47	10.21	10.18	10.17
0.4	10.97	10.50	10.23	10.20	10.19
0	11.00	10.52	10.26	10.22	10.22
-1	11.06	10.58	10.31	10.27	10.27
-6	11.37	10.86	10.57	10.53	10.53
-10	11.60	11.06	10.77	10.73	10.72

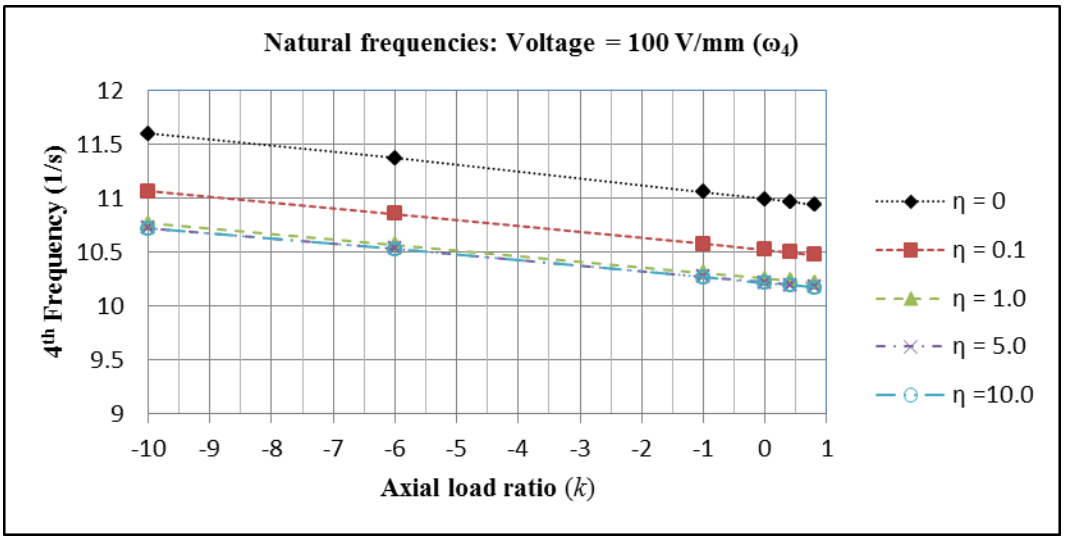

Figure 3.4b: Change in 4th frequency vs axial load ratio: Voltage = 100V

The largest natural frequency for different tip mass ratios always occurs at tensile axial load ratio, when the beam is in tension at a load ratio of k = -10. On the other side of the load ratio spectrum, when the beam is in compression and the beam approaches the buckling load the natural frequencies are smallest.

Table3.1a to Table 3.4d indicate the natural frequncies of the beam with a voltage induced on the top and bottom pieazo actuator. The natural frequencies for the beam increase as we increase the axial load and decrease as we increase the tip mass ratio. The effect of the piezo acutuator is lost when the tensile axial ratio is greater than k = -1.

For the higher modes of vibration, the difference in natural frequency is minimal indicating that the piezo has no effect on the vibation frequencies and that only the first mode of vibration can be significantly altered using a piezo actuator. This is the fundamental mode of vibration which is dominant over the other mode. This also lends it suitable for distributed parameter system control (Bailey *et al*., 1985).

Table 3.4c: 4th frequencies of the beam with a tip mass and axial load: Voltage = 500V.

	Voltage = 500V/mm (ω_4)				
Axial load Ratio (k)	η = 0	η = 0.1	η = 1	η = 5	η =10
0.8	10.94	10.47	10.21	10.18	10.17
0.4	10.97	10.50	10.23	10.20	10.19
0	10.99	10.52	10.26	10.22	10.22
-1	11.06	10.58	10.31	10.27	10.27
-6	11.37	10.86	10.57	10.53	10.53
-10	11.60	11.06	10.77	10.73	10.72

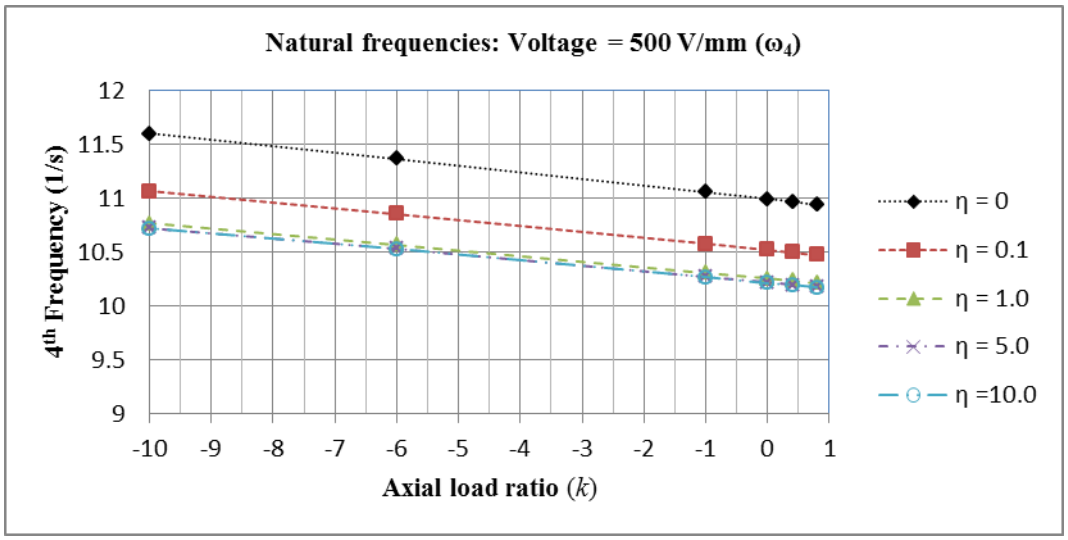

Figure 3.4c: Change in 4th frequency vs axial load ratio: Voltage = 500V

Table 3.4d: 4th frequencies of the beam with a tip mass and axial load: Voltage = 1000V.

	Voltage = 1000V/mm (ω_4)				
Axial load Ratio (k)	$\eta = 0$	$\eta = 0.1$	$\eta = 1$	$\eta = 5$	$\eta = 10$
0.8	10.94	10.47	10.21	10.18	10.17
0.4	10.97	10.50	10.23	10.20	10.19
0	10.99	10.52	10.26	10.22	10.22
-1	11.06	10.58	10.31	10.27	10.27
-6	11.37	10.86	10.57	10.53	10.53
-10	11.60	11.06	10.77	10.73	10.72

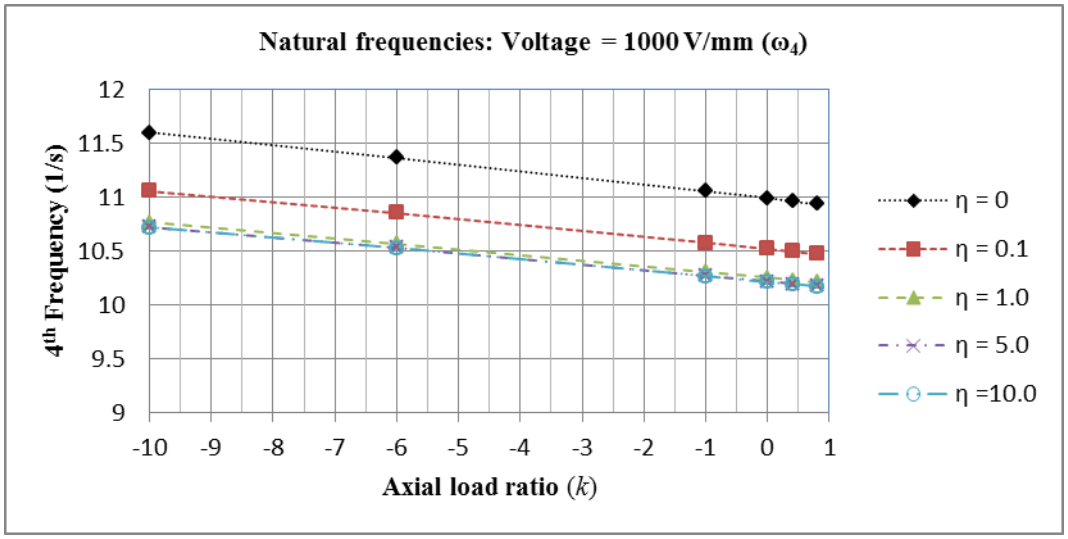

Figure 3.4d: Change in 4th frequency vs axial load ratio: Voltage = 1000V

3.3 Change in natural frequencies for varying axial load, tip mass and voltage

3.3.1 First natural frequencies (fundamental mode)

This section covers the discussion on the changes caused by application of voltage on the natural frequencies of the system. This study concentrates on the first four frequencies (1st, 2nd, 3rd and 4th modes) of the system, where the 1st frequency is the fundamental frequency of the system and dominates all the other modes of vibration. Tables 3.5a to 3.5d show the natural frequencies for particular tip mass ratio, varying axial load ratio and the percentage change in the natural frequencies of the system of an inactive beam ($\bar{V}_+ = 0$V)

and for a beam with active piezo actuators for varying input voltages ($^{-}_{+}V = 100\text{V}, 500\text{V}$ and 1000V).

The aim is to quantify the change in the natural frequency between an inactive ($^{-}_{+}V = 0\text{V}$) and an active beam ($^{-}_{+}V = 100\text{V}, 500\text{V}$ and 1000V) The percentage change is derived by using equation 3.2 below, where $(\omega_n)^i_k$ represents the natural frequency for a particular tip mass ratio (i = 0, 0.1, 1, 5, 10), axial load ratio (k = +0.8, 0, -1, -6, -10) and ($\omega_{V=j}$) is the natural frequency for the varying input voltage (j = 100V , 500V , 1000V).

$$\%\Delta\text{natural frequency}\,(\omega_n)^i_k = \frac{\omega_{V=0} - \omega_{V=j}}{\omega_{V=0}} \times 100 \tag{3.2}$$

From Figures 3.5a to 3.5d we can observe that there is a change in the natural frequency of the beam for the different voltage input, axial load ratio and tip mass ratio. In the first mode of vibration a maximum change of frequency of approximately 44% for $^{-}_{+}V = 1000\text{V}$ input is observed. This high percentage change can be observed when there is a compressive load and decreases as the column is subjected to a tensile load.

From the Figures 3.5a to 3.5d, in the 1st mode of vibration, we can see that the piezo loses its effectiveness and the percentage change in the natural frequency drop to below 2% when the axial load ratio exceeds k = -1. Beyond that the piezo has an insignificant effect on the natural frequency. The effects of the piezo actuator are of importance between k = +0.8 to k = -2. The maximum tensile load for this study will thus be limited to an axial load ratio k = -2, beyond which the beam conforms to the characteristics of an uncontrolled beam. The percentage changes are approximately 2%. The percentage change can be increased at these values for axial load ratio and tip mass ratio by increasing thickness of the piezo layers. This allows for an increased voltage input which in turn alters the moments at the boundaries which directly affects the natural frequencies.

Table 3.5a: 1st Mode frequencies (ω_1) with tip mass ratio, $\eta = 0$

Axial load Ratio (k)	ω_1 V=0V	ω_1 V=100V	$\Delta\%\ \omega_1$ V=100V	ω_1 V=500V	$\Delta\%\ \omega_1$ V=500V	ω_1 V=1000V	$\Delta\%\ \omega_1$ V=1000V
0.8	1.27	1.25	2.15	1.11	12.62	0.66	44.47
0.4	1.66	1.65	0.66	1.61	3.45	1.54	7.39
0	1.88	1.87	0.36	1.84	1.90	1.80	3.97
-1	2.19	2.19	0.16	2.18	0.82	2.16	1.68
-6	2.87	2.87	0.01	2.86	0.13	2.86	0.28
-10	3.15	3.15	0.03	3.15	0.09	3.14	0.17

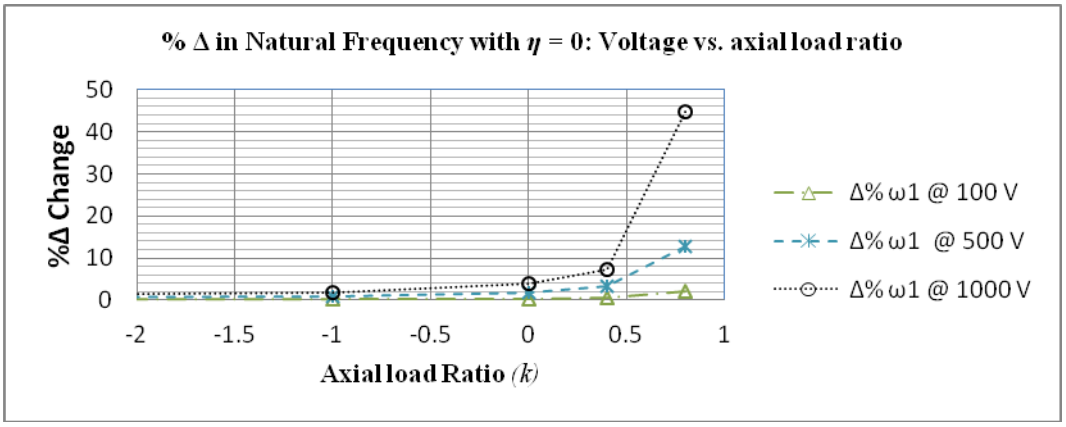

Figure 3.5a: Percentage change in natural frequency ($\eta = 0$)

Table 3.5b: 1st Mode frequencies (ω_1) with tip mass ratio, $\eta = 0.1$

Axial load Ratio (k)	ω_1 V=0V	ω_1 V=100V	$\Delta\%\ \omega_1$ V=100V	ω_1 V=500V	$\Delta\%\ \omega_1$ V=500V	ω_1 V=1000V	$\Delta\%\ \omega_1$ V=1000V
0.8	1.17	1.14	2.17	1.02	12.71	0.66	37.08
0.4	1.52	1.51	0.66	1.47	3.52	1.41	7.53
0	1.72	1.72	0.38	1.69	1.98	1.65	4.12
-1	2.03	2.02	0.18	2.01	0.90	1.99	1.82
-6	2.68	2.68	0.04	2.67	0.18	2.67	0.34
-10	2.96	2.96	0.03	2.95	0.11	2.95	0.21

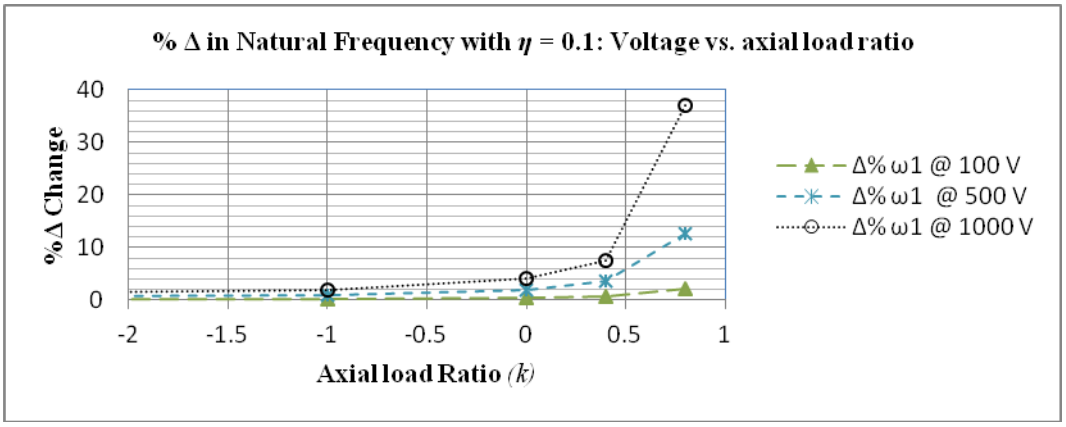

Figure 3.5b: Percentage change in natural frequency ($\eta = 0.1$)

Table 3.5c: 1st Mode frequencies (ω_1) with tip mass ratio, η = 1

Axial load Ratio (k)	ω_1 V=0V	ω_1 V=100V	$\Delta\%\ \omega_1$ V=100V	ω_1 V=500V	$\Delta\%\ \omega_1$ V=500V	ω_1 V=1000V	$\Delta\%\ \omega_1$ V=1000V
0.8	0.84	0.82	2.17	0.73	12.79	0.53	37.23
0.4	1.10	1.09	0.73	1.06	3.67	1.02	7.79
0	1.25	1.24	0.42	1.22	2.10	1.19	4.35
-1	1.48	1.47	0.19	1.46	0.98	1.45	2.00
-6	1.99	1.99	0.04	1.99	0.23	1.98	0.48
-10	2.22	2.21	0.03	2.21	0.15	2.21	0.30

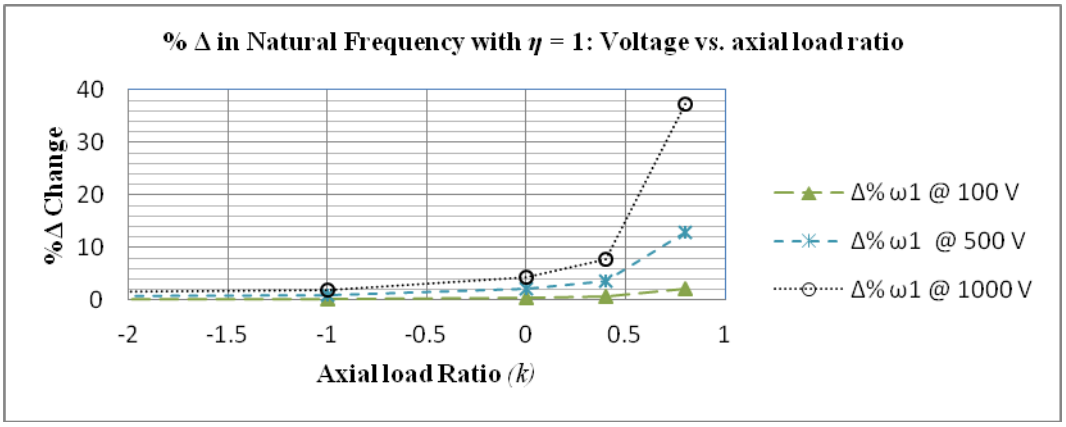

Figure 3.5c: Percentage change in natural frequency (η = 1)

Table 3.5d: 1st Mode frequencies (ω_1) with tip mass ratio, η = 5

Axial load Ratio (k)	ω_1 V=0V	ω_1 V=100V	$\Delta\%\ \omega_1$ V=100V	ω_1 V=500V	$\Delta\%\ \omega_1$ V=500V	ω_1 V=1000V	$\Delta\%\ \omega_1$ V=1000V
0.8	0.58	0.57	2.19	0.51	12.83	0.37	37.27
0.4	0.77	0.76	0.69	0.74	3.66	0.71	7.80
0	0.87	0.87	0.43	0.85	2.14	0.83	4.41
-1	1.03	1.03	0.18	1.02	0.99	1.01	2.04
-6	1.40	1.40	0.06	1.39	0.27	1.39	0.54
-10	1.56	1.56	0.07	1.55	0.20	1.55	0.36

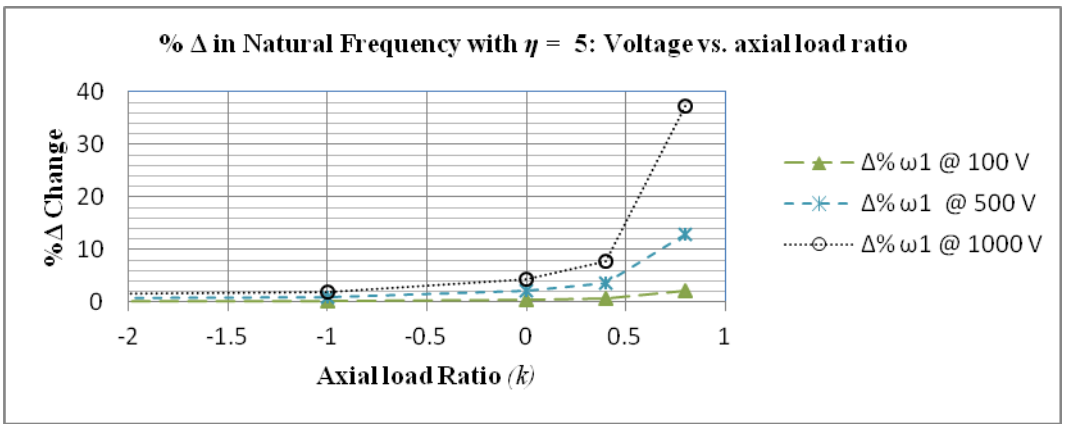

Figure 3.5d: Percentage change in natural frequency (η = 5)

3.3.2 2nd, 3rd and 4th Natural frequency (higher modes)

In the higher modes of vibration, Figures A1-1 to A3-5 in Appendix A1 to A3, it is observed that the piezo has very little or no effect on the frequencies of vibration of the beam. In the second mode of vibration we have a maximum percentage change in natural frequency of 0.4%. From Figures A1-1 to A3-5 it is also noticed that the percentage change decreases to less than 0.02%, as the tip mass ratio increases. The natural frequencies versus axial load at different tip masses indicate that they have a monotonic relation. An increase in the load in tension results in an increase in the natural frequency of the mode of vibration, but as the tip mass increases the natural frequency decreases.

The voltage induced on the piezo layers causes a contraction or extension of the two layers, i.e. bottom and top layer. The resultant strain induces a moment on the beam at the boundaries, and therefore causes a change in the natural frequencies of the beam. The percentage change in the natural frequencies of the beam due to the magnitude of the input voltage is tabulated in Appendix A1 to A3. Another observation is that for a constant tip mass ratio and varying voltage input the curves are stacked on top of each other. The only explanation is that the varying voltage input ($0\text{V} < \overset{-}{+}V \leq 1000\text{V}$) does not have an effect on the natural frequencies of the beam in the 2nd, 3rd and 4th mode of vibration.

3.4 Natural frequencies versus change in tip mass

To investigate the change in natural frequencies of the beam due to the change in tip mass; the change in frequency versus tip mass is plotted in Figures 3.6a to 3.6d, and the natural frequency at zero tip mass is compared with the natural frequencies as the tip mass is varied for a particular axial load. An increase in the induced voltage on the piezo layers significantly changes in the fundamental natural frequencies but the effects become less pronounced in the higher modes. The percentage change can be calculated in the following relation:

$$\%\Delta\text{natural frequency}\left(\omega_n\right)_i^k = \frac{\omega_{\eta=0} - \omega_{\eta=j}}{\omega_{\eta=0}} \times 100 \tag{3.3}$$

where ($\omega_{\eta=j}$) represents the natural frequency for a particular tip mass ratio (j = 0, 0.1, 1, 5), axial load ratio (k = +0.8, 0, -1, -6, -10) and $(\omega_n)_i^k$ is the natural frequency for the varying input voltage (i = 0, 100V, 500V, 1000V).

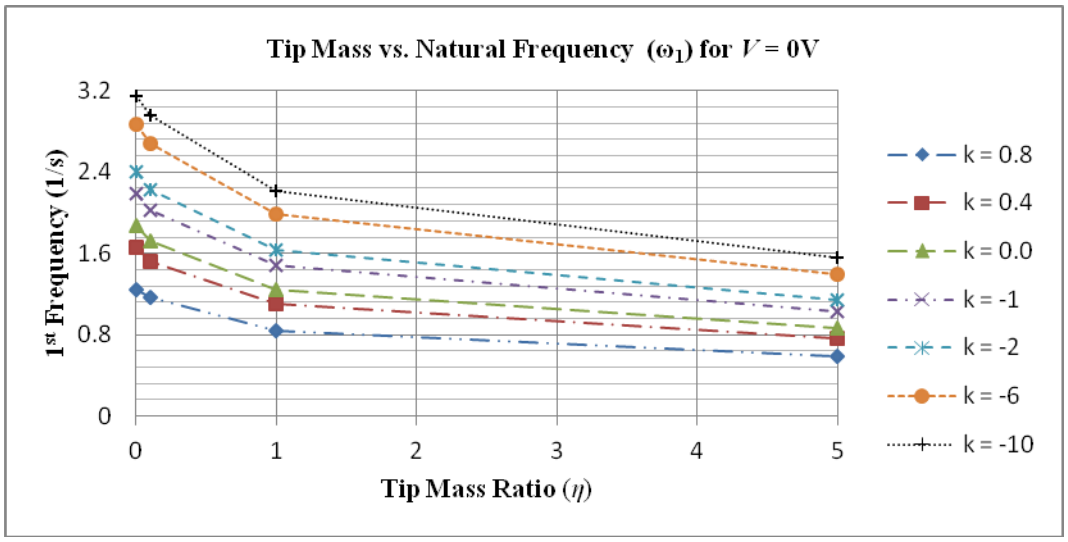

Figure 3.6a: 1st Frequency vs tip mass ratio: Voltage = 0V

When the tip mass ratio is increased in the first mode there is approximately 60% maximum decrease in natural frequency and approximately 20%, 12% and 8% in the 2nd, 3rd and 4th mode, respectively. The slope of the graphs in Figures 3.6a to 3.9d, is much steeper when the tip mass ratio is between (η = 0) and (η = 1) and decreases as the maximum tip mass ratio is approached. As the tip mass ratio increases the slope decreases and the change in natural frequency for an additional mass becomes small. As tip mass ratio increases the beam starts to behave like a clamped-pinned beam (Balachandran *et al.*, 2009).

In the higher modes the slope also levels off when the tip mass ratio goes beyond (η = 1). It is also observed that effective piezo control can be achieved in the fundamental mode (1st mode), because the largest changes in frequency occur in this mode. This is evident when the graphs at zero voltage ($\bar{+}V = 0\text{V}$) Figure 3.6a and at maximum voltage ($\bar{+}V = 1000\text{V}$) Figure 3.6d are compared for the 1th mode frequencies the curves in the graphs are different. Whereas, Figure 3.9a and 3.9d are the plots for the 4th mode frequencies at zero and maximum voltage and the graphs are almost identical.

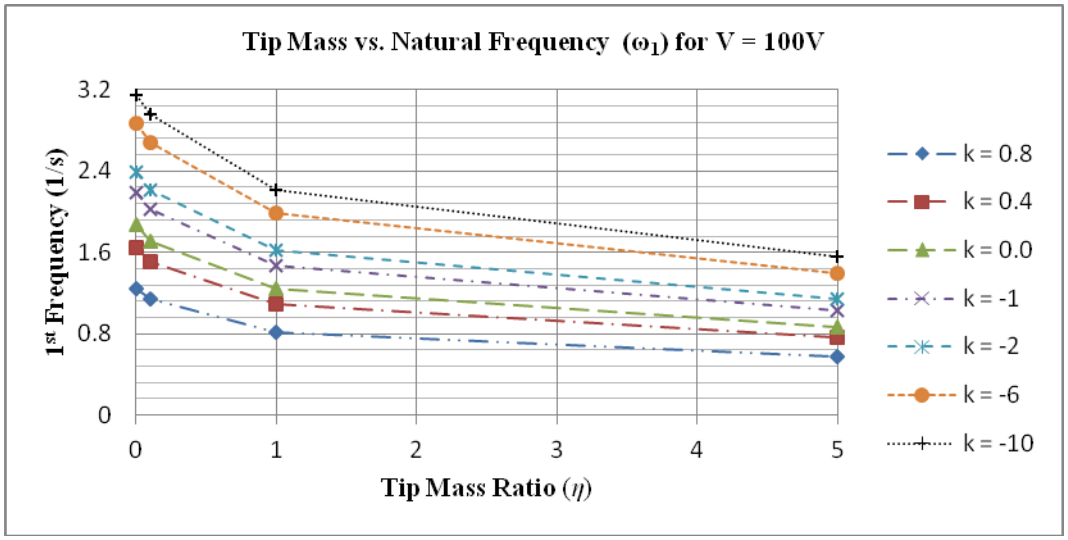

Figure 3.6b: 1st Frequency vs tip mass ratio: Voltage = 100V

The highest natural frequencies (ω = 3.149s^{-1}) occurs when the beam is under tension at (k = -10) and there is zero tip mass (η = 0). When an input voltage of 1000V is applied to the piezo, there is only a slight change in the natural frequency (ω = 3.1438s^{-1}) or 0.17% change.

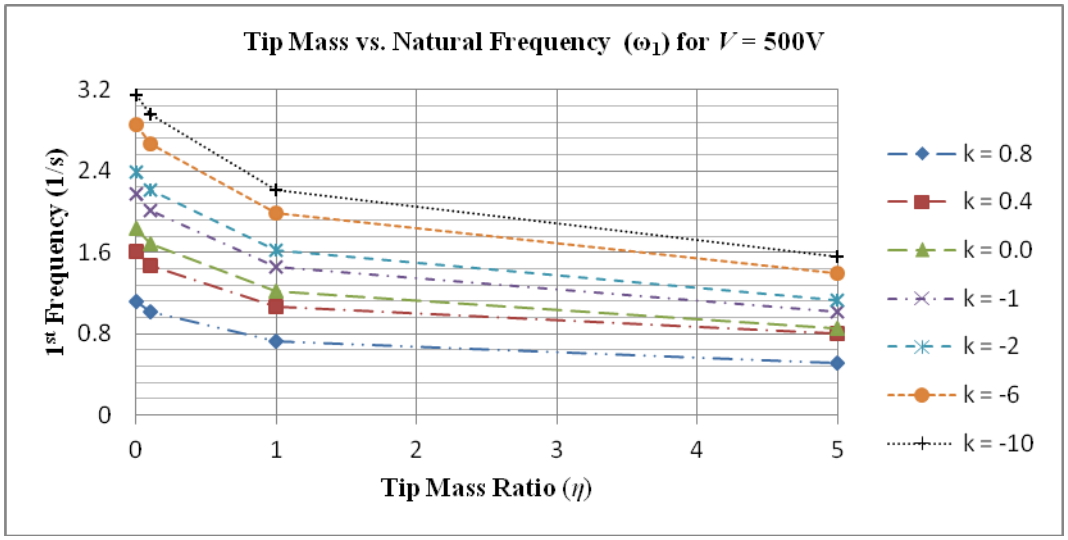

Figure 3.6c: 1st Frequency vs tip mass ratio: Voltage = 500V

This indicates that the piezo produces no noticeable change in the vibration characteristics of the structure. However, when the beam is subject to a compressive axial load (k = +0.8) at zero tip mass ratio (η = 0), the natural frequency when the piezo layers are inactive ($^{-}_{+}V = 0V$) is (ω = 1.2744 s^{-1}), see Figure 3.6a. When an input voltage ($^{-}_{+}V = 1000\text{V}$) is

applied to the bottom and top layer, the natural frequency is significantly reduced to (ω = 0.7051s^{-1}). That represents a change of 44% reduction in the natural frequency.

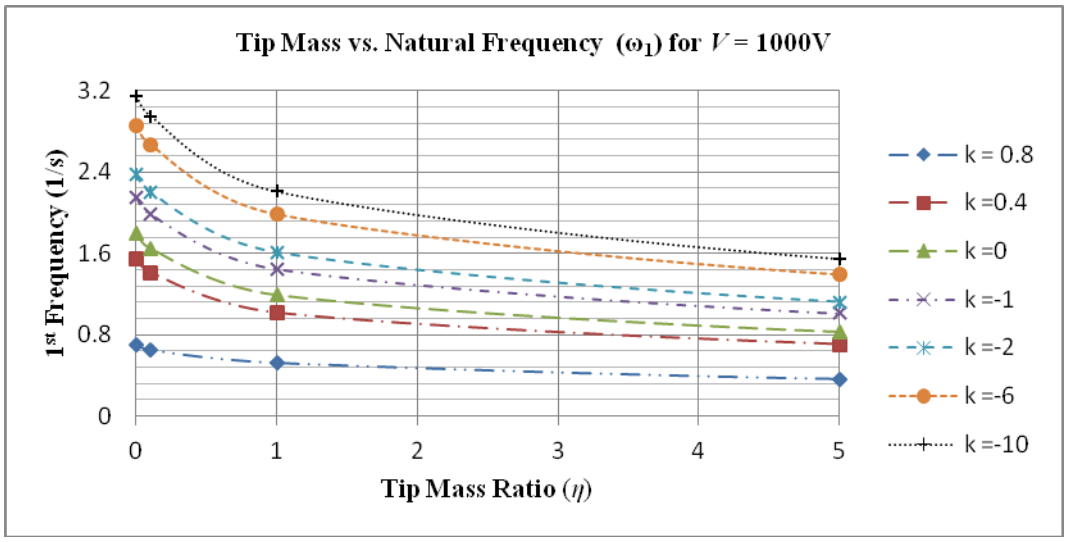

Figure 3.6d: 1st Frequency vs tip mass ratio: Voltage = 1000V

When adding an incremental tip mass there is approximately 8%, 38% and 55% drop in the natural frequencies from the reference point (η = 0) for tip mass ratio of η = 0.1, 1, and 5 respectively. Beyond a tip mass ratio of η = 5 the slope of the curves flatten, which means that a large change in tip mass ratio is required for a slight change in the frequency. So then, as tip mass ratio increases the frequency converges to some value in the limit as $n \to \infty$. This occurs for all the various voltage input to the piezo actuators.

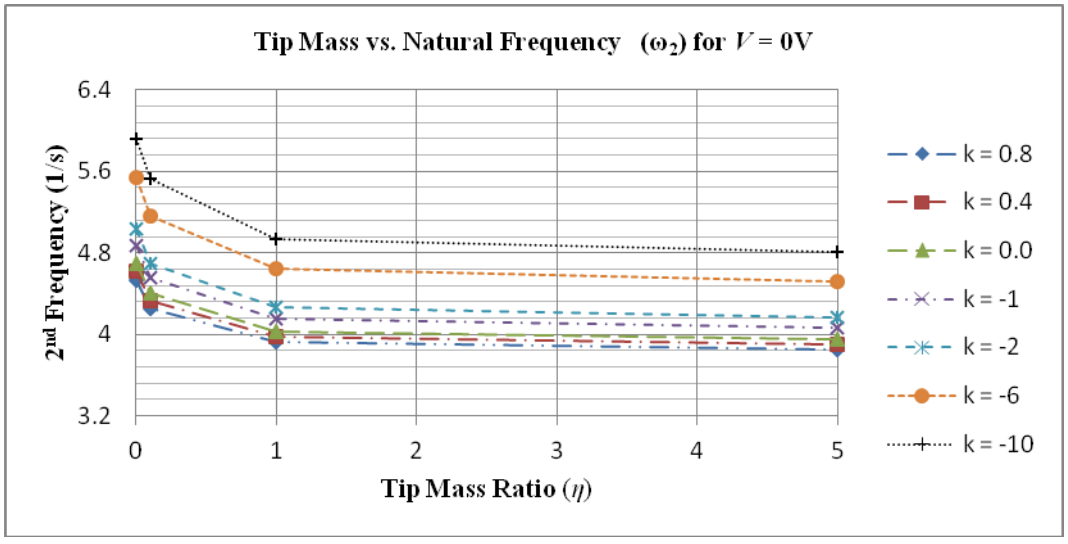

Figure 3.7a: 2nd Frequency vs tip mass ratio: Voltage = 0V

At maximum voltage input ($\overset{-}{+}V = 1000\text{V}$) the frequencies are lower when the beam is in maximum compression (k = +0.8). Figure 3.6a to 3.9d, show that the curves for maximum compressive load are always at the bottom of the set of curves.

At maximum tensile load (k = -10) and zero tip mass ratio (η = 0), the frequencies are the same for the various voltage inputs, indicating the piezo is ineffective. The percentage difference between a beam with zero voltage and a beam with maximum voltage input is 0.33%. In Figure 3.6a and Figure 3.6d, the bottom most curves are different in values when the system is undergoing a compressive load. The top most curves are due the maximum tensile load (k = -10) and again a comparison of the above mentioned figures shows that the curves are identical. This indicates that at maximum tensile load the frequency are not affected by the piezo.

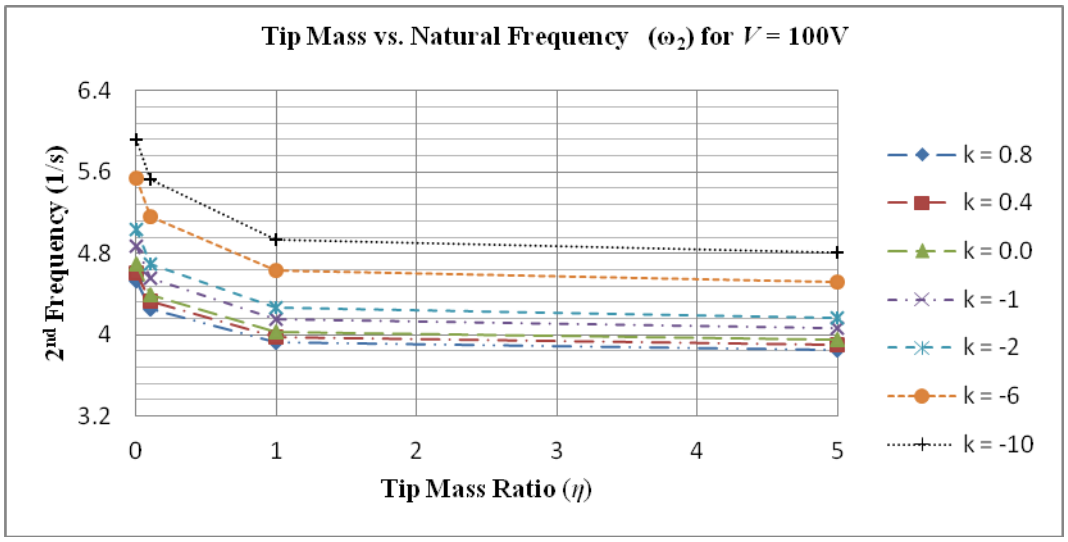

Figure 3.7b: 2nd Frequency vs tip mass ratio: Voltage = 100V

The gradient of the graphs Figure 3.7a to 3.7d decreases as the tip mass ratio increases for the 2nd mode of vibration. This indicates that as the tip mass increases, the percentage change in natural frequency converge. This will resemble a clamped pinned beam (Tse *et al.*, 1979) in the limit as $\eta \rightarrow \infty$.

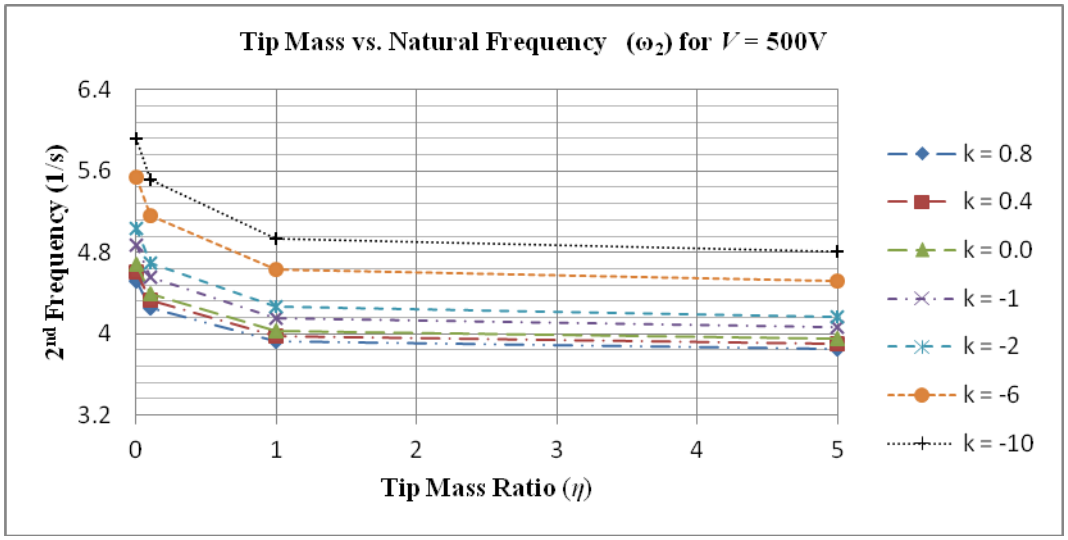

Figure 3.7c: 2nd Frequency vs tip mass ratio: Voltage = 500V

In the 1st mode of vibration Figure 3.6a to 3.6d it is noted that there is a change in gradient as the tip mass ratio of the curves approaches maximum tip mass, $\eta \rightarrow 5$. This indicates that the first natural frequencies of the system will change beyond maximum tip mass ratio ($\eta = 5$), although the difference gets smaller as the tip mass ratio increases.

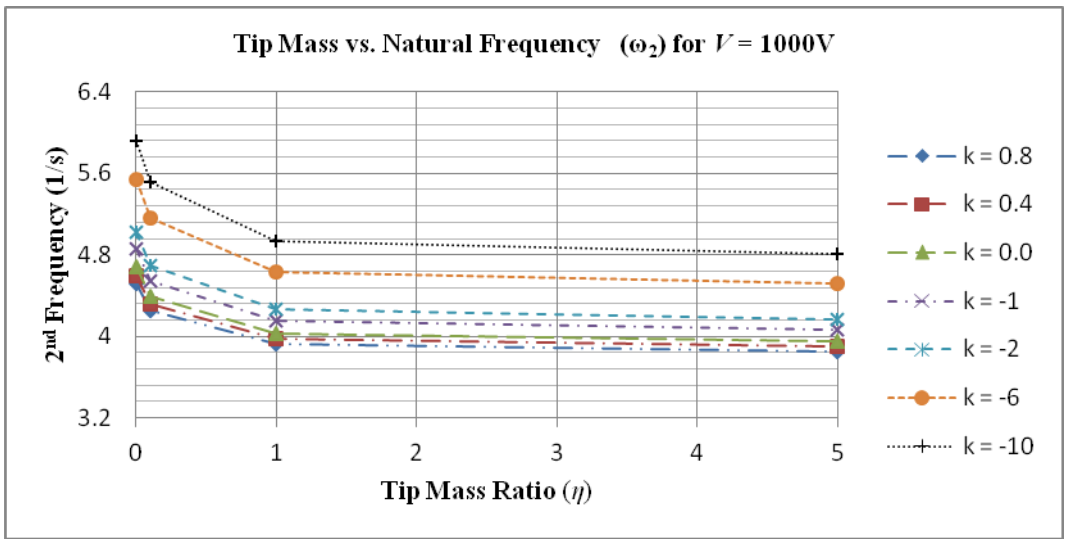

Figure 3.7d: 2nd Frequency vs tip mass ratio: Voltage = 1000V

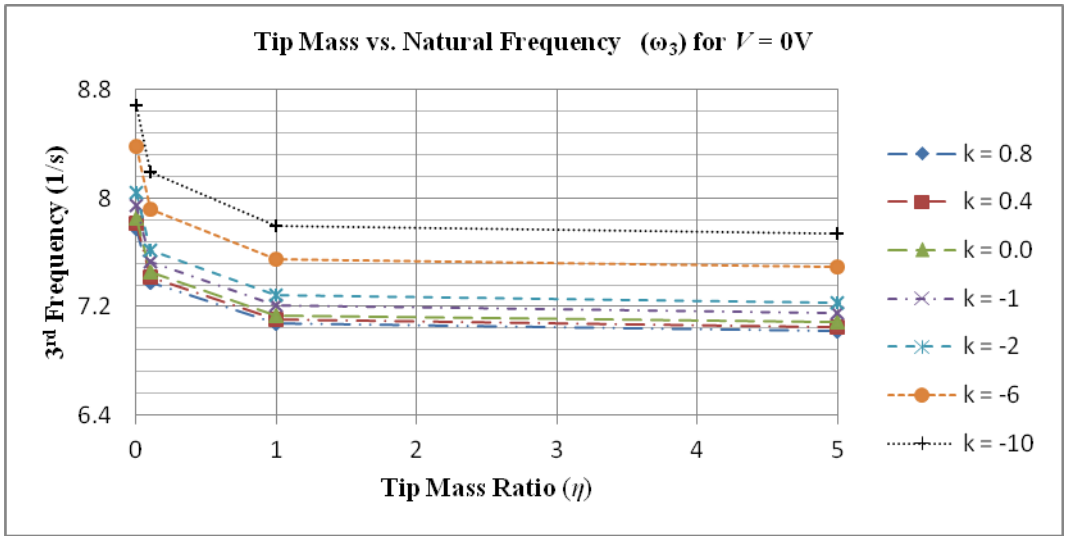

Figure 3.8a: 3rd Frequency vs tip mass ratio: Voltage = 0V

In the 2nd, 3rd, 4th modes of vibration Figure 3.7a to 3.9d the gradient approaches zero when the tip mass ratio (η) is approximately 1. Beyond this point the tip mass dominates the other parameter. For this reason, the maximum tip mass ratio for this investigation was limited to $\eta \leq 5$.

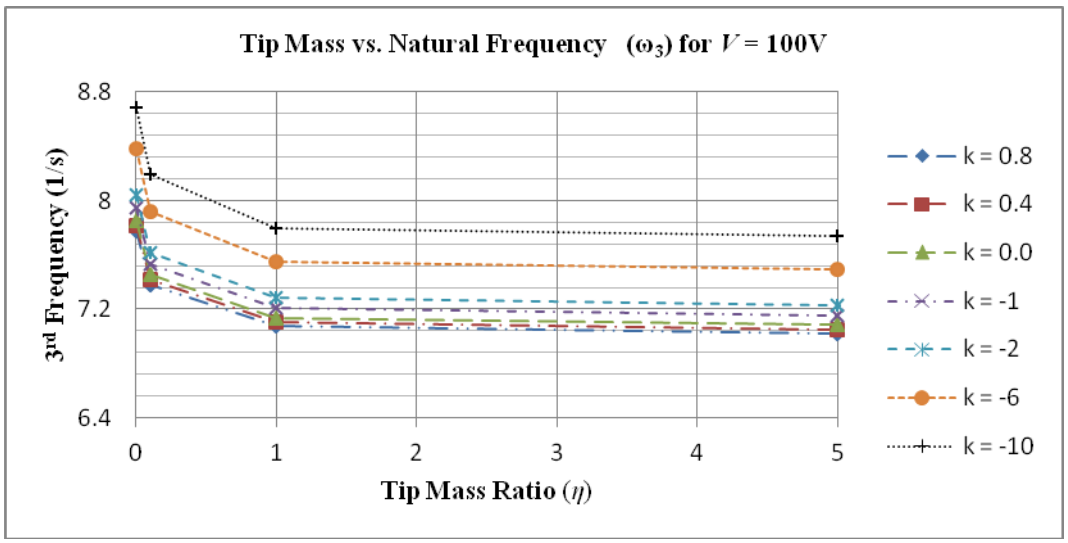

Figure 3.8b: 3rd Frequency vs tip mass ratio: Voltage = 100V

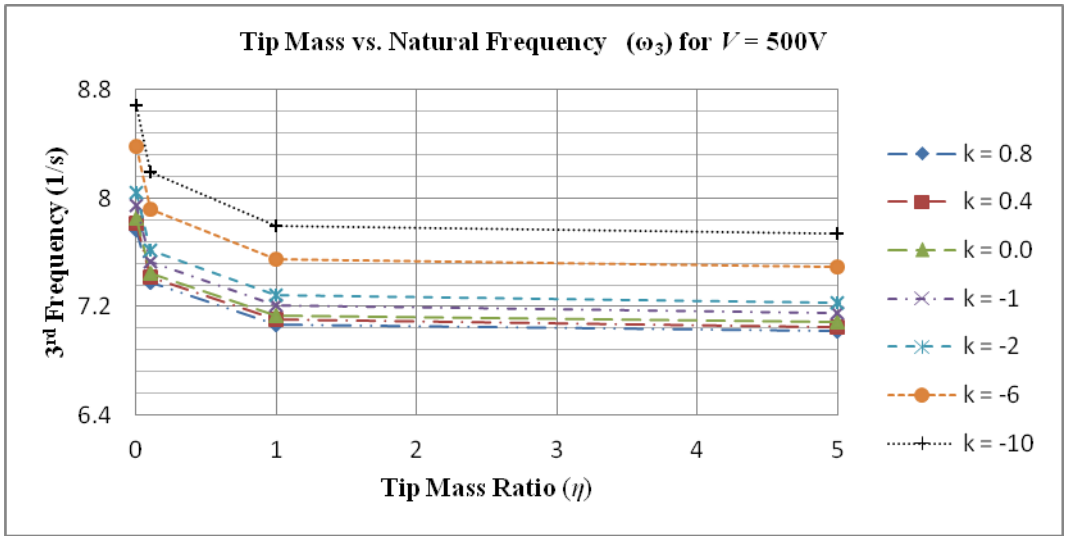

Figure 3.8c: 3rd Frequency vs tip mass ratio: Voltage = 500V

In the 3rd and 4th mode of vibration when the tip mass ratio is beyond η = 1 the gradient of the curves flattens out and the other parameters have an insignificant effect on the frequencies, Figure 3.8a to 3.9d. The increase in voltage input to the piezo actuators does not induce enough strain to alter the vibration characteristics of the system.

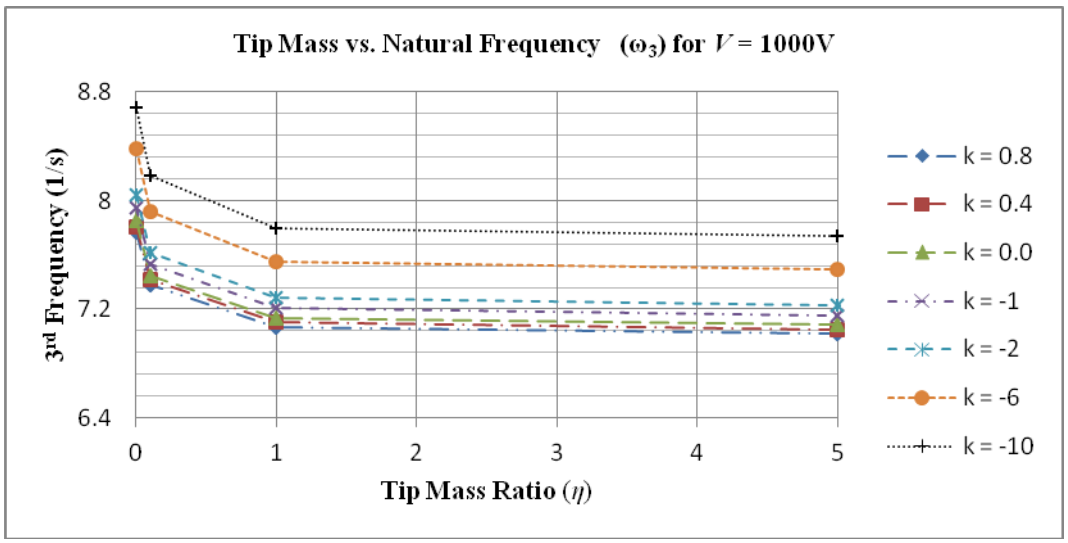

Figure 3.8d: 3rd Frequency vs tip mass ratio: Voltage = 1000V

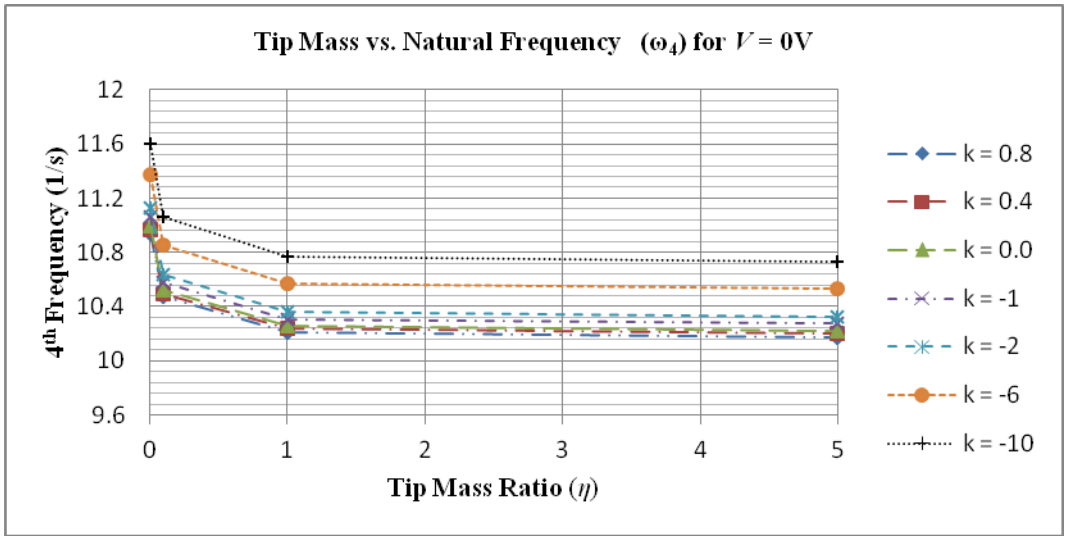

Figure 3.9a: 4th Frequency vs tip mass ratio: Voltage = 0V

When the axial load ratio (k) is constant and the input voltage is varied the percentage change in frequency, between inactive ($\bar{+}V = 0\text{V}$) beam and an active one ($\bar{+}V = 100\text{V}, 500\text{V}$ and 1000V) can be determined. This percentage change drops as the axial load is increased up to k = -1, and thereafter remains constant as the axial load is increased. If the fundamental frequencies (ω_1) are excluded, the largest percentage change in natural frequency ($\Delta\% = 0.3894$) occurs in the 2nd mode of vibration at maximum voltage input and axial load ratio of k = +0.8, see the tables in Appendix A1.

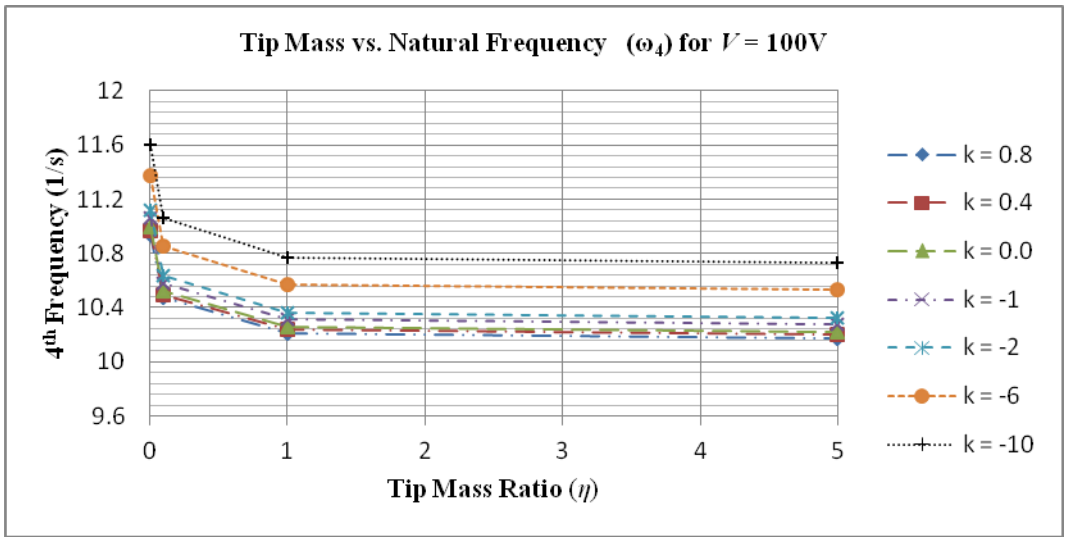

Figure 3.9b: 4th Frequency vs tip mass ratio: Voltage = 100V

This can also be observed in Figures 3.7a to 3.9d, where the slopes of the curves approach zero beyond tip mass ratio $\eta = 1$. The smallest percentage changes in natural frequency for varying axial load ratio and input, occurs in the 4th mode of vibration when the tip mass ratio $\eta = 5$. A further investigation of the graph, Figures 3.7a, shows that the percentage change in natural frequency, between a beam with zero tip mass ($\eta = 0$) and another with varying tip mass ($\eta > 0$), starts to level off as when the tip mass ratio is beyond $\eta \geq 1$, for the 2nd, 3rd and 4th mode.

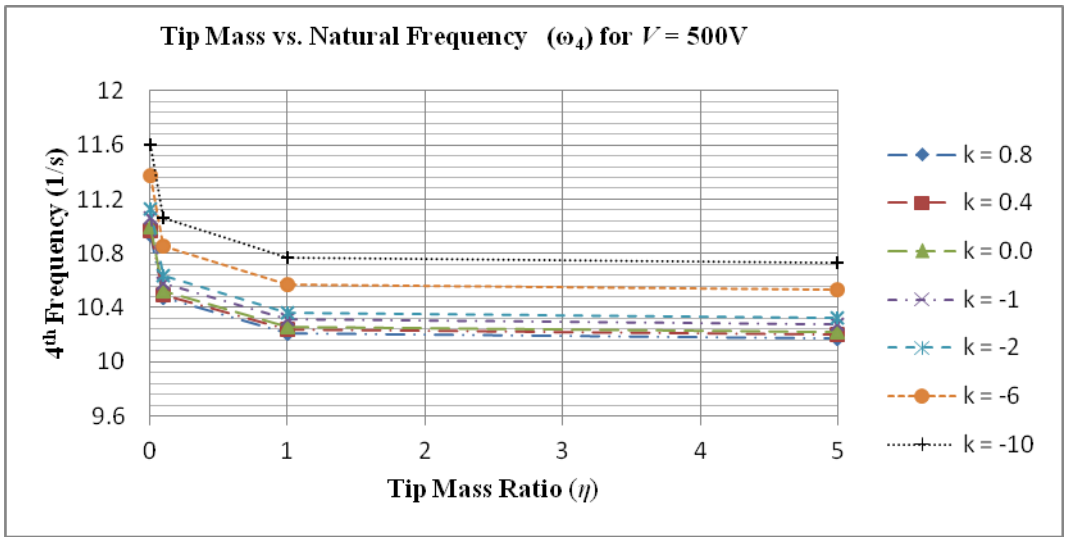

Figure 3.9c: 4th Frequency vs tip mass ratio: Voltage = 500V

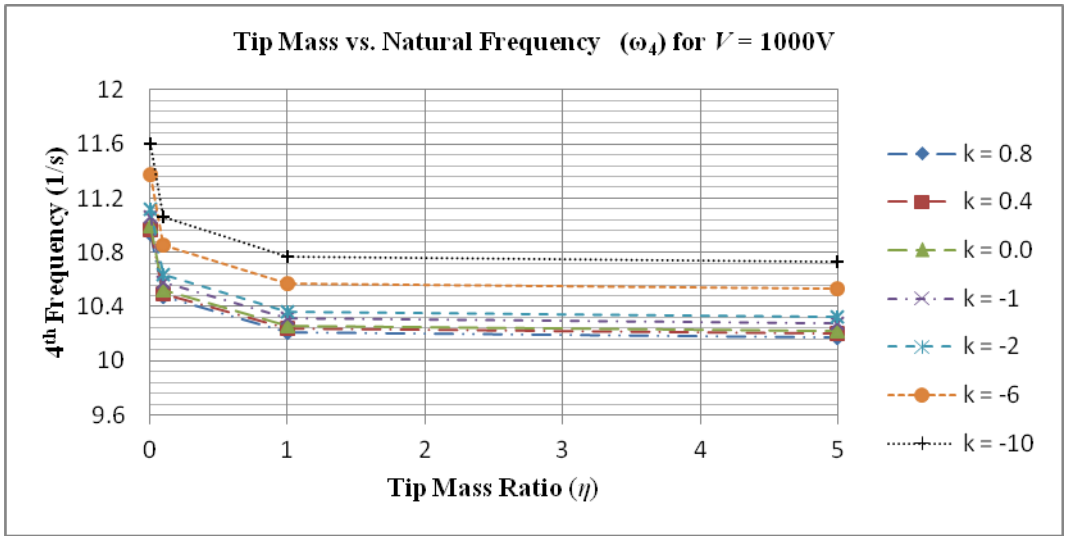

Figure 3.9d: 4th Frequency vs tip mass ratio: Voltage = 1000V

In contrast, the graphs of the 1st mode (Figures 3.6a to 3.6d), show a slope that is much steeper for all voltage input. This leads to the conclusion that the piezo actuators will be

effective at a maximum tip mass ratio η = 5 in the 1st mode, and a tip mass ratio of $\eta \approx 1$ for the 2nd, 3rd and 4th mode of vibration.

Judging from Figures 3.5a to 3.5d, one can clearly see that the graphs for the different voltage input overlap, whereas those of Figure 3.5a to 3.5d indicate a convergence at a tensile load ratio $k \approx -2$. This goes to show that the piezo will not control higher modes but is very effective in the fundamental mode. From the above data, the maximum axial load ratio and tip mass ratio will be limited to k = -2 and η = 5. At these limits, the fundamental mode of vibration, which is the dominant mode, can be controlled. A cursory glance at the figures of the higher modes of vibration for an inactive and an active beam reveal that the curves are identical regardless of the voltage input.

3.5 Percentage change in natural frequencies with change in axial load

Figures 3.10a to 3.13d are the plots of percentage changes in the natural frequency on the column versus axial load. A comparison is made between the frequency of the column with varying axial load ratio (k = +0.8, +0.4, 0, -1, -2, -6, -10) to that of the column with zero axial load ratio (k = 0). The different curves are for varying tip mass ratios.

$$\%\Delta\text{natural frequency}\left(\omega_{V=i}\right)_i^{\eta} = \frac{\omega_{k=0} - \omega_{k=j}}{\omega_{k=0}} \times 100 \tag{3.4}$$

Equation 3.4 is used to calculate the percentage difference in the natural frequency where, $\left(\omega_{V=i}\right)_i^{\eta}$ represents the natural frequency for a particular voltage input (i = 0, 100V, 500V, 1000V), tip mass ratio (η = 0, 0,1, 1, 5, 10) and ($\omega_{k=j}$) is the natural frequency for the varying axial load ratio (j = +0.8,+0.4,0,-1,-2,-6,-10). It is observed that the biggest change occurs at maximum axial load (k = -10) which indicated an increase in the frequency of approximately 80% for a tensile axial load and when the axial load is compressive there is a maximum decrease in frequency of approximately 33% in the first mode of vibration when the piezo actuators are inactive $(\overset{-}{+}V = 0\text{V})$.

When the input voltage to the piezo actuators is increased the natural frequencies of the system change. For 100V input, at a tensile axial load ratio (k = -10), the change in natural frequency is approximately 80% and for compressive axial load ratio (k = +0.8) the change is 33%. When there is an increase the voltage input to 500V, there is a change in the natural frequency of 83% in tension and 39% in compression. At 1000V, the maximum change in natural frequency for at maximum tensile load is 86% and at maximum compressive load ratio the change is 55%.

It is observed that the larger changes in natural frequency when there is axial load and piezo actuators are active. In tension at k = -10 the change are almost identical with a maximum difference of 6% regardless of the state of the piezo actuators (active or inactive), but in compression at k = +0.8 the difference is about 22% when the piezo actuators are inactive compared to when they are active with a maximum input voltage ($\overset{-}{+}V = 1000\text{V}$). In view of that, it will be acceptable to decrease the tensile load ratio threshold. In compression the piezo actuator have notable effect on the natural frequencies.

From the plots Figures 3.10a to 3.13d it is noted that beyond a tensile axial load ratio of k < -2, the different graphs diverge. At this load ratio load, the axial load parameter starts to dominate over the other parameters and thus the maximum axial load ratio is set at k = -2. A closer look shows that at higher vibration modes, the graphs diverge at axial load ratio $k \leq$ -1. The axial load and the tip mass have the opposite effects on the natural frequencies. The former tends to increase the natural frequencies whilst the latter decreases the frequencies. At some point the axial load dominates and its effects are more pronounced.

Given these results the maximum tip mass ratio is limited to $\eta \leq 5$. The percentage change in frequency decreases as the mode number increases. At an axial load ratio k = -2, there is an increase of more than 20% and at axial load ratio k = -1 the change is ±20% in the 1st mode. In the 2nd, 3rd and 4th mode the percentage difference at k = -2 is approximately 5%, 2% and1%, respectively. The graphs also indicate a similar trend in the percentage change in natural frequency in the higher modes of vibration at varying voltage inputs. The percentage difference becomes lower as the mode increases, from a maximum percentage change of approximately 80% at k = -10 and 25% at k = -2, in the higher modes to about 25% at k = -10 and 6% at k = -2.

Furthermore we observe that the graphs for tip mass ratio $\eta = 5$ and $\eta = 10$ overlap, indicating that the tip mass ratio limit can be set at $\eta \leq 5$. With a tip mass ratio of $\eta = 5$ the natural frequencies differ by 0.36% in the first mode, see Table 3.5d, and to a large extent less than 1% in the higher modes, Appendix A1 to A3, Table A1d and A1e, A1d and A2e and Table A3d and A3e. From the above plots, Figures 3.10a to 3.13d indicate the percentage change in frequency for varying tip mass ratios. In the first mode of vibration there is a maximum percentage change of 80% for maximum axial load ratio of k = -10 and about 40% change in maximum compression k = +0.8. These differences are huge and indicate that the column's vibration frequencies are significantly affected. With the piezo voltage input at 1000V there is a significant change in the frequency. In the higher modes of vibration, there is a change of 25% for the 2nd mode, 10% for 3rd mode and 5% for the 4th mode. It can be concluded that the effects on the frequency becomes smaller as the mode of vibration increases.

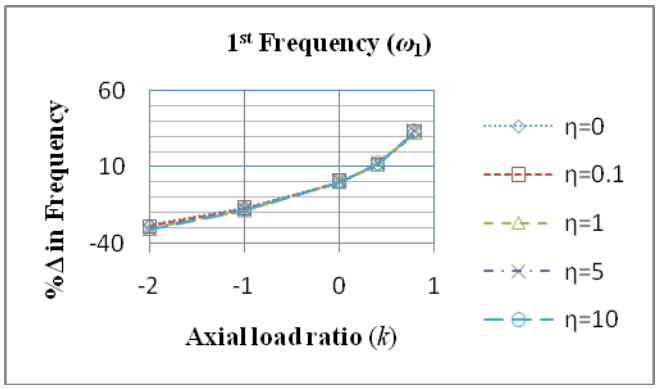

Figure 3.10a: Changes in the natural frequency (ω_1) vs axial load for V = 0V

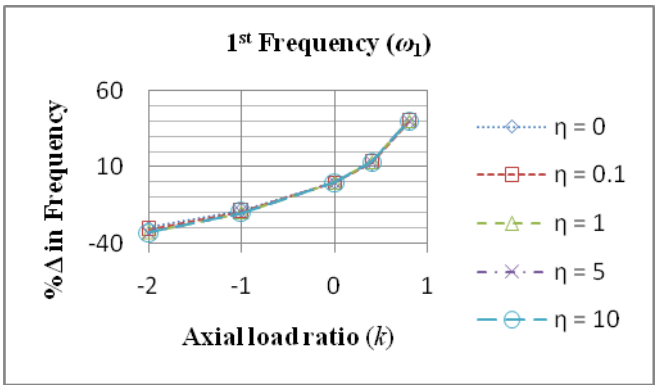

Figure 3.10c: Changes in the natural frequency (ω_1) vs axial load for V = 500V

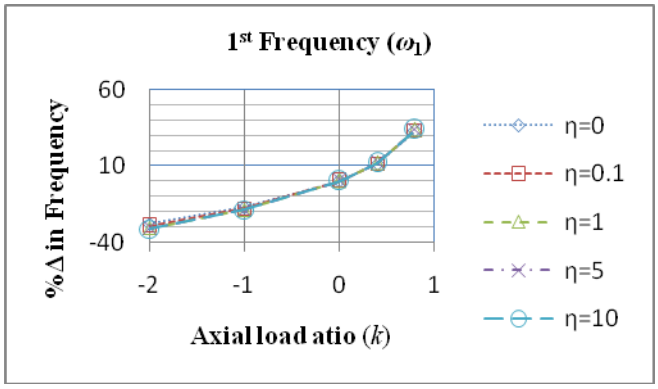

Figure 3.10b: Changes in the natural frequency (ω_1) vs axial load for V = 100V

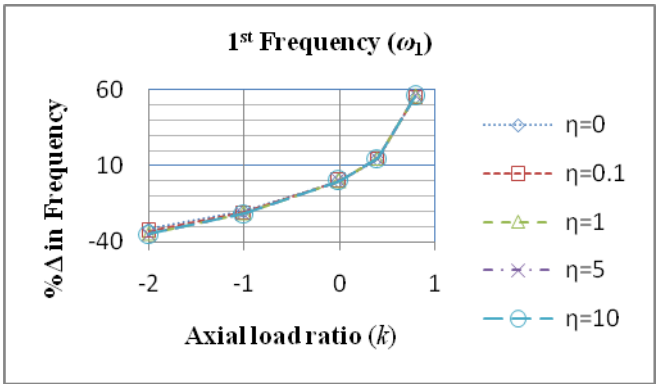

Figure 3.10d: Changes in the natural frequency (ω_1) vs axial load for V = 1000V

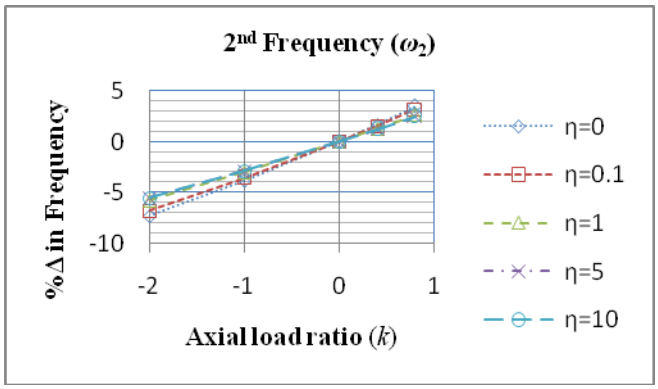

Figure 3.11a: Changes in the natural frequency (ω_2) vs axial load for V = 0V

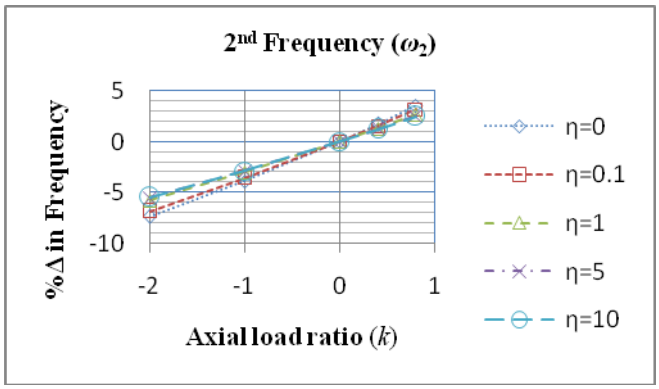

Figure 3.11b: Changes in the natural frequency (ω_2) vs axial load for V = 1000V

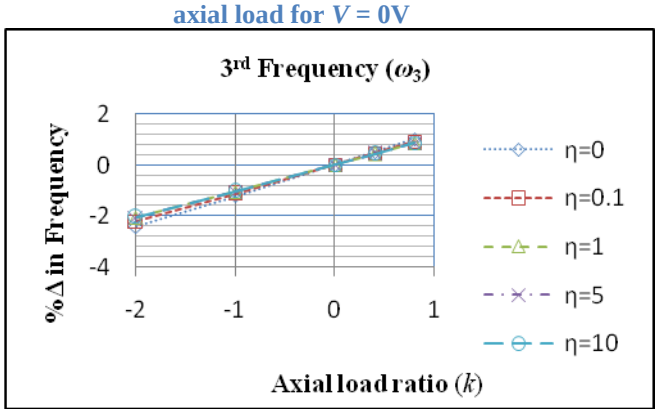

Figure 3.12a: Changes in the natural frequency (ω_3) vs axial load for V = 0V

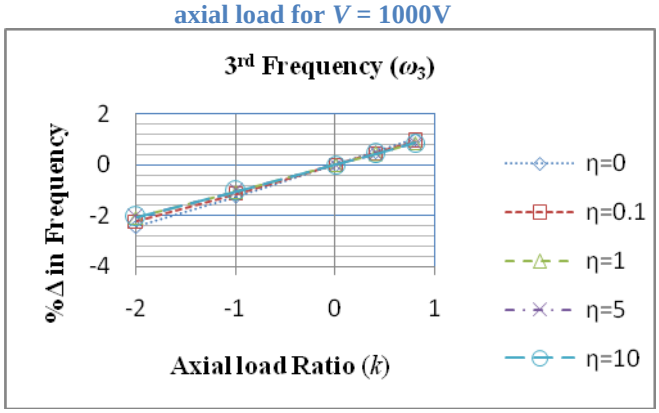

Figure 3.12b: Changes in the natural frequency (ω_3) vs axial load for V = 1000V

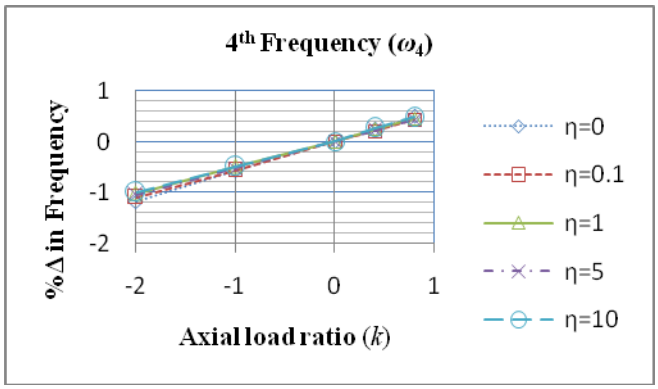

Figure 3.13a: Changes in the natural frequency (ω_4) vs axial load for V = 0V

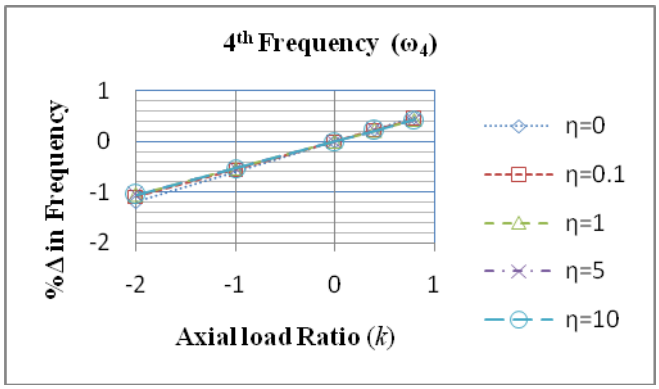

Figure 3.13b: Changes in the natural frequency (ω_4) vs axial load for V = 1000V

Chapter 4 – Computation of frequencies with an extended tip mass

4.1 Determination of the natural frequencies for a beam with an extended tip mass and tip inertia

The natural frequencies of a beam with an extended mass are different from those with a concentrated mass. When dealing with an extended tip mass, one needs to take the effects of the rotary inertia of the tip mass into account and also the fact that the center of gravity of the tip mass is a distance away from the end of the beam. This introduces an additional moment at the end of the beam, where the distance (b_1) in Figure 4.1 below is the moment arm. An investigation into the natural frequencies of a cantilever with an extended tip mass, taking the effects of rotary inertia into account is conducted below. The results are used to compare the change in natural frequencies with change in piezo induced voltage. Figure 4.1 shows a diagram of beam with an extended tip mass, where $b_1 > 0$. Setting $b_1 = 0$ the mass becomes concentrated at the tip.

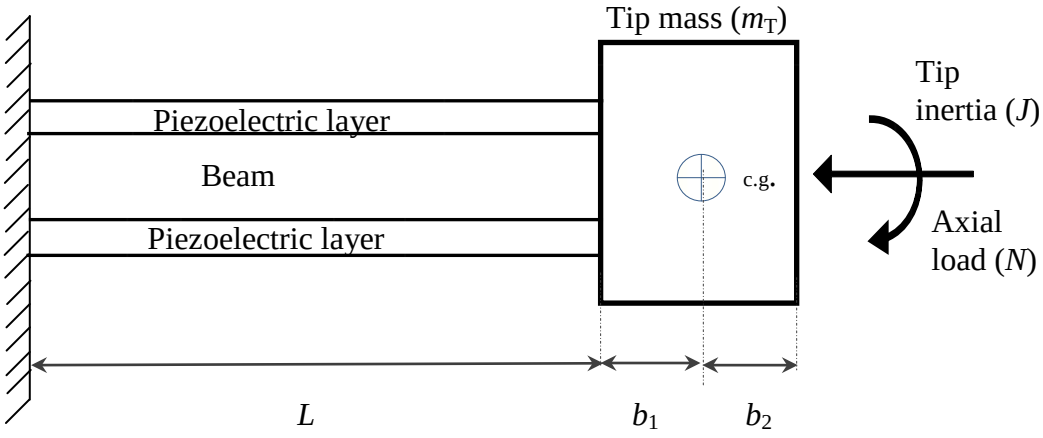

Figure 4.1: Cantilever beam with an extended tip mass

The new boundary conditions can be written in the following manner:

$$\left[E_c I_c \frac{\partial^2 w(L,t)}{\partial x^2} + m_T b_1 \frac{\partial^2 w(L,t)}{\partial t^2} + \left(J + m_T b_1^2 \right) \frac{\partial^3 w(L,t)}{\partial x \partial t^2} - C_{A0} w(L,t) = 0 \right]_{x=L} \quad (4.1)$$

and,

$$\left[E_c I_c \frac{\partial^3 w(L,t)}{\partial x^3} - m_T \frac{\partial^2 w(L,t)}{\partial t^2} + m_T b_1 \frac{\partial^3 w(L,t)}{\partial x \partial t^2} + N \frac{\partial w(L,t)}{\partial x} = 0 \right]_{x=L} \tag{4.2}$$

Equation 4.1 and 4.2 represent the moment and shear boundary conditions at the tip of the beam. In equation 4.1 two additional terms are introduced. The second term accounts for the moment due to the force exerted through the center of the tip mass. The third term accounts for the rotary inertia of the beam as it vibrates transversely. Equation 4.2 has one additional term which is the shear effects at the tip of the beam. Using a separable solution of the form encountered earlier:

$$w(x,t) = \sum_{n=1}^{\infty} X_n(x) T_n(t) \tag{4.3}$$

and the two equations can be written in this form:

$$\begin{aligned} &E_c I_c \frac{\partial^2 \left(X(L)T(t)\right)}{\partial x^2} + m_T b_1 \frac{\partial^2 \left(X(L)T(t)\right)}{\partial t^2} \\ &+ \left(J + m_T b_1^2\right) \frac{\partial^3 \left(X(L)T(t)\right)}{\partial x \partial t^2} - C_{A0} \left(X(L)T(t)\right) = 0 \end{aligned} \tag{4.4}$$

$$\begin{aligned} &E_c I_c X''(L)T(t) + m_T b_1 X(L)\ddot{T}(t) \\ &+ \left(J + m_T b_1^2\right) X'(L)\ddot{T}(t) - C_{A0} X(L)T(t) = 0 \end{aligned} \tag{4.5}$$

Now substitute the time solution $\ddot{T}_n(t) + \omega_n^2 T_n(t) = 0$ into equation 4.4 and divide by $T(t)$ and using equation 2.58a and 2.58b to arrive at the following in short notation:

$$\begin{aligned} &E_c I_c X''(L)T(t) + m_T b_1 X(L)(-\omega^2 T(t)) \\ &+ \left(J + m_T b_1^2\right) X'(L)(-\omega^2 T(t)) - C_{A0} X(L)T(t) = 0 \end{aligned} \tag{4.6}$$

$$E_c I_c X^{''}(L) + (-\omega^2) m_T b_1 X(L) + \left(J + m_T b_1^2\right)(-\omega^2) X^{'}(L) - C_{A0} X(L) T(t) = 0 \tag{4.7}$$

$$X^{''}(L) - b_1 \frac{m_T}{m_c} \frac{m_c \omega^2}{E_c I_c} X(L) - \frac{J}{m_c} \frac{m_c \omega^2}{E_c I_c} X^{'}(L) - b_1^2 \frac{m_T}{m_c} \frac{m_c \omega^2}{E_c I_c} X^{'}(L) - \frac{C_{A0}}{E_c I_c} X(L) = 0 \tag{4.8}$$

where, $J = m_T L^2$

$$X^{''}(L) - b_1 \frac{m_T}{m_c} \frac{m_c \omega^2}{E_c I_c} X(L) - L^2 \frac{m_T}{m_c} \frac{m_c \omega^2}{E_c I_c} X^{'}(L) - b_1^2 \frac{m_T}{m_c} \frac{m_c \omega^2}{E_c I_c} X^{'}(L) - \frac{C_{A0}}{E_c I_c} X(L) = 0 \tag{4.9}$$

$$X^{''}(L) - b_1 \eta a^4 X(L) - L^2 \eta a^4 X^{'}(L) - b_1^2 \eta a^4 X^{'}(L) - C_A X(L) = 0 \tag{4.10}$$

Equation 4.10 above is the moment boundary condition at the end of the beam. Equation 4.11 is the general form of the shear boundary condition at the end of the beam, which is presented in the spatial domain and time domain. After using the general solution and the time solution, the result is expressed in short form in equation 4.16.

$$m_T \frac{\partial^2 \left(X(L)T(t)\right)}{\partial t^2} - m_T b_1 \frac{\partial^3 \left(X(L)T(t)\right)}{\partial x \partial t^2} - E_c I_c \frac{\partial^3 \left(X(L)T(t)\right)}{\partial x^3} - N \frac{\partial \left(X(L)T(t)\right)}{\partial x} = 0 \tag{4.11}$$

$$m_T X(L) \ddot{T}(t) - m_T b_1 X^{'}(L) \ddot{T}(t) - E_c I_c X^{'''}(L) T(t) - N X^{'}(L) T(t) = 0 \tag{4.12}$$

$$m_T X(L)(-\omega^2 T(t)) - m_T b_1 X^{'}(L)(-\omega^2 T(t)) - E_c I_c X^{'''}(L) T(t) - N X^{'}(L) T(t) = 0 \tag{4.13}$$

$$
\begin{aligned}
&-m_T\omega^2 X(L)T(t) + m_T b_1 \omega^2 X^{'}(L)T(t) - E_c I_c X^{'''}(L)T(t) \\
&- NX^{'}(L)T(t) = 0
\end{aligned}
\tag{4.14}
$$

$$
\begin{aligned}
&-\frac{m_T}{m_c}\frac{m_c\omega^2}{E_c I_c} X(L)T(t) - b_1 \frac{m_T}{m_c}\frac{m_c\omega^2}{E_c I_c} X^{'}(L)T(t) - X^{'''}(L)T(t) \\
&-\frac{N}{E_c I_c} X^{'}(L)T(t) = 0
\end{aligned}
\tag{4.15}
$$

$$
X^{'''}(L) + \beta^2 X^{'}(L) + b_1\eta a^4 X^{'}(L) + \eta a^4 X(L) = 0 \tag{4.16}
$$

The above represents the shear boundary condition at the end of the beam in the spatial domain. Equations 4.10 and 4.16 can be used to find the characteristic equation which will give us the natural frequencies of the beam under free vibration. After applying general solution equation 4.17 to the boundary conditions at the free end of the beam, the characteristic equation is derived below:

$$
X_n(x) = C_n\left(\sinh p_{1n}x - \frac{p_{1n}}{p_{2n}}\sin p_{2n}x\right) + B_n\left(\cos p_{2n}x - \cosh p_{1n}x\right) \tag{4.17}
$$

After dropping the subscript (n) and substituting equation 4.17 into the boundary conditions at the free end the result is two equations in B and C. The moment boundary condition is:

$$
\begin{aligned}
&B[(a^4 b_1\eta + C_A - p_1^2)\cosh p_1 L - (a^4 b_1\eta + C_A + p_2^2)\cos p_2 L \\
&+ a^4 p_1\eta(b_1^2 + L^2)(\frac{p_2}{p_1}\sin p_2 L + \sinh p_1 L)] \\
&+ C[\frac{p_1}{p_2}(a^4 b_1\eta + C_A + p_2^2)\sin p_2 L - (a^4 b_1\eta + C_A - p_1^2)\sinh p_1 L \\
&+ a^4 p_1\eta(b_1^2 + L^2)(\cos p_2 L - \cosh p_1 L)] = 0
\end{aligned}
\tag{4.18}
$$

And the shear boundary condition is:

$$
\begin{aligned}
&B[(a^4 b_1 \eta p_2 + p_2^3 - \beta^2 p_2)\sin p_2 L - (a^4 b_1 \eta p_1 + p_1^3 - \beta^2 p_2)\sinh p_1 L \\
&+ a^4 \eta(\cos p_2 L - \cosh p_1 L)] \\
&+ C[\frac{p_1}{p_2}(a^4 b_1 \eta p_2 + p_2^3 - \beta^2 p_2)\cos p_2 L + (-a^4 b_1 \eta p_1 + p_1^3 + \beta^2 p_2)\cosh p_1 L \\
&- a^4 \eta(\frac{p_1}{p_2}\sin p_2 L - \sinh p_1 L)] = 0
\end{aligned} \tag{4.19}
$$

The characteristic equation is determined by solving equation 4.18 for C and substitute the results into equation 4.19. The constant B remains undetermined and can be set to unity and the natural frequencies can be determined for various axial loads, tip mass and piezo voltage input. The characteristic equation can be written in this form:

$$
\begin{aligned}
&p_2 \cos p_2 L\{p_1 \cosh p_1 L[-2a^8 \eta^2 (2b_1^2 + L^2) - 2a^4 b_1 \eta C_A + \\
&C_A \beta^2 + \beta^4 + 2a^4] - a^4 \eta(p_1^2 + p_2^2)(p_1^2(b_1^2 + L^2) - 1)\sinh p_1 L\} \\
&+ \sin p_2 L\{\sinh p_1 L[-p_1^4(a^4 b_1 \eta + C_A + p_2^2) + p_1^2 a^8 \eta^2 (2b_1^2 + L^2) \\
&+ a^4 b_1 \eta(C_A + 2p_2^2 - \beta^2) - \beta^2 p_2^4 (C_A + 2p_2^2) + p_2^2(-a^8 \eta^2 (2b_1^2 + L^2) \\
&+ a^4 b_1 \eta(-C_A - p_1^2 + \beta^2) + C_A(\beta^2 - p_2^2))] - a^4 p_1 \eta(p_1^2 + p_2^2)(p_2^2(b_1^2 + L^2) \\
&+ 1)\cosh p_1 L\} + a^2[2a^8 \eta^2 (2b_1^2 + L^2) + 2a^4 b_1 \eta C_A - C_A \beta^2 - \beta^4 + p_1^4 + p_2^4]
\end{aligned} \tag{4.20}
$$

4.2 Natural frequencies for a beam with extended tip mass

In the previous discussion (Chapter 3), the tip mass was modeled assuming that it is concentrated and therefore dimensionless. In this section a more realistic mass is studied, were the center of gravity for the mass does not pass through the tip of the beam. Figure 4.1 shows the beam with an extended mass such that $b_1 > 0$. For this configuration the effects of rotary inertia of the mass and study the effects of the relevant parameters e.g. tip mass ratio, axial load ratio and piezo voltage input are include. The natural frequencies can be obtained by finding the roots of equation 4.20.

Tables 4.2a to 4.2d and Figure 4.3a to 4.3d are the natural frequencies of a cantilever beam with an extended tip mass subjected to an axial load for a concentrated tip mass, $b_1 = 0$. Beyond an axial load k = -2 the axial load dominates and the effects of piezo control are negligible. The natural frequency increase with axial load ratio and decreases as the tip mass increases for both controlled and uncontrolled beams. As the moment arm to the center of

gravity of the extended tip mass is increased ($b_1 > 0$), the natural frequencies of the beam decrease. When the tip mass ratio is zero the natural frequencies are the same for all $b_1 \geq 0$ but are different for varying voltage inputs. With a compressive load the difference frequency at $k = +0.8$ is about 50% while at $k = -2$ it drops to 1%, which indicates that at beyond $k = -2$ tensile load ratio the piezo cannot be used for effective control of the vibrations. The maximum control voltage was taken to be 1000V/mm where the piezo will breakdown if we increased the input voltage beyond this threshold.

Tables 4.2a to 4.4d indicate the natural frequencies of the beam with tip mass, axial load and voltage input to the piezo layers. Another parameter is introduced and that is the moment arm from the tip of the beam to the line of action of the center of gravity of the tip mass, where $b_1 = 0, L/2, L/1$. When $b_1 = 0$ the system behaves like concentrated tip mass. The results of Tables 3.1a and 4.2a are derived from equation 3.1 and 4.20, respectively. The results in Table 3.1a do not account for rotary inertia at the tip of the beam due to the tip mass, whereas in Table 4.2a, these effects are included. When there tip mass is zero ($\eta = 0$) the results in Table 3.1a, 4.2a, 4.3a and 4.4a are identical for $b_1 \geq 0$ if the voltage is kept the same. In this case equation 4.20 reduces to equation 3.1, the frequency equation without any inertia and this can be verified in Bokaian (1988, 1990).

Figures 4.3a to 3.4d show the plots of natural frequency versus both axial load and tip mass combined, with rotary inertia. The tip mass ratio is varied from ($0 \leq \eta \leq 10$) and the axial load ratio varies from ($-2 \leq k \leq +0.8$) following the discussion in Chapter 3, where we concluded that beyond a tip mass of $\eta > 5$ that the natural frequencies change minimally and the beam behaves like a clamped-pinned beam. It was also concluded that beyond an axial load ratio $k > -2$, the piezo actuators have minimal effect on the natural frequencies of the system. The figures below show that the maximum natural frequency ($\omega < 2.5s^{-1}$) for all combinations of the relevant parameters. The highest natural frequency occurs at $k = -2$ and $\eta = 0$, implying that b_1 can take any value. Furthermore, it is noted that the natural frequencies are almost identical and occur between ($2 \leq \omega \leq 2.5s^{-1}$). This further shows that the axial load dominates all other parameters at this point. For an increasing the tip mass, the natural frequencies decrease and for a decrease in the tensile axial load to compression the natural frequencies also decrease.

The lowest natural frequency occur at (k = +0.8 and η = 10) for $b_1 = L/1$ at maximum voltage input ($\bar{+}V = 1000\text{V}$), and it occurs at a frequency range ($0 \le \omega \le 0.5\text{s}^{-1}$), see Table 4.4d. For all the sets of graphs at varying moment arm, ($b_1 = L/2, L/1$), the lowest natural frequency occurs at maximum voltage input ($\bar{+}V = 1000\text{V}$). From the above, we can deduce that as the moment arm (b_1) is increased, the inertia of the tip mass reduces the natural frequency of the system. Table 4.1 indicates the highest natural frequency of $\omega = 0.360\text{s}^{-1}$ for a beam with a concentrated tip mass and Table 4.1 and 4.4d a natural frequency of $\omega = 0.1460\text{s}^{-1}$ at $b_1 = L/1$ at maximum voltage input ($\bar{+}V = 1000\text{V}$) with inertia taken into consideration. This constitutes a significant decrease of approximately 52% in the natural frequency if we take the moment arm to the center of gravity into consideration in the analysis.

Table 4.1: Lowest natural frequencies for k = +0.8 and η = 10.

Voltage	$b_1 = 0$	$b_1 = L/10$	$b_1 = L/5$	$b_1 = L/2$	$b_1 = L/1$
0V	0.36	0.35	0.34	0.32	0.28
100V	0.35	0.34	0.28	0.31	0.28
500V	0.31	0.30	0.29	0.27	0.24
1000V	0.19	0.19	0.18	0.16	0.15

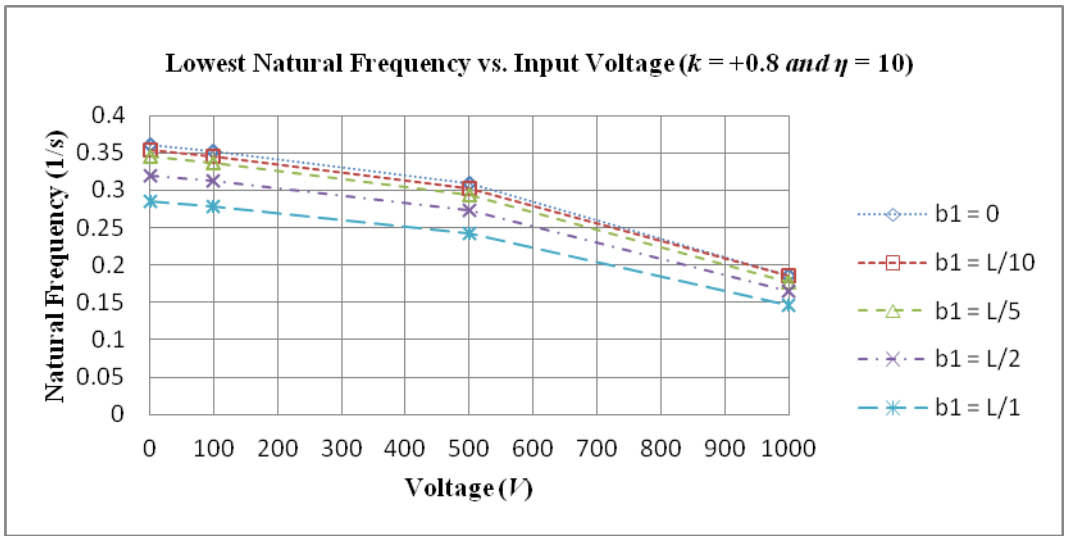

Figure 4.2: Lowest Natural frequencies of system at k = +0.8 and η = 10

In Figures 4.3a to 4.3d the graphs have a range of 0.25 *units* for different natural frequency ranges (color coded accordingly). The lowest range of natural frequencies is ($0 \le \omega \le 0.5\text{s}^{-1}$) when the color of the graph is red and ends where the axial load ratio (k = +0.8) and tip mass ratio (η = 10). The lowest natural frequencies are listed in Table 4.1. As the voltage input to

the piezo actuators is increased from $\bar{+}V = 0\text{V}$ to $1000V$, it is observed that the area increases, indicating that as the voltage increases them system tends to settle more and more at lower frequencies for the combination of parameters.

From the graphs it is also noted that when the axial load ratio is maximum (k = -2 and η = 0) the area of the turquoise shading remains the same for all the above mentioned graphs, Figure 4.3a to 4.3d indicating that around that vicinity, the axial load dominates the other parameters, including the input voltage. The curves in Figure 4.2 show a non-linear change in the natural frequencies such that as the voltage increases, the slope of the curve becomes larger. This indicates that we can achieve greater control/changes of the natural frequencies at higher input voltages, but the input voltage is limited to 1000V/mm to prevent piezo breakdown.

4.3 Fundamental frequencies for a beam with an extended tip mass and rotary inertia

4.3.1 Natural frequencies of a beam with a tip mass, $b_1 = 0$

The tables and figures in this section characterize the natural frequencies of the system. The moment arm, which is the distance from the tip of the beam to the center of gravity of the extended mass, is held constant and the voltage varied to determine the effects of the piezo actuator on the natural frequencies. Every set of four graphs and tables represent a particular moment arm $0 \le L/n \le 1$, where n = ∞, 2, 1. The discussion is limited to the fundamental mode (1st natural frequency) of vibration which is the most important. In the discussion of Chapter 3, it was established that the voltage input in the piezo layers have an insignificant effect on the higher modes of vibration, i.e. 2nd , 3rd, and 4th natural frequency of vibration.

Figure 4.3a represents the natural frequencies of the beam with varying axial load ratio, tip mass ratio and the input voltage to the piezo actuators is zero ($\bar{+}V = 0\text{V}$). It is apparent that the lowest natural occur when η = 10 and k = +0.8 and these occur in the range $0.25 < \omega < 0.5\text{s}^{-1}$ and the largest natural frequencies occur at η = 0 and k = -2 in the range of $2.25 < \omega < 2.5\text{s}^{-1}$. A compressive axial load tends to lower the natural frequencies and a

tensile axial load increases them whereas, a larger tip mass ratio tends to decrease the natural frequencies.

Table 4.2a: 1st Frequency of a beam with a tip mass (b_1 = 0) and rotary inertia at 0V.

Axial load Ratio (k)	η = 0	η = 0.1	η = 1	η = 5	η = 10
+0.8	1.27	1.01	0.63	0.43	0.36
+0.4	1.66	1.33	0.83	0.56	0.47
+0.2	1.78	1.43	0.88	0.60	0.50
0	1.88	1.51	0.93	0.63	0.53
-0.4	2.03	1.64	1.01	0.67	0.53
-1	2.19	1.78	1.09	0.73	0.62
-2	2.40	1.96	1.18	0.79	0.67

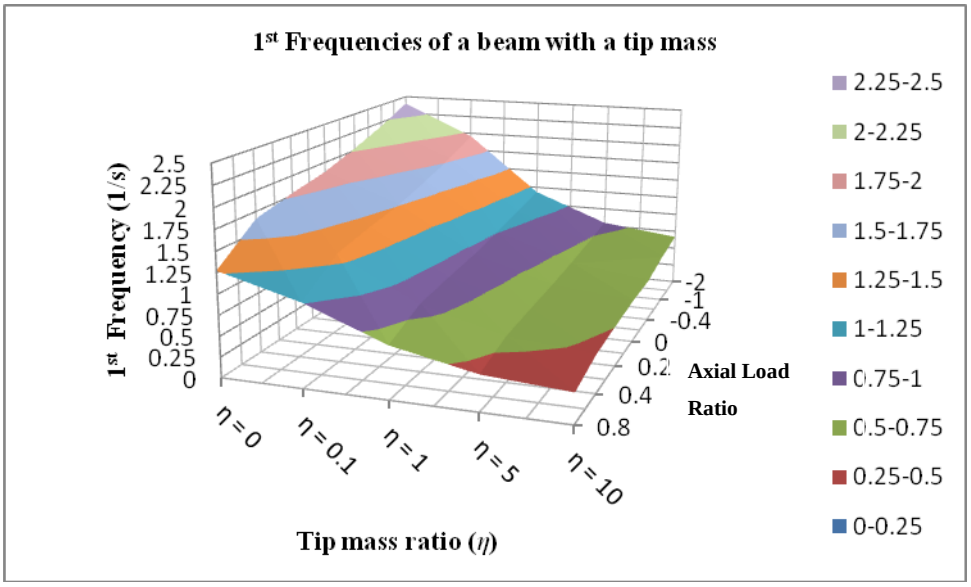

Figure 4.3a: Natural frequency vs axial load and tip mass for b_1 = 0 and V = 0V

When the plots for $\bar{+}V = 100\text{V}$ and $\bar{+}V = 500\text{V}$ in Figures 4.3b and 4.3c are analyzed, it is noted that area covered in the brown ($0.25 < \omega < 0.5\text{s}^{-1}$) increases as the input voltage is increased. This means that due to the increase in the input voltage to the piezo actuators, there is a greater occurrence of the frequencies in the range $0.25 < \omega < 0.5\text{s}^{-1}$. By so doing the natural frequencies of the composite beam are altered by inducing a voltage and it therefore follows that the vibration of the beam can be controlled using piezo actuators.

Table 4.2b: 1st Frequency of a beam with a tip mass (b_1 = 0) and rotary inertia at 100V.

Axial load Ratio (k)	η = 0	η = 0.1	η = 1	η = 5	η = 10
+0.8	1.24	0.99	0.62	0.42	0.35
+0.4	1.65	1.32	0.82	0.55	0.47
+0.2	1.77	1.42	0.88	0.59	0.50
0	1.87	1.50	0.93	0.63	0.53
-0.4	2.02	1.63	1.00	0.68	0.57
-1	2.19	1.78	1.08	0.73	0.61
-2	2.39	1.95	1.18	0.79	0.67

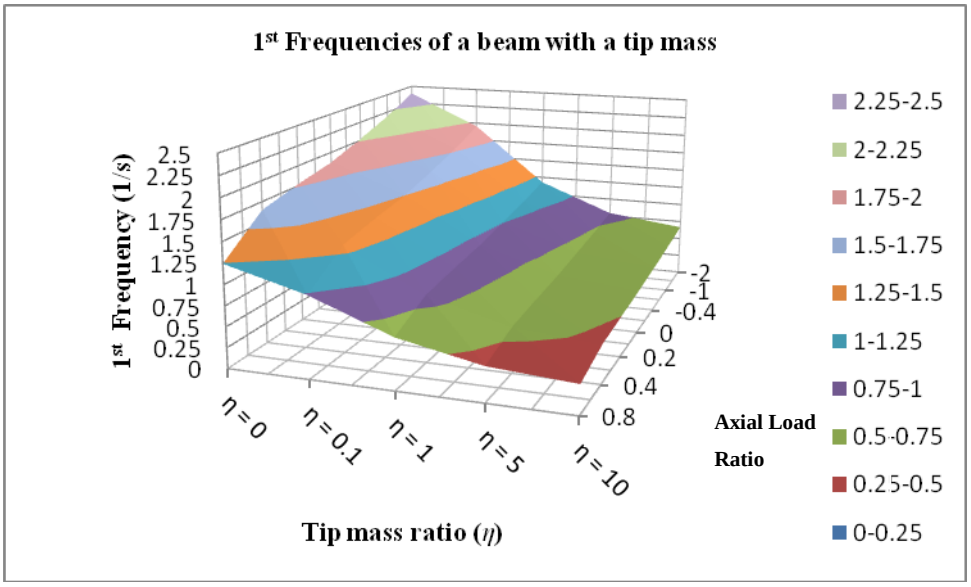

Figure 4.3b: Natural frequency vs axial load and tip mass for b_1 = 0 and V = 100V

At maximum input voltage $(\bar{}_{+}V = 1000\text{V})$ there is the largest decrease in natural frequencies and the lowest of these frequencies are in the range of $0 < \omega < 0.25\text{s}^{-1}$. From Table 4.2d it is noted that the lowest natural frequency is $\omega = 0.1855\text{s}^{-1}$ and occurs at $\eta = 10$ and $k = +0.8$ in comparison to the lowest frequency is ($\omega = 0.3614\text{s}^{-1}$) for an inactive beam, Tables 4.2a and 4.4d shows a 49% decrease in the frequencies when maximum input voltage $(\bar{}_{+}V = 1000\text{V})$ is applied.

The highest natural frequency ($\omega = 2.3972\text{s}^{-1}$) occurs when there is zero tip mass ratio ($\eta = 0$) and at maximum axial load ratio ($k = -2$), for an inactive piezo actuator $(\bar{}_{+}V = 0\text{V})$. When the voltage is increased to a maximum $(\bar{}_{+}V = 1000\text{V})$ there is a decrease in the natural frequency to ($\omega = 2.3709\text{s}^{-1}$), which is a change of approximately 1%. This also supports an

earlier conclusion that the axial load dominates the other parameters when $k \approx -2$. From the Figures 4.3a to 4.3d the area for the frequency ranges of $2.25 < \omega < 2.5 s^{-1}$ is observed to remain constant for the whole voltage range $(\bar{+}V = 0V \text{ to } 1000V)$.

Table 4.2c: 1st Frequency of a beam with a tip mass ($b_1 = 0$) and rotary inertia at 500V.

Axial load Ratio (k)	$\eta = 0$	$\eta = 0.1$	$\eta = 1$	$\eta = 5$	$\eta = 10$
+0.8	1.09	0.87	0.54	0.37	0.31
+0.4	1.60	1.27	0.79	0.54	0.45
+0.2	1.73	1.38	0.86	0.58	0.49
0	1.84	1.47	0.91	0.61	0.52
-0.4	2.00	1.61	0.99	0.67	0.56
-1	2.17	1.76	1.07	0.72	0.61
-2	2.38	1.94	1.17	0.79	0.66

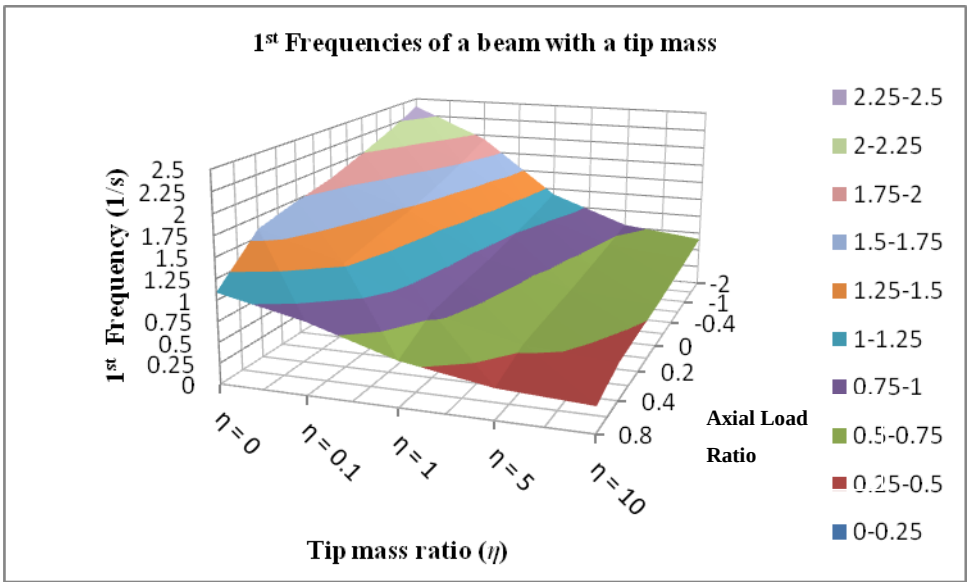

Figure 4.3c: Natural frequency vs axial load and tip mass for $b_1 = 0$ and $V = 500$V

A closer look at the frequencies curves also indicates that the frequencies decrease when an incremental voltage input to the piezo actuators is applied. Taking $\eta = 10$, $k = +0.8$ and $\bar{+}V = 0V$ as our reference point and observe the frequency ranges along the tip mass ratio axis as $\eta \rightarrow 0$, it is noted that the shaded areas covered by the lower frequency ranges increase as the input voltage is varied incrementally from $\bar{+}V = 0V$ to $1000V$. At $\bar{+}V = 0V$ the red area covers 2.5 *units* from the reference point along the tip mass ratio axis, see Figures 4.3a to 4.3d, it is 3 *units*, 3.5 *units* and 6 *units* for a voltage input of 100V, 500V and 1000V,

respectively. Along the axial load ratio axis it is noted that as $k \rightarrow 0$ the area that represents the lowest frequency range remains constant for $\bar{+}V = 0\text{V}, 100\text{V}$ and 500V, with a slight increase at maximum voltage input $(\bar{+}V = 1000\text{V})$

This means that the lower frequency ranges increase and overlap the higher frequencies and the overall results is that the system settles at lower frequencies when the voltage is increased. The biggest changes occur at maximum input voltage $(\bar{+}V = 1000\text{V})$. For example, in Figure 4.3a, the frequency range $0.5 < \omega < 0.75\text{s}^{-1}$ starts at $\eta \approx 2.5$ and ends at $\eta \approx 4.5$. This effect is produce by a combination of an axial load and tip mass only because the induced voltage is zero. In Figure 4.3d, this range of frequency occurs along the tip mass ratio axis between $\eta \approx 0.1$ and $\eta \approx 0$.

Table 4.2d: 1st Frequency of a beam with a tip mass (b_1 = 0) and rotary inertia at 1000V.

Axial load Ratio (k)	η = 0	η = 0.1	η = 1	η = 5	η = 10
+0.8	0.66	0.52	0.33	0.22	0.19
+0.4	1.53	1.21	0.75	0.51	0.33
+0.2	1.68	1.33	0.83	0.56	0.47
0	1.79	1.43	0.88	0.60	0.50
-0.4	1.97	1.58	0.97	0.65	0.55
-1	2.15	1.74	1.06	0.71	0.60
-2	2.37	1.92	1.16	0.78	0.66

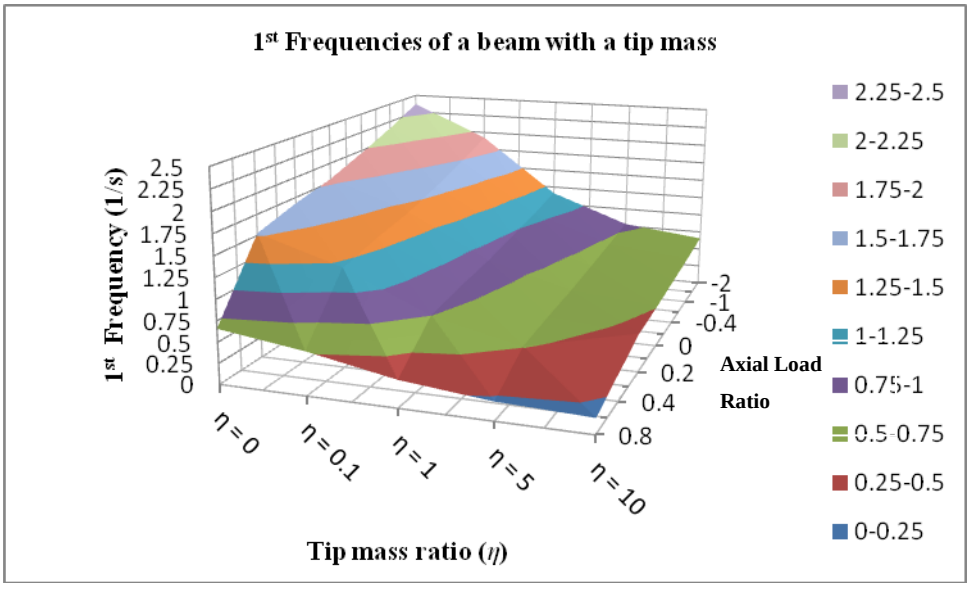

Figure 4.3d: Natural frequency vs axial load and tip mass for b_1 = 0 and V =1000V

This goes further to show that an active piezo actuator, when $V > 0$V, has an attenuating effect on the natural frequencies of the system. At maximum input voltage ($\bar{+}V = 1000$V) as $\eta \rightarrow 10$ and $k \rightarrow 1$ (critical buckling) the lowest frequency range is $0 < \omega < 0.25\text{s}^{-1}$.

4.3.2 Natural frequencies of a beam with extended tip mass and rotary inertia for $b_1 = L/2$

When the moment arm is extended such that b_1 equals half the length of the beam (L) and rotary inertia is taken into account, there are changes in the natural frequencies of the beam. Tables 4.3a to 4.4d and Figures 4.4a to 4.5d show the natural frequencies of the beam for $b_1 > 0$.

Table 4.3a: 1st Frequency of a beam with a tip mass ($b_1 = L/2$) and rotary inertia at 0V.

Axial load Ratio (k)	$\eta = 0$	$\eta = 0.1$	$\eta = 1$	$\eta = 5$	$\eta = 10$
+0.8	1.25	0.93	0.56	0.38	0.32
+0.4	1.66	1.23	0.74	0.50	0.42
+0.2	1.78	1.31	0.79	0.53	0.45
0	1.88	1.39	0.83	0.56	0.47
-0.4	2.03	1.50	0.90	0.60	0.51
-1	2.19	1.64	0.97	0.65	0.55
-2	2.40	1.79	1.06	0.71	0.60

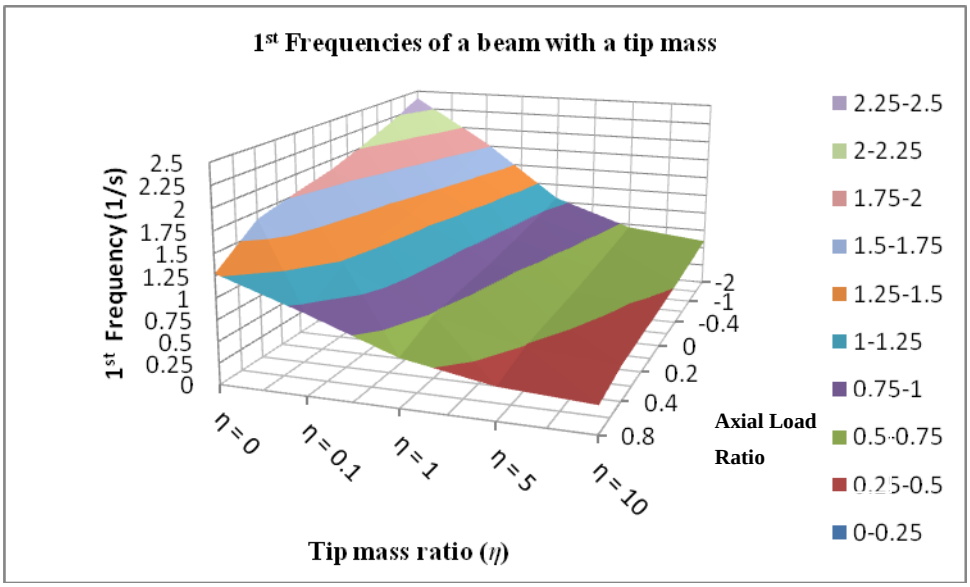

Figure 4.4a: Natural frequency vs axial load and tip mass for $b_1 = L/2$ and $V = 0$V

The lowest natural frequency occurs at η = 10 and k = +0.8 in the range of $0.25 < \omega < 0.5s^{-1}$ when the voltage input to the piezo actuators is $\overset{-}{+}V = 0V$ to $500V$. At maximum voltage input ($\overset{-}{+}V = 1000V$) the frequency range drops to $0 < \omega < 0.25s^{-1}$. This indicates that there is some degree of controllability of the vibrations at maximum input voltage regardless of the size of the moment arm ($0 \leq b_1 \leq L$).

Table 4.3b: 1st Frequency of a beam with a tip mass ($b_1 = L/2$) and rotary inertia at 100V.

Axial load Ratio (k)	η = 0	η = 0.1	η = 1	η = 5	η = 10
+0.8	1.24	0.91	0.55	0.37	0.31
+0.4	1.65	1.22	0.73	0.49	0.41
+0.2	1.77	1.31	0.78	0.53	0.44
0	1.87	1.38	0.83	0.56	0.47
-0.4	2.02	1.50	0.89	0.60	0.50
-1	2.19	1.63	0.97	0.65	0.55
-2	2.30	1.79	1.05	0.71	0.60

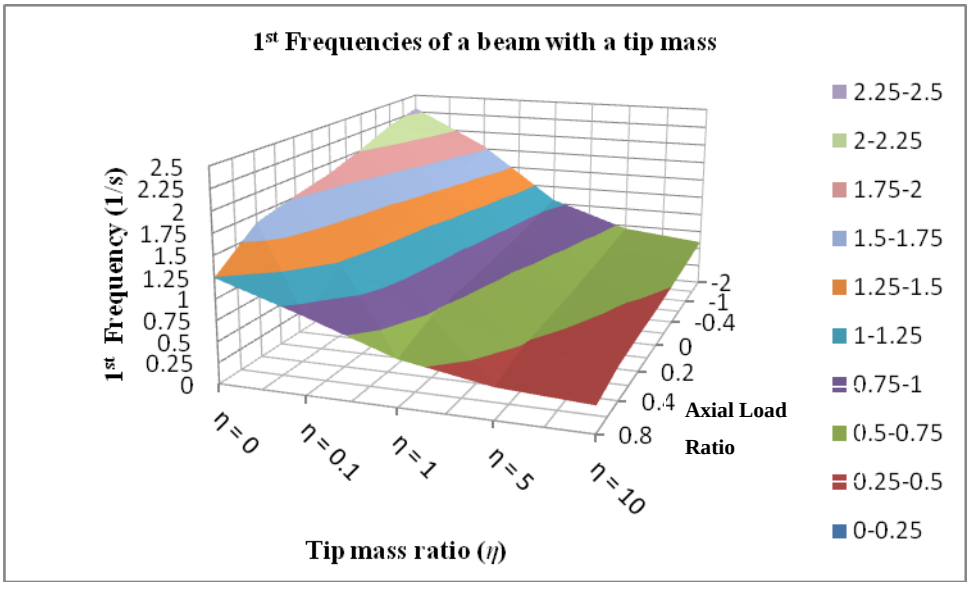

Figure 4.4b: Natural frequency vs axial load and tip mass for $b_1 = L/2$ and V =100V

In the previous section, for b_1 = 0, it was noted that there is an increase in the area or range ($0.25 < \omega < 0.5s^{-1}$) occupied by the lowest natural frequencies and also that inducing a voltage in the piezo actuators increases this area, indicating that the frequencies of the system are reduced for a compressive axial load ratio, a larger tip mass and moment arm

combination. The same phenomenon occurs for $b_1 > 0$, but the initial areas (when the actuators are inactive or active) for the lowest range frequencies are different.

Table 4.3c: 1st Frequency of a beam with a tip mass ($b_1 = L/2$) and rotary inertia at 500V.

Axial load Ratio (k)	$\eta = 0$	$\eta = 0.1$	$\eta = 1$	$\eta = 5$	$\eta = 10$
+0.8	1.09	0.80	0.48	0.32	0.27
+0.4	1.60	1.17	0.71	0.48	0.40
+0.2	1.73	1.27	0.76	0.51	0.43
0	1.84	1.35	0.81	0.54	0.46
-0.4	2.00	1.48	0.88	0.59	0.50
-1	2.17	1.61	0.96	0.64	0.54
-2	2.38	1.78	1.05	0.70	0.59

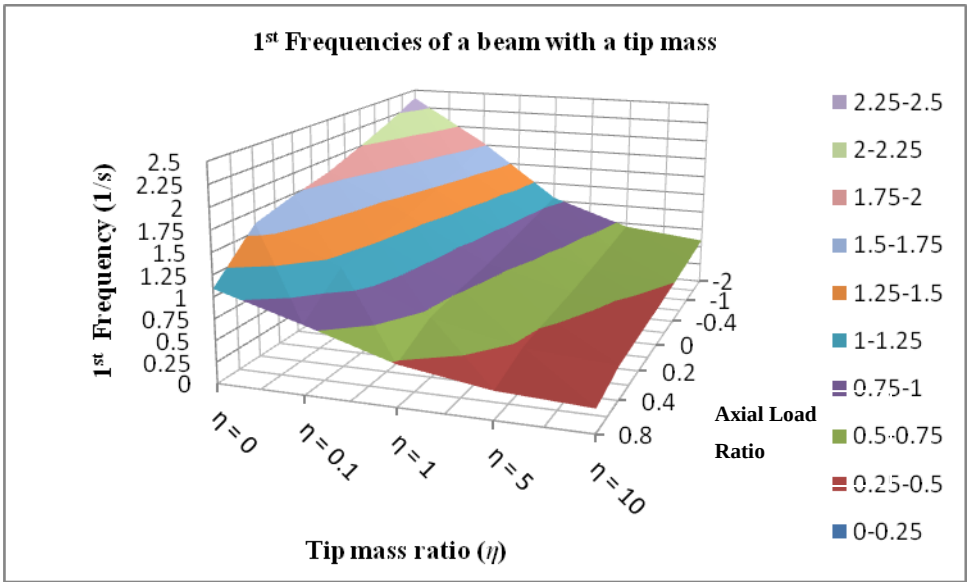

Figure 4.4c: Natural frequency vs axial load and tip mass for $b_1 = L/2$ and V =500V

The area is proportional to the voltage input (Voltage α Area). The area of the lower frequencies for $b_1 = 0$ (Figure 4.3a) is smaller than the area covered when $b_1 = L/2$, Figure 4.4a and $b_1 = L/1$, Figure 4.5a, indicating that as the moment arm is increased the natural frequencies of the beam decrease. These natural frequencies can be further reduced at maximum voltage input to the piezo actuators to a range $0 < \omega < 0.25\ s^{-1}$. When the piezo input voltage is zero, Figure 4.3a, 4.4a and 4.5a show an increase in the area of lowest frequency. This also shows that the moment arm has a significant effect on the frequencies.

Table 4.3d: 1st Frequency of a beam with a tip mass ($b_1 = L/2$) and rotary inertia at 1000V.

Axial load Ratio (k)	$\eta = 0$	$\eta = 0.1$	$\eta = 1$	$\eta = 5$	$\eta = 10$
+0.8	0.66	0.48	0.29	0.20	0.16
+0.4	1.53	1.11	0.67	0.45	0.38
+0.2	1.68	1.23	0.74	0.50	0.42
0	1.79	1.32	0.79	0.53	0.45
-0.4	1.97	1.45	0.86	0.58	0.49
-1	2.15	1.59	0.94	0.63	0.53
-2	2.37	1.76	1.04	0.70	0.59

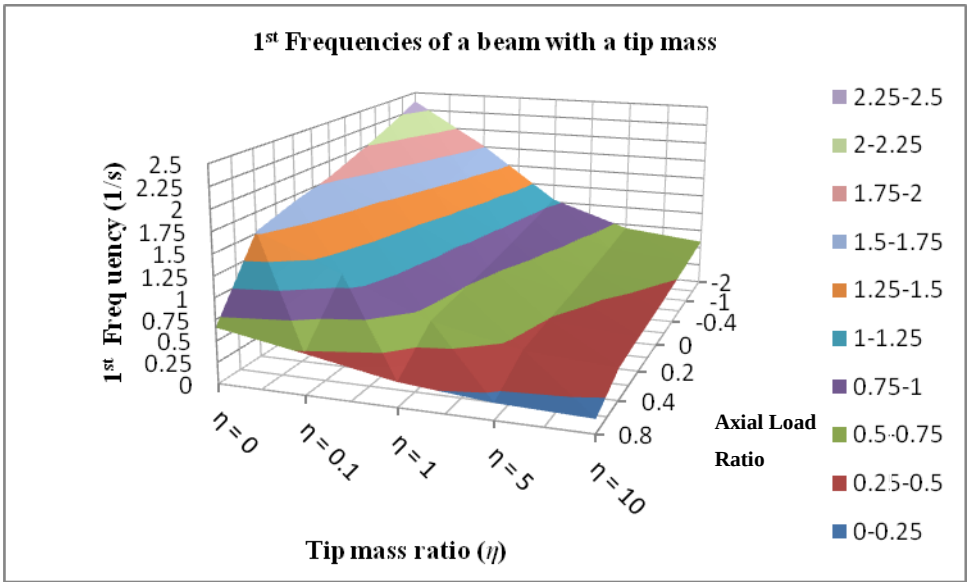

Figure 4.4d: Natural frequency vs axial load and tip mass for $b_1 = L/2$ and V =1000V

4.3.3 Natural frequencies of a beam with extended tip mass and rotary inertia for $b_1 = L/1$

From the data above it is evident that the natural frequencies of the beam can be altered using a piezo actuator and that maximum control can be attained at maximum voltage ($\overset{-}{+}V = 1000\text{V}$). In Figure 4.3a to 4.3d it is noted that the increase in area in red ($0.25 < \omega < 0.5\ \text{s}^{-1}$) is along the tip mass ratio axis (η) for $b_1 = 0$. When $b_1 > 0$ the increase is more pronounced along the axial load ratio axis (k) compared to the case of $b_1 = 0$, see Figures 4.4a to 4.5d. The red area increases as the moment arm increase and drop further into the blue zone were the frequency range is $0 < \omega < 0.25\ \text{s}^{-1}$.

Table 4.4a: 1st Frequency of a beam with a tip mass ($b_1 = L/1$) and rotary inertia at 0V.

Axial load Ratio (k)	$\eta = 0$	$\eta = 0.1$	$\eta = 1$	$\eta = 5$	$\eta = 10$
+0.8	1.25	0.85	0.50	0.34	0.28
+0.4	1.66	1.12	0.66	0.44	0.37
+0.2	1.78	1.20	0.70	0.47	0.40
0	1.88	1.26	0.74	0.50	0.42
-0.4	2.03	1.37	0.80	0.53	0.45
-1	2.19	1.48	0.86	0.58	0.49
-2	2.40	1.62	0.94	0.63	0.53

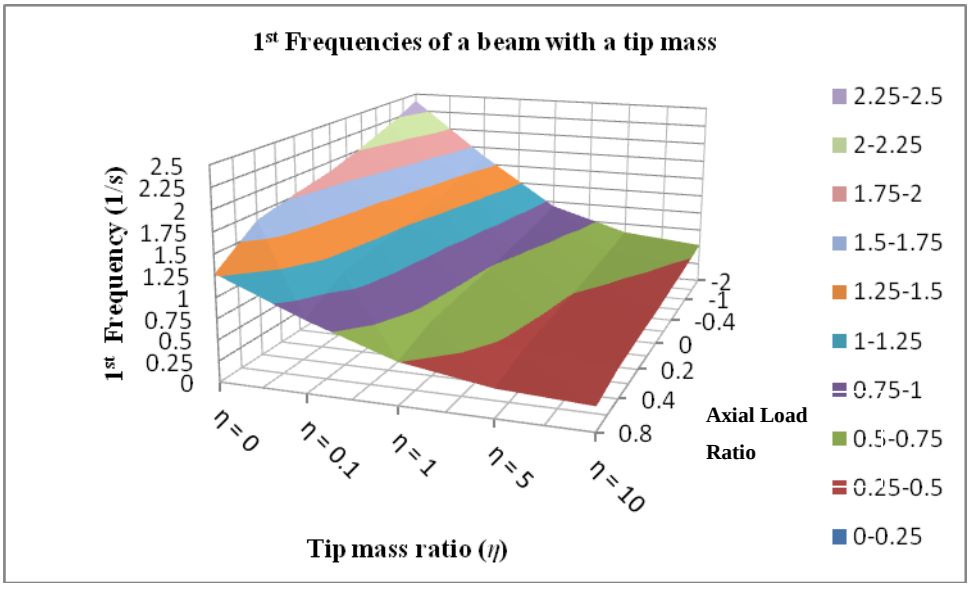

Figure 4.5a: Natural frequency vs axial load and tip mass for $b_1 = L//1$ and $V = 0$V

Figure 4.3a shows the natural frequencies for a beam with inactive piezo layers ($\bar{}_{+}V = 0\text{V}$). Along the axial load ratio axis it is noted that the limit were the area of lowest natural frequencies is at k = +0.2. As we increase the voltage input to the piezo layers it is also noted that the limit changes, Figures 4.3b to 4.3d, to k = +0.2, k = +0.1, k = -0.4 for voltage inputs of, $\bar{}_{+}V = 100\text{V}$, $\bar{}_{+}V = 500\text{V}$, $\bar{}_{+}V = 1000\text{V}$ along η = 10; respectively. It is observed that the largest deviation, when compared to an inactive beam occurs at maximum voltage input. It can be concluded that by increasing the voltage input, the number of natural frequencies occurring in the lowest range can be increased and therefore the vibration characteristics of the system changed.

Table 4.4b: 1st Frequency of a beam with a tip mass ($b_1 = L/1$) and rotary inertia at 100V.

Axial load Ratio (k)	$\eta = 0$	$\eta = 0.1$	$\eta = 1$	$\eta = 5$	$\eta = 10$
+0.8	1.24	0.83	0.49	0.33	0.28
+0.4	1.65	1.11	0.65	0.44	0.37
+0.2	1.77	1.19	0.70	0.47	0.39
0	1.87	1.26	0.73	0.49	0.41
-0.4	2.02	1.36	0.79	0.53	0.45
-1	2.19	1.48	0.86	0.58	0.48
-2	2.39	1.62	0.93	0.63	0.53

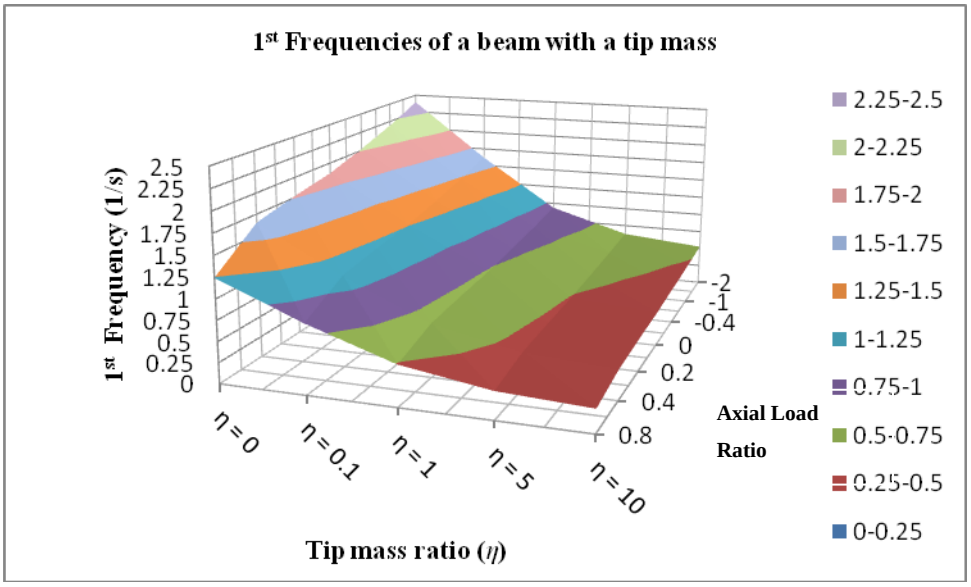

Figure 4.5b: Natural frequency vs axial load and tip mass for $b_1 = L//1$ and V =100V

At maximum voltage input for a concentrated load ($\bar{+}V = 1000$V and $b_1 = 0$) the limit of the area of lowest frequencies ($0.25 < \omega < 0.5s^{-1}$) is $k = 0$ along the axial load ratio axis, see Figure 4.3a to 4.5d. From Figure 4.4d and 4.5d it is noted that the outer limit of the area increases as the moment arm increases along the axial load axis, the lower frequency zone increases from $k = -0.4$ and $k = -1.5$ for $b_1 = L/2$ and $b_1 = L/1$, respectively. By increasing the moment arm more area is captured and thereby attenuates the natural frequencies. The addition of an input voltage adds an additional decrease as discussed earlier. Tables 4.2a to 4.4d show the natural frequencies of the system with all the parameters taken into account.

Table 4.4c: 1st Frequency of a beam with a tip mass ($b_1 = L/1$) and rotary inertia at 500V.

Axial load Ratio (k)	$\eta = 0$	$\eta = 0.1$	$\eta = 1$	$\eta = 5$	$\eta = 10$
+0.8	1.09	0.73	0.43	0.29	0.24
+0.4	1.60	1.07	0.63	0.42	0.35
+0.2	1.73	1.16	0.68	0.46	0.38
0	1.84	1.23	0.72	0.48	0.41
-0.4	2.00	1.34	0.78	0.52	0.44
-1	2.17	1.46	0.85	0.57	0.48
-2	2.38	1.61	0.93	0.62	0.52

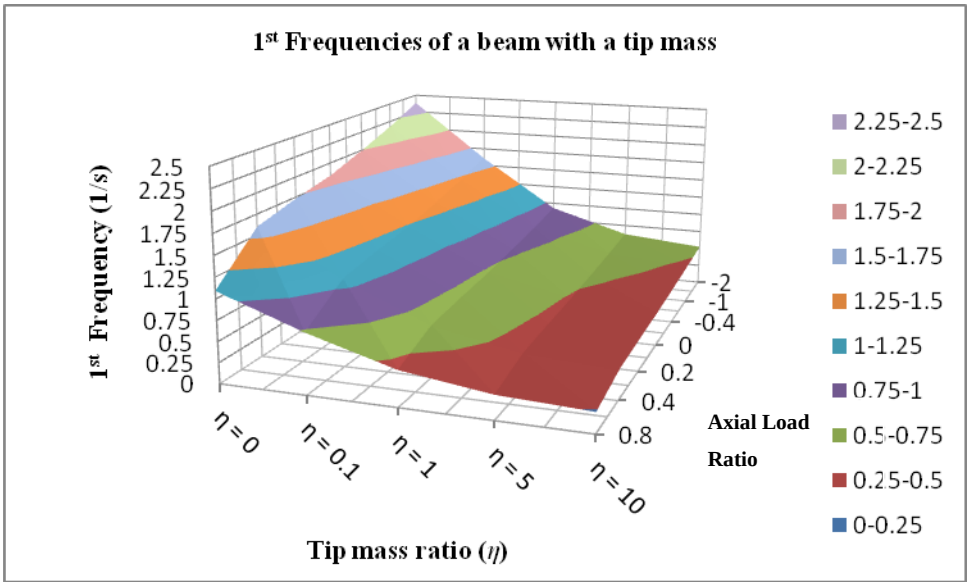

Figure 4.5c: Natural frequency vs axial load and tip mass for $b_1 = L//1$ and $V = 500$V

At $b_1 = 0$, for an inactive beam $(\overset{-}{+}V = 0\text{V})$ the natural frequency is $\omega = 0.3614\text{s}^{-1}$ and at maximum input voltage $(\overset{-}{+}V = 1000\text{V})$ the frequency is $\omega = 0.1855\text{s}^{-1}$, at $b_1 = L/2$ the frequency is $\omega = 0.3202\text{s}^{-1}$ for $\overset{-}{+}V = 0\text{V}$ along with $\omega = 0.1643\text{s}^{-1}$ for $\overset{-}{+}V = 1000\text{V}$ and at $b_1 = L/1$ the frequency is $\omega = 0.2844\text{s}^{-1}$ for $\overset{-}{+}V = 0\text{V}$ along with $\omega = 0.1460\text{s}^{-1}$ for $\overset{-}{+}V = 1000\text{V}$, which represents a decrease of approximately 50% in the natural frequencies.

By keeping the input voltage constant and varying the moment arm, the decrease calculated from the data is approximately 11%. This goes to indicate that the piezo electric actuators have a significant effect on the vibrations.

Table 4.4d: 1st Frequency of a beam with a tip mass ($b_1 = L/1$) and rotary inertia at 1000V.

Axial load Ratio (k)	$\eta = 0$	$\eta = 0.1$	$\eta = 1$	$\eta = 5$	$\eta = 10$
+0.8	0.66	0.44	0.26	0.18	0.15
+0.4	1.53	1.02	0.60	0.40	0.34
+0.2	1.68	1.12	0.66	0.44	0.37
0	1.79	1.20	0.70	0.47	0.40
-0.4	1.97	1.32	0.77	0.51	0.43
-1	2.15	1.44	0.84	0.56	0.47
-2	2.37	1.59	0.92	0.62	0.52

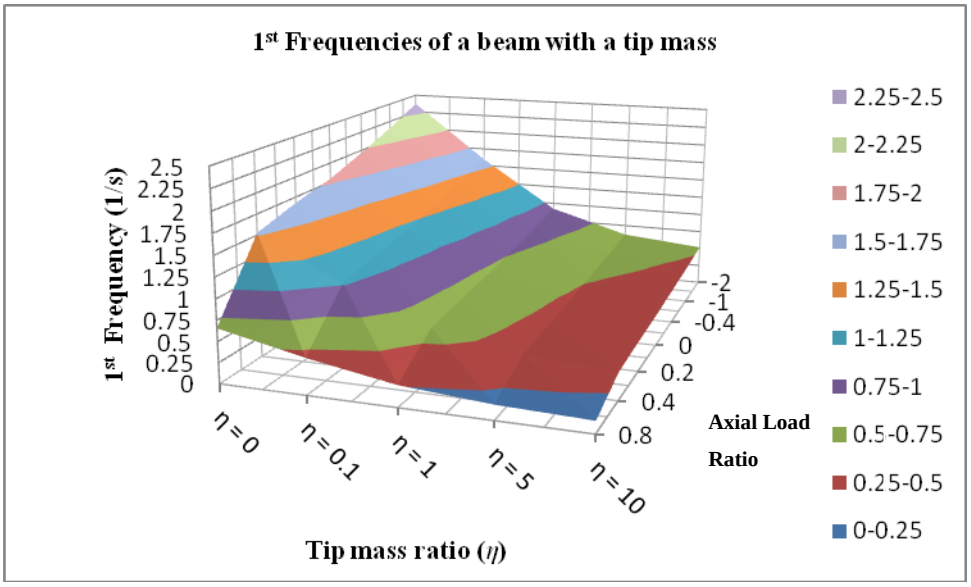

Figure 4.5d: Natural frequency vs axial load and tip mass for $b_1 = L/1$ and V =1000V

Chapter 5 – Effect of actuator thickness and voltage polarity on the frequencies

5.1 Fundamental frequencies for a beam with different actuator thicknesses

So far in the investigation it has been shown that the frequencies of vibration for a cantilevered beam with a tip mass and axial load can be modified with the use of piezo electric actuators. The above investigation was based on the piezo actuators with a thickness of one millimeter ($h_1 = h_2 = 1$mm). With a thickness of 1mm we showed that the piezo actuators were effective within a range of axial load ratio ($+0.8 < k < -2$) and tip mass ratio ($0 < \eta < 5$). According to the literature on piezo actuators it is reasonable to limit the voltage input to $\bar{}_{+}V = 1000\text{V}$ per millimeter to prevent the saturation of the piezo material. In this section the effectiveness of the piezo actuators is investigated when the piezo thickness is increased to 2mm and the input voltage is also increased to $\bar{}_{+}V = 2000\text{V}$, while keeping the overall thickness of the composite the same; that is the thickness of the composite is limited to 12mm. For the 2mm piezo layer thickness ($h_1 = h_2 = 2$mm) the overall thickness of the piezoelectric beam is maintained and therefore the beam thickness is reduced 8mm.

In the earlier sections of this investigation, it is noted that the piezo actuator has an insignificant or zero effect on the higher natural frequencies (ω_n - for $n > 1$) of the beam; and therefore the subsequent investigation focuses on the most relevant mode of vibration, which is the fundamental mode (1^{st} natural frequency). Figure 5.1 shows the plot the of the 1^{st} natural frequency (ω_1) vs. the axial load (k) for different input voltages ($\bar{}_{+}V = 0\text{V}, 1000\text{V}$ and 2000V), where 1000V is applied to the beam with 1mm piezo layers at the top and bottom of the beam and 2000V applied to the beam with 2mm piezo layers at the top and bottom.

It was observed earlier, in Section 3.5, that the piezo actuators are ineffective in controlling the fundamental frequency beyond a particular axial load ratio ($k < -2$). In the plot of Figure 5.1, the tip mass ratio is kept constant ($\eta = 0$) and both the axial load ratio and the voltage are varied. For an axial load $k \leq -2$ the differences in the fundamental modes are

minimal. The largest difference in the frequencies occurs at near critical load when the axial load ratio is k = +0.8.

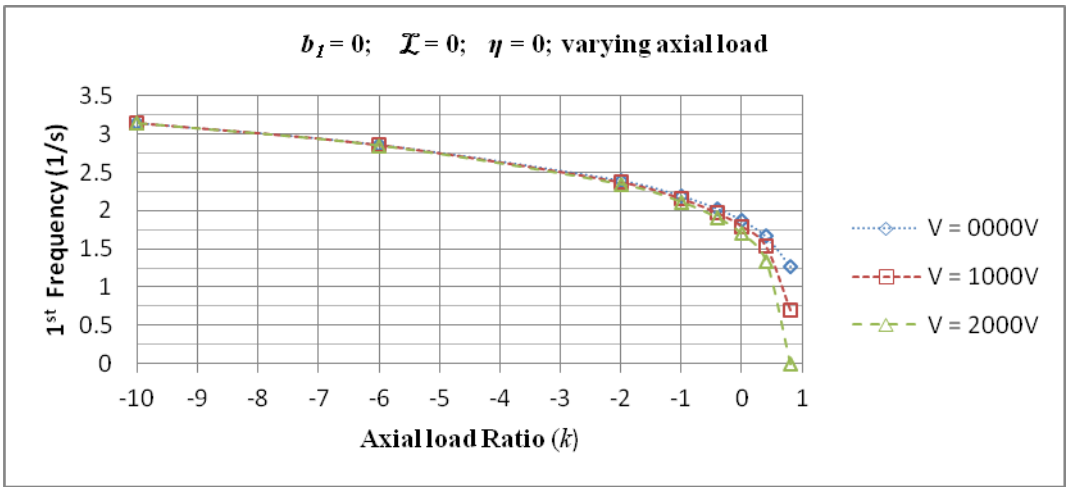

Figure 5.1: 1st Natural frequency vs axial load for different voltages (b_1 = 0)

At k = -2, the natural frequencies are; 2.3972s^{-1} for an uncontrolled beam ($\bar{+}V = 0\text{V}$), 2.3716s^{-1} for a controlled with beam, $\bar{+}V = 1000\text{V}$ and 2.3442s^{-1} for a controlled beam with $\bar{+}V = 2000\text{V}$. The percentage difference at $\bar{+}V = 0\text{V}$ and $\bar{+}V = 1000\text{V}$ is 1.068% and for $\bar{+}V = 0\text{V}$ and $\bar{+}V = 2000\text{V}$ is 2.211%. At k = +0.8 it is noted that there is a large difference between uncontrolled beam and controlled beam, where the frequency of the uncontrolled beam ($\bar{+}V = 0\text{V}$) is 1.2742s^{-1} and for the controlled beam ($\bar{+}V = 1000\text{V}$) is 0.6597s^{-1}. When the voltage is $\bar{+}V = 2000\text{V}$ the beam buckles and there are zero vibrations in the beam. The percentage difference at $\bar{+}V = 0\text{V}$ and $\bar{+}V = 1000\text{V}$ is 44.71% and for $\bar{+}V = 0\text{V}$ and $\bar{+}V = 2000\text{V}$ is 100%.

Again, an observation of Figure 5.1 shows that the natural frequency the system when k = +0.8 and the input voltage is $\bar{+}V = 2000\text{V}$ is zero. By applying an increasing axially compressive load on the beam, the beam buckles. When this occurs, the frequency of vibration approaches zero in the limit ($\omega_1 \rightarrow 0$). In this case the axial load is limited, $N = +0.8P_{cr}$, where P_{cr} is the critical buckling load of the beam.

Therefore by applying $\bar{+}V = 2000\text{V}$ to the piezo actuators, the system goes into buckling, hence the frequency of zero in this case. This buckling load can be determined by setting the frequency parameter (a_4) in the characteristic equation (equation 2.86) to zero and the axial load parameter (β) becomes an unknown which can be used to determine the critical buckling load for the system (Bokaian, 1988). This buckling phenomenon is referred to as divergence and it occurs when the frequency is zero (Abedinnasab *et al.*, 2011).

To further study the fundamental frequencies of the system for a beam with $h_1 = h_2 = 2\text{mm}$ piezo thickness and induced voltage $\bar{+}V = 2000\text{V}$, the axial load ratio is kept constant ($k = 0$). Table 5.1 lists the natural frequencies for a beam without any rotary inertia ($\mathcal{I} = 0$) with a control voltage of $\bar{+}V = 0\text{V}, 1000\text{V}$ and 2000V; and the frequencies of a beam including the rotary effects due to inertia ($\mathcal{I} = 0.146\text{mm}$) at the tip. The left hand side of Table 5.1 shows the frequencies without rotary inertia and the right hand side is the frequencies including rotary inertia. Both sets of frequencies in Table 5.1 are for a concentrated mass is at tip and the moment arm $b_1 = 0$.

Table 5.1: Fundamental frequency of a beam with tip mass ($b_1 = 0$), axial load ($k = 0$), beam thickness ($h_b = 8\text{mm}$) and top and bottom piezo ($h_1 = h_2 = 2\text{mm}$).

$b_1 = 0;\quad \mathcal{I} = 0;\quad k = 0$ (without rotary inertia)				$b_1 = 0;\quad \mathcal{I} = 0.146;\quad k = 0$ (with rotary inertia)			
Tip mass Ratio (η)	$\bar{+}V = 0\text{V}$	$\bar{+}V = 1000\text{V}$	$\bar{+}V = 2000\text{V}$	Tip mass Ratio (η)	$\bar{+}V = 0\text{V}$	$\bar{+}V = 1000\text{V}$	$\bar{+}V = 2000\text{V}$
0	1.88	1.79	1.70	0	1.88	1.79	1.70
0.1	1.72	1.65	1.55	0.1	1.51	1.43	1.34
1	1.25	1.19	1.12	1	0.93	0.88	0.83
5	0.87	0.83	0.78	5	0.63	0.60	0.56
10	0.74	0.70	0.66	10	0.53	0.50	0.47

It is observed that the two parameters, tip mass ratio and induced voltage have the same effects, i.e. an increase the tip mass or the induced voltage results in a decrease in the natural frequencies. The highest frequencies occur when the tip mass ratio is zero ($\eta = 0$, $\omega_1 = 1.8751$) and the voltage is zero ($\bar{+}V = 0\text{V}$) and then decreases to ($\omega_1 = 0.4722$) when the tip mass ratio and the voltage are maximum; $\eta = 10$ and $\bar{+}V = 2000\text{V}$. This represents a percentage change (decrease) of 74.82% from an unloaded and uncontrolled beam to a maximum loaded and controlled beam. If the tip mass ratio is zero ($\eta = 0$) and the tip mass ratio is maximum ($\eta = 10$) the percentage difference is 60.76% and when the tip mass ratio is

minimal (η = 0) and the voltage is zero ($\bar{+}V = 0\text{V}$) and maximum voltage ($\bar{+}V = 2000\text{V}$), the percentage difference is 9.49%. This indicates that the tip mass has a dominant effect on the frequencies as the mass increases and more influence than the induced voltage. This cut-off point can be found when the tip mass is $\eta > 1$, at which point the percentage change levels off, for a beam without inertia and a beam with inertia, see Table 5.1.

As expected, in Figure 5.1 and Table 5.2, the frequencies at zero tip mass (η = 0) at the different voltages ($\bar{+}V = 0\text{V}, 1000\text{V}$ and 2000V) correspond regardless of whether inertia is taken into account or not for any value of the moment arm (b_1). At a voltage of: $\bar{+}V = 0\text{V}, 1000\text{V}$ and 2000V, the frequencies are: ω_1 = 1.8751s^{-1}, 1.7945s^{-1} and 1.6972s^{-1}.

Table 5.2: Fundamental frequency of a beam with tip mass ($b_1 > 0$), axial load ($k = 0$), beam thickness (h_b = 8mm) and top and bottom piezo ($h_1 = h_2$ = 2mm).

$b_1 = L/2$; $\mathcal{L} = 0.146$; $k = 0$ (with rotary inertia)				$b_1 = L/1$; $\mathcal{L} = 0.146$; $k = 0$ (with rotary inertia)			
Tip mass Ratio (η)	$\bar{+}V = 0\text{V}$	$\bar{+}V = 1000\text{V}$	$\bar{+}V = 2000\text{V}$	Tip mass Ratio (η)	$\bar{+}V = 0\text{V}$	$\bar{+}V = 1000\text{V}$	$\bar{+}V = 2000\text{V}$
0	1.88	1.79	1.70	0	1.88	1.79	1.70
0.1	1.39	1.32	1.24	0.1	1.26	1.20	1.12
1	0.83	0.79	0.74	1	0.74	0.70	0.66
5	0.56	0.53	0.50	5	0.50	0.47	0.44
10	0.47	0.45	0.42	10	0.42	0.40	0.37

This is totally in accordance to our expectation because if the tip mass ratio is zero (η = 0), the moment arm (b_1) can be any value and results are the same. Table 5.1 and 5.2 shows that the frequencies decrease as the tip mass ratio and the voltage increase and also that the gradient of the curves is very steep when $0 < \eta < 1$. This shows that there is a bigger change in frequency for a change in tip mass ratio. The gradient of the curves is much smaller when the tip mass ratio $\eta > 1$, meaning that a much larger change in the axial load ratio and the voltage only has a small effect on the natural frequencies. From Table 5.1 and 5.2 the percentage difference of the frequencies for $b_1 = L/2$ and $b_1 = L/1$ can be calculated. For the moment arm $b_1 = L/2$ and $b_1 = L/1$ at a voltage of $\bar{+}V = 0\text{V}$ and 1000V, the difference is ≈ 5 %, and for the moment arm $b_1 = L/2$ and $b_1 = L/1$ at a voltage of $\bar{+}V = 0\text{V}$ and 2000V the difference is $\approx 10\%$. The difference between the curves tends to become constant as the tip mass ratio increases. From the above data it is concluded that if the thickness of the piezo layer and the input voltage are increased, the natural frequencies decreases even further.

5.2 Effect of voltage polarity on frequencies

5.2.1 Increase in the fundamental frequency

If the polarity of the voltage input to the piezoelectric beam are selected according to Table 2.2; such that, the system undergoes a tensile load due to strain induced by the piezo actuator, the natural frequencies increase. Table 5.3 shows the natural frequencies of an uncontrolled beam whilst Table 5.4 and 5.5 shows the frequencies of a controlled beam. The controlled frequencies show a higher difference in the first mode of vibration but only a slight difference in the second, third and fourth mode as in the discussed in Chapter 3. The piezo actuators do not have a notable effect on the second and higher modes of vibration of the system. The zeroth eigenvalue (ω_0) or characteristic value for the frequency equation is trivial, $\omega_0 = 0$ and therefore the tables indicate the fundamental frequency.

The fundamental frequency is increased when a voltage is applied and the values for the increase are shown in Table 5.4 and 5.5. The fundamental frequency can be increased by approximately 17% at maximum compressive load (k = +0.8) for varying tip mass ratio as indicated in Table 5.6. The difference in frequency gap increases as the tip mass ratio increases and levels off for $\eta \geq 5$. In Section 3.2 the investigation uncovered the fact that the natural frequencies for tip mass ratio η = 5 and η = 10 are only slightly different in the first mode and almost identical in the higher modes.

In Table 5.5 the natural frequencies of a controlled beam are listed for an input voltage of $^{+}_{-}V = 2000\text{V}$. In Section 5.1 above the overall thickness of the bottom and top piezo actuators was increased from 1mm to 2mm which allowed us to increase to input voltage. These frequencies are higher compared to the frequencies for an uncontrolled beam and for a controlled beam at $^{+}_{-}V = 1000\text{V}$. The effects on the second natural frequencies due to an increase in the voltage are insignificant. When applying an increased voltage the fundamental frequencies can be further increased up to approximately 28% for compressive loads. That represents an increase of about 10% from an input voltage of $^{+}_{-}V = 1000\text{V}$ at k = +0.8 for tip mass ratio $\eta \leq 10$.

Table 5.3: Fundamental frequencies for uncontrolled beam $\overset{-}{+}V = 0\text{V}$.

	Voltage = 0V (ω_1)				
Axial load Ratio (k)	$\eta = 0$	$\eta = 0.1$	$\eta = 1$	$\eta = 5$	$\eta = 10$
0.8	1.27	1.17	0.84	0.58	0.49
0.4	1.66	1.52	1.10	0.77	0.65
0	1.88	1.72	1.25	0.87	0.74
-1	2.19	2.03	1.48	1.03	0.87
-6	2.87	2.68	1.99	1.40	1.18
-10	3.15	2.96	2.22	1.56	1.32

Table 5.4: Fundamental frequencies for controlled beam $\overset{+}{-}V = 1000\text{V}$.

	Voltage = -1000V (ω_1)				
Axial load Ratio (k)	$\eta = 0$	$\eta = 0.1$	$\eta = 1$	$\eta = 5$	$\eta = 10$
0.8	1.49	1.37	0.99	0.69	0.58
0.4	1.77	1.62	1.18	0.82	0.69
0	1.95	1.79	1.30	0.91	0.77
-1	2.23	2.06	1.51	1.05	0.89
-6	2.87	2.69	2.00	1.40	1.19
-10	3.15	2.96	2.22	1.56	1.32

Table 5.5: Fundamental frequencies for controlled beam $\overset{+}{-}V = 2000\text{V}$.

	Voltage = -2000V (ω_1)				
Axial load ratio (k)	$\eta = 0$	$\eta = 0.1$	$\eta = 1$	$\eta = 5$	$\eta = 10$
0.8	1.63	1.50	1.08	0.76	0.64
0.4	1.85	1.70	1.24	0.86	0.73
0	2.00	1.85	1.34	0.94	0.79
-1	2.26	2.10	1.54	1.07	0.91
-6	2.88	2.70	2.01	1.41	1.19
-10	3.16	2.97	2.23	1.57	1.33

Table 5.7 shows that the increase in the fundamental frequency becomes smaller as the beam is subjected to a tensile load and insignificant beyond k = -1. Using piezo actuators the fundamental frequencies of the system can be increase to make room for a larger range of external excitation frequencies.

Table 5.6: Percentage change in fundamental frequency between uncontrolled $^{-}_{+}V = 0\text{V}$ and controlled beam $^{+}_{-}V = 1000\text{V}$.

	Percentage change in fundamental frequency $\frac{(\omega_1)_{1000\text{V}} - (\omega_1)_{0\text{V}}}{(\omega_1)_{0\text{V}}} \times 100$				
Axial load Ratio (k)	η = 0	η = 0.1	η = 1	η = 5	η =10
0.8	17.22	17.42	17.78	17.83	17.85
0.4	6.34	6.55	6.78	6.90	6.89
0	3.74	3.92	4.17	4.22	4.25
-1	1.70	1.84	2.08	2.15	2.16
-6	0.32	0.39	0.55	0.57	0.58
-10	0.16	0.20	0.32	0.31	0.35

Table 5.7: Percentage change in fundamental frequency between uncontrolled $^{-}_{+}V = 0\text{V}$ and controlled beam $^{+}_{-}V = 2000\text{V}$.

	Percentage change in fundamental frequency $\frac{(\omega_1)_{2000\text{V}} - (\omega_1)_{0\text{V}}}{(\omega_1)_{0\text{V}}} \times 100$.				
Axial load Ratio (k)	η = 0	η = 0.1	η = 1	η = 5	η =10
0.8	28.18	28.63	29.36	29.50	29.54
0.4	11.30	11.70	12.23	12.41	12.41
0	6.86	7.21	7.72	7.83	7.88
-1	3.20	3.47	3.94	4.06	4.06
-6	0.61	0.75	1.05	1.10	1.11
-10	0.31	0.40	0.62	0.65	0.69

5.2.2 Increase in frequency gap between the fundamental and second natural frequency

In Section 2.4 a characteristic equation was developed to give the eigenvalues or natural frequencies. The characteristic values of equation 2.86 are dependent on axial load, tip mass, elastic column and the piezo actuators. The actuation due to the piezo layers is further dependent on material properties, input voltage magnitude, voltage polarity shown in Table 2.2 and the geometric properties (layer thickness, etc.). In this section the polarity of the input voltage is investigated with the view to widen the frequency gap between zero and the fundamental frequency (ω_0 and ω_1) and also between the fundamental frequency and the second natural frequency (ω_1 and ω_2).

Table 5.8a: 1st frequencies for uncontrolled beam $\pm V = 0$V

	Voltage = 0V (ω_1)				
(k)	$\eta = 0$	$\eta = 0.1$	$\eta = 1$	$\eta = 5$	$\eta = 10$
0.8	1.27	1.17	0.84	0.58	0.49
0.4	1.66	1.52	1.10	0.77	0.65
0	1.88	1.72	1.25	0.87	0.74
-1	2.19	2.03	1.48	1.03	0.87
-6	2.87	2.68	1.99	1.40	1.18
-10	3.15	2.96	2.22	1.56	1.32

Table 5.8b: Reduced 1st frequencies for controlled beam $\pm V = 1000$V

	Voltage = 1000V (ω_1)				
(k)	$\eta = 0$	$\eta = 0.1$	$\eta = 1$	$\eta = 5$	$\eta = 10$
0.8	0.66	0.73	0.53	0.37	0.31
0.4	1.54	1.41	1.02	0.71	0.60
0	1.79	1.65	1.19	0.83	0.70
-1	2.15	1.99	1.45	1.01	0.85
-6	2.86	2.67	1.98	1.39	1.18
-10	3.14	2.95	2.21	1.55	1.31

Table 5.8c: Reduced 1st frequencies for controlled beam $\pm V = 2000$V

	Voltage = 2000V (ω_1)				
(k)	$\eta = 0$	$\eta = 0.1$	$\eta = 1$	$\eta = 5$	$\eta = 10$
0.8	**	**	**	**	**
0.4	1.34	1.22	0.88	0.61	0.52
0	1.70	1.55	1.12	0.78	0.66
-1	2.11	1.94	1.41	0.98	0.83
-6	2.85	2.66	1.97	1.38	1.17
-10	3.14	2.94	2.20	1.54	1.31

**-- indicates zero frequency due to buckling.

Table 5.9b: 2nd frequencies for uncontrolled beam $\pm V = 0$V

	Voltage = 0V (ω_2)				
(k)	$\eta = 0$	$\eta = 0.1$	$\eta = 1$	$\eta = 5$	$\eta = 10$
0.8	4.53	4.26	3.93	3.85	3.84
0.4	4.62	4.33	3.98	3.90	3.89
0	4.69	4.40	4.03	3.95	3.94
-1	4.88	4.56	4.15	4.06	4.05
-6	5.55	5.17	4.64	4.52	4.51
-10	5.92	5.52	4.94	4.81	4.79

Table 5.9a: Reduced 2nd frequencies for controlled beam $\pm V = 1000$V

	Voltage = 1000V (ω_2)				
(k)	$\eta = 0$	$\eta = 0.1$	$\eta = 1$	$\eta = 5$	$\eta = 10$
0.8	4.51	4.25	3.92	3.85	3.84
0.4	4.60	4.32	3.98	3.90	3.89
0	4.68	4.39	4.03	3.95	3.94
-1	4.86	4.55	4.15	4.06	4.05
-6	5.54	5.16	4.64	4.52	4.51
-10	5.92	5.52	4.94	4.81	4.79

Table 5.9b: Reduced 2nd frequencies for controlled beam $\pm V = 2000$V

	Voltage = 2000V (ω_2)				
(k)	$\eta = 0$	$\eta = 0.1$	$\eta = 1$	$\eta = 5$	$\eta = 10$
0.8	4.49	4.24	3.92	3.85	3.84
0.4	4.58	4.31	3.97	3.90	3.89
0	4.66	4.38	4.03	3.95	3.94
-1	4.85	4.54	4.15	4.06	4.05
-6	5.53	5.15	4.64	4.52	4.51
-10	5.91	5.51	4.93	4.80	4.79

The effects of a varying voltage were established in Section 3.2. Tables 5.8a to 5.8c and Tables 5.9a to 5.9c show the first and second natural frequencies for an uncontrolled and controlled piezoelectric beam. It was noted in Section 3.3, Table 3.5d, that there is a maximum reduction in the fundamental frequency of 44% at zero tip mass ratio ($\eta = 0$) and maximum compressive load ($k = +0.8$). The reduction at maximum compressive axial load ratio remains high at 37% as the tip mass ratio is varied to $\eta = 10$. At zero axial load ($k = 0$) the reduction is approximately 4% for all cases in the fundamental mode. When an increasing tensile load is applied the difference decreases dramatically to less than 0.5%. In

the second and higher modes of vibration the maximim difference is less that 0.5% and therefore negligible.

Table 5.10: Difference between 1st and 2nd reduced frequencies for uncontrolled beam $\bar{}_{+}V = 0\text{V}$

	Voltage = 0V (ω_2 - ω_1)				
Axial load Ratio (k)	η = 0	η = 0.1	η = 1	η = 5	η =10
0.8	3.26	3.10	3.09	3.27	3.35
0.4	2.95	2.81	2.88	3.13	3.24
0	2.82	2.68	2.78	3.08	3.20
-1	2.68	2.53	2.68	3.03	3.18
-6	2.68	2.49	2.65	3.13	3.32
-10	2.78	2.57	2.72	3.25	3.47

Table 5.11: Difference between 1st and 2nd reduced frequencies for controlled beam $^{+}_{-}V = 1000\text{V}$

	Voltage = 1000V (ω_2 - ω_1)				
Axial load Ratio (k)	η = 0	η = 0.1	η = 1	η = 5	η =10
0.8	3.85	3.52	3.40	3.48	3.53
0.4	3.06	2.91	2.96	3.19	3.29
0	2.88	2.74	2.84	3.12	3.23
-1	2.71	2.56	2.70	3.05	3.20
-6	2.68	2.49	2.66	3.13	3.33
-10	2.77	2.57	2.73	3.25	3.47

Table 5.12: Difference between 1st and 2nd reduced frequencies for controlled beam $^{+}_{-}V = 2000\text{V}$

	Voltage = 2000V (ω_2 - ω_1)				
Axial load Ratio (k)	η = 0	η = 0.1	η = 1	η = 5	η =10
0.8	***	***	***	***	***
0.4	3.24	3.09	3.10	3.29	3.37
0	2.96	2.82	2.91	3.17	3.28
-1	2.74	2.59	2.74	3.08	3.22
-6	2.68	2.49	2.67	3.14	3.34
-10	2.77	2.57	2.73	3.26	3.48

***-- the difference cannot be expressed due to buckling of beam.

The frequency gap between the first and the second natural frequency is important in the design of structures. A mechanical structure has natural frequencies that are determined from the geometric and material properties. If these properties are unchanged the resonant frequencies remain unchanged and an external applied excitation frequency should fall within

this band of frequencies to prevent resonance. Tables 5.10 to 5.12 show the frequency gap between the first and the second natural frequency for an uncontrolled beam and a controlled beam. The frequency gap is significantly large for a compressive axial load and is reduced when a tensile load is applied. From the above discussion it is concluded that the difference is mainly due to the decrease if the fundamental frequency because the decrease in the second frequencies due to piezoelectric layers is negligible. A larger frequency gap is preferred in the design of mechanical structures because a larger band of excitation frequencies can be accommodated by the structure before it reaches resonance.

Table 5.13: Percentage change in frequency gap between uncontrolled $\bar{}_{+}V = 0\text{V}$ and controlled beam $\overset{+}{-}V = 1000\text{V}$.

	Change in frequency gap for 1st and 2nd frequency. $\frac{(\omega_2-\omega_1)_{0\text{V}}-(\omega_2-\omega_1)_{1000\text{V}}}{(\omega_1)_{0\text{V}}}\times 100$				
Axial load Ratio (k)	$\eta = 0$	$\eta = 0.1$	$\eta = 1$	$\eta = 5$	$\eta = 10$
0.8	18.33	13.59	10.02	6.63	5.49
0.4	3.59	3.71	2.89	1.90	1.55
0	2.32	2.26	1.86	1.23	1.01
-1	1.01	1.09	1.02	0.68	0.55
-6	0.03	0.12	0.29	0.21	0.18
-10	0.04	0.04	0.17	0.18	0.12

Table 5.14: Percentage difference in frequency gap between uncontrolled $\bar{}_{+}V = 0\text{V}$ and controlled beam $\overset{+}{-}V = 2000\text{V}$.

	Change in frequency gap for 1st and 2nd frequency. $\frac{(\omega_2-\omega_1)_{0\text{V}}-(\omega_2-\omega_1)_{2000\text{V}}}{(\omega_1)_{0\text{V}}}\times 100$				
Axial load Ratio (k)	$\eta = 0$	$\eta = 0.1$	$\eta = 1$	$\eta = 5$	$\eta = 10$
0.8	***	***	***	***	***
0.4	9.80	9.94	7.58	4.95	4.05
0	5.13	5.46	4.41	2.89	2.37
-1	2.06	2.48	2.30	1.53	1.24
-6	0.07	0.32	0.64	0.47	0.40
-10	0.06	0.08	0.40	0.34	0.26

***-- the percentage cannot be expressed due to buckling of beam.

The percentage difference between the frequency gap for an uncontrolled and controlled beam is highest for a compressive load ratio of k = +0.8 indicating that the system is most sensitve to the piezo actuators in compression. The percentage difference drops off as the tip mass ratio is increased because the higher mode frequencies converge rapidly to those of a

clamped pinned beam as the tip mass ratio increases ($\eta \rightarrow \infty$). The maximum increase in the gap is 18% whilst the minimum increase is 5% at compressive load. As the axial load changes to tension the difference decreases in a rapid fashion indicating that the piezo actuator loses its efficacy. In tensile load the fundamental frequencies decrease sharply within the axial load ratio range mentioned above in Table 5.13 and 5.14; and less so in the second frequencies. The percentage change in frequency gap for 1st and 2nd frequency becomes smaller and the piezo loses its effectiveness leading to the controlled beam resembling the uncontrolled beam.

In Table 5.8c when a compressive load of k = +0.8 and the control voltage input is increased to $\bar{}_{+}V = 2000\text{V}$ the beam undergoes buckling and therefore experiences no vibrations. The results at k = +0.8 for an input voltage of $\bar{}_{+}V = 2000\text{V}$ will not be analyzed further due to the buckling phenomenon. When the axial load ratio is k = +0.4 and a voltage of $\bar{}_{+}V = 2000\text{V}$ is applied buckling can be avoided. At k = +0.4 the change in the frequency gap is 9.80% compared to 3.59% for $\bar{}_{+}V = 2000\text{V}$ and $\bar{}_{+}V = 1000\text{V}$, respectively. It is noted in Tables 5.13 and 5.14 that the frequency gap between the first and the second frequencies can be doubled by increasing the voltage to $\bar{}_{+}V = 2000\text{V}$. When the tensile axial load is applied and $k \leq$ -1 the change in the frequency gap is approximately 2% and therefore insignificant.

Chapter 6 – Mode shapes of vibrating piezoelectric beam

6.1 First mode shapes for a beam with a concentrated tip mass

The deflection profiles of the beam in free vibration can be determined from the general solution, equation 2.62. Using the boundary conditions at the fixed end, the two constants A_n and D_n can be eliminated and the general solution is expressed in equation 6.1 in terms of two constants. The constants C_n and B_n are obtained from satisfying the boundary conditions at the free end.

$$X_n(x) = C_n\left(\sinh\, p_{1n}x - \frac{p_{1n}}{p_{2n}}\sin\, p_{2n}x\right) + B_n\left(\cos\, p_{2n}x - \cosh\, p_{1n}x\right) \tag{6.1}$$

After inserting the general solution into equation 4.1 and equation 4.2, the two equations below can be computed in terms of the remaining two constants where, for a concentrated mass $b_1 = 0$ and equation 4.18 and 4.19 reduce to equation 6.2 and 6.3 below.

$$C_n = +B_n \cdot \frac{\left[\left(p_{2n}^2 + C_A\right)\cos\, p_{2n}L + \left(p_{1n}^2 - C_A\right)\cosh\, p_{1n}L\right]}{\left[\frac{p_{1n}}{p_{2n}}\left(p_{2n}^2 + C_A\right)\sin\, p_{2n}L + \left(p_{1n}^2 - C_A\right)\sinh\, p_{1n}L\right]} \tag{6.2}$$

and,

$$B_n = -C_n\,\frac{p_{1n}}{p_{2n}}\left[\frac{\left(p_{2n}^2 - \beta^2\right)\cos\, p_{2n}L + \left(p_{1n}^2 + \beta^2\right)\cosh\, p_{1n}L + \eta a_n^4\left(\frac{1}{p_{1n}}\sinh\, p_{1n}L - \frac{1}{p_{2n}}\sin\, p_{2n}L\right)}{\left(p_{2n}^2 - \beta^2\right)\sin\, p_{2n}L - \frac{p_{1n}}{p_{2n}}\left(p_{1n}^2 + \beta^2\right)\sinh\, p_{1n}L + \eta a_n^4\left(\frac{1}{p_{2n}}\cos\, p_{2n}L - \frac{1}{p_{2n}}\cosh\, p_{1n}L\right)}\right] \tag{6.3}$$

By inserting C_n from equation 6.2 into equation 6.1 and 6.3 a general solution is obtained in terms of B_n alone; and therefore B_n can set to unity or any arbitrary constant. Below are the curves of the shape functions for a beam with tip mass, axial load and a voltage applied to the piezo actuator layers.

To investigate the tip deflection as the tip mass ratio is varied incrementally, hold the axial load constant (k = 0) and plot the first mode of vibration for incremental varying tip mass ratio's. In Section 3.4 the effect of tip mass on the natural frequencies was investigated and a conclusion was reached that as the tip mass increases the natural frequencies decrease, this can be observed in Figure 3.6a to 3.9d. It is also observed in Figure 3.1a to 3.4d that a compressive axial load decreases the natural frequencies, whilst a tensile axial load will increase the natural frequencies; see Table 3.1a to 3.4d. The same conclusion can be drawn for all the modes of vibration from the data in the above mentioned tables and figures for a concentrated tip mass, where the center of gravity of the mass coincides with the tip of the beam at x = 0.146m.

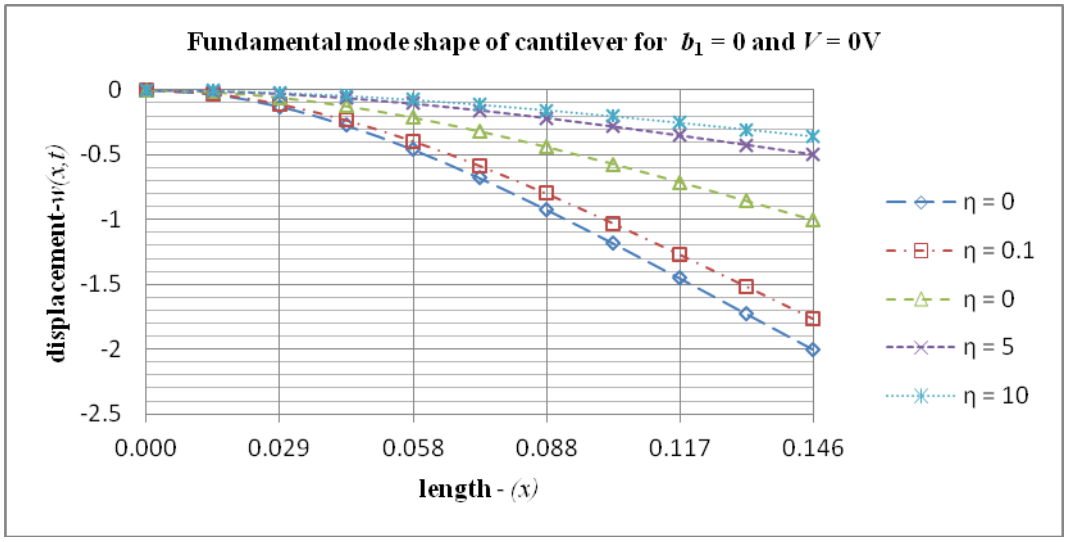

Figure 6.1: 1st Mode shape of vibration with inactive piezo actuators for Voltage = 0V

Figure 6.1 illustrates the 1st mode shapes of vibration for the system with zero input voltage ($\bar{+}V = 0\text{V}$) to the piezo actuators and zero axial load (k = 0). Figure 6.2 illustrates the 1st mode of vibration with maximum input voltage ($\bar{+}V = 1000\text{V}$) and an axial load ratio of zero (k = 0). In both figures it is observed that the transverse displacement of the tip is smallest

when the tip mass ratio is maximum (η = 10). As the tip mass ratio is decreased, there is an increment in tip deflection and the maximum deflection occurs at zero tip mass ratio (η = 0).

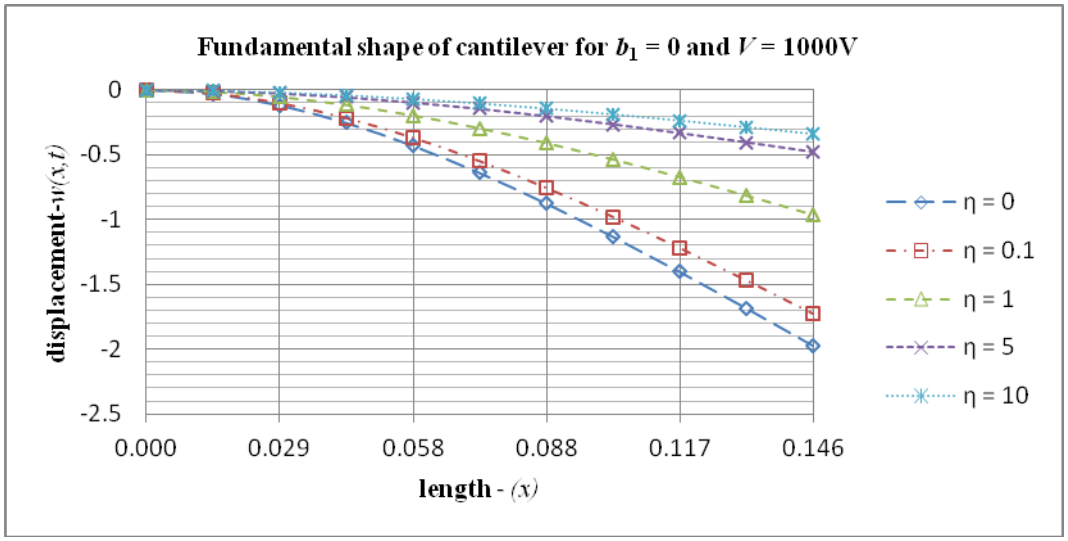

Figure 6.2: 1st Mode shape of vibration with active piezo actuators for Voltage = 1000V

In previous discussions about the relation between the natural frequencies and the tip mass it was concluded that as the tip mass ratio is increased, the natural frequencies of the system decrease. From the above figures, Figure 6.1 and 6.2, it is observed that as the tip mass ratio is increased, the tip deflection decreases. From this observation, it can be further asserted that as the natural frequency if the system decreases the tip deflection of the beam decreases accordingly. The curves in Figure 6.1 and 6.2 show a uniform change in the tip deflection as the tip mass changes. To verify the 1st mode shapes the first four first mode shapes: 1st, 2nd, 3rd and 4th mode shapes are plotted and compared to those attained in Balachandran *et al*., (2009). For the 1st mode it is not clear if the shape is the identical to that obtained by Balachandran *et al*., (2009) since the nature of the problem does not allow us to determine all the four constants (A_n, B_n, C_n and D_n) in the general solution of equation 2.62 and 6.1. The amplitude of the vibration cannot be determined until a time dependent initial conditions of the system is specified. The 2nd, 3rd and 4th mode shapes are plotted in the Appendix C1 and C2. The roots of the mode shapes in the higher modes of vibration are identical to those obtained by Balachandran *et al*., (2009), and so it follows that when the input voltage is set to zero ($\bar{+}V = 0\text{V}$), zero axial load ratio (k = 0) the 1st vibration mode shape should be similar to that attained in Balachandran *et al*., (2009).

Figure 6.2 shows the mode shape of an active beam with a maximum input voltage of 1000V. There are slight changes in the mode shape and the tip deflection but these are not apparent because as mentioned earlier, the nature of the solution only gives us the shape of the mode and not the amplitude. Nevertheless, it is observed that as the tip mass increases, the tip displacement decreases, i.e. as $\eta \rightarrow \infty$ the displacement $w(L,t) \rightarrow 0$ and the system resembles a clamped-hinged beam.

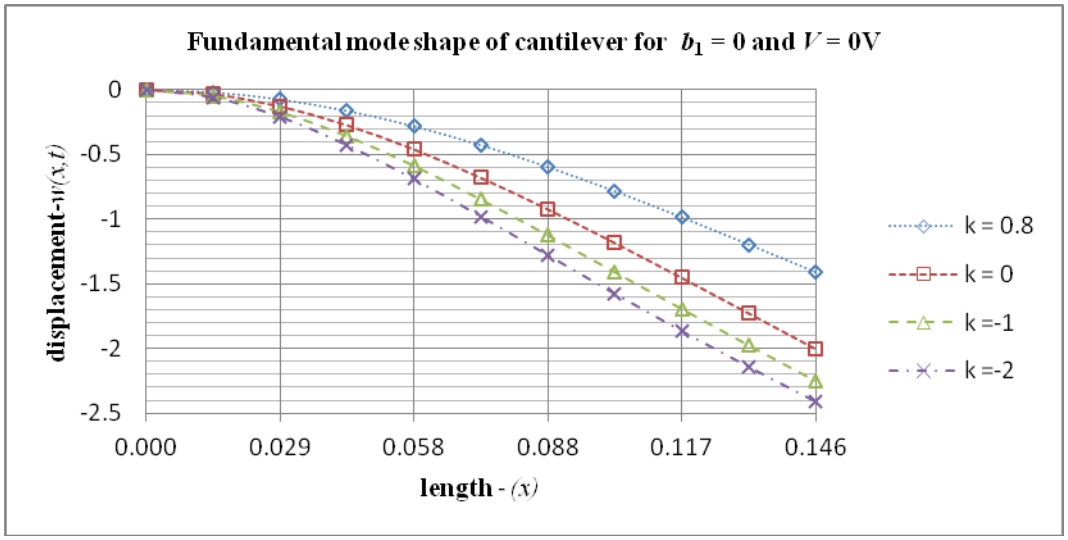

Figure 6.3: 1st Mode shape of vibration with inactive piezo actuators for Voltage = 0V

In Figure 6.3 and 6.4 the effect of the tip mass is eliminated by setting it to zero (η = 0) to investigate the effect of the piezo actuators on the modes shape if the axial load ratio is varied. Table 3.1a to 3.4d contains the natural frequencies for a beam with a tip mass and concentrated load where our area of interest is the column for zero tip mass (η = 0).

Applying a compressive load (k = +0.8) on the column produces the smallest tip deflection as observed in Figure 6.3 and when a tensile load ($k \leq 0$) is applied, the tip deflection of the vibration mode increases accordingly. From this data it is deduced that when a compressive load is applied, the tip displacement of the mode is decreased and when a tensile load is applied, the displacement increases for the vibration modes concerned.

In Section 3.2 it was noted that when the column is subjected to compressive load, the natural frequencies decrease and that a tensile load increases the natural frequencies. From the discussion on the tip mass above, Figure 6.1 and 6.2, it is also observed that as the natural

frequency decreases, so will the tip displacement of the mode of vibration, a finding which is agreeable with Balachandran *et al*., (2009).

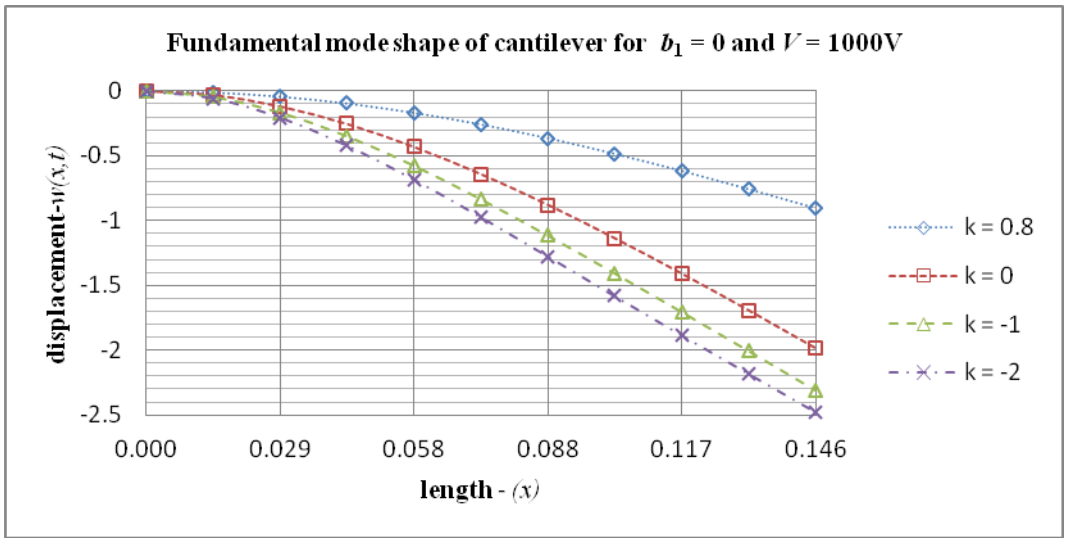

Figure 6.4: 1st Mode shape of vibration with active piezo actuators for Voltage =1000V

The data above suggest that as the natural frequency of the system decreases so will the displacement of the tip for the mode of vibration. The opposite should also hold true i.e. higher the natural frequency of the system, the higher the tip displacement of the mode of vibration. This statement can be affirmed in Figure 6.3 and 6.4.

Figure 6.4 represents the mode shape for an active beam with maximum input voltage ($\bar{}_{+}V = 1000\text{V}$). It is observed from this figure that the largest change in tip displacement occurs for the compressive load. From Section 3.3 it was found that the largest change in natural frequency occurs at maximum compressive load (k = +0.8) and maximum tip mass ratio (η = 10). Clearly, there are some changes in the tip displacement on the mode shape when an input voltage is applied to the piezo actuators. It is observed that in all cases, the tip displacement was diminished but the amplitude of vibration is not specified.

6.2 Mode shapes for a beam with an extended tip mass and rotary inertia ($b_1 > 0$)

The deflection profiles of the beam can be determined from the natural frequencies attained in section 4.3 in addition to using equations 6.4, 6.5 and 6.6 below. Equations 6.5 and 6.6 are obtain from the boundary conditions on the free end of the beam at $x = L$ using the general solution.

$$X_n(x) = C_n\left(\sinh p_{1n}x - \frac{p_{1n}}{p_{2n}}\sin p_{2n}x\right) + B_n\left(\cos p_{2n}x - \cosh p_{1n}x\right) \tag{6.4}$$

where,

$$C_n = \frac{-B_n(C_n^{11} + C_n^{12} + C_n^{13} + C_n^{14} + C_n^{15} + C_n^{16})}{C_n^{21} + C_n^{22} + C_n^{23} + C_n^{24} + C_n^{25} + C_n^{26} + C_n^{27}} \tag{6.5}$$

and,

$$C_n^{11} = -a^4\eta\mathrm{Cos}(p_2L)b_1p_2 \qquad C_n^{21} = \mathrm{Sin}(p_2L)b_1(a^4\eta b_1 + C_A)p_1$$

$$C_n^{12} = \mathrm{Cosh}(p_1L)(a^4\eta b_1 + C_A)p_2 \qquad C_n^{22} = -\mathrm{Sinh}(p_1L)(a^4\eta b_1 + C_A)p_2$$

$$C_n^{13} = a^4\eta\mathrm{Sinh}(p_1L)(\mathcal{L}^2 + b_1^2)p_1p_2 \qquad C_n^{23} = a^4\mathcal{L}^2\eta\mathrm{Cos}(p_2L)b_1p_1p_2$$

$$C_n^{14} = -\mathrm{Cosh}(p_1L)p_1^2p_2 \qquad C_n^{24} = a^4\eta\mathrm{Cos}(p_2L)b_1b_1^2p_1p_2$$

$$C_n^{15} = a^4\eta\mathrm{Sin}(p_2L)b_1(\mathcal{L}^2 + b_1^2)p_2^2 \qquad C_n^{25} = -a^4\eta\mathrm{Cosh}(p_1L)(\mathcal{L}^2 + b_1^2)p_1p_2$$

$$C_n^{16} = -\mathrm{Cos}(p_2L)b_1p_2(C_A + p_2^2) \qquad C_n^{26} = \mathrm{Sinh}(p_1L)p_1^2p_2$$

$$C_n^{27} = \mathrm{Sin}(p_2L)b_1p_1p_2^2$$

also,

$$B_n = \frac{-C_n(B_n^{11} + B_n^{12} + B_n^{13} + B_n^{14})}{B_n^{21} + B_n^{22} + B_n^{23} + B_n^{24}} \tag{6.6}$$

and,

$$B_n^{11} = -a^4\eta \mathrm{Sin}(p_2 L) b_1 p_1 \qquad B_n^{21} = a^4\eta \mathrm{Cos}(p_2 L) b_1 p_2$$

$$B_n^{12} = a^4\eta \mathrm{Sinh}(p_1 L) p_2 \qquad B_n^{22} = -a^4\eta \mathrm{Cosh}(p_1 L) p_2$$

$$B_n^{13} = \mathrm{Cosh}(p_1 L) p_1 (\beta^2 + a^4\eta b_1 + p_1^2) \qquad B_n^{23} = -\mathrm{Sinh}(p_1 L) p_1 (\beta^2 + a^4\eta b_1 + p_1^2) p_2$$

$$B_n^{14} = -\mathrm{Cos}(p_2 L) b_1 p_1 p_2 (\beta^2 + a^4\eta b_1 - p_2^2) \qquad B_n^{24} = -\mathrm{Sin}(p_2 L) b_1 p_2^2 (\beta^2 + a^4\eta b_1 - p_2^2)$$

By inserting C_n, in equation 6.5, into equations 6.4 and 6.6 a general solution is obtained in terms of B_n alone; and therefore B_n can be solved such that the tip displacement of the beam is a non-dimensional constant equal to unity (1). According to Merovitch, (2001), the amplitude of the mode shape cannot be determined uniquely but the shape form will be unique.

Chapter 7 – Dynamic behaviour of a piezoelectric beam subject to initial conditions

7.1 Initial value problem and the eigenfunction expansion series

In Section 2.2 the differential equation governing the vibration of a beam with axial load and tip mass were introduced. The boundary conditions for this particular configuration were presented in Section 2.3. Equation 7.1 represents the Partial Differential Equation (PDE) governing the vibration of the beam:

$$E_c I_c \frac{\partial^4 w}{\partial x^4} + N \frac{\partial^2 w}{\partial x^2} + \rho A \frac{\partial^2 w}{\partial t^2} = f(x,t) \tag{7.1}$$

The different boundary conditions at the fixed end of the beam and the free end of the beam are mentioned in Section 2.3. The boundary conditions were used to generate the characteristic values that satisfy the boundary conditions. To determine the dynamic solution to this problem, the sum of the eigenfunctions derived above are subjected to an initial velocity of the beam of zero, $v(x,0) = 0$ and the tip displacement will be two units, $w(L,0) = 2$. The sum of all the initial values of all the eigenfunctions is required to be 2 units. For this partial differential equation a separable solution (equation 7.2) is assumed:

$$w(x,t) = \sum_{n=1}^{\infty} X_n(x) T_n(t) \tag{7.2}$$

Equation 7.2 is an eigenfunction expansion series of all the modes of vibration which represents a complete solution of the problem. This solution is the sum of an infinite number of eigenfunctions and is approximated with the first six eigenfunctions for the different loading conditions. The first six eigenfunctions provide a satisfactory approximation with a small residual error, which is investigated later in the study. In the space domain the solution is:

$$X_n(x) = C_n\left(\sinh p_{1n}x - \frac{p_{1n}}{p_{2n}}\sin p_{2n}x\right) + B_n\left(\cos p_{2n}x - \cosh p_{1n}x\right) \tag{7.3}$$

where,

$$C_n = +B_n \cdot \frac{\left[\left(p_{2n}^2 + C_A\right)\cos p_{2n}L + \left(p_{1n}^2 - C_A\right)\cosh p_{1n}L\right]}{\left[\frac{p_{1n}}{p_{2n}}\left(p_{2n}^2 + C_A\right)\sin p_{2n}L + \left(p_{1n}^2 - C_A\right)\sinh p_{1n}L\right]} \tag{7.4}$$

and,

$$B_n = -C_n \frac{p_{1n}}{p_{2n}}\left[\frac{\left(p_{2n}^2 - \beta^2\right)\cos p_{2n}L + \left(p_{1n}^2 + \beta^2\right)\cosh p_{1n}L + \eta a_n^4\left(\frac{1}{p_{1n}}\sinh p_{1n}L - \frac{1}{p_{2n}}\sin p_{2n}L\right)}{\left(p_{2n}^2 - \beta^2\right)\sin p_{2n}L - \frac{p_{1n}}{p_{2n}}\left(p_{1n}^2 + \beta^2\right)\sinh p_{1n}L + \eta a_n^4\left(\frac{1}{p_{2n}}\cos p_{2n}L - \frac{1}{p_{2n}}\cosh p_{1n}L\right)}\right] \tag{7.5}$$

And in the temporal domain the solution is:

$$T_n(t) = E_n \sin \omega_n t + F_n \cos \omega_n t \tag{7.6}$$

After simplifying equations 7.3 to 7.6 and inserting the results into equation 7.2; B_n, E_n and F_n remain unknown and the equations is:

$$w(x,t) = \sum_{n=1}^{\infty} B_n X_n(x)[E_n \sin \omega_n t + F_n \cos \omega_n t] \tag{7.7a}$$

$$w(x,t) = \sum_{n=1}^{\infty} X_n(x)[\overline{E}_n \sin \omega_n t + \overline{F}_n \cos \omega_n t] \tag{7.7b}$$

The two constants (B_n and E_n) and (B_n and F_n) in equation 7.7 can be combined into two unknown constant to solve using the initial conditions. The new constant then becomes:

$$\overline{E}_n = B_n E_n \ , \quad \text{and} \quad \overline{F}_n = B_n F_n \tag{7.8}$$

The constant F_n is associated with the unique n^{th} eigenvalue for every mode of vibration. In this study the first 6 eigenfunctions are utilized to estimate the initial displacement along the beam. These constants in equation 7.9 can be determine from the initial conditions at time zero (t = 0).

$$w(x,t) = \overline{F_1}X_1(x)T_1(t) + \overline{F_2}X_2(x)T_2(t) + \overline{F_3}X_3(x)T_3(t) + \overline{F_4}X_4(x)T_4(t) + \overline{F_5}X_5(x)T_5(t) + \overline{F_6}X_6(x)T_6(t) + ... + \overline{F_n}X_n(x)T_n(t) \quad (7.9)$$

where the initial conditions are the displacement and the velocity of the beam at time equal to zero:

$$w(x,0) = \overline{X}_1(x) \quad (7.10)$$

where $\overline{X}_1(x)$ is the displacement of the beam with zero voltage ($\bar{+}V = 0\text{V}$) input for the piezo actuators, zero tip mass ($\eta = 0$)and zero axial load ($k = 0$). This configuration is that of a plain cantilever beam and the initial tip deflection $w(L,0) = \overline{X}_1(L) = 2$ is chosen as a condition for normalization of the series of eigenfunctions for the beam.

$$\frac{dw(x,0)}{dt} = 0 \quad (7.11)$$

From the above initial condition the solution in the time domain is $T_n(t) = \overline{F}_n \cos\omega_n t$. At time zero ($t = 0$), $T_n(0) = \overline{F}_n(1)$ in equation 7.7 and therefore:

$$\overline{F_1}X_1(x) + \overline{F_2}X_2(x) + \overline{F_3}X_3(x) + \overline{F_4}X_4(x) + \overline{F_5}X_5(x) + \overline{F_6}X_6(x) + ... + \overline{F_n}X_n(x) = \overline{X}_1(x) \quad (7.12)$$

The spatial function $X_n(x)$ will be used as X_n and $T_n(t)$ will be used as T_n. Multiply equation (110) by the corresponding eigenfunctions to generate equations 7.13a to 7.13g.

$$\overline{F_1}X_1X_1 + \overline{F_2}X_2X_1 + \overline{F_3}X_3X_1 + \overline{F_4}X_4X_1 + \overline{F_5}X_5X_1 + \overline{F_6}X_6X_1 + ... + \overline{F_n}X_nX_1 = \overline{X}_1X_1 \quad (7.13a)$$

$$\overline{F_1}X_1X_2 + \overline{F_2}X_2X_2 + \overline{F_3}X_3X_2 + \overline{F_4}X_4X_2 + \overline{F_5}X_5X_2 + \overline{F_6}X_6X_2 + ... + \overline{F_n}X_nX_2 = \overline{X}_1X_2 \quad (7.13b)$$

$$\overline{F_1}X_1X_3 + \overline{F_2}X_2X_3 + \overline{F_3}X_3X_3 + \overline{F_4}X_4X_3 + \overline{F_5}X_5X_3 + \overline{F_6}X_6X_3 + ... + \overline{F_n}X_nX_3 = \overline{X}_1X_3 \quad (7.13c)$$

$$\overline{F_1}X_1X_4 + \overline{F_2}X_2X_4 + \overline{F_3}X_3X_4 + \overline{F_4}X_4X_4 + \overline{F_5}X_5X_4 + \overline{F_6}X_6X_4 + ... + \overline{F_n}X_nX_4 = \overline{X}_1X_4 \quad (7.13d)$$

$$\overline{F_1}X_1X_5 + \overline{F_2}X_2X_5 + \overline{F_3}X_3X_5 + \overline{F_4}X_4X_5 + \overline{F_5}X_5X_5 + \overline{F_6}X_6X_5 + ... + \overline{F_n}X_nX_5 = \overline{X}_1X_5 \quad (7.13e)$$

$$\overline{F_1}X_1X_6 + \overline{F_2}X_2X_6 + \overline{F_3}X_3X_6 + \overline{F_4}X_4X_6 + \overline{F_5}X_5X_6 + \overline{F_6}X_6X_6 + ... + \overline{F_n}X_nX_6 = \overline{X}_1X_6 \quad (7.13f)$$

$$\overline{F}_1 X_1 X_n + \overline{F}_2 X_2 X_n + \overline{F}_3 X_3 X_n + \overline{F}_4 X_4 X_n + \overline{F}_5 X_5 X_n + \overline{F}_6 X_6 X_n + \ldots + \overline{F}_n X_n X_n = \overline{X}_1 X_n \quad (7.13g)$$

This generates an infinite series of equations with infinite number unknown constants ($\overline{F}_{1.....n}$) which can be solved simultaneously after integrating the terms on the LHS and RHS over the length of the beam in equations 7.13a to 7.13g. Equation 7.13a to 7.13g can be presented in matrix notation by letting $\mathcal{X}_{ij} = \int_0^L X_i X_j dx$ and $\overline{\mathcal{X}}_{ij} = \int_0^L \overline{X}_i X_j dx$:

$$\begin{bmatrix} \mathcal{X}_{11} & \mathcal{X}_{12} & \mathcal{X}_{13} & \cdots & \cdots & \mathcal{X}_{1n} \\ \mathcal{X}_{21} & \mathcal{X}_{22} & \mathcal{X}_{23} & \cdots & \cdots & \mathcal{X}_{2n} \\ \mathcal{X}_{31} & \mathcal{X}_{32} & \mathcal{X}_{33} & \cdots & \cdots & \mathcal{X}_{3n} \\ \cdots & \cdots & \cdots & \cdots & \cdots & \cdots \\ \cdots & \cdots & \cdots & \cdots & \cdots & \cdots \\ \mathcal{X}_{n1} & \mathcal{X}_{n2} & \ldots\mathcal{X}_{n3}. & \cdots & \cdots & \mathcal{X}_{nn} \end{bmatrix} \begin{bmatrix} \overline{F}_1 \\ \overline{F}_2 \\ \overline{F}_3 \\ \cdots \\ \cdots \\ \overline{F}_n \end{bmatrix} = \begin{bmatrix} \overline{\mathcal{X}}_{11} \\ \overline{\mathcal{X}}_{12} \\ \overline{\mathcal{X}}_{13} \\ \cdots \\ \cdots \\ \overline{\mathcal{X}}_{1n} \end{bmatrix} \quad (7.14a)$$

were $\boldsymbol{A}$ is an $(n \times n)$ matrix, $\boldsymbol{F}$ is an $(n \times 1)$ vector and $\boldsymbol{C}$ is an $(n \times 1)$ vector.

$$\boldsymbol{AF} = \boldsymbol{C} \text{ therefore } \boldsymbol{F} = \boldsymbol{A}^{-1}\boldsymbol{C} \quad (7.14b)$$

7.2 Convergence of the eigenfunction series expansion

The total solution for this problem is composed of an infinite number of functions $X_n(x)$ and $T_n(t)$, where $n \in \{1,2,3,\ldots. \infty\}$ that satisfy the boundary conditions and differential equation for a beam with axial load, tip mass and piezo actuators. All these individual functions can be considered a solution to the initial value problem, but in most cases when using a single function to estimate the initial condition, the estimated solution is unacceptable. For example, in equation 7.10 above, the displacement along the beam can be characterized with a function $\overline{X}_1(x)$ at time zero (t = 0). For this function, $\overline{X}_1(x)$ the tip mass ratio is zero (η = 0), the axial load ratio is zero (k = 0) and the voltage input into the piezo is zero $(\overset{-}{}_{+}V = 0\text{V})$.

In this case, the initial function is chosen as the exact solution for a cantilevered beam and it is therefore noted in Figure 7.1 that for tip mass ratio is zero (η = 0), the axial load ratio is zero (k = 0) the tip displacement remains the same regardless of the number of eigenfunctions

used to estimate the solution. For this case, the constants ($\overline{F}_{1.....n}$) in equations 713a to 7.13g can be solved and it is found that only the constant that is associated with the first mode of vibration of a cantilevered beam is non-zero. The constants associated with the higher modes of vibration approach zero in the limit.

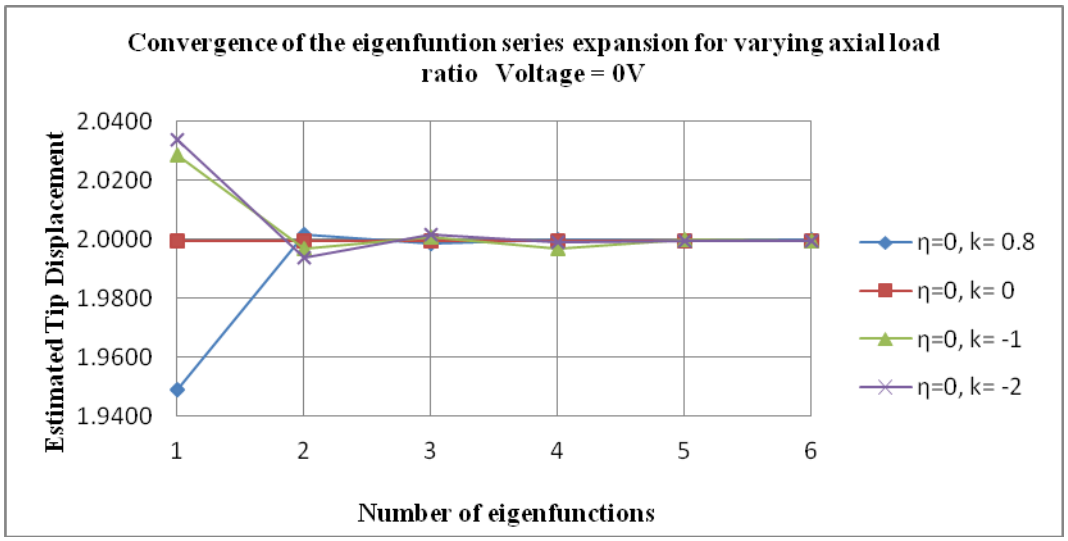

Figure 7.1: Convergence of eigenfunction expansion for Voltage = 0V

The rest of the constants ($\overline{F}_{2.....n}$) are infinitesimal and therefore, their associated eigenfunctions do not contribute to the estimation of the displacement. In this case it is adequate to use one solution to solve the initial value problem. This is a special case as can be observed from Figure 7.1. When the tip mass ratio is non-zero ($\eta \neq 0$), the axial load ratio is non-zero ($k \neq 0$) there is variation in the displacements as the number of eigenfunctions in the series expansion increases.

From Figures 7.1 and 7.2 it is noted that for certain combinations of axial load ratio and tip mass ratio the displacements are not identical. This means that the series of eigenfunctions does not satisfy the initial condition exactly and the sum of the functions approaches a critical point, which is a displacement of two units at the tip of the beam, $\overline{X}_1(L) = 2$. In other words, the relation below should hold true.

$$\lim_{n\to\infty} \sum_{i=1}^{n} \overline{F}_i X_i(x) T_i(t) = \overline{X}_1(x) \tag{7.15}$$

If the sum of the functions does not satisfy the initial conditions exactly there will be some residual (ϵ). This residual should be kept very small to render the approximation as close to the exact solution as possible.

$$\left|\sum_{i=1}^{n} \overline{F}_i X_i(x) T_i(0) - \overline{X}_1(x)\right| < \epsilon \tag{7.16}$$

If the tip mass ratio is disregarded (η = 0), Figure 7.1 shows that the largest residual occurs when only the first mode is used to approximate the initial function. The biggest percentage difference in the exact solution and the approximate solution is 2.54% for a compressive axial load (k = +0.8). For maximum axial load ratio (k = -2), the absolute value of the percentage difference in displacement residual is 1.68% at the same tip mass ratio. When the numbers of eigenfunctions used to approximate the solution is increased, the maximum percentage difference drops to 0.0288% for a six eigenfunction expansion. This difference is so small and the first six functions are adequate to approximate the initial conditions. In Figures 7.1 and 7.2 the estimated displacement at the tip is shown. It can be clearly seen that a single eigenfunction solution expansion is not adequate to satisfy the initial value problem. As the numbers increase beyond the first three eigenfunctions, $X_1(L)$, $X_2(L)$ and $X_3(L)$ the series resonates about the exact solution such that the total sum of the contributions is 2 units

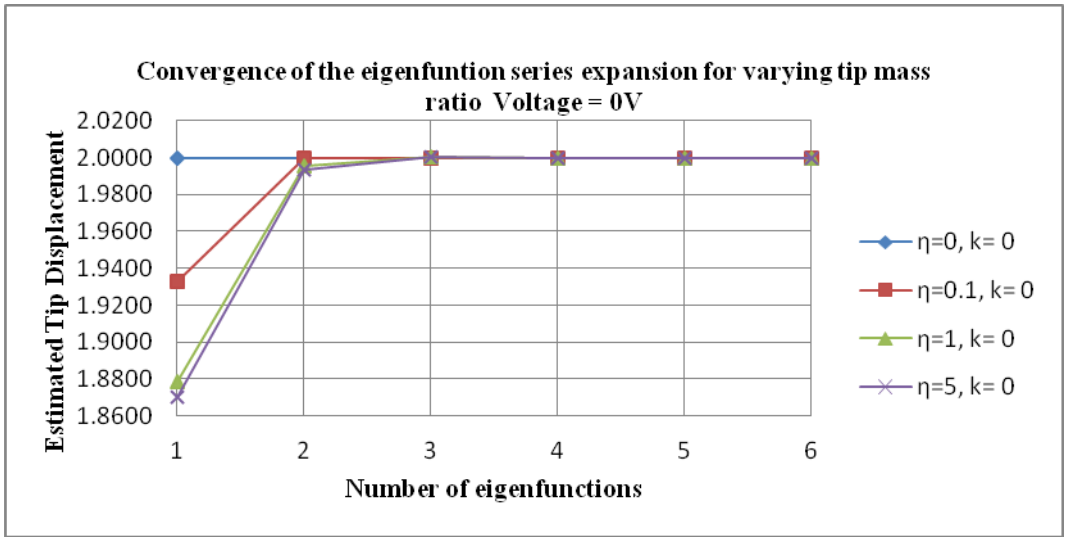

Figure 7.2: Convergence of eigenfunction expansion for Voltage = 0V

$$w(x,t) = \overline{X}_1(x) + \epsilon \quad \text{and} \quad w(x,t) = \overline{X}_1(x) - \epsilon \tag{7.17}$$

From the tables and figures above increasing the number of terms in the series beyond four (4) increases the accuracy of the eigenfunction expansion marginally. Therefore the number of terms used to estimate the solution is limited to six (6) terms. This study seeks to find out the effects of the piezo on the structure and so it is also of interest to investigate the convergence of the eigenfunction expansion when the piezo actuators are active ($\bar{+}V = 1000\text{V}$). Figure 7.3 and 7.4 show the tip displacement for an incremental number of eigenfunctions for an active beam. Right away it is noted that the results from using the first eigenfunction solution do not match those of a cantilevered beam, which is $\overline{X}_1(L) = 2$.

The biggest variation in the tip displacement occurs when only one eigenfunction is used to estimate the solution. When the tip mass ratio and the axial load ratio is varied, it is noted that the largest residual occurs when there is no tip mass (η = 0) and the beam is in compression (k = +0.8). This difference amounts to a 4.24% percentage difference compared to the initial value, $\overline{X}_1(L) = 2$ at time zero (t = 0). The difference is also apparent when there is no tip mass (η = 0) and axial load (k = +0.8) but the piezo actuators are active ($\bar{+}V = 1000\text{V}$); and amounts to 1.06% compared to 0.02% for an inactive beam ($\bar{+}V = 0\text{V}$).

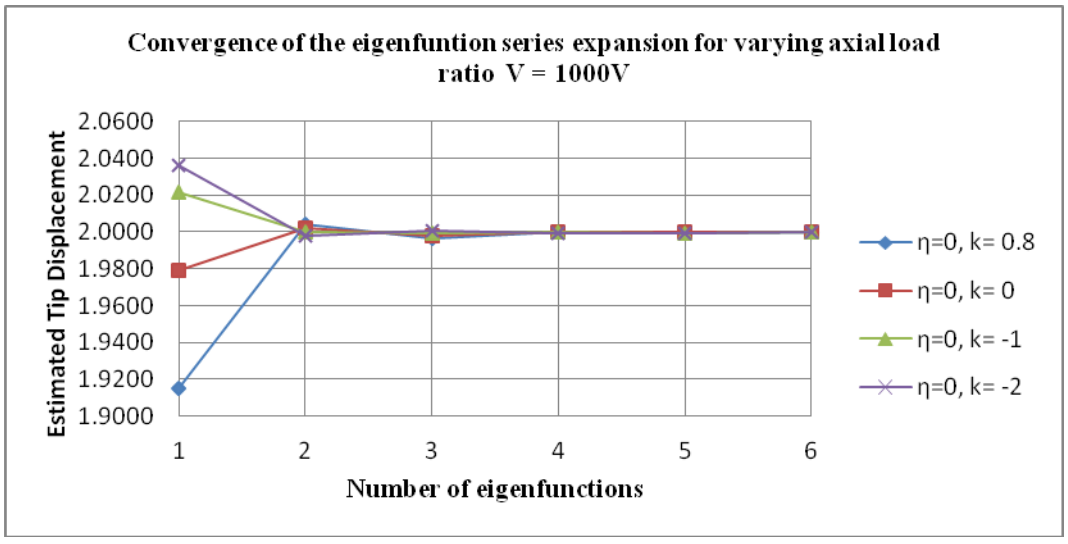

Figure 7.3: Convergence of eigenfunction expansion for Voltage =1000V

For the extreme loading, compression (k = +0.8) and tension (k = -2), the largest percentage variation in the tip displacement is noted, 4.24% and -1.8073%. By increasing the number of eigenfunctions to six, the percentage difference drop to 0.0153% and 0.0083%, for (η = 0, k = +0.8) and (η = 0, k = -2), respectively. In Figure 7.3 and 7.4 the eigenfunction series converges to $\overline{X}_1(L) = 2$. The same observation was made earlier when the piezo actuators were inactive $(\bar{+}V = 0\text{V})$ in Figures 7.1 and 7.2

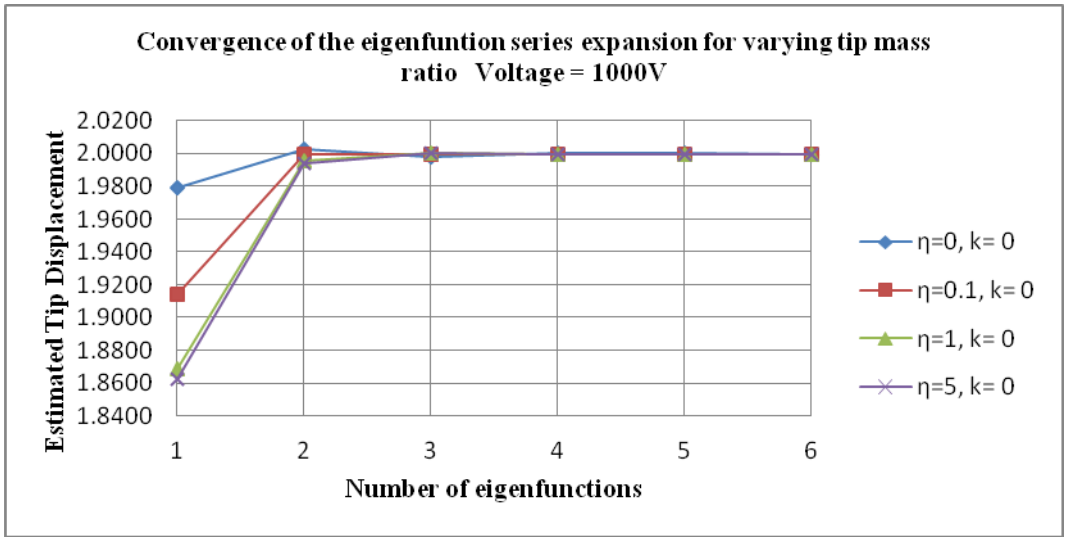

Figure 7.4: Convergence of eigenfunction expansion for Voltage =1000V

If the axial load is kept constant and the tip mass varied, it is observed that the largest percentage difference of 6.90% occurs when the tip mass ratio is maximum (η = 5) and 1.0568% when there is no tip mass (η = 0). Again, as the number of terms in the series is increased, the approximation converges to the exact solution. For six terms (n = 6) in the eigenfunction expansion series, the percentage difference is approximately 0.02%.

7.3 Complete dynamic solution

The full solution to this problem is made up of a sum of an infinite number of functions. All these functions contribute to the transverse displacement and the total amplitude of vibration of the full solution. Because of our choice of the initial displacement function, the tip displacement is $w(L,0) = 2$. A summary inspection of Tables 7.1 to 7.4 shows that the initial amplitude at the tip of the beam is almost identical to two (2) *units*, with a small residual

($\epsilon >> 1$). This residual is expressed in equation 7.16 above and in the present problem 0.0083% < ϵ < 0.0322% percentage difference. In Table 7.1 to 7.4 it is observed that the fundamental (1st) mode of vibration contributes the largest displacement to the amplitude, while the other modes only contribute a smaller percentage of the amplitude.

Table 7.1: Tip deflection contribution of individual eigenfunctions with $\bar{V}_{+} = 0\text{V}$ for varying axial load ratios (k).

No. of eigen functions V=0V	Tip Displacement V= 0V ; η = 0; k = 0.8	Tip Displacement V= 0V ; η = 0; k = 0	Tip Displacement V= 0V ; η = 0; k = -1	Tip Displacement V= 0V ; η = 0; k = -2
1st	2.0755	1.9994	1.9237	1.8643
2nd	-0.0690	0.0001	0.0673	0.1186
3rd	-0.0042	0.0000	0.0050	0.0097
4th	-0.0018	0.0000	0.0022	0.0043
5th	-0.0005	0.0000	0.0006	0.0011
6th	-0.0003	0.0000	0.0004	0.0007
$w(L,0)$	1.9999	1.9995	1.9991	1.9987

When the tip mass is zero (η = 0) and the axial load is zero (k = 0), the first mode of vibration contributes 99.97% of the sum of the displacements and the rest of the modes 0.005% (the rest of the displacement can be accounted for in the residual (ϵ). In Table 7.1 it is observed that the second (2nd) mode contributes a displacement of 0.0001 *units* at the tip and all the other modes contribute zero. In the second mode of vibration it is concluded that the maximum amplitude of vibration will be 0.0001 *units*, which in turn tells us that the associated constant $\bar{F}_n$, is infinitesimal ($\bar{F}_n \to 0$). All the modes of vibration exhibit a sinusoidal behavior which is characterized by the solution derived in Section 7.1:

$$w(x,t) = \bar{F}_n X_n(x) \cos \omega_n t \tag{7.17}$$

This study does not take damping into account; whether it is natural damping or forced damping of the structure. The solution in equation 7.17 has no damping and therefore it is expected that the maximum amplitudes for the different modes will be maintained for $t > 0$. In Table 7.1 to 7.4, it is observed that the contribution of the second mode to the overall amplitude becomes more significant as the tip mass ratio (η) and the axial load ratio (k) are varied. In Table 7.1 the first mode contributes for 103.78%, 99.97%, 96.19% and 93.22% to the total amplitude for a constant mass ratio (η) for an axial load of k = +0.8, 0, -1, -2. The

second mode contributes -3.45%, 0.005%, 3.365% and 5.93% for the same axial loading. The negative or positive sign of the contribution is significant in that it tell us that the first mode is overestimated or underestimated compared to the initial displacement function. If the estimate of the first mode is bigger than two (2) *units*, then the first mode overestimates the amplitude and if it is under two, the amplitude is underestimated.

Table 7.2: Tip deflection contribution of individual eigenfunctions with $\bar{}_{+}V = 0\text{V}$ for varying mass ratios (η).

No. of eigen functions V=0V	Tip Displacement V= 0V ; η = 0; k = 0	Tip Displacement V= 0V ; η = 0.1; k = 0	Tip Displacement V= 0V ; η = 1; k = 0	Tip Displacement V= 0V ; η = 5; k = 0
1st	1.9994	1.8777	1.6351	1.5983
2nd	0.0001	0.1225	0.3675	0.4022
3rd	0.0000	-0.0005	-0.0029	-0.0010
4th	0.0000	-0.0002	-0.0002	-0.0001
5th	0.0000	-0.0001	0.0000	0.0000
6th	0.0000	0.0000	0.0000	0.0000
$w(L,0)$	1.9995	1.9995	1.9995	1.9995

From the tables it is noted that the contribution can be a positive or negative addition. The sum of the individual contributions $w_n(L,0)$ in Table 7.1 to 7.4 adds up to approximately two units with a very small residual.

Table 7.3: Tip deflection contribution of individual eigenfunctions with $\bar{}_{+}V = 1000\text{V}$ for varying axial load ratios (k).

No. of eigen functions V=1000V	Tip Displacement V= 1000V ; η = 0; k = 0.8	Tip Displacement V= 1000V ; η = 0; k = 0	Tip Displacement V= 1000V ; η = 0; k = -1	Tip Displacement V= 1000V ; η = 0; k = -2
1st	2.1222	2.0404	1.9588	1.8947
2nd	-0.1042	-0.0298	0.0429	0.0985
3rd	-0.0104	-0.0060	-0.0007	0.0042
4th	-0.0040	-0.0022	0.0001	0.0022
5th	-0.0015	-0.0010	-0.0004	0.0001
6th	-0.0006	-0.0006	-0.0002	0.0001
$w(L,0)$	2.0014	2.0008	2.0004	2.0000

When the axial load (k) is kept constant and the tip mass (η) varied, in Table 7.2, the first mode contributes 99.97% , 93.885%, 81.755% and 79.915% and the second mode contributes

0.005%, 6.125%, 18.375% and 20.11%. The second most significant contributions to the total amplitude can be attributed to second mode of vibration. The rest of the modes have some contribution to make but will not affect the vibrations in any significant way.

Table 7.4: Tip deflection contribution of individual eigenfunctions with $^{+}_{-}V = 1000\text{V}$ for varying mass ratios (η).

No. of eigen functions V=1000V	Tip Displacement V= 1000V ; η = 0; k = 0	Tip Displacement V= 1000V ; η = 0.1; k = 0	Tip Displacement V= 1000V ; η = 1; k = 0	Tip Displacement V= 1000V ; η = 5; k = 0
1st	2.0404	1.8553	1.6207	1.5859
2nd	-0.0298	0.1444	0.3819	0.4147
3rd	-0.0060	0.0000	-0.0029	-0.0010
4th	-0.0022	-0.0002	-0.0002	-0.0001
5th	-0.0010	0.0000	0.0000	0.0000
6th	-0.0006	0.0000	0.0000	0.0000
$w(L,0)$	2.0008	1.9995	1.9995	1.9995

In Table 7.3 and 7.4, the same trends are observed as above for a beam with inactive piezo actuators. In Table 7.3, when both the tip mass ratio, axial load ratio are zero and the piezo is active $(^{-}_{+}V = 1000\text{V})$; the second modes has a large contribution to the amplitude -1.49% as oppose to 0.005% for an inactive piezo $(^{-}_{+}V = 0\text{V})$. It is further noticed that the higher modes contribute when the beam is active $(^{-}_{+}V = 1000\text{V})$ in all cases and also that in Tables 7.1 to 7.4 most of the higher modes make a contribution to the initial tip displacement.

The largest tip displacement is 2.0014 units which corresponds to zero voltage $(^{-}_{+}V = 0\text{V})$, zero tip mass ratio (η = 0) and tensile load (k = +0.8); and that represents a 0.07% overestimate; and the lowest tip displacement is 1.9987 units which corresponds to maximum voltage $(^{-}_{+}V = 1000\text{V})$, zero tip mass ratio ($\eta$ = 0) and maximum compressive load (k = -2) and that represents an under estimate of 0.065%. The residual (ϵ) is approximately 0.0014 *units.*

The general solution to this problem is derived by using the method of separation of variables which entails two solutions, one in the spatial domain and the other in the time domain. The

solution in the time domain involves a sinusoidal function ($F_n \cos \omega_n t$) in which the circular frequency (ω_n) and the period ($\mathcal{T}$) can be written as:

$$\omega_n = \left(\frac{R_n}{L}\right)^2 \sqrt{\frac{E_c I_c}{m_c}} \tag{7.18}$$

$$\mathcal{T} = \frac{2\pi}{\omega_n} \tag{7.19}$$

The period ($\mathcal{T}$) is the time taken for the system to complete one full oscillation. From the above equations it is noted that the circular frequency and the period are directly linked to natural frequency (R_n) of vibration. For example, R_1 = 1.8751 for the first natural frequency of vibration for cantilevered beam. For the different combinations of parameters: voltage, tip mass, axial load, extended mass, etc., the natural frequencies are unique and if follows that the circular frequency (ω_n) and the period ($\mathcal{T}$) are unique for all possible combinations of parameters. After separation of variables the differential equation that describes the motion of the beam with respect to time becomes:

$$\ddot{T}_n(t) + \omega_n^2 T(t) = 0 \tag{7.20}$$

with a general solution:

$$T_n(t) = \overline{E}_n \sin \omega_n t + \overline{F}_n \cos \omega_n t \tag{7.21}$$

From equation 7.19 and 7.20 above, the period can be determined and in the Figure 7.5 below the phase angle or phase constant ($\varnothing$) can be defined. Figure 7.6 shows a periodic function with the phase and the period of oscillation. The phase angle helps to determine the first peak of the harmonic oscillation. To analyze the above, choose two constants ($\varnothing$) and (G) which can be satisfied in the figure below.

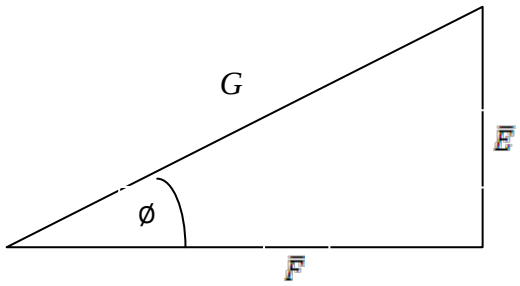

Figure 7.5: Right angled triangle that shows the relation between (ø) and (G)

Therefore after using Pythagoras:

$$G = \sqrt{\bar{F}_n + \bar{E}_n} \tag{7.22}$$

Noting that,

$$\cos\varphi = \frac{\bar{F}_n}{G} \quad \text{and} \quad \sin\varphi = \frac{\bar{E}_n}{G} \quad \text{also,} \quad \tan\varphi = \frac{\bar{E}_n}{\bar{F}_n} \tag{7.23}$$

$$T_n(t) = G\left(\frac{\bar{E}_n}{G}\sin\omega_n t + \frac{\bar{F}_n}{G}\cos\omega_n t\right) \tag{7.24a}$$

$$T_n(t) = G\left(\sin\phi\sin\omega_n t + \cos\phi\cos\omega_n t\right) \tag{7.24b}$$

And by using the cosine addition formula:

$$T_n(t) = G\cos(\omega_n t - \phi) \tag{7.25}$$

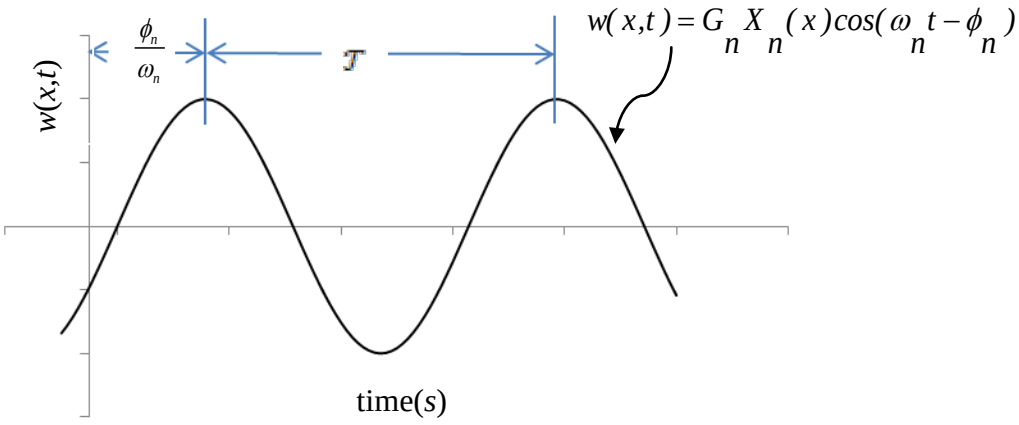

Figure 7.6: Phase angle (ø) and period (T) of oscillation

7.4 Oscillation of the beam for $b_1 = 0$

In this section the oscillation of the beam for a concentrated tip mass ($b_1 = 0$) is investigated and thereafter the discussion is expanded to the results obtained for an extended tip mass ($b_1 > 0$). Figure 7.7 shows the effects of the axial load and the tip mass on the frequency of vibration of the beam. It has been noted that as the axial load ratio increases from a compressive load to a tensile load, the frequency of vibration increases and as we increase the tip mass ratio, the frequency of vibration decreases.

The minimum number of oscillations occurs at an axial load ratio of k = +0.8 and a tip mass ratio of η = 5 and it is 24.20Hz for zero voltage and 6.38Hz for maximum voltage, whereas the maximum oscillations occur at maximum tensile loading k = -2 and tip mass ratio η = 0 and the frequency is 755.16Hz for zero voltage and 738.72Hz for maximum voltage. The percentage difference at zero tip mass ratio (η = 0) and axial load ratio (k = +0.8) is approximately 73.20% for an uncontrolled $(\bar{+}V = 0\text{V})$ and a controlled $(\bar{+}V = 1000\text{V})$ beam; and as the load ratio is increased to k = 0, -1 and -2; it becomes 8.62%, 3.69% and 2.18%, respectively. The above mentioned oscillations are due to the first or fundamental harmonic. In Figures 7.10 to 7.13, the oscillation amplitude contribution of the first harmonic is larger than in the other two harmonics. The second harmonic amplitude contributions to the full solution increase as the tip mass increases and therefore this harmonic will be of interest when mapping out the oscillations the beam. The third and higher harmonics of the series have a negligible amplitude contribution because as the number of functions (n) used in the full solution is increased, the amplitudes of the higher harmonics tend to zero because $\bar{F}_n \to 0$, as $n \to \infty$.

Figures 7.7 to 7.9 show the oscillation frequencies of the beam. For a compressive load a significant amount of control of the vibrations is achieved and as the axial load ratio increases the piezo actuator loses its efficacy up to approximately 3%. Figures 7.7 to 7.9 show the frequencies as the axial load ratio for a particular tip mass ratio (η = 0, 0.1, 1, 5) is varied and the moment arm is kept constant at b_1 = 0, L/2, L/1. From these figures it is noted that the curves decrease monotonically for the relation between the frequency and the axial load ratio. What is most significant is that the frequency difference between a controlled and an uncontrolled beam decreases as the axial load ratio is increased. Figure 7.7 to 7.9 show an

overlap in the frequencies for a controlled and an uncontrolled beam at approximately k = -2. That indicates clearly that the piezo actuator has an insignificant effect on the vibrations of the system. When a tip mass is added, Figure 7.7(*b*) to 7.7(*d*) show a decrease in the frequencies of oscillation.

For a compressive load the difference is largest and decreases as the axial load ratio increases, where the curves converge at an axial load ratio of approximately k = -2 . These masses tend to attenuate the vibrations of the system and added to the effects of the piezo actuator, decrease the vibration of the system further. For a tip mass ratio η = 0, 0.1, 1, 5 the difference in the frequencies of the controlled and uncontrolled beam is approximately 73% in compression and approximately 3% at maximum tensile load. Therefore it is reasonable to conclude that the piezo actuators have some notable contribution to the change in frequency of oscillation of the beam.

The above discussion is based on the first harmonic which is represented by the lowest frequency on the amplitude spectrum plot, Figures 7.10 to 7.13. The plots also indicate the 2^{nd} and 3^{rd} harmonic of the vibration and contribute to the overall vibration profile of the beam. From these figures it is noted that the frequency difference between a controlled beam and an uncontrolled beam is below 1% and this goes to show that the piezo actuators have minimal effect on the frequency of oscillation in the 2^{nd} and 3^{rd} harmonic. From this data it can be concluded that the 1^{st} harmonics are dominant and by altering the frequencies of these harmonics the vibration characteristics of the beam can be altered.

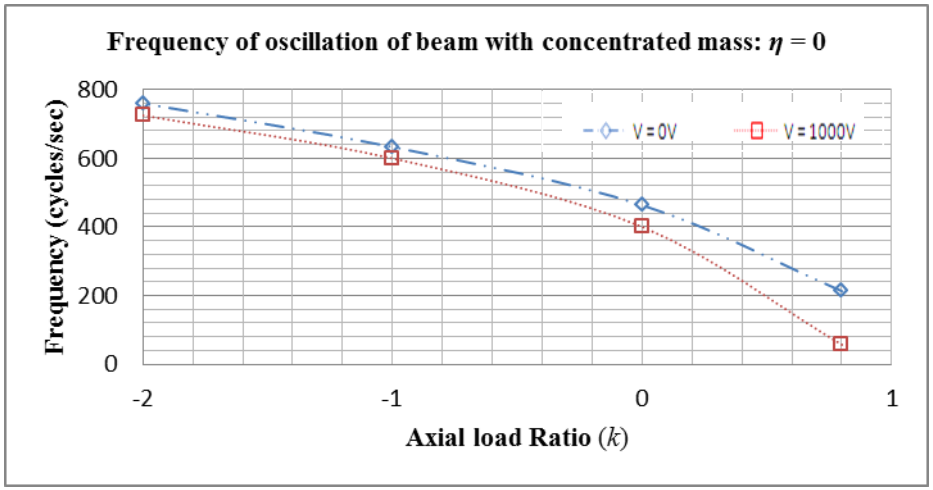

(*a*)

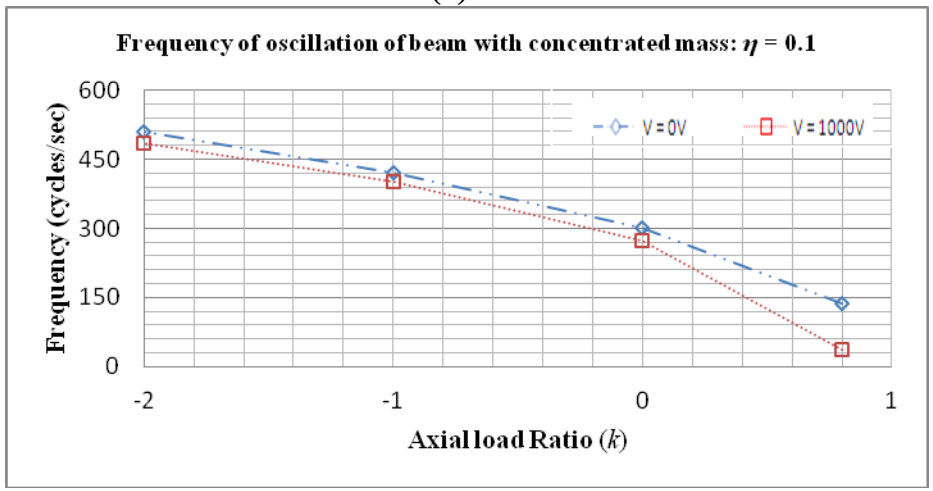

(*b*)

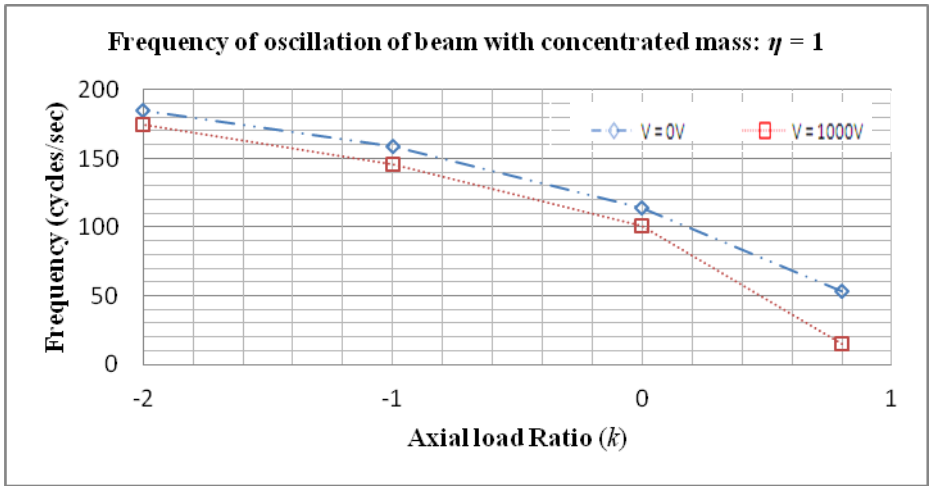

(*c*)

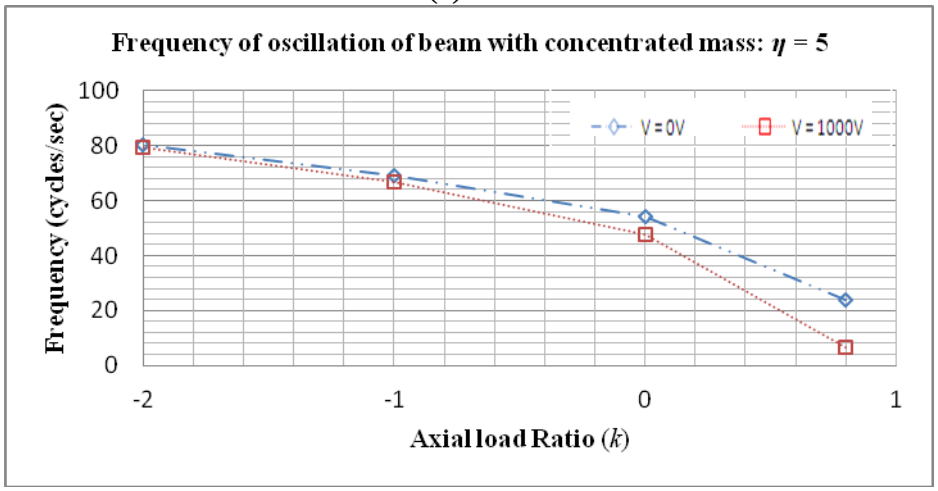

(*d*)

Figure 7.7: Frequencies for controlled and uncontrolled beams for $b_1 = 0$. (*a*) $\eta = 0$, (*b*) $\eta = 0.1$, (*c*) $\eta = 1$ and (*d*) $\eta = 5$

7.5 Oscillation of the beam for $b_1 = L/2$

In this section the mass in not concentrated such that the center of gravity of the attached mass does not coincide with tip of the beam. The extension of the beam is regarded weightless and in addition the effects of rotary inertia on the vibrations of the beam are included. From Figure 7.8 below, it can be observed that there are changes in the oscillation frequencies of the system, noting that as the axial load ratio is increased the frequencies increase. The maximum frequency occurs when the axial load ratio is k = -2 and the beam is under maximum tensile load.

In Figure 7.8 the effects of the axial load and tip mass on the oscillation frequencies, when the center of gravity of the tip mass is half the length of the beam away from the tip is demonstrated. It is noted from Figure 7.7(a), 7.8(a) and 7.9(a) that the maximum oscillation frequency is ~760Hz for maximum tensile load (k = -2) and zero tip mass ratio (η = 0) for all cases. This should be expected since the extension is weightless and therefore its length does not add any mass at the tip. Furthermore, the percentage difference at maximum tip mass ratio and maximum tensile axial load ratio are approximately zero. This indicates that the piezo actuator has no effect on the system at those limits.

When the load ratio is tensile ($k \geq$ -1) the frequency of oscillation of the beam are identical for maximum axial load ratio (η = 5). This indicates that the piezo layer have no effect on the oscillation of the tip for large tip masses and axial load ratio in excess of k = -1.

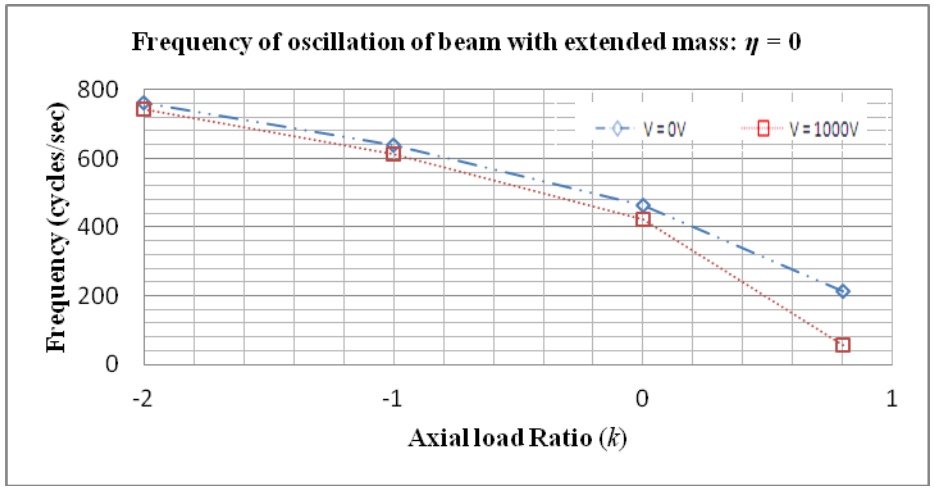

(*a*)

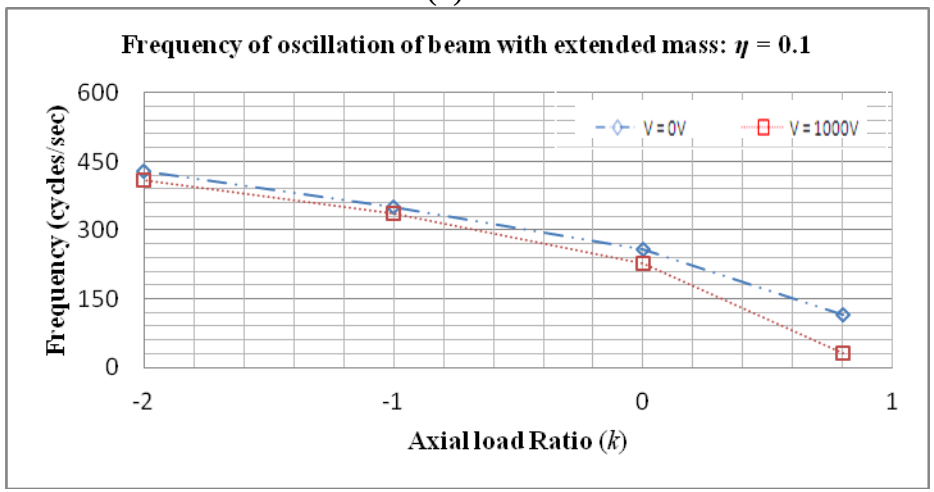

(*b*)

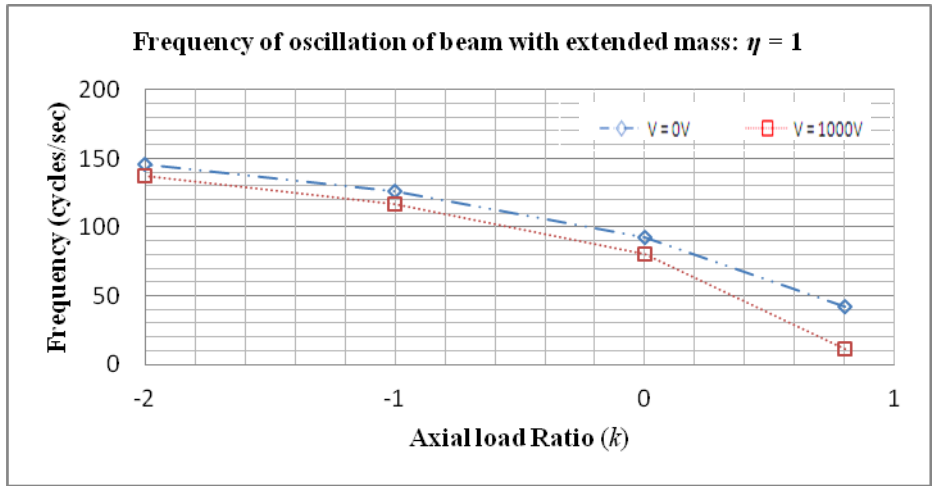

(*c*)

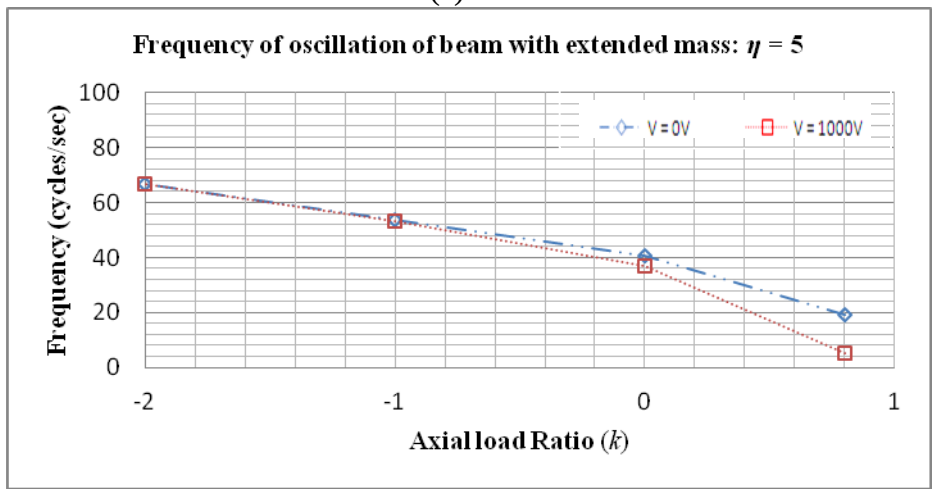

(*d*)

Figure 7.8: Frequencies for controlled and uncontrolled beams for $b_1 = L/2$. (*a*) $\eta = 0$, (*b*) $\eta = 0.1$, (*c*) $\eta = 1$ and (*d*) $\eta = 5$

7.6 Oscillation of the beam for $b_1 = L/1$

For an extension with a length equal to the length of the beam the results are presented in Figure 7.9. In these figures the same trends are noted as was observed earlier in the analysis, with $b_1 = 0$ and $b_1 = L/2$. In this instance there is a further drop in the oscillation frequencies of the beam. There is a percentage drop of 21.29% and a percentage drop of 19.2% for an uncontrolled beam $(\bar{+}V = 0\text{V})$ and for a controlled beam $(\bar{+}V = 1000\text{V})$ for a compressive load (k = +0.8) and tip mass ratio $\eta = 5$, when $b_1 = L/2$ and $b_1 = L/1$, respectively.

The lowest frequencies of oscillation are obtained when the moment arm is maximum ($b_1 = L/1$) and the effects due to rotary inertia are taken in to account. When the frequencies of oscillation for a moment arm of zero ($b_1 = 0$) and the maximum moment arm ($b_1 = L/1$), a percentage difference of 35.79% for an uncontrolled beam and 38.79% for a controlled beam is noted. This conclusively suggests that the length of the extension has a significant effect on the oscillation at the tip of the beam.

From Figure 7.9 the convergence of the two graphs occurs at k = -1. The effect of the tip mass is to reduce the natural frequencies of the system, as observed in earlier discussion in Chapter 4 and the extension at the tip of the beam also contributes to the lowering of the oscillation frequencies. This effect manifests itself in the oscillation of the tip of the beam were slower oscillations are noted.

Again it is observed that the frequencies of oscillation of the tip in Figure 7.7 to 7.9 are identical when the tip mass ratio of the system is zero ($\eta = 0$) for both the uncontrolled and the controlled beam. The percentage difference for an axial load of k = - 1 for η = 0, 0.1, 1, 5 is 1.984%, 4.345%, 4.81% and 4.76%, respectively.

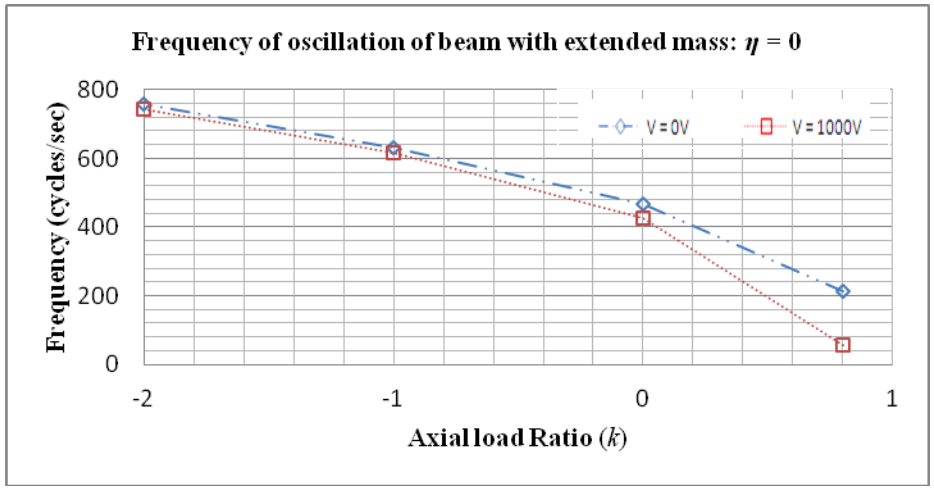

(*a*)

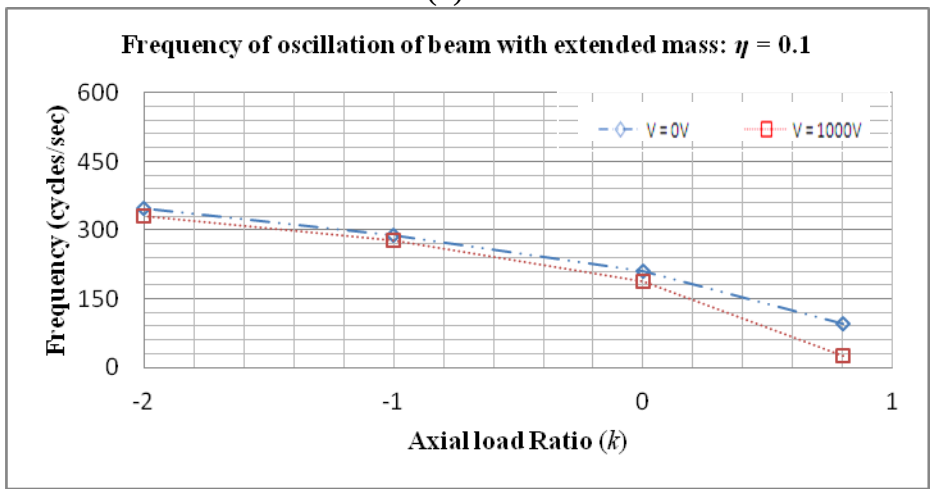

(*b*)

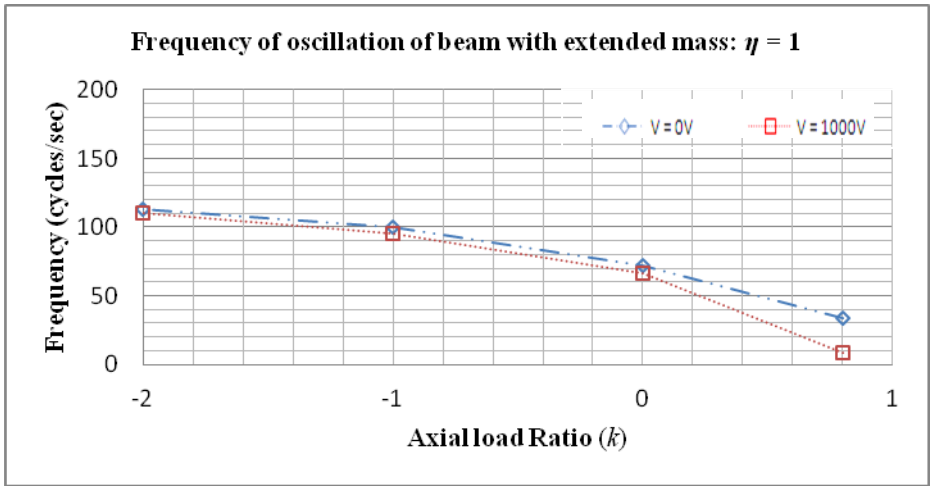

(*c*)

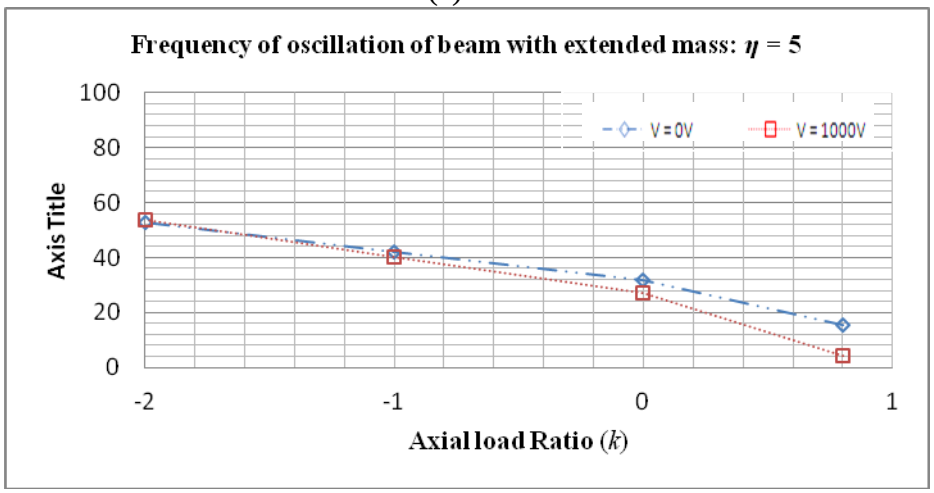

(*d*)

Figure 7.9: Frequencies for controlled and uncontrolled beams for $b_1 = L/1$. (*a*) $\eta = 0$, (*b*) $\eta = 0.1$, (*c*) $\eta = 1$ and (*d*) $\eta = 5$

7.7 Amplitude spectrum for the cantilevered beam

In Figures 7.10 to 7.13 the dynamic solution of the problem is plotted and the amplitude spectrum is indicated in the figures below. The dynamic solution function is made up of series of eigenfunctions which can be summarized in the following equation:

$$w(x,t) = \sum_{n=1}^{6} \overline{F}_n X_n(x) \cos \omega_n t \tag{7.26}$$

The first term, $\overline{F}_n X_n(x)$, represent the amplitude of the vibration and the second term, $\cos \omega_n t$, contains the oscillation frequency of the beam. These two parameters, amplitude and frequency, are represented in the amplitude spectrum plots in Figures 7.10 to 7.13. From the amplitude spectrum figures it is noted that the dynamic solution, Figures 7.10a to 7.10d, 7.11a to 7.11d, 7.12a to 7.12d and 7.13a to 7.13d, are a sum of a series of cosines with different amplitudes and cyclic frequency. The different harmonics are shown in the amplitude spectrum figures and from these figures the magnitude of the effect that a particular harmonic has on the entire system can be determined. This however does not tell us about the phase (ø) of the harmonic. The phase gives us information to determine if the harmonics are constructive or destructive when added together.

The amplitude spectrum plots show only the first three oscillation frequencies of the system. This can be justified by using the findings in Section 6.2, where it was concluded that six (6) eigenfunctions would converge to a reasonable estimation. Furthermore, Figure 7.1 to 7.4 shows that three functions are adequate and therefore only the first three harmonics are shown in the figures.

In Section 7.4 to 7.6 the frequencies of oscillations for the various combinations of axial load, tip mass, piezo electric field and the length of extension of the tip mass were discussed based on the fundamental mode (1st eigenfunction – $w_1(L,t)$,where $n = 1$) . However, the complete solution is composed of a sum of an infinite number of eigenfunctions $n \in \{1,2,3,\ldots \infty\}$ and therefore the higher modes $n > 1$ cannot be neglected even though the piezo actuators have a negligible effect on those frequencies. For this reason, it is observed that the oscillation plots of Figures 7.10 to 7.13 are not smooth. The initial displacement of the beam is defined as the

first mode of a cantilever beam. In the Figures 7.10(*b*), 7.10(*f*) and 7.10(*j*) the second harmonics have extremely small amplitudes. Table 7.1 indicates that at $\bar{V}_{+} = 0\text{V}$ and $k = 0$ the tip displacement is 1.9994 units which is identical to the exact solution and therefore the second harmonic contributes zero displacement to the initial deflection of the tip. When the axial load, tip mass and voltage are included the amplitude of the second harmonics increase and contribute to the initial amplitude. The harmonics are out of phase and have different amplitudes and periods and when combined produce the jagged curves of Figure 7.10 to 7.13.

In Figures 7.10 to 7.13 it is observed that the contribution of the second harmonic becomes larger as the tip mass increases and the piezoelectric experiences maximum voltage input.
The increase in the amplitude of the second harmonic can also be attributed to the non-orthogonality of the initial displacement function to the second mode eigenfunction.

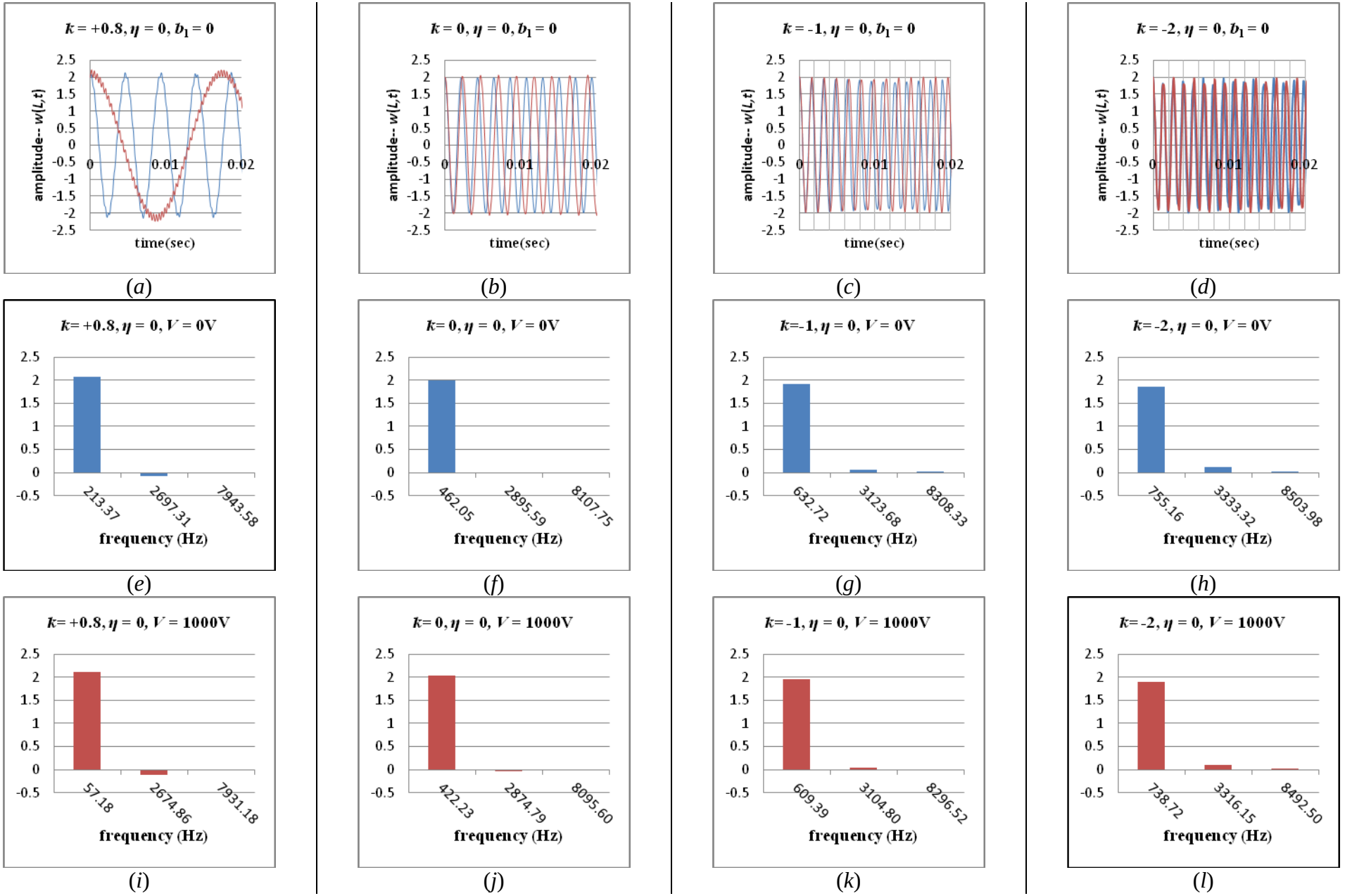

Figure 7.10: (*a*) to (*d*): Oscillation of uncontrolled beam and controlled beams. (*e*) to (*h*): Amplitude spectrum of uncontrolled beams. (*i*) to (*l*): Amplitude spectrum of controlled beams; $\eta = 0$ 0V 1000V

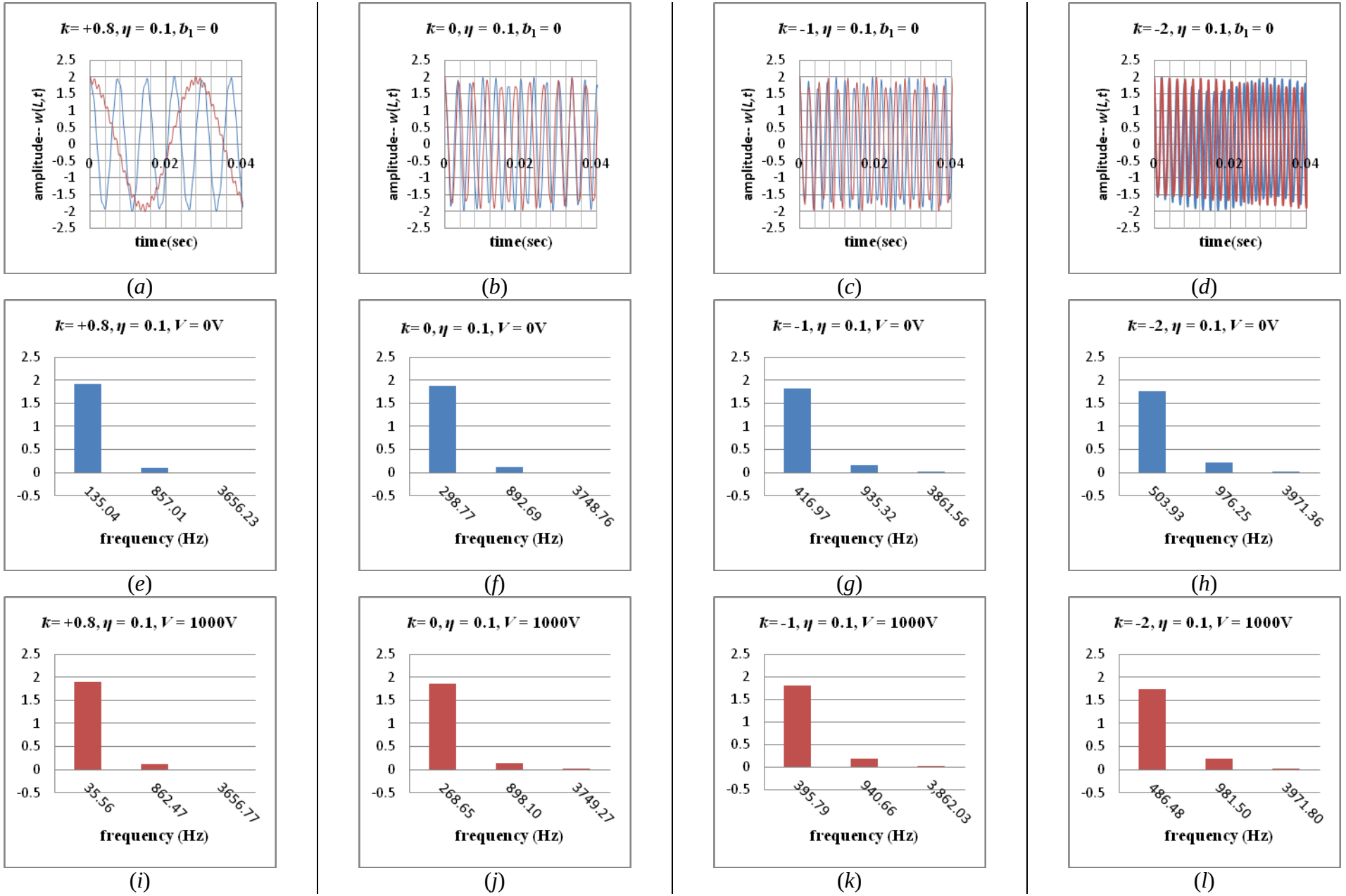

Figure 7.11: (*a*) to (*d*): Oscillation of uncontrolled beam and controlled beams. (*e*) to (*h*): Amplitude spectrum of uncontrolled beams. (*i*) to (*l*): Amplitude spectrum of controlled beams; $\eta = 0.1$ 0V 1000V

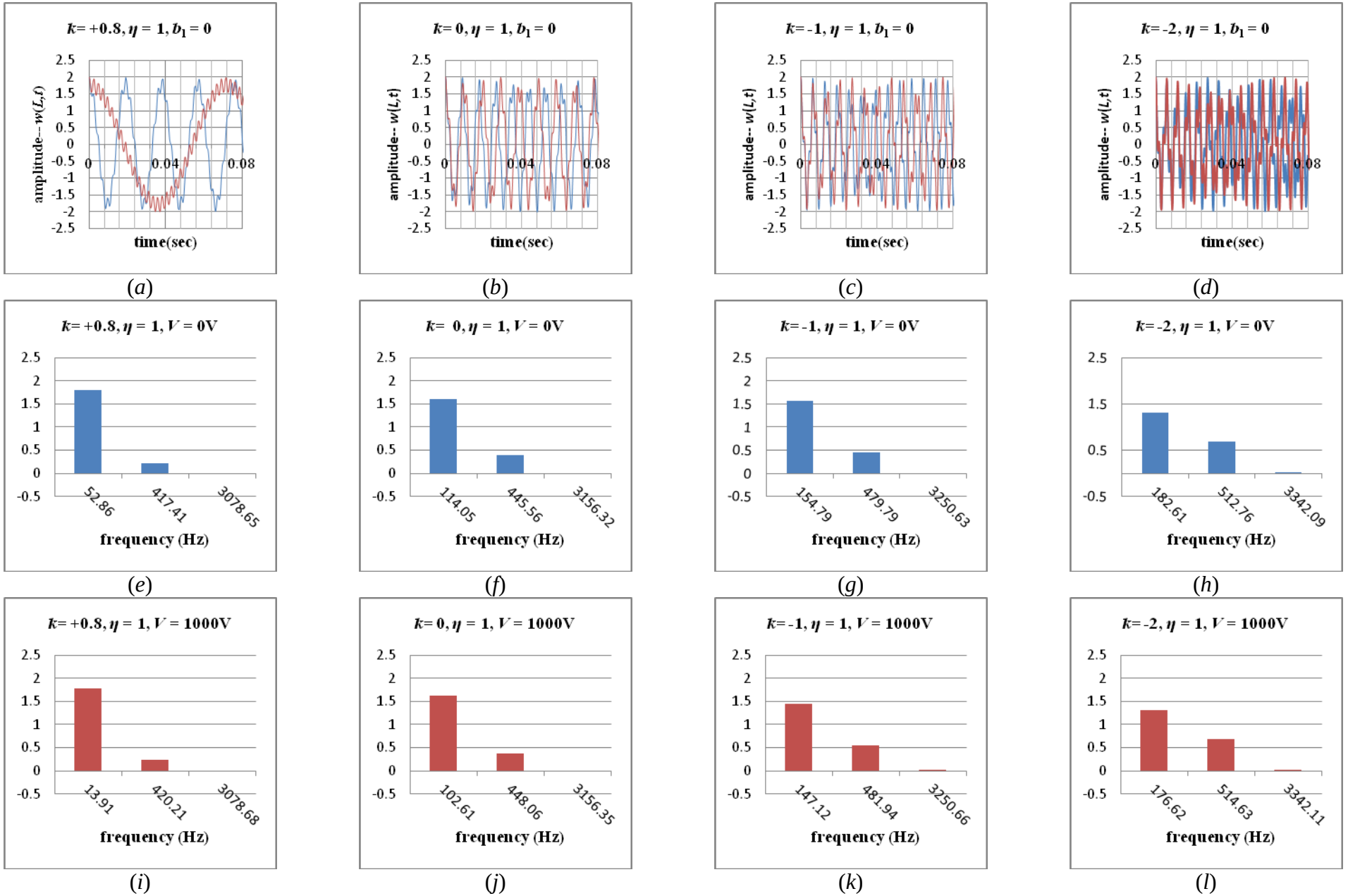

Figure 7.12: (*a*) to (*d*): Oscillation of uncontrolled beam and controlled beams. (*e*) to (*h*): Amplitude spectrum of uncontrolled beams. (*i*) to (*l*): Amplitude spectrum of controlled beams; $\eta = 1$ 0V 1000V

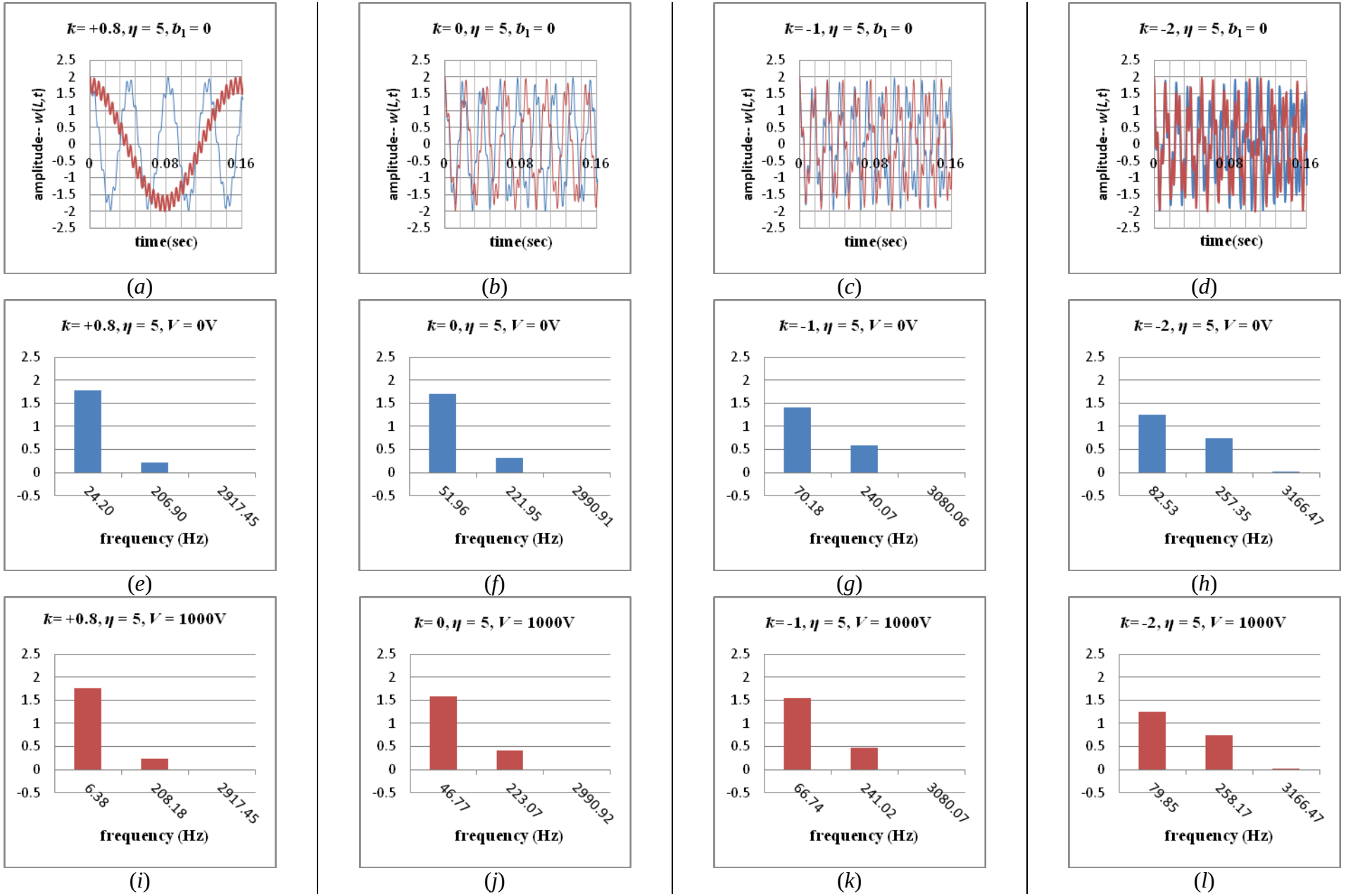

Figure 7.13: (*a*) to (*d*): Oscillation of uncontrolled beam and controlled beams. (*e*) to (*h*): Amplitude spectrum of uncontrolled beams. (*i*) to (*l*): Amplitude spectrum of controlled beams; $\eta = 5$ 0V 1000V

Chapter 8 – Conclusions

8.1 Conclusion

In the investigation carried out in this study the aim is to study the effects of piezoelectric actuators on the frequencies of a cantilevered beam with tip mass and axial load at the free end. The voltage input into the piezo layers causes a change in the frequencies of vibration. The tip mass is modeled as a concentrated mass and an extended mass. Piezoelectric actuators were used to modify the moments at the free end of the beam, which in turn alters the natural frequencies of the beam. The piezoelectric actuators can be used to adjust the boundary conditions such that the frequencies of vibration can be increased or decreased. In this study, more emphasis is dedicated the reduction of frequencies, but it was shown that the natural can be increased. Classic beam theory was used to approximate the vibration characteristics of the system. The eigenvalues that govern the solution were altered using piezoelectric actuators by modifying the moments generated at the boundaries of the piezoelectric beam.

Piezo actuators have an attractive quality because they can convert mechanical strain into electric potential or electric potential into mechanical strain. To produce a desired strain, a limited amount of voltage can be induced to avoid piezo breakdown. The manufacturers' data for piezo patches recommend 1000V/mm of thickness. The piezoelectric composite beam is made from two actuators of equal thickness on the top and bottom surface of an elastic column sandwiched in the middle. The governing equations for the model were developed to allow for discrete voltage inputs to the piezo layers to decrease or increase the natural frequencies.

The thickness of the piezo was increased from 1mm to 2mm and the input voltage from 1000V to 2000V resulting in a further reduction of the frequencies. At $\eta = 0$, a 40% reduction in the frequency can be attained for $k = +0.8$ and 2% for $k = -2$ for 1mm thickness and that frequency reduction is doubled by increasing the piezo layers to 2mm. When the thicknesses of the piezo are increased while keeping the cross sectional area constant the system resembles a bimorph piezo beam.

A compressive axial load reduces the natural frequencies and when the natural frequencies approach zero, the beam approaches buckling mode and tensile axial load increases the frequency. This loading causes an overestimation or underestimation in the approximation of the initial value of the displacement of the beam determined from the first harmonic's amplitude. This over estimation is corrected by the second and higher harmonics with a negative or positive displacement such that the sum of all the amplitudes in the different harmonics adds up to the stipulated initial condition for an uncontrolled and controlled beam. A tensile axial load increases the natural frequencies and the piezo electric actuators are effective up to maximum axial load ratio k = -2. The tip mass has the effect lowering the natural frequencies. As the tip mass increases, the behavior of the piezo electric cantilevered bean changes to that of a clamped-pinned beam and the piezo actuators loose effectiveness when the mass becomes too large. The beam tip mass ratio in this investigation is limited to $\eta = 5$, to allow for control of the frequencies using piezo actuators.

For a concentrated tip mass the center of gravity of the mass coincides with the end of the beam. The line of action of the center of gravity for an extended mass goes through a point which lies at some distance away from the tip of the beam. In this case a moment arm is introduced and the analysis also takes rotary inertia in consideration. The effect of rotary inertia is to lower the frequencies. A concentrated mass yields higher natural frequencies compared to those of an extended mass with inertia. Both the concentrated and extended mass has the effect of lowering of the natural frequencies. In addition, the tip mass has an effect of increasing the amplitude of the second harmonic. If the eigenfunction for a particular harmonic is not orthogonal to the initial displacement function, the second and higher modes contribute to the vibration profile of the beam.

The line of action of the center of gravity for this investigation is zero (L/∞) for concentrated load, half length ($L/2$) of the beam and full length ($L/1$) of the beam from the tip of the column. At maximum tip mass, zero axial load and zero voltage the frequencies are $0.6288s^{-1}$, $0.5588s^{-1}$ and $0.4954s^{-1}$ for (L/∞), ($L/2$) and ($L/1$), respectively. This indicates that the tip mass extension will lower the frequencies. The dimensions of the mass have to be taken into consideration for a more accurate and realistic model.

The following 4 parameters tend to lower the frequencies of vibration: (1) compressive axial load, (2) tip mass, (3) moment arm (extension) and (4) piezo actuators. A tensile load has the

opposite effect and tends to increase the frequencies. In this study, the percentage level of reduction caused by the first three parameters mentioned above was not investigated. Even though the total frequency reduction is made up of contributions from the end conditions (axial load, tip mass and moment arm) the piezo actuator also contribute significantly within the limits outlined ($-2 < k < +0.8$ and $0 < \eta < 5$).

To obtain a solution to this boundary value problem a separable solution is employed. The dynamic part of the solution produces harmonics that are associated with the eigenfunctions. The sum of these periodic harmonics gives us a vibration profile of the piezoelectric beam. In free vibration there are an infinite number of modes and these modes are characterized by the natural frequencies where the first mode is derived from the 1st natural frequency, the second mode by the second 2nd frequency, etc. The 1st mode is the fundamental mode and the most important in the analysis of the system. The vibrations on the piezo electric beam are affected by piezo actuation most significantly in the fundamental mode. The 2nd modes frequencies are affected minimally and the higher modes effects are negligible.

The solution of the problem is achieved with the use of six eigenfunctions. Normally, this type of approximate solution would require an infinite number of eigenfunctions to arrive at the exact solution. In this case, the use of six eigenfunctions is adequate and yields a residual error of approximately 0.0015% compared to the exact solution which is a function defined by the first mode of free vibration for a plain cantilever beam.

8.2 Future research

Further studies will be undertaken to analyze a beam with tip mass and axial load where we can damp out the vibration of the system. Because the system is a distributed parameter system using Lyapunov's direct method the vibrations can be damped out. This method has been proven to be effective in damping out the fundamental mode. Further research will be undertaken in the field of nanomaterial where CNT are used as sensors. Vibration analysis of these materials can be utilized and the frequency profile generated used to identify molecules that attach to the nanotubes e.g. bacteria, viruses, chemicals, etc. The analysis will be conducted using nonlocal theories for bending and surface effects due to the surface to bulk ratio will be studied.

Bibliography

[1] Abedinnasab MH, Kamali Eigoli A, Zohoor H and Vossoughi GH (2011) On the influence of centerline strain on the stability of a bimorph piezo-actuated micro beam *Scientia Iranica* B **18(6)** pp. 1246-1252

[2] APC International LTD. (2013) Piezo Theory http://www.americanpiezo.com/piezo-theory/pzt.html

[3] Bailey T and Hubbard JE (1985) Distributed piezoelectric-polymer active vibration control of a cantilever beam *Journal of Guidance, Control and Dynamics*. **8** pp. 605-611

[4] Balachandran B and Magrab EB (2009) *ibrations* Toronto, Canada: CENGAGE Learning

[5] Baras JS and Zhuang Y (1992) Active vibration damping using smart materials *Workshop on Distributed Parameter Modeling and Control of Flexible Aerospace Systems* Williamsburg, VA.

[6] Banks HT, Smith RC and Wang Y *Smart Material Structures: Modeling, Estimation and Control*, Willey, Chichester and Masson, Paris, 1996

[7] Belouettar S, Azar L, Daya EM, Laptev V and Potier-Ferry M (2008) Active control of nonlinear vibration of sandwich piezoelectric beams: A simplified approach *Computer and Structures* **86** pp. 386-397

[8] Benjeddou A (2000) Advances in piezoelectric finite element modeling of adaptive structural elements: a survey *Computers and Structures* **76** pp. 347-363

[9] Blevins RD (1979) *Formulas of natural frequencies and mode shapes* New York: Van Nostrand Reinhold pp. 101-113

[10] Bokaian A (1988) Natural frequencies of beams under compressive axial loads *Journal of Sound and Vibration* **126(1)** pp. 49-65

[11] Bokaian A (1990) Natural frequencies of beams under tensile axial loads *Journal of Sound and Vibration* **142(2)** pp. 481-498

[12] Brissaud M, Ledren S and Gonnard P (2003) Modeling of a cantilever non-symmetric piezoelectric bimorph **Vol. 13**, pp. 832-844 *Journal of Micromechanics and Micro engineering* IOP Publishing Ltd, United Kingdom

[13] Burke SE and Hubbard Jr. JE (1987) Active vibration control of a simply supported beam using a spatially distributed actuator *IEEE Control Systems Magazine* **Aug.** pp. 25-30

[14] Chien-Chang Lin and Huag-Nan Huang (1999) Vibration control of beam-plates with bonded piezoelectric sensors and actuators, *Computers and Structures* **73** pp. 239-248

[15] Cook-Chennault KA, Thambi N, Sastry AM (2008) Powering MEMS portable devices – a review of non-regenerative and regenerative power supply systems with emphasis on piezoelectricity energy harvesting systems. *Smart Material Structures 2008*; 17:043001

[16] Crawley EF and de Luis J (1990) Use of piezoelectric actuators as elements of intelligent structures **Vol. 25(10)** pp. 1373-1385 *American Institute of Aeronautics and Astronautics* New York, NY

[17] de Silva CW (2000) Vibration Signal Analysis *Vibration: Fundamentals and Practice* Boca Raton: CRC Press LLC

[18] Deveo DL and Pisano AP (1997) Modeling and optimal design of piezoelectric cantilever micro-actuators *Journal of Microelectromechanical Systems* **Vol. 6** pp 266-270

[19] Duffy KJ, Adali S (1991)) Optimal fibre orientation of anti-symmetric hybrid laminates for maximum fundamental frequency and frequency separation *Journal of Sound and Vibration* **146**(2) pp. 181-190

[20] Dunsch R and Breguet JM (2007) Unified mechanical approach to piezoelectric modeling *Sensors and Actuators* **A 134** pp. 436-446

[21] Edwards, Jr. CH and Penny DE (1989) *Elementary Differential Equations: With Boundary Value Problems.* (New Jersey: Prentice Hall)

[22] Ertuk, A (2012) Assumed-modes modeling of piezoelectric energy harvesters: Euler-Bernoulli, Rayleigh and Timoshenko models with axial deformations, *Computers and Structures* **106-107** pp. 214-227

[23] Fridman Y and Abramovich H (2008) Enhanced structural behavior of flexible laminated composite beams *Composite Structures Elsevier Ltd.* **Vol. 82** pp. 140-154

[24] Gardonio P and Elliot SJ (2005) Modal response of a beam with a sensor-actuator pair for the implementation of velocity feedback control *Journal of Sound and Vibration* **284** pp. 1-22

[25] Gaundenzi P, Carbonaro R and Benzi E (2000) Control of beam vibrations by means of piezoelectric devices: theory and experiments *Journal of Composite Structures* **50** pp. 376-379

[26] Ge SS, Lee TH, Zhu G and Hong F (2000) Variable control of a distributed-parameter flexible beam *Journal of Robotic Systems* **18(1)** pp. 17-27

[27] Gere J M and Goodno B J (2009) *Mechanics of Materials* (Stamford, CT: CENGAGE Learning)

[28] Gökdağ H and Kopmaz O (2005) Coupled bending and torsional vibration of a beam with in-span and tip attachments *of Sound and Vibration* **287** pp. 591-610

[29] Gürdal Z, Haftka RT and Hajela P (1999) *Design and optimization of laminated composite materials* (New York: John Wiley & Sons)

[30] Habib MS and Radcliffe CJ (1991) Active damping of distributed parameter beam transverse vibration *Journal of Dynamic System, Measurement, and Control*. **Vol. 113** pp. 295-299

[31] Inman DJ (2006) *Vibration with control* (England: John Wiley & Sons Ltd.)

[32] Inman DJ (2001) Active modal control for smart structures *Philoso. Trans. Royal Soc., Ser.* **A 359** (1778) pp. 205-219

[33] Janker P, Claeyssen F, Grohmann B, Christmann M, Lorkowski T, LeLetty R and Sosniki O, Pages A (2008) New Actuators for Aircraft and Space Applications *ACTUATOR 2008, 11th International Conference on New Actuators*, Bremen, Germany 9-11 June 2008

[34] Kalamkarov AL and Drozdov AD (1996) Intelligent composite structures: general theory and applications *International Journal of Solid Structures*. **Vol. 33**, **No.29** pp. 4411-4429

[35] Kapuria S and Alam N (2006) Efficient layer-wise finite element model for dynamic analysis of laminated piezoelectric beams *Computer Methods in Applied Mechanics and Engineering* **195** pp. 2742-2760

[36] Kayacik Ö, Brusch Jr. JC, Sloss JM, Adali S and Sadek IS (2008) Integral equation approach for piezo patch vibration control of beams with various types of damping *Computers and Structures* **86** pp. 357-366

[37] Kim SJ and Jones JD (1991) Optimal design of piezo actuators for active noise and vibration control. *American Institute of Aeronautics and Astronautics* New York, NY **Vol. 19** pp. 2047-2053

[38] Lee SY, Ko B and Yang W (2005) Theoretical modeling, experiments and optimization of piezoelectric multi-morph *Smart Material Structures* **14** pp. 1343-1352

[39] Lumentut MF and Horward IM (2011) Analytical and experimental comparisons of electromechanical vibration response of a piezoelectric bimorph beam for power harvesting *Mechanical Systems and Signal Processing* **36** (2013) 66-86

[40] Magrab EB (2007) Natural frequencies and mode shapes of Timoshenko beams with attachments *Journal of Vibration and Control* **13(7)**: pp. 905-934

[41] Mansour MO, Arafa MH and Megahed SM (2010) Resonator with magnetically adjustable natural frequency for vibration energy harvesting *Sensors and Actuators* **A 163** pp. 297-303

[42] Mei C (2011) Studying the effects of lumped end mass on vibrations of a Timoshenko beam using a wave based approach *Journal of Vibration and Control*. **18(5)** pp. 733-742

[43] Meirovitch L (2001) *Fundamentals of Vibrations* (New York: McGraw-Hill)

[44] Meriam JL and Kraige LG, *Engineering Mechanics: dynamics*. New York: John Wiley and Sons, 2001

[45] Oliveira A, Sousa P and Costa Branco PJ (2004) Surface deformation by piezoelectric actuator: from Park and Agrawal models to a simplified model formulation *Sensors and Actuators* **A 115** pp. 235-244

[46] Park JK and Moon WK (2004) Constitutive relations for piezoelectric benders under various boundary conditions *Sensors and Actuators* **A 115** pp. 159-167

[47] PI Ceramic GmbH (2013) Piezoelectric Actuator Materials http://www.piceramic.com/piezo_tutorial.php

[48] Pourki F (1993) Active distributed damping of flexible structures using piezo-electric actuators/sensors *Mechanics Research Communications*. **Vol. 20**, **4** pp. 279-285

[49] Pourki F (1993) Distributed controllers for flexible structures using piezo-electric actuators /sensors *Proceedings of the 32nd Conference an Decision and Control* pp. 1367-1370

[50] Preumont A *Vibration Control of Active Structures*, 2nd ed. Kluwer Academic Publishers, London 2002

[51] Qiu ZC, Zhang XM, Wu HX and Zhang HH (2007) Optimum placement and active vibration control for piezoelectric smart flexible cantilever plate *Journal of Sound and Vibration* **301** pp. 521-543

[52] Rezazadeh G, Fathalilou M and Shabani R (2009) Static and dynamic stabilities of a microbeam actuated by a piezoelectric voltage *Journal Microsystem Technologies* **15** pp. 1785-1791

[53] Sadek I, Kucuk I, Zeini E and Adali S (2009) Optimal boundary control of dynamics responses of piezo actuating micro-beams *Applied Mathematical Modelling* **33** pp. 3343-3353

[54] Shaker FJ (1975) *Effect of axial load on mode shapes and frequencies of beams.* Lewis Research Center: NASA TN D-8109

[55] Shu YC and Lien IC (2006) Analysis of power output for piezoelectric energy harvesting systems Smart Materials and Structures **15** pp. 1499-1512

[56] Shudong Yu and Siyuan He (2012) Accurate free vibration analysis of cantilever piezoelectric panel carrying a rigid mass *Journal of Vibration and Control* **19(8)** pp. 1187–1198

[57] Sloss JM, Adali S, Sadek LS and Bruch Jr. JC (1999) Piezoelectric displacement feedback control with time delay *SPIE Conference on Mathematics and Control in Smart Structures*. **SPIE Vol. 3667** pp. 649-656

[58] Smith RC (2005) *Smart Materials Systems: Model Development* (Philadelphia, PA: Society for Industrial and Applied Mathematics (SIAM))

[59] Spier C, Bruch, Jr. JC, Sloss JM, Adali S and Sadek IS (2009) Placement of multiple piezo patch sensors and actuators for a cantilevered beam to maximize frequency and frequency gaps *Journal of Vibration and Control,* **15(5):** pp. 643-670

[60] Srinivasan AV and McFarland DM (2000) *Smart structures: analysis and design* (New York: Cambridge University Press)

[61] Stanton SC, Ertuk A, Mann BP, Inmann DJ (2010) Nonlinear piezoelectricity in electrostatic energy harvesters : modeling and experimental identification *Journal of Applied Physics* **108**:074903

[62] Timoshenko S, Young DH and Weaver Jr. W (1974) *Vibration Problems in Engineering* (New York: John Wiley & Sons)

[63] Trindale MA and Benjeddou A (2002) Hybrid active-passive damping treatments using viscoelastic and piezoelectric materials: Review and assessment *Journal of Vibration and Control* **8** pp. 699-745

[64] Tse FS, Morse IE and Hinkle RT (1979) *Mechanical Vibrations: Theory and Applications* (Boston, MA: Allyn and Bacon, Inc.)

[65] Wang QM and Cross LE (1999) Constitutive equations of symmetrical triple layer piezoelectric benders *IEEE Trans. Ultrasonics Ferroelectric Frequency Control* **46(6)** pp. 1343-51

[66] Wang QM, Du XH, Xu B and Cross LE (1999) Electromechanical coupling and output efficiency of piezoelectric bending actuators *IEEE Trans. Ultrasonics Ferroelectric Frequency Control* **46(3)** pp. 638-646

[67] Weinberg MS (1999) Working equations for piezoelectric actuators and sensors *Journal of Microelectromechanical Systems* **Vol. 8** pp. 529-533

[68] Wood RJ, Steltz E and Fearing RS (2005) Optimal energy density piezoelectric bending actuators *Sensors and Actuators* **A 119** pp. 476-488

[69] Yang Y, Ju C and Kiong Soh C (2002) Analytical and semi-analytical solutions for cantilevered column using a piezo-electric actuator *Smart Material Structures* **12** pp. 193-203

[70] Yim W and Singh SN (2003) Adaptive output feedback force control of a cantilever beam using a piezoelectric actuator *Journal of Vibration and Control*. **9** pp. 567-581

[71] Young D and Felgar, Jr., RP (1949) Tables of Characteristic Functions Representing Normal Modes of Vibration of a Beam **No. 4913** *University of Texas, Austin* Austin, TX

Appendix

A1. Second natural frequencies.

Table A1 1: 2nd Mode frequencies (ω_2) with tip ass ratio, η = 0

(k)	ω_2 V=0V	ω_2 V=100V	Δ% ω_2 V=100V	ω_2 V=500V	Δ% ω_2 V=500V	ω_2 V=1000V	Δ% ω_2 V=1000V
0.8	4.531	4.528	0.05	4.522	0.2	4.513	0.39
0.4	4.615	4.613	0.04	4.607	0.18	4.598	0.36
0	4.694	4.693	0.03	4.686	0.16	4.679	0.36
-1	4.875	4.874	0.02	4.869	0.13	4.862	0.27
-6	5.545	5.544	0.02	5.541	0.07	5.537	0.14
-10	5.924	5.923	0.024	5.921	0.05	5.918	0.10

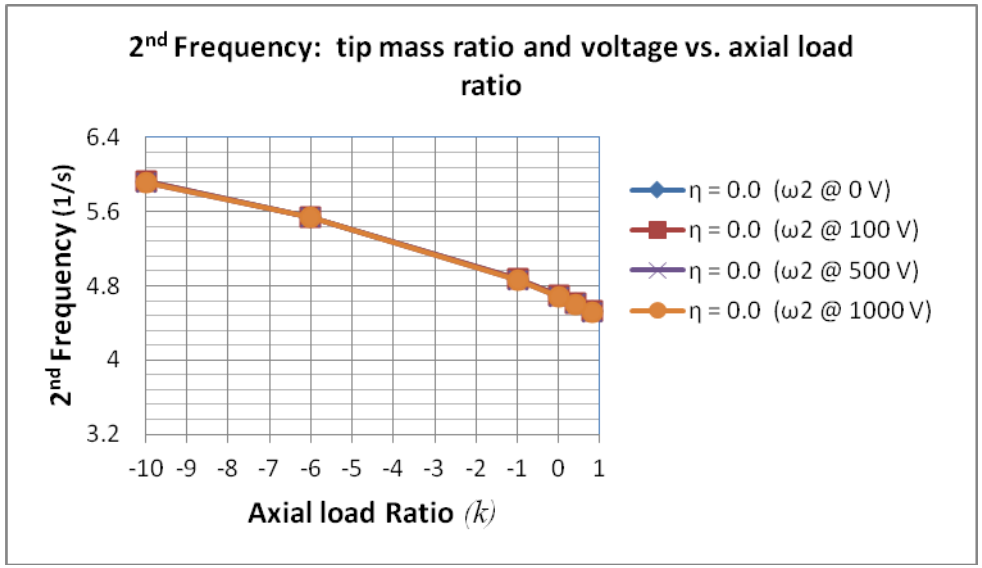

Figure A1 1: Natural frequency vs axial load: Tip mass ratio (η = 0)

Table A1 2: 2nd Mode frequencies (ω_2) with tip ass ratio, η = 0.1

(k)	ω_2 V=0V	ω_2 V=100V	Δ% ω_2 V=100V	ω_2 V=500V	Δ% ω_2 V=500V	ω_2 V=1000V	Δ% ω_2 V=1000V
8	4.26	4.259	0.03	4.254	0.14	4.248	0.27
0.4	4.331	4.330	0.02	4.326	0.12	4.320	0.24
0	4.400	4.398	0.02	4.394	0.12	4.389	0.24
-1	4.557	4.556	0.01	4.553	0.1	4.548	0.20
-6	5.165	5.165	0.01	5.162	0.06	5.159	0.12
-10	5.524	5.523	0.01	5.521	0.05	5.519	0.09

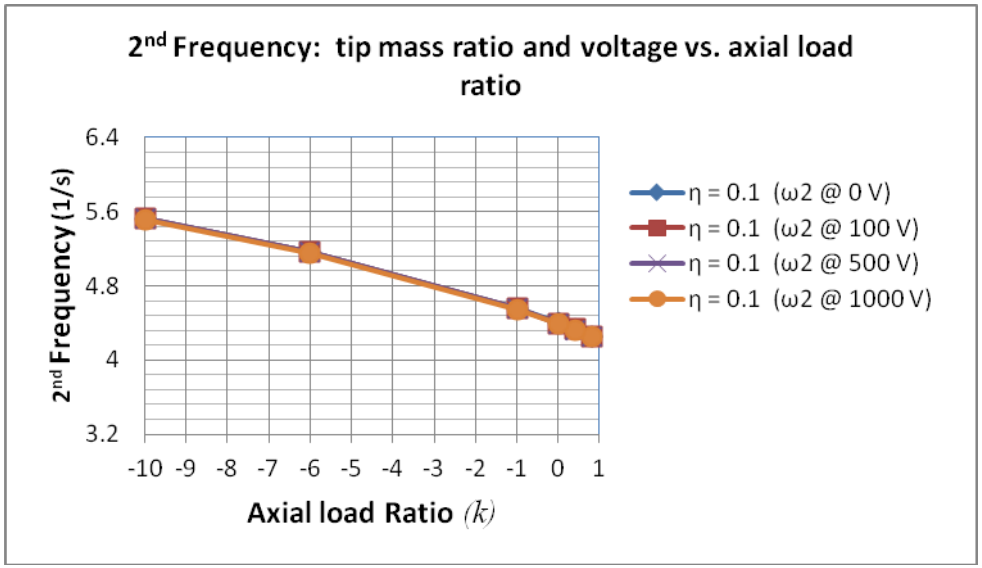

Figure A1 2: Natural frequency vs axial load: Tip mass ratio (η = 0.1)

Table A1 3: 2nd Mode frequencies (ω_2) with tip ass ratio, η = 1

(k)	ω_2 V=0V	ω_2 V=100V	$\Delta\%\ \omega_2$ V=100V	ω_2 V=500V	$\Delta\%\ \omega_2$ V=500V	ω_2 V=1000V	$\Delta\%\ \omega_2$ V=1000V
0.8	3.925	3.925	0.01	3.924	0.04	3.922	0.07
0.4	3.979	3.979	0.004	3.978	0.03	3.977	0.06
0	4.0311	4.031	0.01	4.030	0.03	4.029	0.06
-1	4.153	4.153	0.01	4.152	0.03	4.151	0.06
-6	4.639	4.638	0.01	4.638	0.03	4.637	0.05
-10	4.937	4.936	0.01	4.936	0.02	4.935	0.04

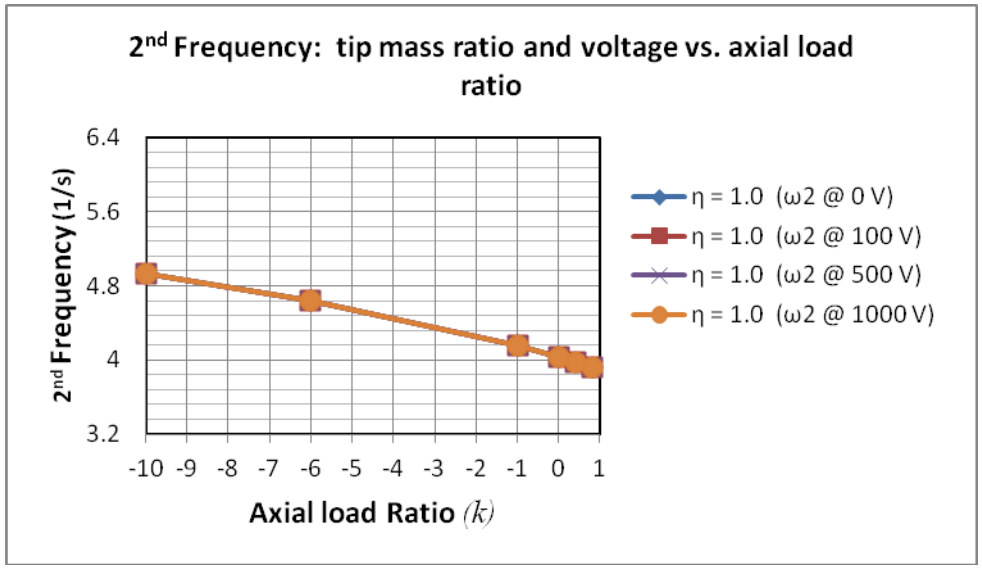

Figure A1 3: Natural frequency vs axial load: Tip mass ratio (η = 1)

Table A1 4: 2nd Mode frequencies (ω_2) with tip ass ratio, η = 5

(k)	ω_2 V=0V	ω_2 V=100V	$\Delta\%\ \omega_2$ V=100V	ω_2 V=500V	$\Delta\%\ \omega_2$ V=500V	ω_2 V=1000V	$\Delta\%\ \omega_2$ V=1000V
0.8	3.851	3.850	0.01	3.850	0.02	3.850	0.03
0.4	3.901	3.901	-0.004	3.901	002	3.901	0.01
0	3.950	3.950	0.001	3.950	0.01	3.949	0.01
-1	4.064	4.064	-0.003	4.064	0.01	4.064	0.01
-6	4.523	4.522	0.01	4.522	0.01	4.522	0.02
-10	4.805	4.805	0.0004	4.805	0.004	4.805	0.01

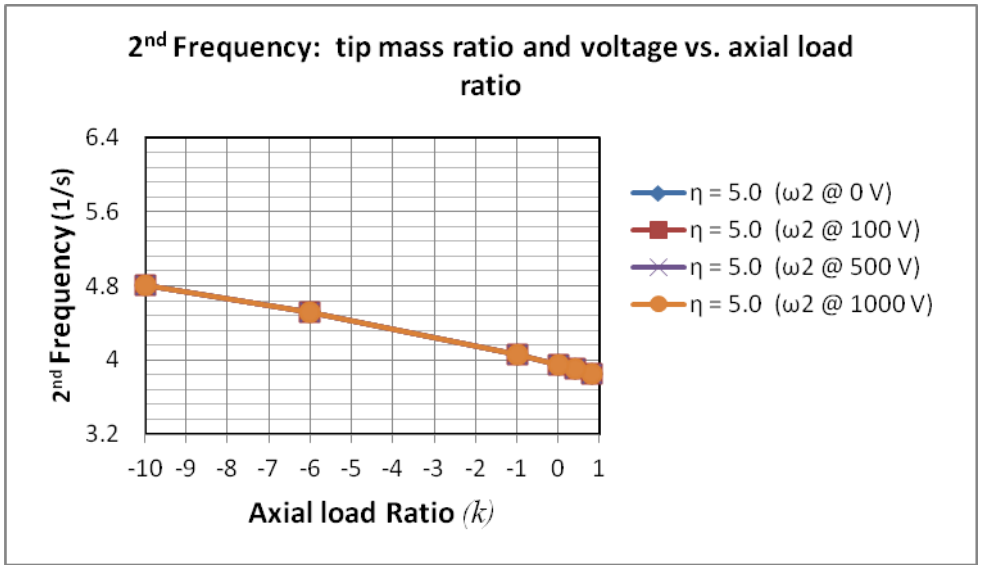

Figure A1 4: Natural frequency vs axial load: Tip mass ratio (η = 5)

Table A1 5: 2nd Mode frequencies (ω_2) with tip ass ratio, η = 10

(k)	ω_2 V=0V	ω_2 V=100V	$\Delta\%$ ω_2 V=100V	ω_2 V=500V	$\Delta\%$ ω_2 V=500V	ω_2 V=1000V	$\Delta\%$ ω_2 V=1000V
0.8	3.840	3.840	-0.0004	3.840	0.01	3.840	0.01
0.4	3.890	3.890	0.004	3.890	0.01	3.890	0.01
0	3.938	3.938	-0.01	3.938	-0.01	3.9381	0.01
-1	4.052	4.052	0.01	4.052	0.01	4.051	0.01
-6	4.506	4.506	-0.0004	4.506	0.004	4.506	0.003
-10	4.787	4.787	-0.001	4.787	0.003	4.787	0.002

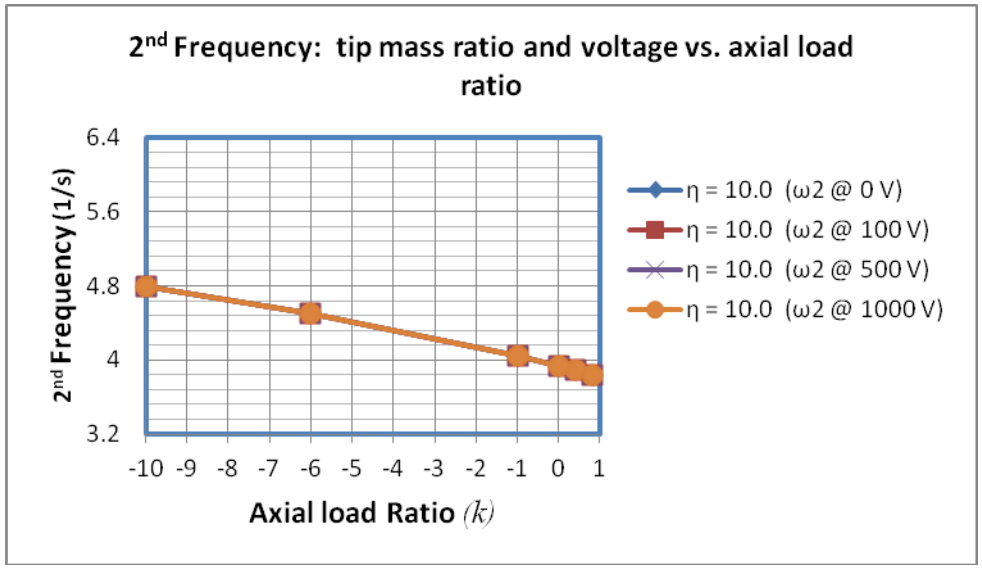

Figure A1 5: Natural frequency vs axial load: Tip mass ratio (η = 10)

A2. Third natural frequencies.

Table A2 1: 3rd Mode frequencies (ω_3) with tip ass ratio, η = 0

(k)	ω_3 V=0V	ω_3 V=100V	$\Delta\%$ ω_3 V=100V	ω_3 V=500V	$\Delta\%$ ω_3 V=500V	ω_3 V=1000V	$\Delta\%$ ω_3 V=1000V
0.8	7.775	7.774	0.01	7.772	0.04	7.769	0.07
0.4	7.815	7.815	0.01	7.812	0.03	7.810	0.07
0	7.855	7.854	0.01	7.852	0.04	7.849	0.07
-1	7.951	7.951	0.002	7.949	0.03	7.940	0.06
-6	8.386	8.386	0.005	8.384	0.02	8.382	0.05
-10	8.687	8.687	0.004	8.685	0.02	8.683	0.04

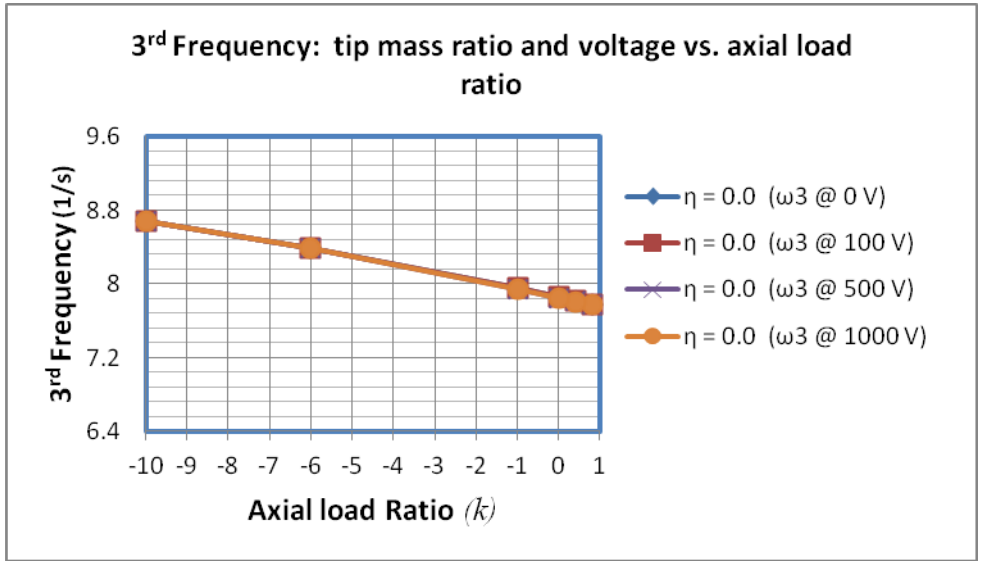

Figure A2 1: Natural frequency vs axial load: Tip mass ratio (η = 0)

Table A2 2: 3rd Mode frequencies (ω_3) with tip ass ratio, η = 0.1

(k)	ω_3 V=0V	ω_3 V=100V	$\Delta\%$ ω_3 V=100V	ω_3 V=500V	$\Delta\%$ ω_3 V=500V	ω_3 V=1000V	$\Delta\%$ ω_3 V=1000V
0.8	7.382	7.382	0.01	7.380	0.02	7.379	0.04
0.4	7.417	7.416	0.01	7.415	0.02	7.414	0.04
0	7.451	7.451	0.003	7.450	0.02	7.448	0.04
-1	7.535	7.535	0.003	7.534	0.0	7.532	0.04
-6	7.919	7.919	0.003	7.918	0.02	7.916	0.03
-10	8.191	8.190	0.01	8.189	0.02	8.188	0.03

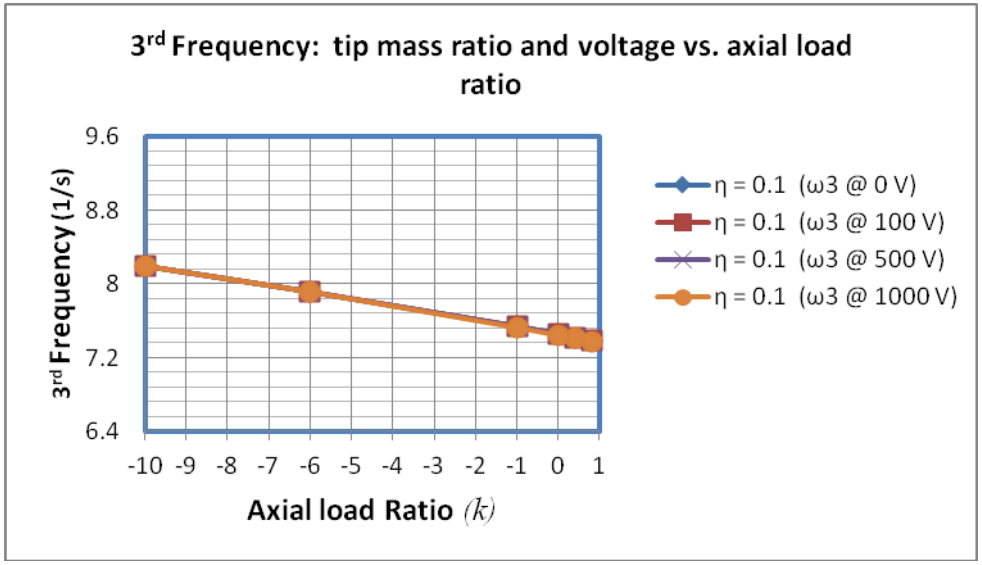

Figure A2 2: Natural frequency vs axial load: Tip mass ratio (η = 0.1)

Table A2 3: 3rd Mode frequencies (ω_3) with tip ass ratio, η = 1

(k)	ω_3 V=0V	ω_3 V=100V	$\Delta\%$ ω_3 V=100V	ω_3 V=500V	$\Delta\%$ ω_3 V=500V	ω_3 V=1000V	$\Delta\%$ ω_3 V=1000V
0.8	7.073	7.072	0.002	7.072	0.005	7.072	0.008
0.4	7.103	7.103	-0.006	7.103	-0.003	7.104	0.001
0	7.134	7.134	-0.001	7.134	0.001	7.134	0.004
-1	7.209	7.209	-0.001	7.209	0.001	7.209	0.004
-6	7.553	7.553	0.003	7.553	0.005	7.552	0.008
-10	7.797	7.797	-6E-04	7.797	0.001	7.797	0.004

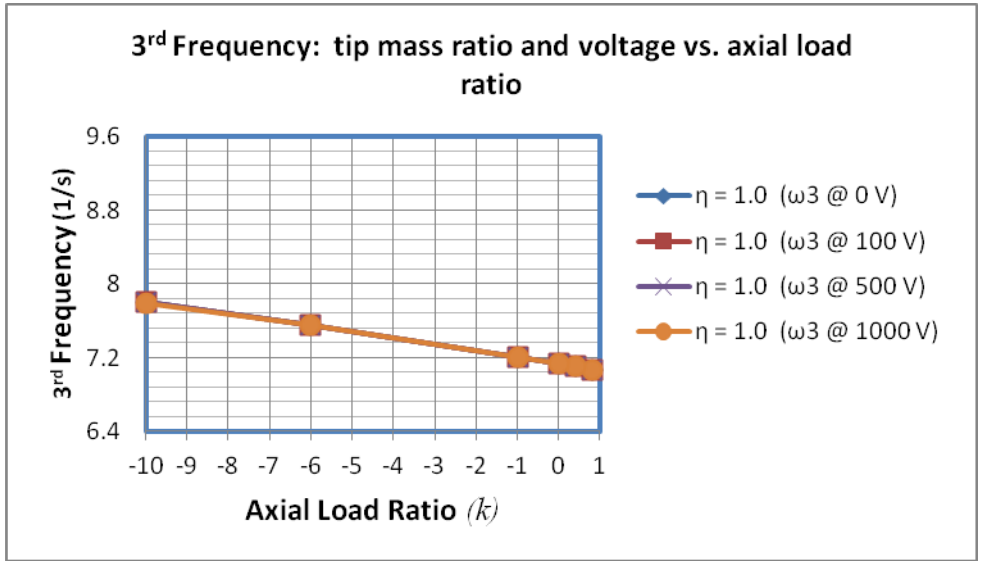

Figure A2 3: Natural frequency vs axial load: Tip mass ratio (η = 1)

Table A2 4: 3rd Mode frequencies (ω_3) with tip ass ratio, η = 5

(k)	ω_3 V=0V	ω_3 V=100V	$\Delta\%$ ω_3 V=100V	ω_3 V=500V	$\Delta\%$ ω_3 V=500V	ω_3 V=1000V	$\Delta\%$ ω_3 V=1000V
0.8	7.022	7.022	-1E-04	7.022	0.0004	7.022	0.0011
0.4	7.052	7.052	0.0005	7.052	0.001	7.052	0.0017
0	7.083	7.083	-4E-04	7.082	0.0001	7.082	0.0008
-1	7.157	7.157	-3E-04	7.156	0.0002	7.156	0.0009
-6	7.496	7.496	-7E-04	7.496	-3E-04	7.495	0.0002
-10	7.737	7.737	-3E-05	7.737	0.0003	7.737	0.0008

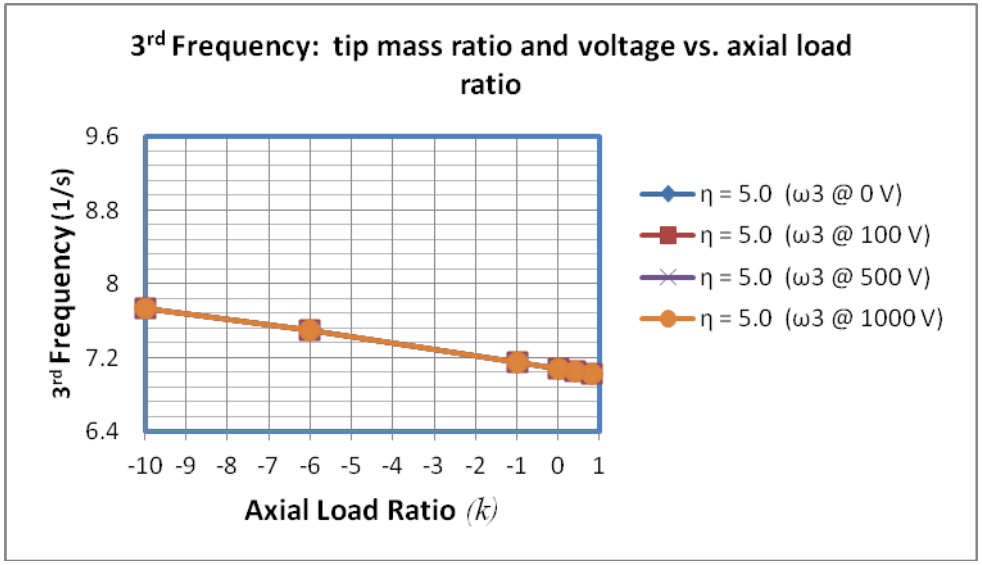

Figure A2 4: Natural frequency vs axial load: Tip mass ratio (η = 5)

Table A2 5: 3rd Mode frequencies (ω_3) with tip ass ratio, η = 10

(k)	ω_3 V=0V	ω_3 V=100V	$\Delta\%$ ω_3 V=100V	ω_3 V=500V	$\Delta\%$ ω_3 V=500V	ω_3 V=1000V	$\Delta\%$ ω_3 V=1000V
0.8	7.015	7.015	0.0001	7.015	0.0004	7.015	0.0007
0.4	7.045	7.054	-0.12	7.045	0.0003	7.045	0.0006
0	7.076	7.076	0.01	7.076	0.0058	7.076	0.006
-1	7.149	7.149	-0.01	7.149	-0.006	7.149	-0.006
-6	7.488	7.488	0.001	7.488	0.0008	7.488	0.001
-10	7.729	7.729	0.01	7.729	0.005	7.729	0.006

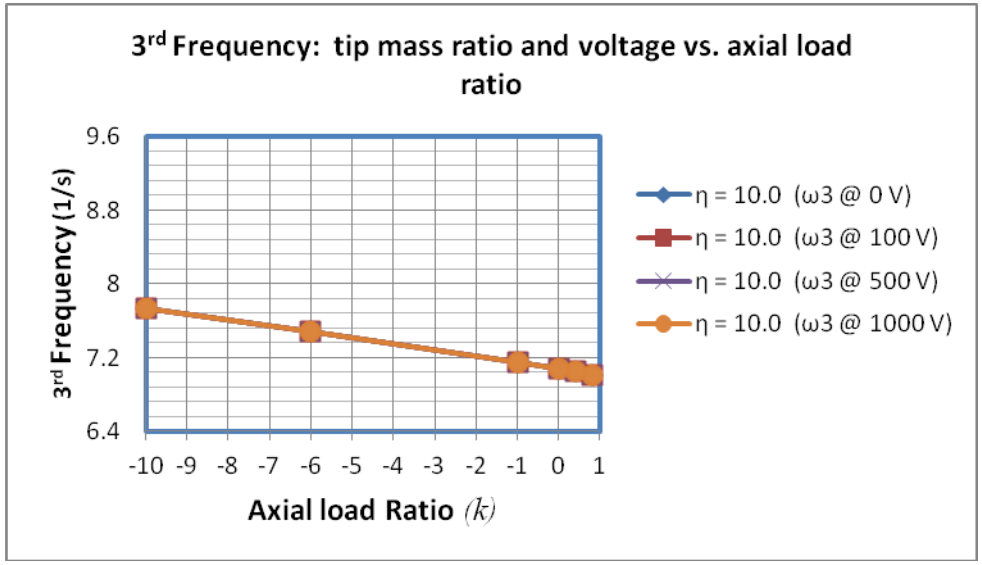

Figure A2 5: Natural frequency vs axial load: Tip mass ratio (η = 10)

A3. Fourth natural frequencies.

Table A3 1: 4th Mode frequencies (ω_4) with tip ass ratio, η = 0

(k)	ω_4 V=0V	ω_4 V=100V	$\Delta\%$ ω_4 V=100V	ω_4 V=500V	$\Delta\%$ ω_4 V=500V	ω_4 V=1000V	$\Delta\%$ ω_4 V=1000V
0.8	10.942	10.942	-0	10.941	0.01	10.939	0.02
0.4	10.969	10.969	0.002	10.968	0.01	10.966	0.02
0	10.996	10.995	0.007	10.994	0.02	10.993	0.03
-1	11.060	11.061	-0.01	11.060	0.001	11.059	0.01
-6	11.373	11.373	0.002	11.372	0.01	11.371	0.02
-10	11.600	11.604	-0.04	11.603	-0.03	11.602	-0.02

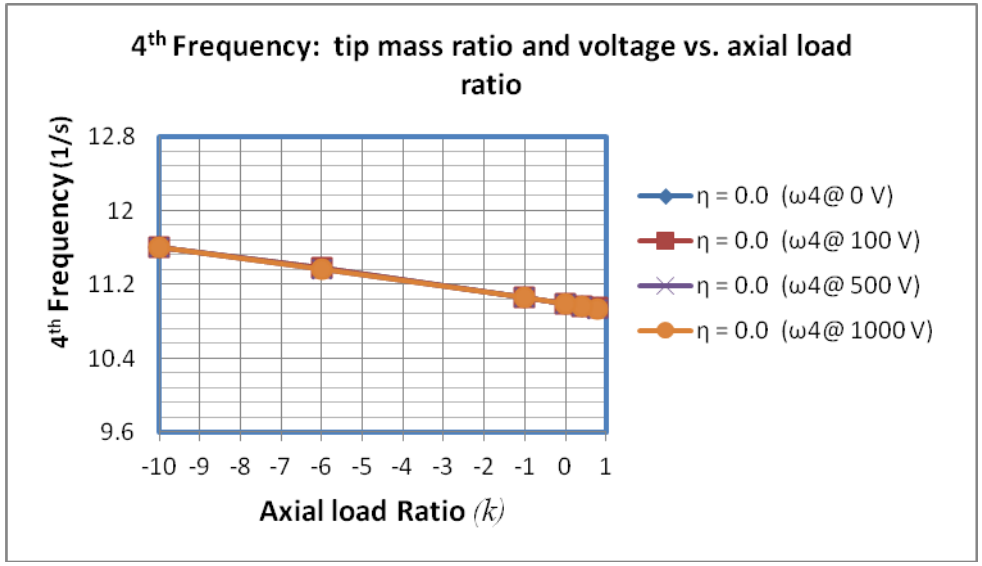

Figure A3 1: Natural frequency vs axial load: Tip mass ratio (η = 0)

Table A3 2: 4th Mode frequencies (ω_4) with tip ass ratio, η = 0.1

(k)	ω_4 V=0V	ω_4 V=100V	$\Delta\%$ ω_4 V=100V	ω_4 V=500V	$\Delta\%$ ω_4 V=500V	ω_4 V=1000V	$\Delta\%$ ω_4 V=1000V
0.8	10.475	10.475	0.001	10.474	0.005	10.474	0.01
0.4	10.498	10.492	0.06	10.498	0.005	10.497	0.01
0	10.520	10.522	-0.02	10.521	-0.01	10.521	-0.006
-1	10.580	10.580	0.004	10.579	0.008	10.579	0.01
-6	10.856	10.856	0.001	10.856	0.005	10.855	0.01
-10	11.060	11.063	-0.03	11.063	-0.03	11.062	-0.02

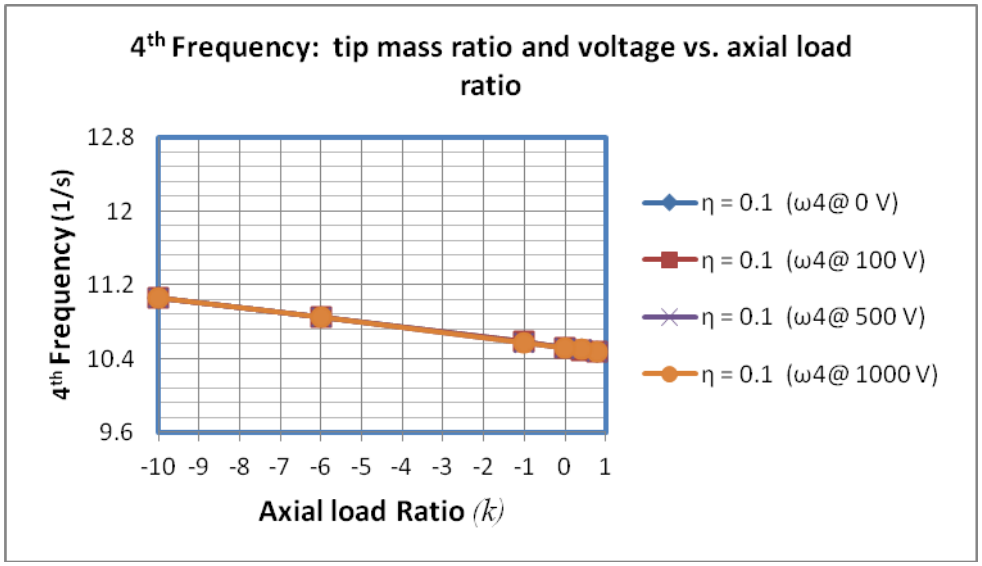

Figure A3 2: Natural frequency vs axial load: Tip mass ratio (η = 0.1)

Table A3 3: 4th Mode frequencies (ω_4) with tip ass ratio, η = 1

(k)	ω_4 V=0V	ω_4 V=100V	$\Delta\%$ ω_4 V=100V	ω_4 V=500V	$\Delta\%$ ω_4 V=500V	ω_4 V=1000V	$\Delta\%$ ω_4 V=1000V
0.8	10.212	10.212	-0	10.212	0.0006	10.212	0.001
0.4	10.235	10.235	2E-04	10.235	0.0008	10.234	0.002
0	10.260	10.257	0.033	10.257	0.03	10.256	0.03
-1	10.310	10.311	-0.01	10.311	-0.01	10.311	-0.01
-6	10.571	10.571	3E-04	10.571	0.0009	10.571	0.002
-10	10.770	10.766	0.04	10.766	0.04	10.766	0.04

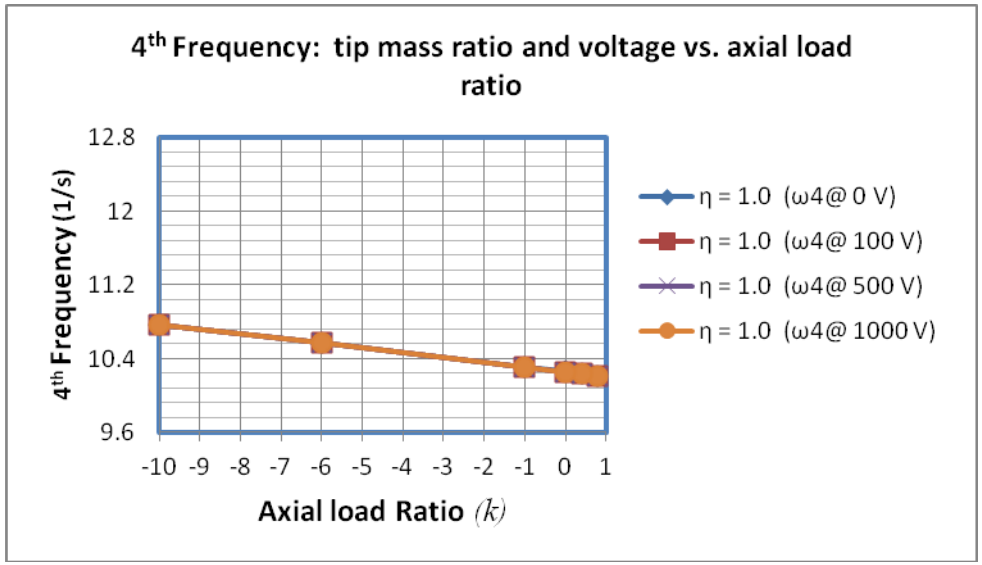

Figure A3 3: Natural frequency vs axial load: Tip mass ratio (η = 1)

Table A3 4: 4th Mode frequencies (ω_4) with tip ass ratio, η = 5

(k)	ω_4 V=0V	ω_4 V=100V	$\Delta\%$ ω_4 V=100V	ω_4 V=500V	$\Delta\%$ ω_4 V=500V	ω_4 V=1000V	$\Delta\%$ ω_4 V=1000V
0.8	10.176	10.176	-0	10.176	-6E-05	10.176	8.8E-05
0.4	10.198	10.198	4E-04	10.198	0.0005	10.198	0.0007
0	10.220	10.220	4E-04	10.220	0.0005	10.220	0.0006
-1	10.274	10.274	-0	10.274	1E-04	10.274	0.0002
-6	10.533	10.533	1E-04	10.533	0.0002	10.533	0.0004
-10	10.727	10.726	4E-04	10.726	0.0006	10.726	0.0007

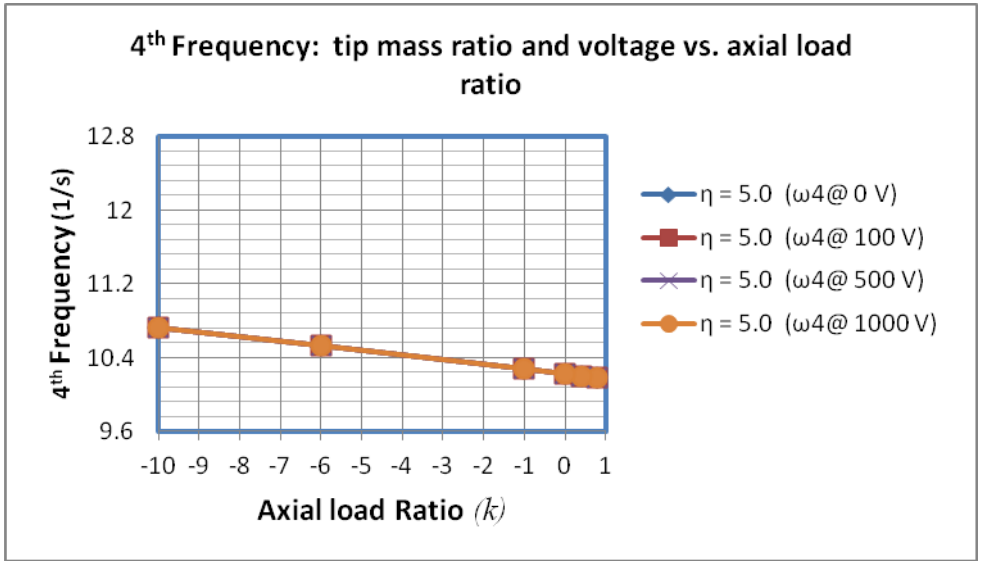

Figure A3 4: Natural frequency vs axial load: Tip mass ratio (η = 5)

Table A3 5: 4th Mode frequencies (ω_4) with tip ass ratio, η = 10

(k)	ω_4 V=0V	ω_4 V=100V	$\Delta\%$ ω_4 V=100V	ω_4 V=500V	$\Delta\%$ ω_4 V=500V	ω_4 V=1000V	$\Delta\%$ ω_4 V=1000V
0.8	10.171	10.171	0.00001	10.171	0.00007	10.171	0.0002
0.4	10.193	10.193	0.00002	10.193	0.00007	10.193	0.0002
0	10.215	10.215	0.00001	10.215	0.00007	10.215	0.0002
-1	10.269	10.269	0.00002	10.269	0.00007	10.269	0.0001
-6	10.528	10.528	0.000009	10.528	0.00005	10.528	0.0001
-10	10.721	10.721	0.000009	10.721	0.00006	10.721	0.0001

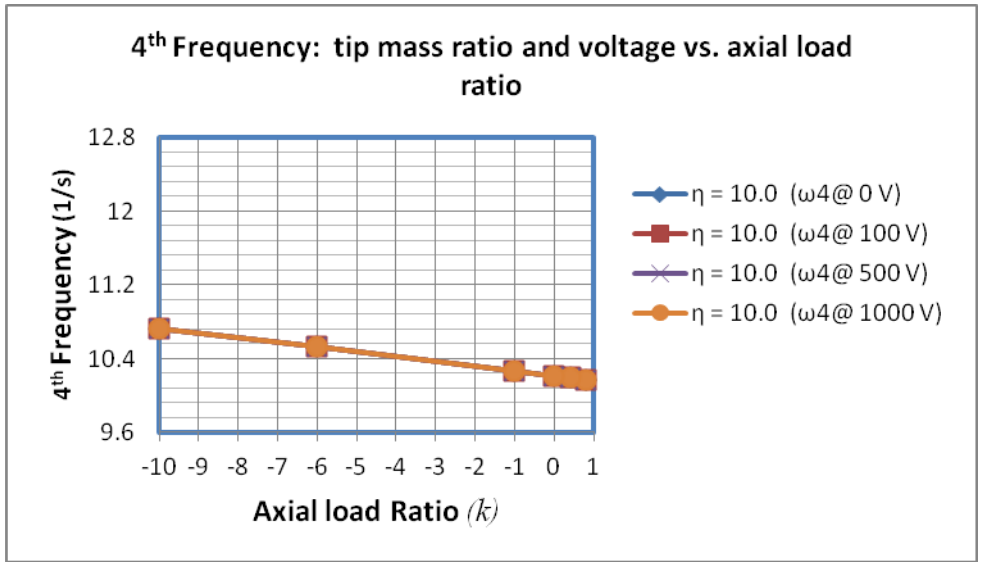

Figure A3 5: Natural frequency vs axial load: Tip mass ratio (η = 10)

B1. Natural frequencies with $b_1 = L/10$.

Table B1 1: Natural frequencies of a beam with a concentrated tip mass ($b_1 = L/10$) including the effects rotary inertia at 0V.

Axial load Ratio (k)	η = 0	η = 0.1	η = 1	η = 5	η = 10
+0.8	1.2472	0.9992	0.6206	0.4195	0.3533
+0.4	1.6629	1.3115	0.8096	0.5467	0.4603
+0.2	1.7800	1.4073	0.8664	0.5847	0.4922
0	1.8751	1.4860	0.9123	0.6153	0.5180
-0.4	2.0256	1.6121	0.9844	0.6634	0.5584
-1	2.1943	1.7552	1.0639	0.7162	0.6027
-2	2.3972	1.9293	1.1569	0.7776	0.6543

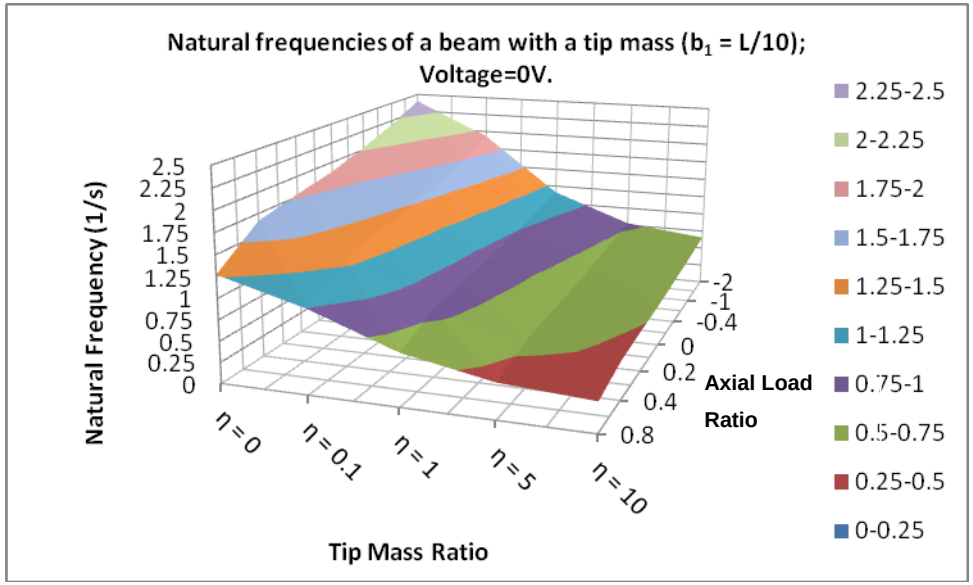

Figure B1 1: Changes in the natural frequency vs axial load and tip mass ($b_1 = L/10$)

Table B1 2: Natural frequencies of a beam with a concentrated tip mass ($b_1 = L/10$) including the effects rotary inertia at 100V.

Axial load Ratio (k)	η = 0	η = 0.1	η = 1	η = 5	η = 10
+0.8	1.2442	0.9748	0.6054	0.4093	0.3446
+0.4	1.6509	1.3009	0.8031	0.5223	0.4566
+0.2	1.7706	1.3988	0.8611	0.5811	0.4892
0	1.8675	1.4788	0.9079	0.6124	0.5155
-0.4	2.0201	1.6064	0.9810	0.6611	0.5564
-1	2.1903	1.7508	1.0613	0.7144	0.6012
-2	2.3946	1.9260	1.1550	0.7763	0.6532

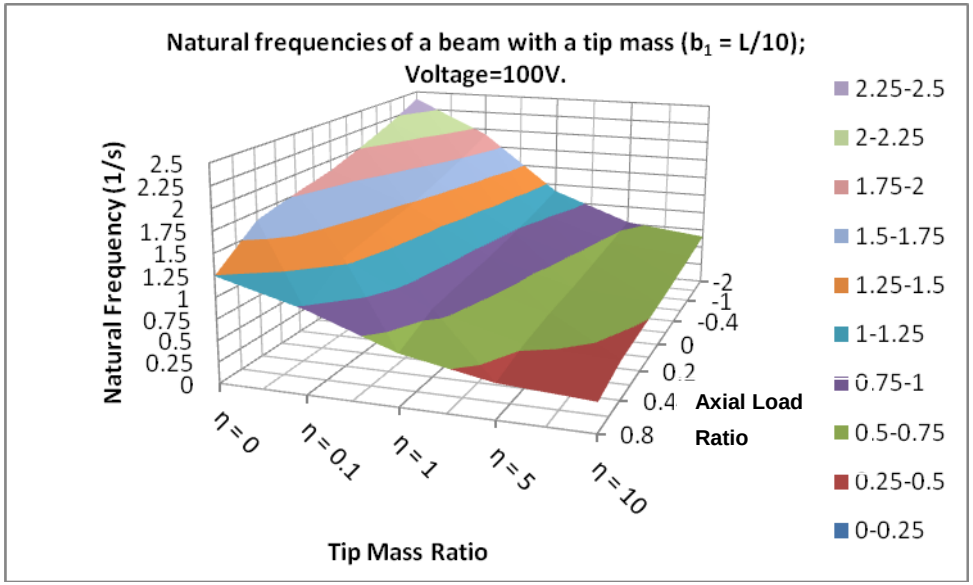

Figure B1 2: Changes in the natural frequency vs axial load and tip mass ($b_1 = L/10$)

Table B1 3: Natural frequencies of a beam with a concentrated tip mass ($b_1 = L/10$) including the effects rotary inertia at 500V.

Axial load Ratio (k)	$\eta = 0$	$\eta = 0.1$	$\eta = 1$	$\eta = 5$	$\eta = 10$
+0.8	1.0929	0.8532	0.5298	0.3582	0.3017
+0.4	1.5995	1.2561	0.7755	0.5237	0.4409
+0.2	1.7313	1.3632	0.8393	0.5664	0.4769
0	1.8356	1.4488	0.8896	0.6001	0.5052
-0.4	1.9971	1.5831	0.9669	0.6517	0.5485
-1	2.1743	1.7329	1.0507	0.7073	0.5953
-2	2.3843	1.9125	1.1473	0.7712	0.6489

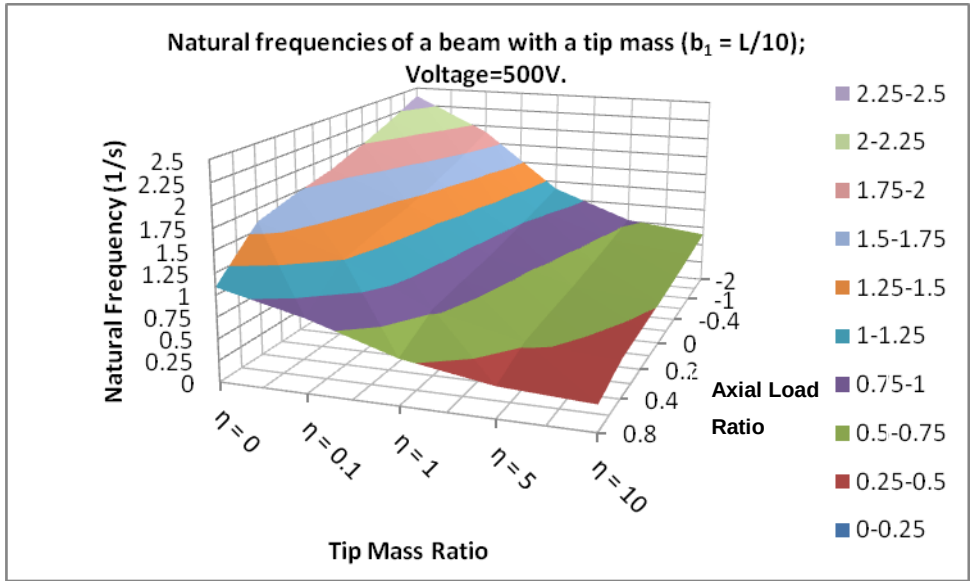

Figure B1 3: Changes in the natural frequency vs axial load and tip mass ($b_1 = L/10$)

Table B1 4: Natural frequencies of a beam with a concentrated tip mass ($b_1 = L/10$) including the effects rotary inertia at 1000V.

Axial load Ratio (k)	$\eta = 0$	$\eta = 0.1$	$\eta = 1$	$\eta = 5$	$\eta = 10$
+0.8	0.6597	0.5127	0.3184	0.2153	0.1813
+0.4	1.5258	1.1932	0.7367	0.4975	0.4189
+0.2	1.6770	1.3149	0.8096	0.5465	0.4601
0	1.7925	1.4091	0.8652	0.5837	0.4914
-0.4	1.9666	1.5529	0.9487	0.6394	0.5382
-1	2.1534	1.7100	1.0371	0.6983	0.5877
-2	2.3709	1.8956	1.1376	0.7648	0.6435

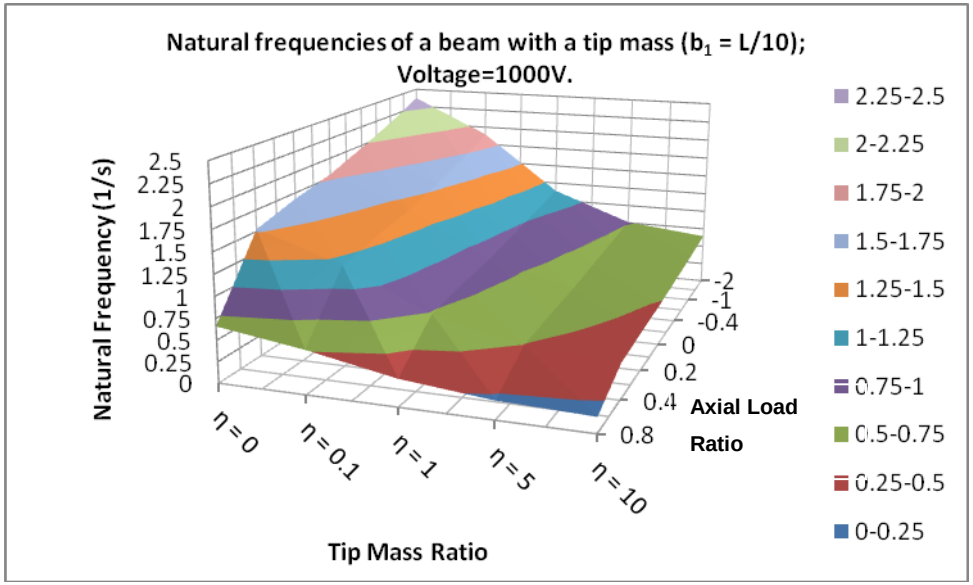

Figure B1 4: Changes in the natural frequency vs axial load and tip mass ($b_1 = L/10$)

B2. Natural frequencies with $b_1 = L/5$.

Table B2 1: Natural frequencies of a beam with a concentrated tip mass ($b_1 = L/5$) including the effects rotary inertia at 0V.

Axial load Ratio (k)	$\eta = 0$	$\eta = 0.1$	$\eta = 1$	$\eta = 5$	$\eta = 10$
+0.8	1.2472	0.9838	0.6065	0.4096	0.3449
+0.4	1.6629	1.2910	0.7915	0.5340	0.4495
+0.2	1.7800	1.3853	0.8470	0.5712	0.4808
0	1.8751	1.4627	0.8920	0.6012	0.5061
-0.4	2.0256	1.5865	0.9628	0.6484	0.5457
-1	2.1943	1.7271	1.0410	0.7004	0.5894
-2	2.3972	1.8978	1.1328	0.7612	0.6404

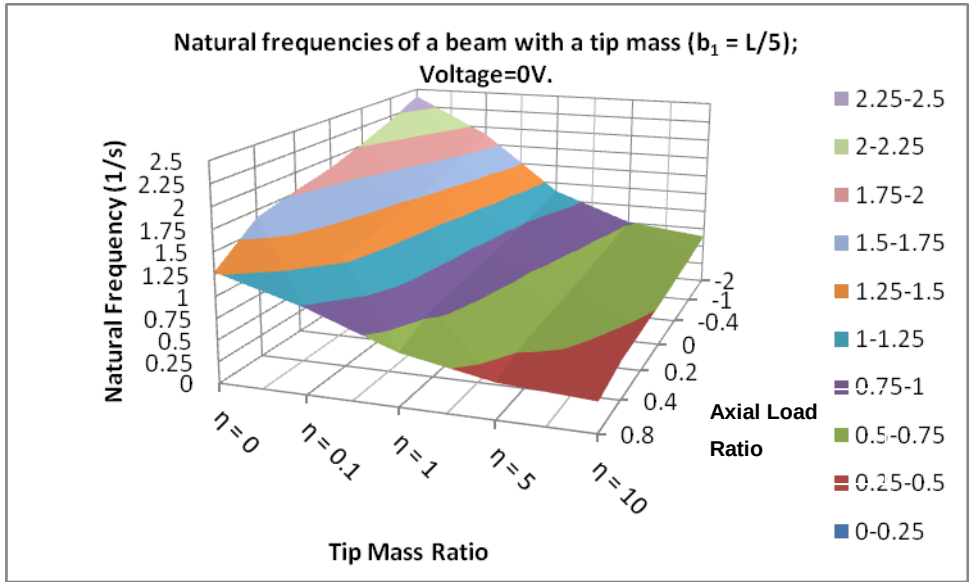

Figure B2 1: Changes in the natural frequency vs axial load and tip mass ($b_1 = L/5$)

Table B2 2: Natural frequencies of a beam with a concentrated tip mass ($b_1 = L/5$) including the effects rotary inertia at 100V.

Axial load Ratio (k)	$\eta = 0$	$\eta = 0.1$	$\eta = 1$	$\eta = 5$	$\eta = 10$
+0.8	1.2442	0.9597	0.5917	0.3996	0.3365
+0.4	1.6509	1.2806	0.7851	0.5297	0.4459
+0.2	1.7706	1.3769	0.8419	0.5677	0.4779
0	1.8675	1.4555	0.8877	0.5983	0.5036
-0.4	2.0201	1.5809	0.9594	0.6462	0.5438
-1	2.1903	1.7227	1.0384	0.6987	0.5880
-2	2.3946	1.8945	1.1309	0.7599	0.6394

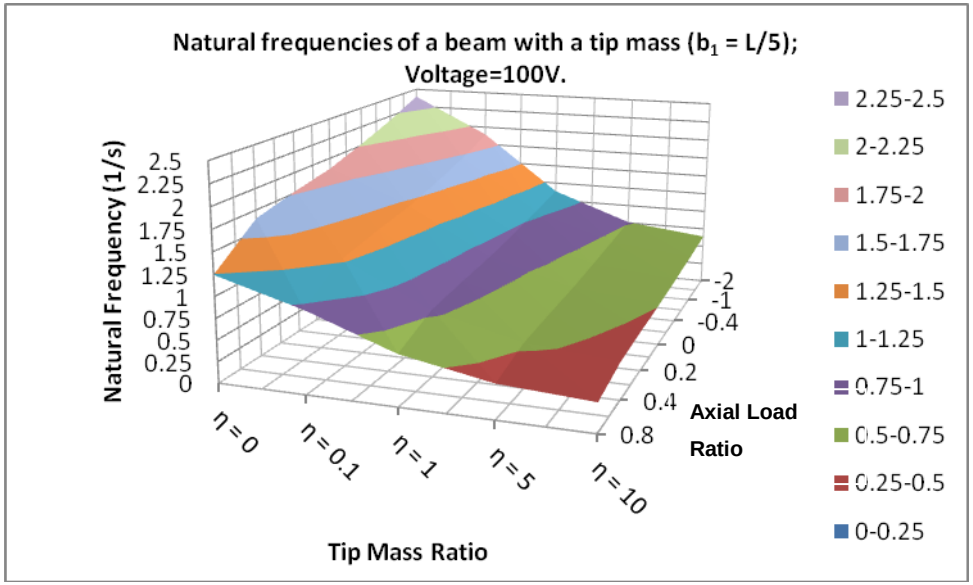

Figure B2 2: Changes in the natural frequency vs axial load and tip mass ($b_1 = L/5$)

Table B2 3: Natural frequencies of a beam with a concentrated tip mass ($b_1 = L/5$) including the effects rotary inertia at 500V.

Axial load Ratio (k)	$\eta = 0$	$\eta = 0.1$	$\eta = 1$	$\eta = 5$	$\eta = 10$
+0.8	1.0929	0.8400	0.5178	0.3498	0.2945
+0.4	1.5995	1.2365	0.7581	0.5115	0.4306
+0.2	1.7313	1.3418	0.8205	0.5533	0.4658
0	1.8356	1.4260	0.8698	0.5863	0.4935
-0.4	1.9971	1.5580	0.9457	0.6370	0.5361
-1	2.1743	1.7051	1.0280	0.6917	0.5821
-2	2.3843	1.8813	1.1233	0.7549	0.6352

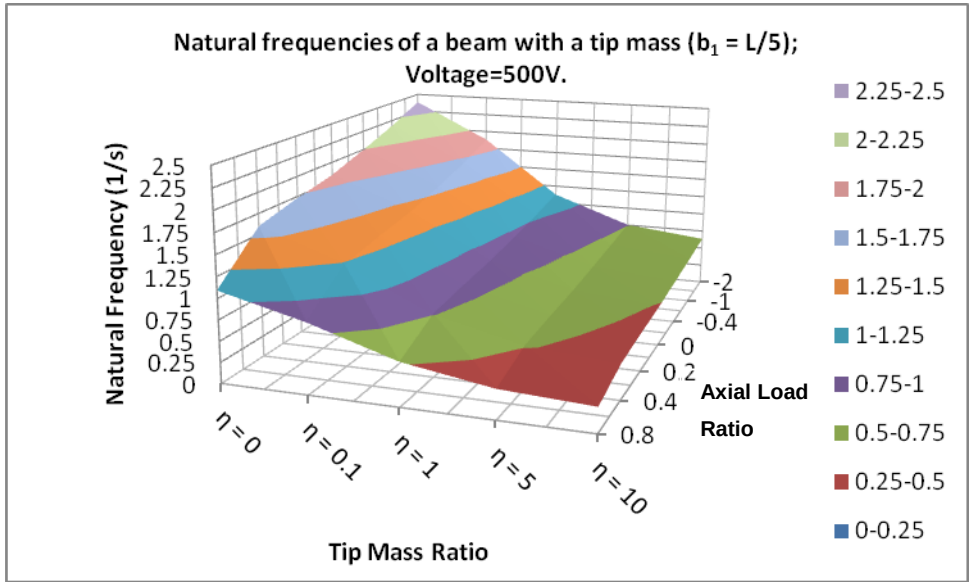

Figure B2 3: Changes in the natural frequency vs axial load and tip mass ($b_1 = L/5$)

Table B2 4: Natural frequencies of a beam with a concentrated tip mass ($b_1 = L/5$) including the effects rotary inertia at 1000V.

Axial load Ratio (k)	$\eta = 0$	$\eta = 0.1$	$\eta = 1$	$\eta = 5$	$\eta = 10$
+0.8	0.6597	0.5047	0.3112	0.2102	0.1770
+0.4	1.5258	1.1745	0.7201	0.4859	0.4091
+0.2	1.6770	1.2943	0.7915	0.5338	0.4494
0	1.7925	1.3868	0.8450	0.5703	0.4801
-0.4	1.9666	1.5282	0.9278	0.6250	0.5260
-1	2.1534	1.6825	1.0147	0.6828	0.5746
-2	2.3709	1.8646	1.1137	0.7485	0.6298

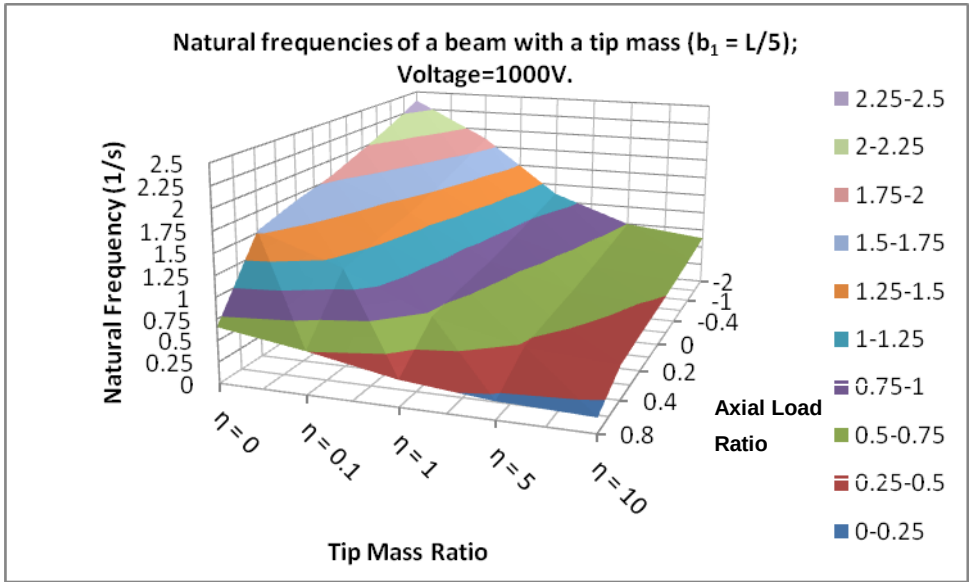

Figure B2 4: Changes in the natural frequency vs axial load and tip mass ($b_1 = L/5$)

C1. Mode shapes 0V and 1000V for $\eta = 0$

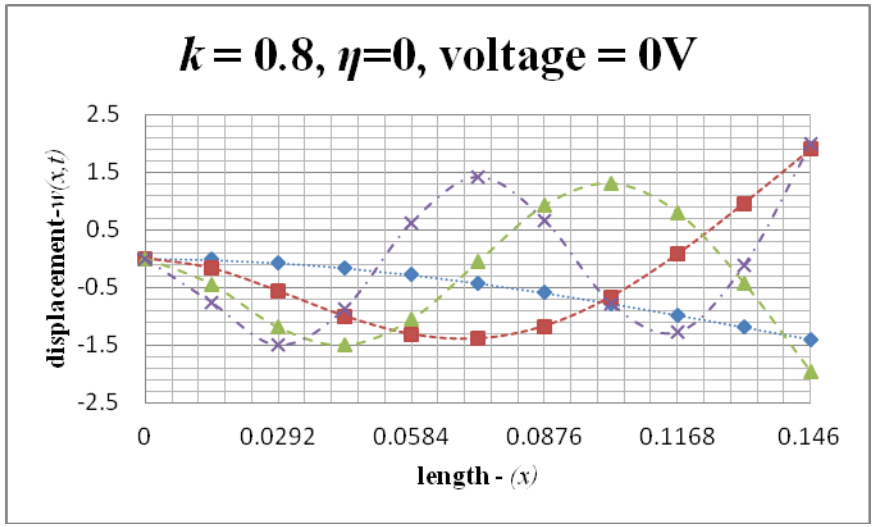

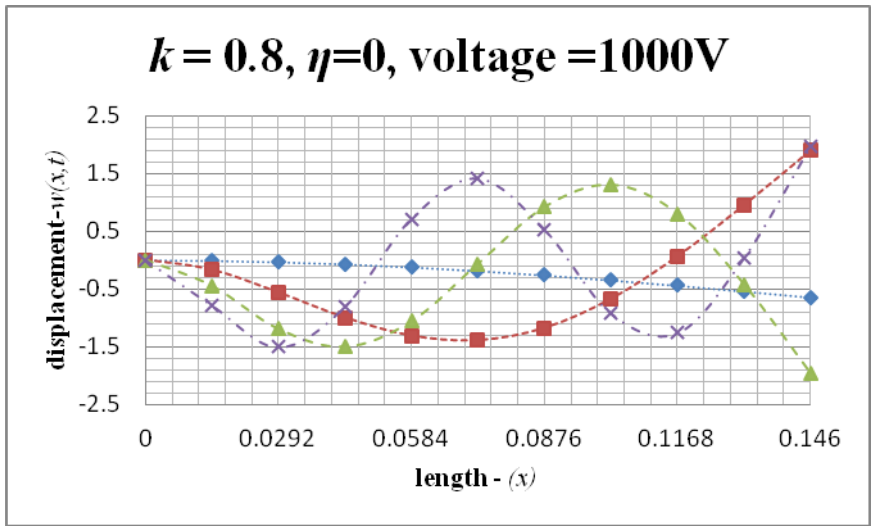

Figure C1 1: First four mode shapes for $k = +0.8$

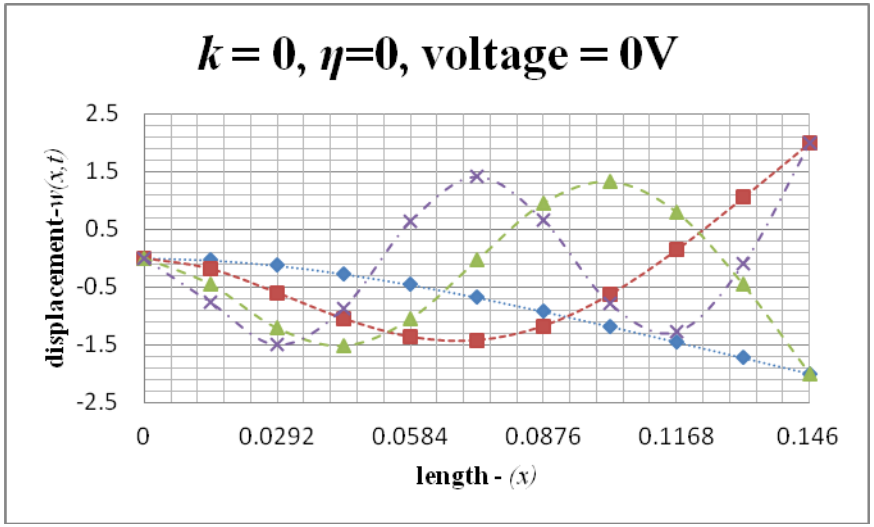

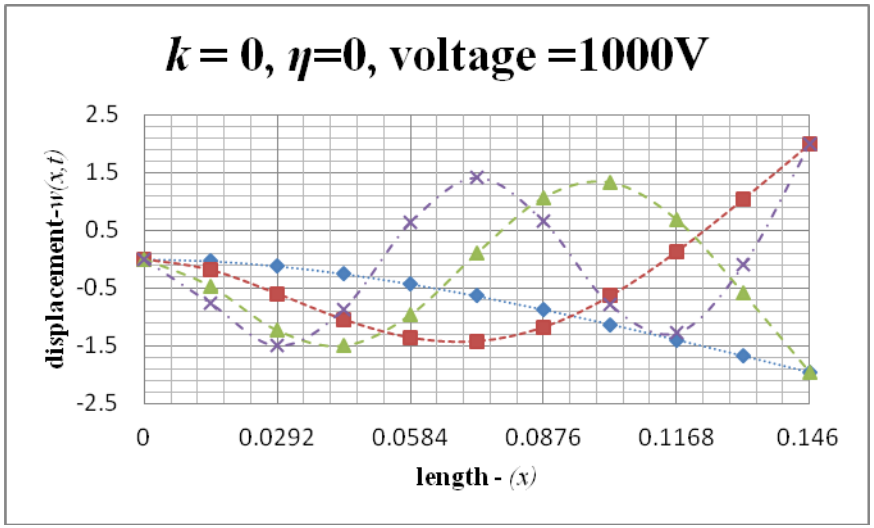

Figure C1 2: .First four mode shapes for $k = 0$

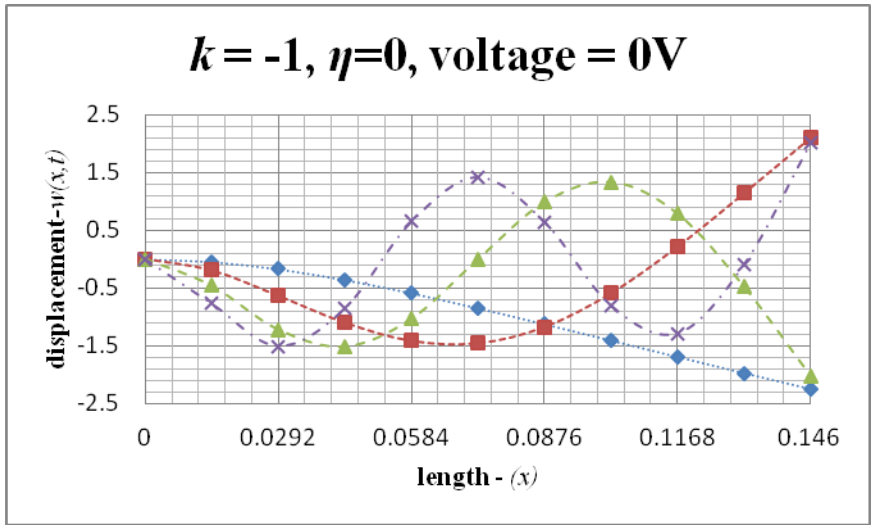

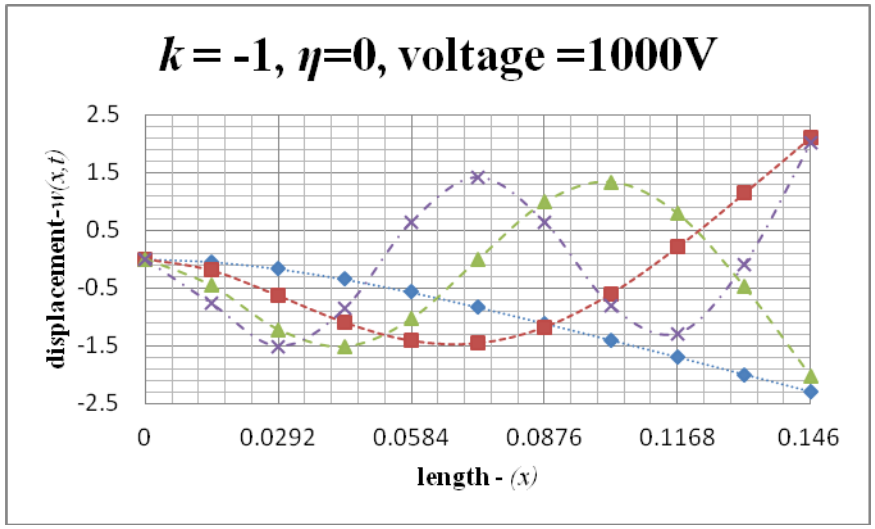

Figure C1 3: First four mode shapes for k = -1

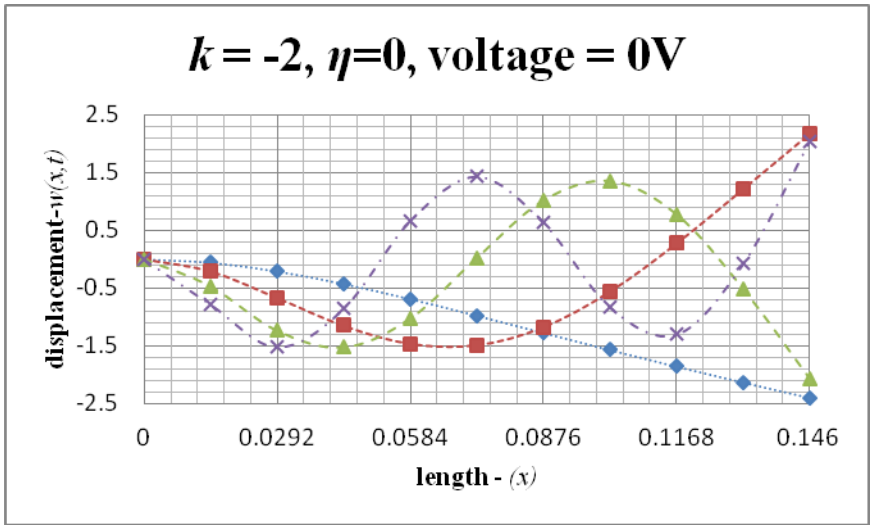

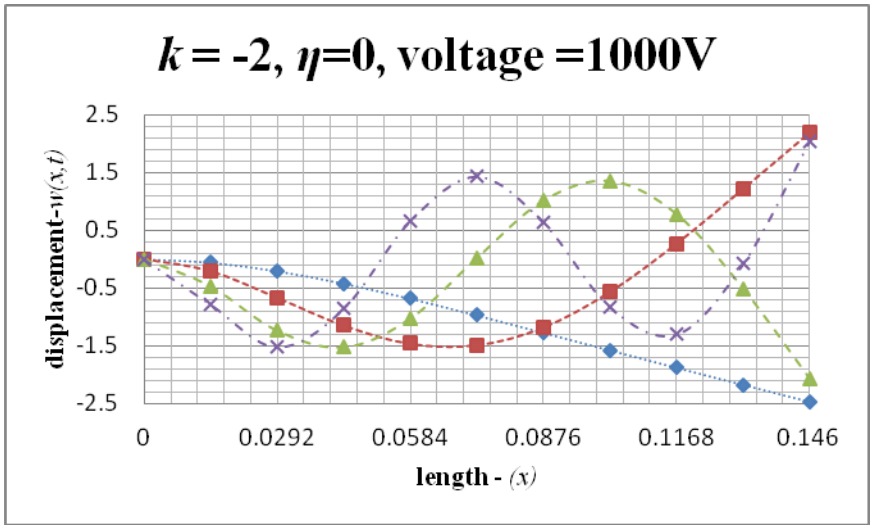

Figure C1 4: First four mode shapes k = -2

C2. Mode shapes for different tip masses $k = 0$

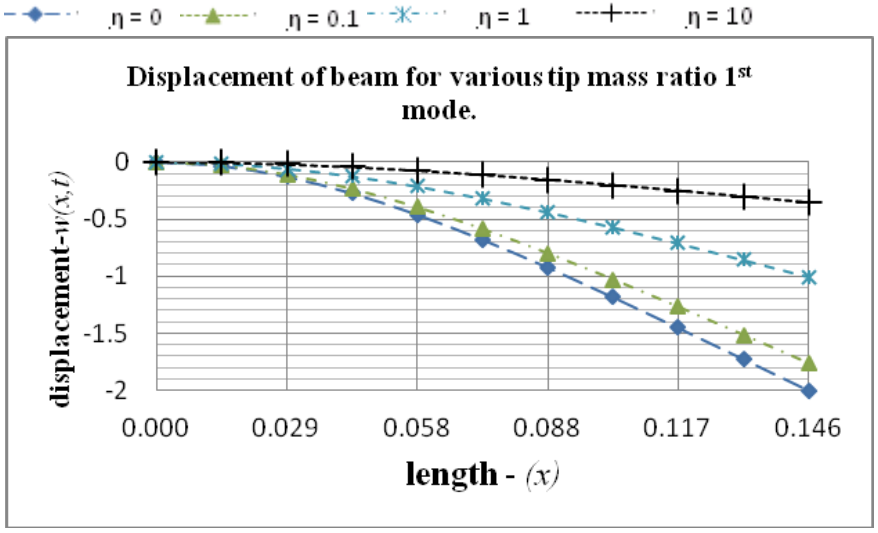

Figure C2 1: Fundamental mode shapes

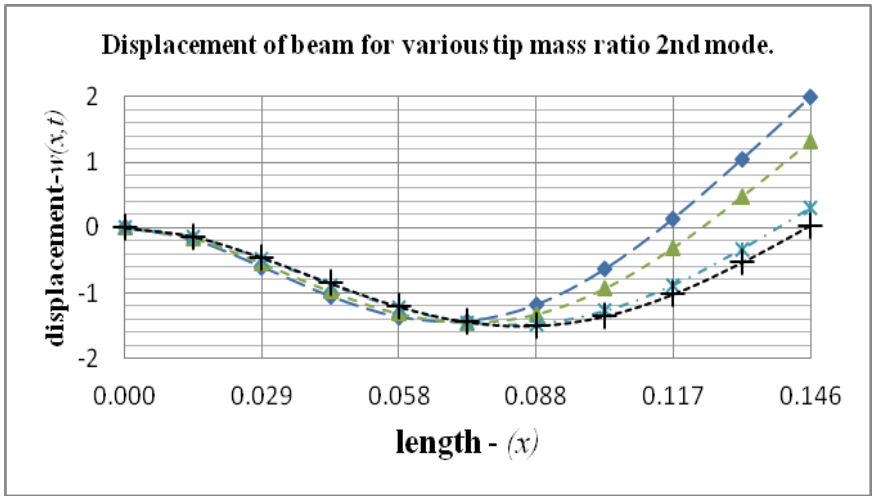

Figure C2 2: Second mode shapes

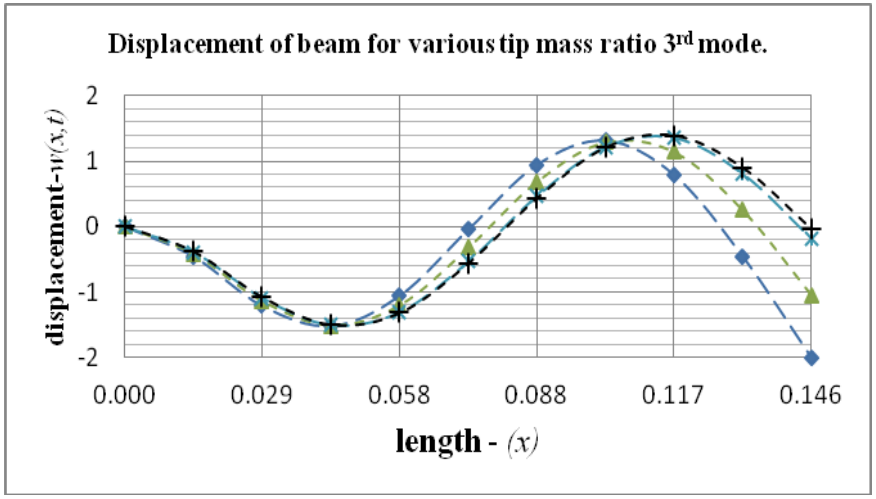

Figure C2 3: Third mode shapes

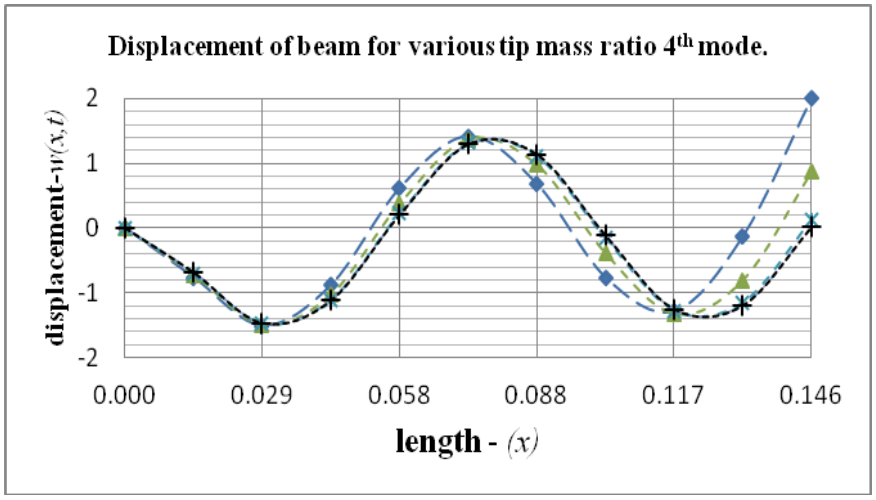

Figure C2 4: Fourth mode shapes